MEASURABLE BRAIN AND COGNITIVE RESERVE: THE IMPLICATION OF NEUROIMAGING BIOMARKERS IN THE NORMAL AGING PROCESS

EDITED BY: Chu-Chung Huang, Ching-Po Lin, Kenji Toba and Duan Xu
PUBLISHED IN: Frontiers in Aging Neuroscience

frontiers Research Topics

ISSN 1664-8714
ISBN 978-2-83250-341-6
DOI 10.3389/978-2-83250-341-6

About Frontiers

Frontiers is more than just an open-access publisher of scholarly articles: it is a pioneering approach to the world of academia, radically improving the way scholarly research is managed. The grand vision of Frontiers is a world where all people have an equal opportunity to seek, share and generate knowledge. Frontiers provides immediate and permanent online open access to all its publications, but this alone is not enough to realize our grand goals.

Frontiers Journal Series

The Frontiers Journal Series is a multi-tier and interdisciplinary set of open-access, online journals, promising a paradigm shift from the current review, selection and dissemination processes in academic publishing. All Frontiers journals are driven by researchers for researchers; therefore, they constitute a service to the scholarly community. At the same time, the Frontiers Journal Series operates on a revolutionary invention, the tiered publishing system, initially addressing specific communities of scholars, and gradually climbing up to broader public understanding, thus serving the interests of the lay society, too.

Dedication to Quality

Each Frontiers article is a landmark of the highest quality, thanks to genuinely collaborative interactions between authors and review editors, who include some of the world's best academicians. Research must be certified by peers before entering a stream of knowledge that may eventually reach the public - and shape society; therefore, Frontiers only applies the most rigorous and unbiased reviews.
Frontiers revolutionizes research publishing by freely delivering the most outstanding research, evaluated with no bias from both the academic and social point of view. By applying the most advanced information technologies, Frontiers is catapulting scholarly publishing into a new generation.

What are Frontiers Research Topics?

Frontiers Research Topics are very popular trademarks of the Frontiers Journals Series: they are collections of at least ten articles, all centered on a particular subject. With their unique mix of varied contributions from Original Research to Review Articles, Frontiers Research Topics unify the most influential researchers, the latest key findings and historical advances in a hot research area! Find out more on how to host your own Frontiers Research Topic or contribute to one as an author by contacting the Frontiers Editorial Office: frontiersin.org/about/contact

MEASURABLE BRAIN AND COGNITIVE RESERVE: THE IMPLICATION OF NEUROIMAGING BIOMARKERS IN THE NORMAL AGING PROCESS

Topic Editors:
Chu-Chung Huang, East China Normal University, China
Ching-Po Lin, National Yang-Ming University, Taiwan
Kenji Toba, Tokyo Metropolitan Institute of Gerontology, Japan
Duan Xu, University of California, San Francisco, United States

Citation: Huang, C.-C., Lin, C.-P., Toba, K., Xu, D., eds. (2022). Measurable Brain and Cognitive Reserve: The Implication of Neuroimaging Biomarkers in the Normal Aging Process. Lausanne: Frontiers Media SA.
doi: 10.3389/978-2-83250-341-6

Table of Contents

frontiers | Frontiers in Aging Neuroscience

TYPE Editorial
PUBLISHED 13 September 2022
DOI 10.3389/fnagi.2022.1020435

OPEN ACCESS

EDITED AND REVIEWED BY
Kristy A. Nielson,
Marquette University, United States

*CORRESPONDENCE
Chu-Chung Huang
czhuang@psy.ecnu.edu.cn

SPECIALTY SECTION
This article was submitted to Neurocognitive Aging and Behavior, a section of the journal Frontiers in Aging Neuroscience

RECEIVED 16 August 2022
ACCEPTED 26 August 2022
PUBLISHED 13 September 2022

CITATION
Huang C-C, Lin C-P, Toba K and Xu D (2022) Editorial: Measurable brain and cognitive reserve: The implication of neuroimaging biomarkers in the normal aging process.
Front. Aging Neurosci. 14:1020435.
doi: 10.3389/fnagi.2022.1020435

Editorial: Measurable brain and cognitive reserve: The implication of neuroimaging biomarkers in the normal aging process

Chu-Chung Huang[1,2]*, Ching-Po Lin[3,4,5], Kenji Toba[6] and Duan Xu[7]

[1]Shanghai Key Laboratory of Brain Functional Genomics (Ministry of Education), Affiliated Mental Health Center (ECNU), School of Psychology and Cognitive Science, East China Normal University, Shanghai, China, [2]Shanghai Changning Mental Health Center, Shanghai, China, [3]Institute of Neuroscience, National Yang Ming Chiao Tung University, Taipei, Taiwan, [4]Brain Research Center, National Yang Ming Chiao Tung University, Taipei, Taiwan, [5]Center for Healthy Longevity and Aging Sciences, National Yang Ming Chiao Tung University, Taipei, Taiwan, [6]Tokyo Metropolitan Institute of Gerontology, Tokyo, Japan, [7]Department of Radiology and Biomedical Imaging, University of California, San Francisco, San Francisco, CA, United States

KEYWORDS

cognitive reserve, brain reserve hypothesis, neuroimage, aging, lifespan

Editorial on the Research Topic
Measurable brain and cognitive reserve: The implication of neuroimaging biomarkers in the normal aging process

Cognitive aging is universal, but individual trajectories vary widely. Many older adults are capable of maintaining good physical, psychological, and social functioning until the end of life, called "successful aging" (Rowe and Kahn, 1997). It is believed that these individuals are more resistant to neuropathological challenges, and their cognition ages more slowly. By observing the resilient nature of these "successfully aging" brains, "reserve" concepts are constructed to explain such heterogeneity among individuals.

In the theory of brain reserve (BR), individuals with higher brain volumes or neural resources are better able to resist pathological damage and aging-related changes (Satz, 1993). Meanwhile, cognitive reserve (CR) suggests that pre-acquired cognitive skills, such as IQ, education, occupational attainment, exercise, and leisure activities, enrich the brain's networks to cope with brain atrophy or damage (Stern, 2013). Both theories seek to explain individual heterogeneity. With the advent of neuroimaging techniques, recent studies have made significant progress in measuring brain capacity to predict one's cognitive aging trajectory and health status. This helps fulfill the BR and CR theories at the practical level (Cabeza et al., 2018; Groot et al., 2018; Cole et al., 2019; Stern et al., 2019).

In this Research Topic, advanced neuroimaging techniques were used to investigate or estimate the effects of CR in the normal aging process and populations with neurodegenerative disorders.

Given that the concept of CR is related to the cognitive resiliency of an individual's brain during neural challenges. Lee et al. utilized the AD neuropathology—tau, amyloid—and cortical thickness using T1-MRI to predict cognitive function, the residuals of which is conceptualized as CR to associate with disease progression. They demonstrated that the effect of CR can be different according to the disease status, that higher CR was related to a mitigated decline in CU individuals, while it was associated with exacerbated cognitive decline in the AD spectrum. Using FDG-PET, Kato et al. investigated the effect of CR on amnestic MCI. Among MCI patients showing clinical AD patterns based on Silverman's classification, glucose hypometabolism was observed in the high-education group compared with the low-education group. Furthermore, cognitive decline was more rapid in the high-education group over 3 years. Although using education as a proxy of CR remains debatable, this study indicates that individuals with higher CR may instead suffer a greater cognitive decline in the face of pathological brain changes. Since brain atrophy is often accompanied by cognitive decline, Imabayashi et al. demonstrated brain volume atrophy composite scores in medial temporal regions were deemed as early AD markers in the evaluation of early volume changes in cognitively normal participants (CN). They found that CN with positive amyloid instead shows enlarged left medial temporal volume than those without amyloid deposition, which might be explained by an increase in brain volume as a mechanism to compensate for AD pathology in the preclinical stage to maintain cognitive performance. Using multimodal neuroimaging techniques, Kim et al. proposed the negative behavioral reserve (nBR) hypothesis (predicted negative symptoms using neuroimaging markers) to explain individual variability in behavioral problems in frontotemporal dementia. Their findings suggest that participants with higher nBR have lower negative symptoms and are associated with lesser atrophy in the frontotemporal cortex and greater white matter integrity. These findings imply that individuals with greater BR may have fewer clinical symptoms than those with the same neuropathological burden. Toh and Siow utilized a new diffusion MRI algorithm that analyzes the diffusivity along perivascular spaces (ALPS) to assess glymphatic activity (Taoka et al., 2017), which is related to the efficiency of waste clearance in the brain. The ALPS index showed lower values in ischemic stroke patients than normal controls, suggesting impaired glymphatic function. Additionally, the ALPS index can increase with time since stroke onset, suggesting glymphatic function recovery. This study provides evidence for assessing brain health using diffusion-based ALPS estimates.

The studies by Lee et al., Kato et al., Imabatyshi et al., and Toh and Siow provide neuroimaging evidence for individuals susceptible or resistant to neuropathology. Based on their findings, the effect of CR may vary depending on the disease spectrum stage. Future studies should consider the compensatory effect or the role of brain structural and functional changes longitudinally.

Hsieh and Yang investigated the association of diffusion parameter changes in brain white matter (WM) with cognition in 114 mid-aged adults within a 2-year interval. While some brain-cognition associations can be found in the cross-sectional dataset, only the association between WM integrity and processing speed could be replicated in both cross-sectional and longitudinal datasets. These findings support aging-related changes in processing speed over the 2-year interval and highlight the necessity of longitudinal design for studies of aging-related cognition. A longitudinal study by Pur et al. examined age-related changes in brain structural connectivity (SC) and functional connectivity (FC) within 2 years in older adults using diffusion-weighted imaging and resting-state functional MRI. They demonstrated that age-related cognitive declines could be supported by a distinct positive and negative contribution of SC and FC. The results suggest a tendency to preserve structural connections but decline functional ones during the cognitive aging process, which may imply the neural basis of cognitive reserve that protects against aging-related degeneration. Wei et al. compared the dynamic FC using resting-state fMRI between those with subjective cognitive decline (SCD) and a control group. The study demonstrated that changes in frontoparietal dynamic connectivity could occur early in the preclinical stage of SCD, which suggests the critical role of dynamic FC of FPN in balancing subjective and objective cognition.

Hsieh and Yang and Pur et al. focus on longitudinal changes from the brain network perspective. Wei et al. demonstrated the dynamic FC changes at the stage before objective cognition declines. These studies shed insight into cognitive reserve research using neuroimaging techniques, that balancing segregation and integration at the network level could be essential to brain health status instead of relying on traditional localizationism concepts.

Leisure activity (LA) engagement in later life has been associated with greater cognitive reserve; however, how it influences brain health remains unclear. Iizuka et al. classified 482 participants into four different subtypes of LA engagement according to how many types of LA they are currently engaged in. The results demonstrated that people who engaged in $\geq$3

types of LAs showed greater hippocampal volume and gray matter volume, which was more pronounced among males than females. Even though most domains of cognition decline with age, language is an exception that remains stable from adulthood to later life. In this regard, Yeh et al. examined whether different brain regions are in charge between young and older adults during idioms processing. They found that older adults showed higher accuracy for frequent idioms and equivalent accuracy for infrequent idioms than younger adults. In addition, older adults exhibited higher functional activations in the bilateral frontotemporal and medial frontoparietal regions. This study provides evidence for the alternative view that aging may not necessarily be solely accompanied by decline.

The cognitive reserve emphasizes the importance of acquired experiences throughout early lifetime. The studies by Iizuka et al. and Yeh et al. provide in-depth evidence in support of this hypothesis, utilizing neuroimaging measurements to explain individual differences in cognitive abilities.

The above contributions are but a few papers collected in this Research Topic addressing important issues about how reserve can be measured across the human lifespan using multimodal neuroimaging techniques. Future studies will endeavor to leverage the variety of neuroimaging methods to explain the heterogeneity of human behavior and cognition, and discover the underlying neural mechanism of the reserve. More importantly, interventional study designs should be considered to assess and clarify the neurobiological effects of mental, physical training or active lifestyles on cognitive reserve.

Author contributions

C-CH drafted the manuscript. C-PL, KT, and DX reviewed it. All authors contributed to the article and approved the submitted version.

Acknowledgments

We would like to warmly thank the editorial board, editor, and our colleagues who served as reviewers in this Research Topic. We are very grateful for their professionalism and support.

Conflict of interest

The authors declare that the research was conducted in the absence of any commercial or financial relationships that could be construed as a potential conflict of interest.

Publisher's note

References

Cabeza, R., Albert, M., Belleville, S., Craik, F. I., Duarte, A., Grady, C. L., et al. (2018). Maintenance, reserve and compensation: the cognitive neuroscience of healthy ageing. *Nat. Rev. Neurosci.* 19, 701–710. doi: 10.1038/s41583-018-0068-2

Cole, J. H., Marioni, R. E., Harris, S. E., and Deary, I. J. (2019). Brain age and other bodily 'ages': implications for neuropsychiatry. *Mol. Psychiatr.* 24, 266–281. doi: 10.1038/s41380-018-0098-1

Groot, C., van Loenhoud, A. C., Barkhof, F., van Berckel, B. N. M., Koene, T., Teunissen, C. C., et al. (2018). Differential effects of cognitive reserve and brain reserve on cognition in Alzheimer disease. *Neurology.* 90, e149–e156. doi: 10.1212/WNL.0000000000004802

Rowe, J. W., and Kahn, R. L. (1997). Successful aging. *Gerontologist.* 37, 433–440. doi: 10.1093/geront/37.4.433

Satz, P. (1993). Brain reserve capacity on symptom onset after brain injury: a formulation and review of evidence for threshold theory. *Neuropsychology.* 7, 273–295. doi: 10.1037/0894-4105.7.3.273

Stern, Y. (2013). Cognitive reserve: implications for assessment and intervention. *Folia Phoniatr Logop* 65, 49–54. doi: 10.1159/000353443

Stern, Y., Barnes, C. A., Grady, C., Jones, R. N., and Raz, N. (2019). Brain reserve, cognitive reserve, compensation, and maintenance: operationalization, validity, and mechanisms of cognitive resilience. *Neurobiol. Aging.* 83, 124–129. doi: 10.1016/j.neurobiolaging.2019.03.022

Taoka, T., Masutani, Y., Kawai, H., Nakane, T., Matsuoka, K., Yasuno, F., et al. (2017). Evaluation of glymphatic system activity with the diffusion MR technique: diffusion tensor image analysis along the perivascular space (DTI-ALPS) in Alzheimer's disease cases. *Jpn J. Radiol.* 35, 172–178. doi: 10.1007/s11604-017-0617-z

frontiers in Aging Neuroscience

ORIGINAL RESEARCH
published: 08 November 2021
doi: 10.3389/fnagi.2021.756249

Glymphatic Dysfunction in Patients With Ischemic Stroke

Cheng Hong Toh[1,2]* *and Tiing Yee Siow*[1]

[1] Department of Medical Imaging and Intervention, Chang Gung Memorial Hospital at Linkou, Taoyuan, Taiwan, [2] Chang Gung University College of Medicine, Taoyuan, Taiwan

Objectives: Rodent experiments have provided some insight into the changes of glymphatic function in ischemic stroke. The diffusion tensor image analysis along the perivascular space (DTI-ALPS) method offers an opportunity for the noninvasive investigation of the glymphatic system in patients with ischemic stroke. We aimed to investigate the changes of glymphatic function in ischemic stroke and the factors associated with the changes.

Materials and Methods: A total of 50 patients (mean age 56.7 years; 30 men) and 44 normal subjects (mean age 53.3 years; 23 men) who had preoperative diffusion-tensor imaging for calculation of the analysis along the perivascular space (ALPS) index were retrospectively included. Information collected from each patient included sex, age, time since stroke onset, infarct location, hemorrhagic change, infarct volume, infarct apparent diffusion coefficient (ADC), infarct fractional anisotropy (FA), and ALPS index of both hemispheres. Interhemispheric differences in ALPS index (infarct side vs. contralateral normal side) were assessed with a paired *t*-test in all patients. ALPS index was normalized by calculating ALPS ratios (right-to-left and left-to-right) for comparisons between patients and normal subjects. Comparisons of ALPS ratios between patients and normal subjects were performed using analysis of covariance with adjustments for age and sex. Linear regression analyses were performed to identify factors associated with the ALPS index.

Results: In patients, the mean ALPS index ipsilateral to infarct was 1.162 ± 0.126, significantly lower ($P < 0.001$) than that of the contralateral side (1.335 ± 0.160). The right-to-left ALPS index ratio of patients with right cerebral infarct was 0.84 ± 0.08, significantly lower ($P < 0.001$) than that of normal subjects (0.95 ± 0.07). The left-to-right ALPS ratio of patients with left cerebral infarct was 0.92 ± 0.09, significantly ($P < 0.001$) lower than that of normal subjects (1.05 ± 0.08). On multiple linear regression analysis, time since stroke onset (β = 0.794, $P < 0.001$) was the only factor associated with the ALPS index.

Conclusion: The ALPS index showed lower values in ischemic stroke suggesting impaired glymphatic function. Following initial impairment, the ALPS index increased with the time since stroke onset, which is suggestive of glymphatic function recovery.

Keywords: neuroimaging biomarkers, ischemic stroke, diffusion tensor imaging, ALPS (analysis along perivascular space) index, glymphatic function

OPEN ACCESS

Edited by:
Ching-Po Lin,
National Yang-Ming University, Taiwan

Reviewed by:
Toshiaki Taoka,
Nagoya University, Japan
Vijay Venkatraman,
The University of Melbourne, Australia

***Correspondence:**
Cheng Hong Toh
eldomtoh@hotmail.com

Received: *10 August 2021*
Accepted: *11 October 2021*
Published: *08 November 2021*

Citation:
Toh CH and Siow TY (2021) Glymphatic Dysfunction in Patients With Ischemic Stroke. Front. Aging Neurosci. 13:756249. doi: 10.3389/fnagi.2021.756249

INTRODUCTION

The glymphatic system has been recently recognized as a pathway for waste clearance and maintaining fluid balance in the brain's parenchymal interstitium (Rasmussen et al., 2018). Cerebrospinal fluid (CSF) from the subarachnoid space flows into brain parenchyma through periarterial spaces of the penetrating arteries and under the influence of Aquaporin-4 water channels mixes with parenchymal interstitial fluid. The interstitial fluid and its solutes then move into the perivenous and perineuronal spaces thereafter leaving the brain parenchyma. The discovery of the glymphatic system led to a new perspective on the pathogenesis of many brain diseases including ischemic stroke (Mestre et al., 2020).

Rodent experiments have provided some insights into the changes in glymphatic function associated with ischemic stroke. It is widely accepted that interstitial fluid clearance in the glymphatic system is reduced after ischemic infarct (Ji et al., 2021; Lv et al., 2021). Despite that substantial knowledge has been gained from animal studies, further research is necessary to confirm if findings regarding the glymphatic system of animals apply to humans. Understanding the role of the glymphatic system in the pathophysiological process of ischemic stroke may help develop treatments that promote poststroke functional recovery. Comprehensive human research on the glymphatic system, however, is limited by the invasiveness of current evaluation tools (e.g., intrathecal contrast medium injection) (Ringstad et al., 2018; Edeklev et al., 2019; Watts et al., 2019).

Diffusion magnetic resonance imaging (MRI) has emerged as a noninvasive tool for human glymphatic system assessment. Analysis along the perivascular space (ALPS) index is a diffusion metric derived from diffusion tensor imaging (DTI) (Taoka et al., 2017). It estimates the diffusivity along with the perivascular spaces of medullary veins and has been used to assess glymphatic activity in clinical conditions including Alzheimer's disease (Taoka et al., 2017; Steward et al., 2021), normal pressure hydrocephalus (Yokota et al., 2019; Bae et al., 2021), Parkinson's disease (Chen et al., 2021; McKnight et al., 2021), age-related iron deposition (Zhou W. et al., 2020), diabetic-associated cognitive impairment (Yang et al., 2020), and tumor-associated brain edema (Toh et al., 2021; Toh and Siow, 2021).

The ALPS index offers an opportunity for the noninvasive investigation of the human glymphatic system, and thus, we took advantage of this method to evaluate the glymphatic system in patients with ischemic stroke. We aimed to investigate the changes of the ALPS index, which suggests a glymphatic function in ischemic stroke, and factors associated with the changes.

MATERIALS AND METHODS

Study Subjects

Approval for reviewing the clinical data and preoperative MRI studies of patients was obtained from our Institutional Review Board. Between 2014 and 2018, a total of 58 consecutive patients with a diagnosis of ischemic stroke underwent preoperative DTI at our institution. Stroke onset time for each patient in this study was the estimate entered in the clinical record by the stroke neurologist. Patients who had an unknown time of stroke onset were not included in the study.

A total of eight patients were excluded due to posterior circulation infarct (n = 1), previous nonlacunar infarct (n = 1), bilateral cerebral infarction (n = 1), previously skull or brain surgery (n = 3), and time since stroke onset >60 days (n = 2). Thus, a total of 50 patients were analyzed. No patients had begun any thrombolytic or other recanalization therapies at the time of their MRI studies.

Patients were divided into two groups based on infarct volume ($\leq$20 cm^3 vs. >20 cm^3) (Meng and Ji, 2021) and time since stroke onset ($\leq$14 days vs. >14 days) (Kanekar et al., 2012). According to a meta-analysis of research on predictive factors in ischemic stroke, the infarct volume cut-point of 50 ml is sensitive in differentiating favorable and unfavorable outcomes (Meng and Ji, 2021). On the other hand, restoration of blood–brain barrier, resolution of vasogenic edema, and cleaning up of necrotic tissue begin after 14 days (Kanekar et al., 2012).

As healthy controls, 44 subjects (21 women, 23 men; mean age 53.3 $\pm$ 9.9 years; age range 27–83 years) with normal brain MRI examinations were also included.

Clinical and Imaging Information

Medical records and MRI studies of the patient were retrospectively reviewed to collect clinical and imaging information including sex, age, and time since stroke onset (time interval between MRI examination and stroke onset time), and infarct location (right or left cerebral hemisphere).

Magnetic Resonance Imaging

All MRI studies were performed using a 3T unit (Magnetom Tim Trio, Siemens, Erlangen, Germany) with a 12-channel phased-array head coil. All examinations included T2-weighted, FLAIR, susceptibility-weighted, DTI, and T1-weighted sequences acquired in the transverse plane before and after administration of 0.1 mmol/kg body weight gadopentetate dimeglumine (Magnevist; Schering, Berlin, Germany).

Diffusion tensor imaging was performed using a single-shot EPI with the following parameters: TR ms/TE ms, 5,800/83; diffusion gradient encoding in 20 directions; b = 0, 1,000 s/mm^2; FOV, 256 × 256 mm; matrix size, 128 × 128; section thickness, 2 mm; and number of signals acquired, 4. A total of 50–60 sections without intersection gaps were used to cover the cerebral hemispheres, brainstem, and cerebellum. Generalized autocalibrating partially parallel acquisitions (GRAPPA) with a reduction factor set at 2 were used during DTI acquisitions. Contrast-enhanced T1-weighted images (TR/TE, 2,000/2.63 ms; section thickness, 1 mm; TI, 900 ms; acquisition matrix, 224 × 256 and FOV, 224 × 256 mm) were acquired after completion of the DTI sequence.

Image Post-processing and Analysis

A software nordicICE (nordic Image Control and Evaluation Version 2, Nordic Imaging Lab, Bergen, Norway) was used for all volume measurements and for processing of diffusion-tensor data. The diffusion-weighted images were co-registered

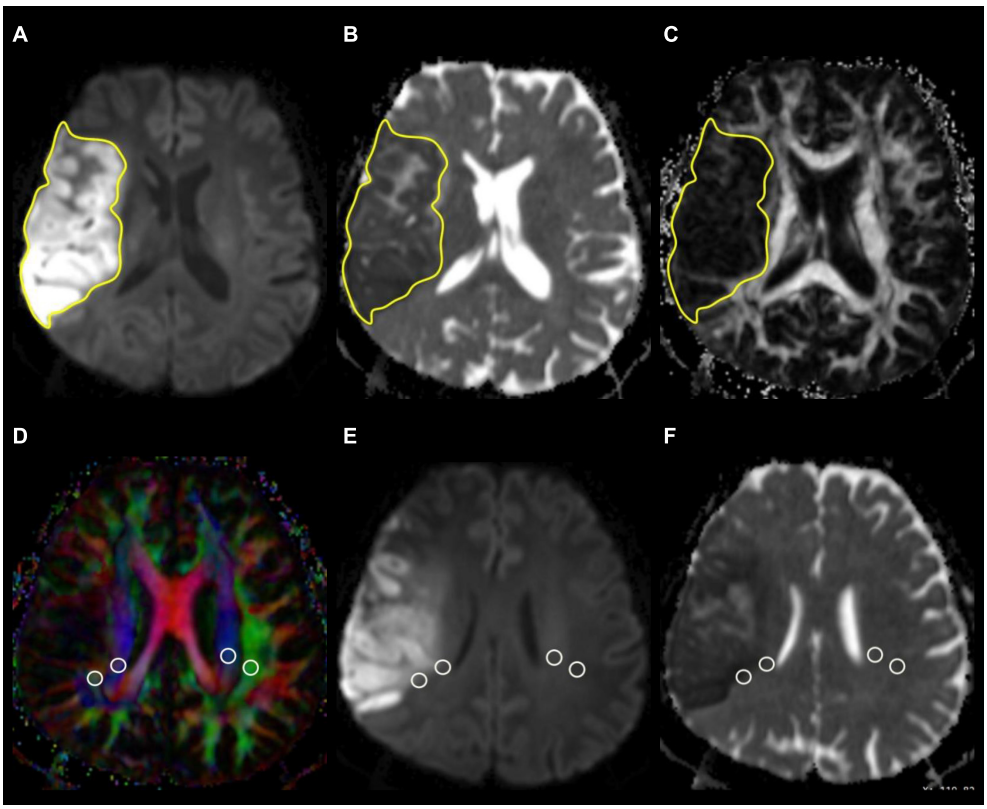

FIGURE 1 | Example of how regions of interest (ROIs) were segmented. Transverse isotropic diffusion-weighted **(A)**, apparent diffusion coefficient **(B)**, and fractional anisotropy images show manually drawn ROIs for measurement of infarct volume, ADC, and FA values. Directionally encoded color map **(D)** illustrates ROIs of projection (blue area) and association (green area) fibers in bilateral periventricular regions. On the co-registered isotropic diffusion-weighted **(E)** and apparent diffusion coefficient **(F)** images, these ROIs do not include infarcted tissue.

to the non-diffusion-weighted (b = 0) images to minimize the artifacts induced by eddy current and subject motion. Fractional anisotropy (FA) and apparent diffusion coefficient (ADC) were calculated from diffusion-tensor data using standard algorithms (Mukherjee et al., 2008; Toh and Castillo, 2021).

All images were co-registered based on a 3D nonrigid transformation and mutual information (Sundar et al., 2007). The adequacy of registration was visually assessed, and manual adjustments were performed by changing transformation parameters of translation, rotation, and/or scaling as necessary. Two neuroradiologists (with 16 and 6 years of experience) independently performed all measurements.

Measurement of Infarct Volume

The infarct volume was measured on FLAIR or isotropic DW images, depending on the lesion conspicuity and infarct stage, with reference to ADC, T2-weighted, and contrast-enhanced T1-weighted images. A polygonal region of interest (ROI) was manually drawn to include the entire infarct on each isotropic DW or FLAIR image. The ROIs on all images were then combined to form a whole infarct volume of interest for calculations of infarct volume. An example of ROI segmentation is shown in **Figure 1**.

Measurements of Infarct Apparent Diffusion Coefficient and Fractional Anisotropy Values

Infarct ADC and FA values were measured using the same ROIs drawn on DW or FLAIR images. The ROIs were adjusted so as not to include regions with hemorrhagic change. Mean ADC and FA values of the whole infarct volume were calculated by averaging the values of all slices with the infarct volume of each slice taken into account.

Measurement of Analysis Along the Perivascular Space Index

The DTI-ALPS method (Taoka et al., 2017, 2021) was used to evaluate the glymphatic function. This method evaluates the diffusivity along with the perivascular space on a transverse slice at the level of the lateral ventricle body. The medullary veins, accompanied by their perivascular spaces, run perpendicular to the ventricular walls at the level of the lateral ventricular bodies in a right-left or left-right direction (i.e., x-axis in image coordinate). In this level, the corticofugal corona radiata projection fibers run in the craniocaudal direction (i.e., z-axis in image coordinate) adjacent to the lateral ventricles. The superior longitudinal fascicle, which represents the association fibers, runs in the

anterior-posterior direction (i.e., *y*-axis in image coordinate) and is located lateral to the corona radiata. As the perivascular space is nearly perpendicular to both the projection fibers and association fibers, the major difference between *x*-axis diffusivity in both fibers (D_{xxproj} and D_{xxassoc} for *x*-axis diffusivity in projection fiber and association fiber, respectively) and the diffusivity that is perpendicular to the *x*-axis and to the direction of fiber tracts (*y*-axis for projection fiber, where the diffusivity is denoted as D_{yyproj}; *z*-axis for association fiber, where the diffusivity is denoted as D_{zzassoc}) is the existence of perivascular space. To quantify glymphatic activity, the ALPS index is defined as follows:

$$\text{ALPS index} = \frac{\text{mean}\left(D_{xxproj}, D_{xxassoc}\right)}{\text{mean}\left(D_{yyproj}, D_{zzassoc}\right)} \quad (1)$$

Diffusion metric images were generated by using 3D Slicer version 4.10.2.[1] ROIs of projection (mean size, 18 ± 14 mm^2) and association fibers (mean size, 16 ± 13 mm^2) of both cerebral hemispheres were drawn on a slice at the level of the lateral ventricular body based on a directionality encoded map with reference to the co-registered ADC, isotropic DW, and FLAIR images so as not to include infarcted tissue. ALPS index was computed according to the Equation 1 above1. An example of ROI placement for ALPS index measurement is shown in **Figure 1**.

Statistical Analysis

A commercially available statistical software package (SPSS 22; IBM, Armonk, NY, United States) was used for the analysis, and *P*-values < 0.05 were considered to indicate a statistical significance. Continuous variables are denoted as mean ± SD unless otherwise noted. The Kolmogorov–Smirnov test was used to assess the normality of continuous variables and guide the selection of a parametric or nonparametric test for the comparison of variables. Variance inflation factors were used to detect multicollinearity.

The interobserver variability in the measurements of infarct volume, ADC, FA, and ALPS index was assessed by intraclass correlation coefficients (ICCs) with 95% confidence intervals (CIs) based on an absolute-agreement, two-way random effects model. The final values of all measurements were obtained by taking the mean of the independent measurements of two observers.

To evaluate the changes of glymphatic function in ischemic strokes, interhemispheric differences in ALPS index (infarct side vs. contralateral normal side) were assessed with a paired *t*-test in all patients. ALPS index was normalized by calculating ALPS ratios (right-to-left and left-to-right) for comparisons between patients and normal subjects. For patients with right cerebral infarct, their right-to-left ALPS index ratio was compared with that of normal subjects. For patients with left cerebral infarct, their left-to-right ALPS index ratio was compared with that of normal subjects. The comparisons between patients and normal subjects were analyzed using analysis of covariance with adjustments for age and sex.

[1]http://www.slicer.org

TABLE 1 | Characteristics of patients and normal subjects.

Characteristics	Patient	Normal subject
No. of subjects	50	44
Mean age ± SD (year)	56.7 ± 15.2	53.3 ± 9.9
Sex		
Woman	20	21
Man	30	23
Infarct location		
Right cerebral	32	
Left cerebral	18	
Hemorrhagic change		
No	31	
Yes	19	
Infarct volume (cm^3)	34.07 ± 44.55	
Infarct ADC (10^{-6} mm^2/s)	709.13 ± 310.39	
Infarct FA	0.149 ± 0.086	
Time since stroke onset (day)	17.1 ± 14.8	
Mean ALPS index		
Ipsilateral to infarct	1.162 ± 0.126	
Contralateral to infarct	1.335 ± 0.160	

Except where indicated, data are numbers of patients.
ADC, apparent diffusion coefficient; ALPS, analysis along the perivascular space; FA, fractional anisotropy; SD, standard deviation.

Among patients with ischemic stroke, group differences in ALPS index according to infarct volume (≤20 cm^3 vs. >20 cm^3) and time since stroke onset (≤14 days vs. >14 days) were assessed with analysis of covariance with adjustments for age and sex. Univariable linear regression analysis was first used to evaluate the associations of ALPS index with age, sex, infarct volume, infarct ADC, infarct FA, the presence of hemorrhagic change, and the time since stroke onset. All variables were entered as potential covariates in the stepwise multivariable linear regression analysis to identify independent factors associated with the ALPS index.

RESULTS

Among 50 patients (20 women, 30 men; mean age, 56.7 ± 15.2 years), 32 (64%) patients had right cerebral infarct and 19 (38%) patients showed hemorrhagic change. The mean time since stroke onset was 17.1 ± 14.8 days (range, 1–60). The mean infarct volume (cm^3) of 50 patients was 34.07 ± 44.55 (range, 4.12–134.14). **Table 1** summarizes patient characteristics and all measurements. There were excellent interobserver agreements in the measurements of infarct volumes (ICC = 0.802, 95% CI = 0.792–0.814, $P < 0.001$), infarct ADC (ICC = 0.956, 95% CI = 0.950–0.958, $P < 0.001$), infarct FA (ICC = 0.912, 95% CI = 0.906–0.918, $P < 0.001$), and bilateral ALPS indices (ICC = 0.838, 95% CI = 0.821–0.844, $P < 0.001$).

In patients, the mean ALPS index ipsilateral to infarct was 1.162 ± 0.126, significantly ($P < 0.001$) lower than that of the contralateral side (1.335 ± 0.160). The interhemispheric differences in the ALPS index are illustrated in **Figure 2**. Comparisons of ALPS index ratios between patients and normal subjects are summarized in **Table 2**. The right-to-left ALPS index

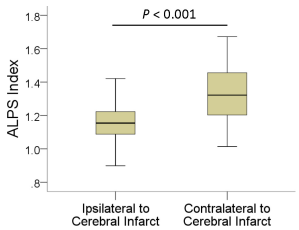

FIGURE 2 | Boxplot shows interhemispheric differences in the ALPS index.

TABLE 2 | Comparisons of right-to-left and left-to-right ALPS index ratios between patients and normal subjects.

Variable	ALPS index ratio	*P*-value	95% CI
Right-to-left ALPS index ratio		<0.001	−13.99, −7.05
Patient with right cerebral infarct (*n* = 32)	0.84 ± 0.08		
Normal subject (*n* = 44)	0.95 ± 0.07		
Left-to-right ALPS index ratio		<0.001	−18.28, −7.79
Patient with left cerebral infarct (*n* = 18)	0.92 ± 0.09		
Normal subject (*n* = 44)	1.05 ± 0.08		

Data are mean ± SD.
ALPS, analysis along the perivascular space; CI, confidence interval.

ratio of patients with right cerebral infarct was 0.84 ± 0.08, significantly ($P < 0.001$) lower than that of normal subjects (0.95 ± 0.07). The left-to-right ALPS ratio of patients with left cerebral infarct was 0.92 ± 0.09, significantly ($P < 0.001$) lower than that of normal subjects (1.05 ± 0.08). **Figure 3** shows the differences in ALPS index ratios between patients and normal subjects.

Table 3 shows the group differences in ALPS index according to infarct volume (≤20 cm^3 vs. >20 cm^3) and time since stroke onset (≤14 days vs. >14 days). ALPS index was significantly higher in patients with infarct volume smaller than 20 cm^3 ($P = 004$) and time since stroke onset longer than 14 days ($P < 0.001$). **Figure 4** shows the differences in the ALPS index with regard to infarct volume and time since stroke onset.

Results of univariable and multivariable linear regression analyses of factors associated with ALPS index are summarized in **Table 4**. On univariable linear regression analysis, ALPS index ipsilateral to the infarct correlated with infarct volume (β = −0.348, $P = 0.013$), infarct FA (β = 0.376, $P = 0.007$), presence of hemorrhagic change (β = −0.297, $P = 0.036$), and time since stroke onset (β = 0.794, $P < 0.001$). The associations of ALPS index with age ($P = 0.594$), sex ($P = 0.061$), and infarct ADC ($P = 0.734$) were not statistically significant. On stepwise multiple linear regression analysis, time since stroke onset (β = 0.794, $P < 0.001$) was the only factor associated with ALPS index. **Figure 5** illustrates the correlations of ALPS index with infarct volume, infarct ADC, infarct FA, and time since stroke onset.

DISCUSSION

In this study, the glymphatic function was impaired in ischemic stroke, as reflected by lower ALPS index in cerebral hemispheres with infarct when compared with that of contralateral normal hemispheres and normal subjects. In addition, the ALPS index increased with the time since stroke onset, suggesting glymphatic function recovery following initial impairment. To our knowledge, this is the first human study reporting the dynamic changes of glymphatic function in ischemic stroke.

The ALPS index may serve as a marker of the function of interstitial fluid clearance as it measures the diffusivity and thus efflux rates of interstitial fluid in the perivascular spaces of deep medullary veins. The ALPS index has been shown to reflect glymphatic dysfunction in diseases known to have impaired clearance function. In patients with dementia, the ALPS index correlates with the Mini-Mental State Examination score of patients (Taoka et al., 2017). In patients with normal pressure hydrocephalus, there is a significant decrease in the ALPS index (Yokota et al., 2019; Bae et al., 2021). In this study, the ALPS index was significantly decreased in cerebral hemispheres with infarct and that may imply impaired glymphatic function and

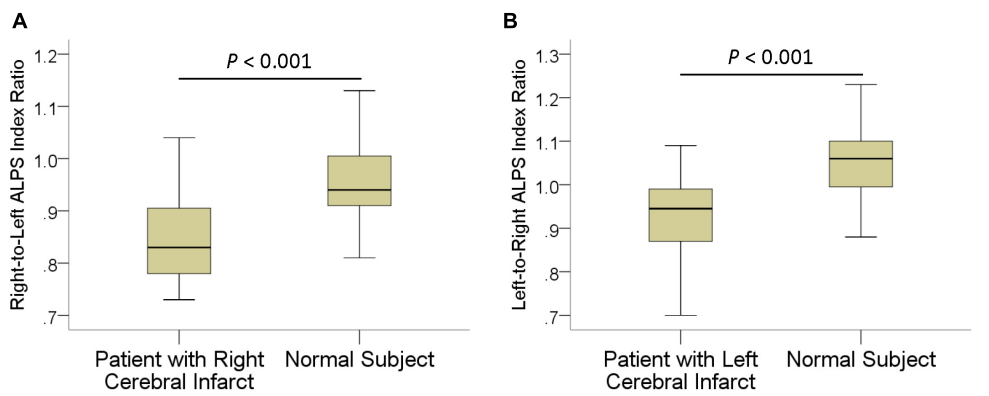

FIGURE 3 | Boxplots show differences in right-to-left **(A)** and left-to-right **(B)** ALPS index ratios between patients with ischemic stroke and normal subjects.

TABLE 3 | Group differences in ALPS index according to infarct volume and time since stroke onset.

Variable	ALPS index	*P*-value	95% CI
Infarct volume (cm^3)		0.004	0.038, 0.181
≤20 (*n* = 33)	1.189 ± 0.133		
>20 (*n* = 17)	1.110 ± 0.094		
Time since stroke onset (day)		<0.001	0.093, 0.215
≤14 (*n* = 32)	1.108 ± 0.087		
>14 (*n* = 18)	1.259 ± 0.129		

Data are mean ± SD.
ALPS, analysis along the perivascular space; CI, confidence interval.

reduced interstitial fluid clearance, similar to that observed in animal studies (Ji et al., 2021; Lv et al., 2021).

It is widely accepted that interstitial fluid clearance is reduced after ischemic stroke in animal studies (Lv et al., 2021). Impaired CSF circulation in the glymphatic system after ischemic stroke has been a consistent finding (Gaberel et al., 2014; Yang et al., 2015; Lin et al., 2020). After ischemic stroke, there was a delay in the clearance of fluorescent traces in the infarct core (Zbesko et al., 2018) as well as amyloid deposits along with perivascular spaces (Arbel-Ornath et al., 2013). Using the middle cerebral artery occlusion model, a recent study found that glymphatic function in ipsilateral substantia nigra and ventral thalamic nucleus was impaired (Gaberel et al., 2014). In our study, we also observed a decrease of glymphatic function in the cerebral hemisphere with ischemic stroke, similar to what has been reported in animal studies. To the best of our knowledge, ischemic stroke-associated glymphatic function impairment has never been reported in human studies.

In this study, we observed a gradual increase of ALPS index with the time since stroke onset, as evidenced by an inverse association between the two. This finding may suggest glymphatic function recovery following initial impairment. The clinical significance of this phenomenon is unclear, and it may have important implications in the pathogenesis of poststroke dementia, which is one of the most common and severe consequences of stroke (Pantoni, 2017). It has been demonstrated that extracellular fluid present in infarct areas (i.e., liquefactive necrosis) is harmful to primary cultured cortical and hippocampal neurons (Zbesko et al., 2018). Impaired tau clearance, which has been implicated in the pathogenesis of poststroke dementia (Zhao et al., 2014), was observed in a study using a rat model of poststroke dementia (Back et al., 2020). In transgenic mice overexpressing human Slit2 (*Slit2-Tg*), cognition was improved *via* accelerating glymphatic clearance after ischemic stroke. Therefore, we speculate that the gradual increase of glymphatic function in patients with ischemic stroke serves to remove fluid and waste associated with tissue destruction in the ischemic infarct.

To date, no studies have reported the longitudinal or dynamic changes of glymphatic function in ischemic stroke. The mechanism of the glymphatic function recovery is not known, and we speculate that it may be the result of glymphatic pathway remodeling. As described in glioma-bearing mice, the glymphatic function is increased by extensive growth of meningeal lymphatic vessels, which is downstream of the glymphatic pathway (Zhou Y. et al., 2020; Wu et al., 2021). The glymphatic pathway remodeling helps fluid clearance and reduction of peritumoral brain edema (Hu et al., 2020). In mice with defective meningeal lymphatic vessels, impaired drainage of brain parenchymal interstitial fluid aggravates peritumoral brain edema. In meningiomas, remodeling of the glymphatic pathway has also been proposed to explain the inverse association between peritumoral edema volume and glymphatic function measured with the ALPS index (Toh et al., 2021). Further studies are needed to determine if glymphatic pathway remodeling occurs in ischemic infarct and its association with glymphatic function recovery.

The ADC and FA are useful in tissue characterization. ADC measures the magnitude of water diffusivity and reflects cytotoxic edema and changes of extracellular matrix volume in infarcted tissue (Nagaraja, 2021). ADC is useful in estimating the lesion age in ischemic stroke (Lansberg et al., 2001). FA, on the other hand, measures the directionality of water flow and may be associated with axonal injury after stroke (Bhagat et al., 2006). Although infarct volume (Vogt et al., 2012), infarct ADC

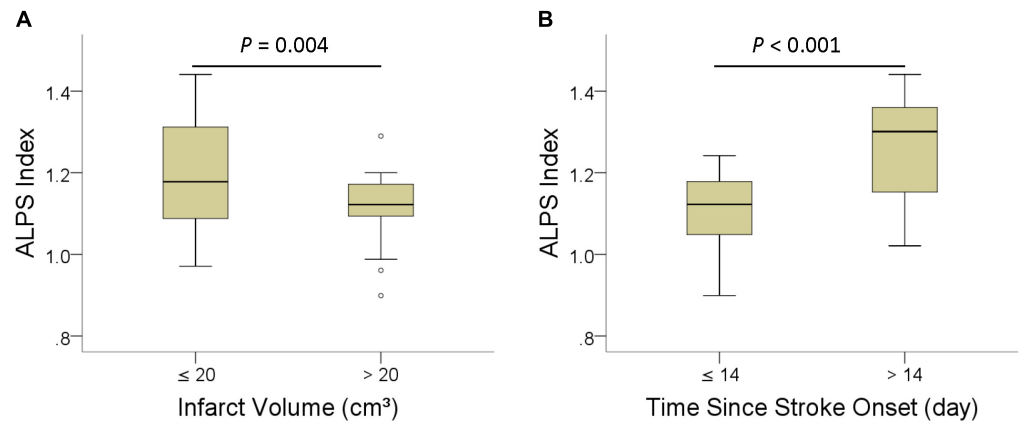

FIGURE 4 | Boxplots of ALPS index with regard to infarct volume **(A)**, and **(B)** time since stroke onset.

TABLE 4 | Univariable and multivariable linear regression analyses of factors associated with ALPS index.

Characteristics	ALPS index							
	Univariate linear regression				Multivariate linear regression			
	B	SE	β	*P*-value	B	SE	β	*P*-value
Age	−0.001	0.001	−0.077	0.594				
Sex	−0.068	0.036	−0.267	0.061				
Infarct volume	−0.001	0.000	−0.348	0.013				
Infarct ADC	−0.002	0.000	−0.049	0.734				
Infarct FA	0.548	0.195	0.376	0.007				
Hemorrhagic change	−0.007	0.036	−0.297	0.036				
Time after stroke onset	0.007	0.001	0.794	< 0.001	0.007	0.001	0.794	<0.001

ALPS, analysis along the perivascular space; SD, standard deviation; B, unstandardized coefficient; β, standardized coefficient; SE, standard error.

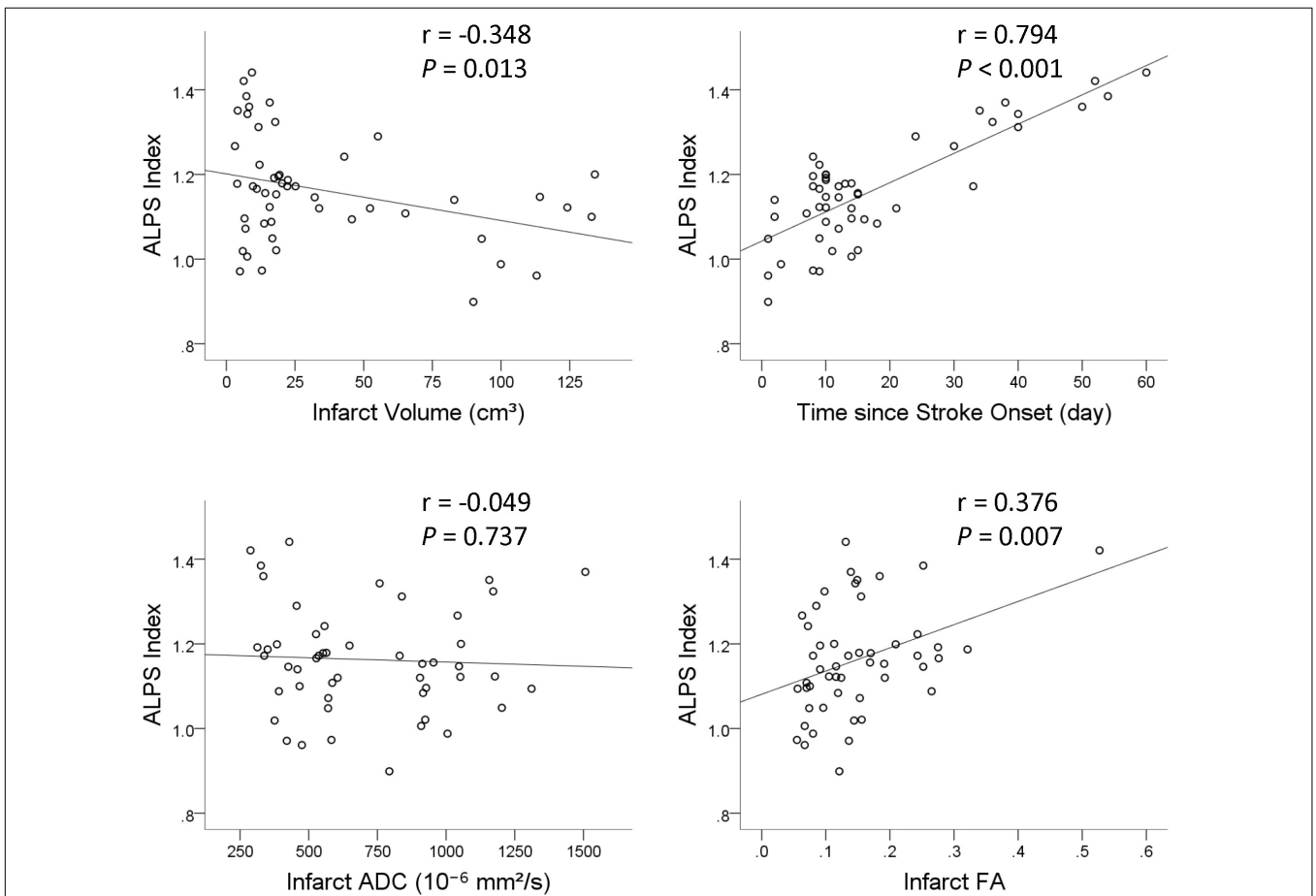

FIGURE 5 | Scatterplots with regression line show the correlations of ALPS index with infarct volume, time since stroke onset, infarct apparent diffusion coefficient (ADC), and infarct fractional anisotropy (FA).

(Nagaraja, 2021), infarct FA (Sotak, 2002; Moura et al., 2019), and hemorrhagic change (Kastrup et al., 2008) may predict outcomes of patients with ischemic stroke, they were not associated with the glymphatic function in our study. Rather, other factors such as Aquaporin-4 and meningeal lymphatics may have more significant roles in regulating the function of the glymphatic system (Lv et al., 2021).

Magnetic resonance imaging examinations performed after intrathecal injection of gadolinium-based contrast agents have confirmed the presence of the glymphatic system in the human brain (Zhou Y. et al., 2020). However, this method is invasive, and the off-label use of gadolinium-based contrast agents has potential neurotoxicity. DTI-ALPS method, in contrast, is noninvasive and has been shown to be highly reproducible

in a recent study (Taoka et al., 2021). It allows investigating longitudinal changes of glymphatic function in the same subjects as well as comparison of glymphatic function across different patient groups. This method may help establish the predictive and prognostic roles of glymphatic function in patients with ischemic stroke.

In this study, the ischemic stroke-associated glymphatic dysfunction seen in animal studies was demonstrated in humans using the ALPS index. The ALPS index has been shown to reflect glymphatic function in several neurological disorders and to correlate with cognitive impairment (Taoka et al., 2017; Yang et al., 2020; Chen et al., 2021; Steward et al., 2021). However, its role as a neuroimaging biomarker of cognitive function in healthy elderly is not yet established. Recently, glymphatic failure has been proposed as a final common pathway to dementia (Nedergaard and Goldman, 2020). Hence, imaging markers that can detect glymphatic dysfunction and cognitive function decline may have important roles in early intervention. Our study further supports the ALPS index as a potential neuroimaging marker of glymphatic function and prospective investigation of the ALPS index as a measure of cognitive reserve in the normal aging process.

There are limitations to our study. First, the glymphatic system has only recently been recognized, and there are no well-established noninvasive methods to measure its function in humans. In our study, the efflux of interstitial fluid at perivenous space was measured. Further studies are needed to establish the correlation between ALPS index and interstitial fluid excretion function. Second, the imaging time points of patients in this study were between day 1 and day 60 after stroke onset. Longitudinal data on temporal changes of ALPS index in the individual patient was not available. These pieces of information would be helpful to confirm the phenomenon that glymphatic function recovers following initial impairment in patients with ischemic stroke. Third, the small sample size of our study may limit comprehensive subgroup analysis stratified by infarct volume and time since stroke onset as well as multivariate analysis of each potential factor associated with glymphatic function.

CONCLUSION

In conclusion, the ALPS index showed lower values in ischemic stroke suggesting impaired glymphatic function. Following initial impairment, the ALPS index increased with the time since stroke onset, which is suggestive of glymphatic function recovery. However, larger series and prospective studies are needed to reach a definitive conclusion on changes in glymphatic function in patients with ischemic strokes.

DATA AVAILABILITY STATEMENT

The raw data supporting the conclusions of this article will be made available by the authors, without undue reservation.

ETHICS STATEMENT

The studies involving human participants were reviewed and approved by the Chang Gung Medical Foundation Institutional Review Board. Written informed consent for participation was not required for this study in accordance with the national legislation and the institutional requirements.

AUTHOR CONTRIBUTIONS

CT and TS contributed to the conception and design of the study and the acquisition and analysis of the data. CT contributed to drafting the text and preparation of figures, and wrote the first draft of the manuscript. Both authors read and approved the final manuscript.

REFERENCES

Arbel-Ornath, M., Hudry, E., Eikermann-Haerter, K., Hou, S., Gregory, J. L., Zhao, L., et al. (2013). Interstitial fluid drainage is impaired in ischemic stroke and Alzheimer's disease mouse models. *Acta Neuropathol.* 126, 353–364. doi: 10.1007/s00401-013-1145-2

Back, D. B., Choi, B. R., Han, J. S., Kwon, K. J., Choi, D. H., Shin, C. Y., et al. (2020). Characterization of Tauopathy in a rat model of post-stroke dementia combining acute infarct and chronic cerebral hypoperfusion. *Int. J. Mol. Sci.* 21:6929. doi: 10.3390/ijms21186929

Bae, Y. J., Choi, B. S., Kim, J. M., Choi, J. H., Cho, S. J., and Kim, J. H. (2021). Altered glymphatic system in idiopathic normal pressure hydrocephalus. *Parkinsonism Relat. Disord.* 82, 56–60. doi: 10.1016/j.parkreldis.2020.11.009

Bhagat, Y. A., Emery, D. J., Shuaib, A., Sher, F., Rizvi, N. H., Akhtar, N., et al. (2006). The relationship between diffusion anisotropy and time of onset after stroke. *J. Cereb. Blood Flow Metab.* 26, 1442–1450. doi: 10.1038/sj.jcbfm.9600294

Chen, H. L., Chen, P. C., Lu, C. H., Tsai, N. W., Yu, C. C., Chou, K. H., et al. (2021). Associations among cognitive functions, plasma DNA, and diffusion tensor image along the perivascular space (DTI-ALPS) in patients with Parkinson's disease. *Oxid. Med. Cell Longev* 2021:4034509. doi: 10.1155/2021/4034509

Edeklev, C. S., Halvorsen, M., Løvland, G., Vatnehol, S. A. S., Gjertsen, Ø., Nedregaard, B., et al. (2019). Intrathecal use of gadobutrol for glymphatic MR imaging: prospective Safety study of 100 patients. *AJNR Am. J. Neuroradiol.* 40, 1257–1264. doi: 10.3174/ajnr.A6136

Gaberel, T., Gakuba, C., Goulay, R., Martinez De Lizarrondo, S., Hanouz, J. L., Emery, E., et al. (2014). Impaired glymphatic perfusion after strokes revealed by contrast-enhanced MRI: a new target for fibrinolysis? *Stroke* 45, 3092–3096. doi: 10.1161/strokeaha.114.006617

Hu, X., Deng, Q., Ma, L., Li, Q., Chen, Y., Liao, Y., et al. (2020). Meningeal lymphatic vessels regulate brain tumor drainage and immunity. *Cell Res.* 30, 229–243. doi: 10.1038/s41422-020-0287-8

Ji, C., Yu, X., Xu, W., Lenahan, C., Tu, S., and Shao, A. (2021). The role of glymphatic system in the cerebral edema formation after ischemic stroke. *Exp. Neurol.* 340:113685. doi: 10.1016/j.expneurol.2021.113685

Kanekar, S. G., Zacharia, T., and Roller, R. (2012). Imaging of stroke: part 2, Pathophysiology at the molecular and cellular levels and corresponding imaging changes. *AJR Am. J. Roentgenol.* 198, 63–74. doi: 10.2214/ajr.10.7312

Kastrup, A., Gröschel, K., Ringer, T. M., Redecker, C., Cordesmeyer, R., Witte, O. W., et al. (2008). Early disruption of the blood-brain barrier after thrombolytic therapy predicts hemorrhage in patients with acute stroke. *Stroke* 39, 2385–2387. doi: 10.1161/strokeaha.107.505420

Lansberg, M. G., Thijs, V. N., O'brien, M. W., Ali, J. O., De Crespigny, A. J., Tong, D. C., et al. (2001). Evolution of apparent diffusion coefficient, diffusion-weighted, and T2-weighted signal intensity of acute stroke. *AJNR Am. J. Neuroradiol.* 22, 637–644.

Lin, L., Hao, X., Li, C., Sun, C., Wang, X., Yin, L., et al. (2020). Impaired glymphatic system in secondary degeneration areas after ischemic stroke in rats. *J. Stroke Cerebrovasc. Dis.* 29:104828. doi: 10.1016/j.jstrokecerebrovasdis.2020.104828

Lv, T., Zhao, B., Hu, Q., and Zhang, X. (2021). The Glymphatic system: a novel therapeutic target for stroke treatment. *Front. Aging Neurosci.* 13:689098. doi: 10.3389/fnagi.2021.689098

McKnight, C. D., Trujillo, P., Lopez, A. M., Petersen, K., Considine, C., Lin, Y. C., et al. (2021). Diffusion along perivascular spaces reveals evidence supportive of glymphatic function impairment in Parkinson disease. *Parkinsonism Relat. Disord.* 89, 98–104. doi: 10.1016/j.parkreldis.2021.06.004

Meng, X., and Ji, J. (2021). Infarct volume and outcome of cerebral ischaemia, a systematic review and meta-analysis. *Int. J. Clin. Pract.* 75:e14773. doi: 10.1111/ijcp.14773

Mestre, H., Du, T., Sweeney, A. M., Liu, G., Samson, A. J., Peng, W., et al. (2020). Cerebrospinal fluid influx drives acute ischemic tissue swelling. *Science* 367:eaax7171. doi: 10.1126/science.aax7171

Moura, L. M., Luccas, R., De Paiva, J. P. Q., Amaro, E. Jr., Leemans, A., Leite, C. D. C., et al. (2019). Diffusion tensor imaging biomarkers to predict motor outcomes in stroke: a narrative review. *Front. Neurol.* 10:445. doi: 10.3389/fneur.2019.00445

Mukherjee, P., Berman, J. I., Chung, S. W., Hess, C. P., and Henry, R. G. (2008). Diffusion tensor MR imaging and fiber tractography: theoretic underpinnings. *AJNR Am. J. Neuroradiol.* 29, 632–641. doi: 10.3174/ajnr.A1051

Nagaraja, N. (2021). Diffusion weighted imaging in acute ischemic stroke: a review of its interpretation pitfalls and advanced diffusion imaging application. *J. Neurol. Sci.* 425:117435. doi: 10.1016/j.jns.2021.117435

Nedergaard, M., and Goldman, S. A. (2020). Glymphatic failure as a final common pathway to dementia. *Science* 370, 50–56. doi: 10.1126/science.abb8739

Pantoni, L. (2017). Have stroke neurologists entered the arena of stroke-related cognitive dysfunctions? Not yet, but they should! *Stroke* 48, 1441–1442. doi: 10.1161/strokeaha.117.016869

Rasmussen, M. K., Mestre, H., and Nedergaard, M. (2018). The glymphatic pathway in neurological disorders. *Lancet Neurol.* 17, 1016–1024. doi: 10.1016/s1474-4422(18)30318-1

Ringstad, G., Valnes, L. M., Dale, A. M., Pripp, A. H., Vatnehol, S. S., Emblem, K. E., et al. (2018). Brain-wide glymphatic enhancement and clearance in humans assessed with MRI. *JCI Insight* 3:e121537. doi: 10.1172/jci.insight.121537

Sotak, C. H. (2002). The role of diffusion tensor imaging in the evaluation of ischemic brain injury - a review. *NMR Biomed.* 15, 561–569. doi: 10.1002/nbm.786

Steward, C. E., Venkatraman, V. K., Lui, E., Malpas, C. B., Ellis, K. A., Cyarto, E. V., et al. (2021). Assessment of the DTI-ALPS parameter along the perivascular space in older adults at risk of dementia. *J. Neuroimaging* 31, 569–578. doi: 10.1111/jon.12837

Sundar, H., Shen, D., Biros, G., Xu, C., and Davatzikos, C. (2007). Robust computation of mutual information using spatially adaptive meshes. *Med. Image Comput. Comput. Assist. Interv.* 10, 950–958. doi: 10.1007/978-3-540-75757-3_115

Taoka, T., Ito, R., Nakamichi, R., Kamagata, K., Sakai, M., Kawai, H., et al. (2021). Reproducibility of diffusion tensor image analysis along the perivascular space (DTI-ALPS) for evaluating interstitial fluid diffusivity and glymphatic function: CHanges in Alps index on Multiple conditiON acquIsition eXperiment (CHAMONIX) study. *Jpn J Radiol.* doi: 10.1007/s11604-021-01187-5 [Epub Online ahead of print].

Taoka, T., Masutani, Y., Kawai, H., Nakane, T., Matsuoka, K., Yasuno, F., et al. (2017). Evaluation of glymphatic system activity with the diffusion MR technique: diffusion tensor image analysis along the perivascular space (DTI-ALPS) in Alzheimer's disease cases. *Jpn. J. Radiol.* 35, 172–178. doi: 10.1007/s11604-017-0617-z

Toh, C. H., and Castillo, M. (2021). Peritumoral brain edema volume in meningioma correlates with tumor fractional anisotropy but not apparent diffusion coefficient or cerebral blood volume. *Neuroradiology* 63, 1263–1270. doi: 10.1007/s00234-021-02646-6

Toh, C. H., and Siow, T. Y. (2021). Factors associated with dysfunction of glymphatic system in patients with glioma. *Front. Oncol.* 11:744318. doi: 10.3389/fonc.2021.744318

Toh, C. H., Siow, T. Y., and Castillo, M. (2021). Peritumoral brain edema in meningiomas may be related to glymphatic dysfunction. *Front. Neurosci.* 15:674898. doi: 10.3389/fnins.2021.674898

Vogt, G., Laage, R., Shuaib, A., and Schneider, A. (2012). Initial lesion volume is an independent predictor of clinical stroke outcome at day 90: an analysis of the Virtual International Stroke Trials Archive (VISTA) database. *Stroke* 43, 1266–1272. doi: 10.1161/strokeaha.111.646570

Watts, R., Steinklein, J. M., Waldman, L., Zhou, X., and Filippi, C. G. (2019). Measuring glymphatic flow in man using quantitative contrast-enhanced MRI. *AJNR Am. J. Neuroradiol.* 40, 648–651. doi: 10.3174/ajnr.A5931

Wu, C. H., Lirng, J. F., Ling, Y. H., Wang, Y. F., Wu, H. M., Fuh, J. L., et al. (2021). Noninvasive characterization of human glymphatics and meningeal lymphatics in an in vivo model of blood-brain barrier leakage. *Ann. Neurol.* 89, 111–124. doi: 10.1002/ana.25928

Yang, C., Liu, Z., Li, H., Zhai, F., Liu, J., and Bian, J. (2015). Aquaporin-4 knockdown ameliorates hypoxic-ischemic cerebral edema in newborn piglets. *IUBMB Life* 67, 182–190. doi: 10.1002/iub.1356

Yang, G., Deng, N., Liu, Y., Gu, Y., and Yao, X. (2020). Evaluation of glymphatic system using diffusion MR technique in T2DM Cases. *Front. Hum. Neurosci.* 14:300. doi: 10.3389/fnhum.2020.00300

Yokota, H., Vijayasarathi, A., Cekic, M., Hirata, Y., Linetsky, M., Ho, M., et al. (2019). Diagnostic performance of glymphatic system evaluation using diffusion tensor imaging in idiopathic normal pressure hydrocephalus and mimickers. *Curr. Gerontol. Geriatr. Res.* 2019:5675014. doi: 10.1155/2019/5675014

Zbesko, J. C., Nguyen, T. V., Yang, T., Frye, J. B., Hussain, O., Hayes, M., et al. (2018). Glial scars are permeable to the neurotoxic environment of chronic stroke infarcts. *Neurobiol. Dis.* 112, 63–78. doi: 10.1016/j.nbd.2018.01.007

Zhao, Y., Gu, J. H., Dai, C. L., Liu, Q., Iqbal, K., Liu, F., et al. (2014). Chronic cerebral hypoperfusion causes decrease of O-GlcNAcylation, hyperphosphorylation of tau and behavioral deficits in mice. *Front. Aging Neurosci.* 6:10. doi: 10.3389/fnagi.2014.00010

Zhou, W., Shen, B., Shen, W. Q., Chen, H., Zheng, Y. F., and Fei, J. J. (2020). Dysfunction of the Glymphatic System Might Be Related to Iron Deposition in the Normal Aging Brain. *Front. Aging Neurosci.* 12:559603. doi: 10.3389/fnagi.2020.559603

Zhou, Y., Cai, J., Zhang, W., Gong, X., Yan, S., Zhang, K., et al. (2020). Impairment of the glymphatic pathway and putative meningeal lymphatic vessels in the aging human. *Ann. Neurol.* 87, 357–369. doi: 10.1002/ana.25670

Conflict of Interest: The authors declare that the research was conducted in the absence of any commercial or financial relationships that could be construed as a potential conflict of interest.

Publisher's Note: All claims expressed in this article are solely those of the authors and do not necessarily represent those of their affiliated organizations, or those of the publisher, the editors and the reviewers. Any product that may be evaluated in this article, or claim that may be made by its manufacturer, is not guaranteed or endorsed by the publisher.

frontiers in Aging Neuroscience

ORIGINAL RESEARCH
published: 30 November 2021
doi: 10.3389/fnagi.2021.758562

Leisure Activity Variety and Brain Volume Among Community-Dwelling Older Adults: Analysis of the Neuron to Environmental Impact Across Generations Study Data

Ai Iizuka[1], Hiroshi Murayama[1], Masaki Machida[2], Shiho Amagasa[2], Shigeru Inoue[2], Takeo Fujiwara[3] and Yugo Shobugawa[4]*

[1] Research Team for Social Participation and Community Health, Tokyo Metropolitan Institute of Gerontology, Tokyo, Japan, [2] Department of Preventive Medicine and Public Health, Tokyo Medical University, Tokyo, Japan, [3] Department of Global Health Promotion, Tokyo Medical and Dental University, Tokyo, Japan, [4] Department of Active Ageing, Niigata University Graduate School of Medical and Dental Sciences, Niigata, Japan

OPEN ACCESS

Edited by:
Chu-Chung Huang,
East China Normal University, China

Reviewed by:
Lindsay S. Nagamatsu,
Western University, Canada
Akira Monji,
Saga University, Japan
Lei Yu,
Rush Alzheimer's Disease Center, United States

****Correspondence:***
Hiroshi Murayama
murayama@tmig.or.jp

Received: *14 August 2021*
Accepted: *04 November 2021*
Published: *30 November 2021*

Citation:
Iizuka A, Murayama H, Machida M, Amagasa S, Inoue S, Fujiwara T and Shobugawa Y (2021) Leisure Activity Variety and Brain Volume Among Community-Dwelling Older Adults: Analysis of the Neuron to Environmental Impact Across Generations Study Data. Front. Aging Neurosci. 13:758562. doi: 10.3389/fnagi.2021.758562

Background: Recent findings indicate that leisure activity (LA) delays cognitive decline and reduces the risk of dementia. However, the association between LA and brain volume remains unclear. This study aimed to examine the association between LA variety and brain volume with a focus on the hippocampus and gray matter.

Methods: Data were obtained from the baseline survey of the Neuron to Environmental Impact across Generations study, which had targeted community-dwelling older adults living in Niigata, Japan. We divided LAs into 10 categories, and counted the number of categories of activities in which the participants engaged. We classified them as follows: 0 (i.e., no activity), 1, 2, or $\geq$ 3 types. Brain volume was assessed through magnetic resonance imaging, and hippocampal and gray matter volumes were ascertained.

Results: The sample size was 482. Multiple linear regression analysis showed that hippocampal and gray matter volumes were significantly greater among participants with $\geq$ 3 types of LAs than among their no-activity counterparts. Hippocampal volume was significantly greater among those who engaged in one type of LA than among those who engaged in no such activity. Sex-stratified analysis revealed that hippocampal volumes were significantly greater among males who engaged in $\geq$ 3 types of LAs and one type of LA. However, no such association was found among females.

Conclusion: The present findings suggest that engaging in a wide range of LAs is related to hippocampal and gray matter volumes. Furthermore, there was a sex difference in the association between LA variety and brain volume.

Keywords: brain reserve, brain volume, hippocampus, gray matter, leisure activity, magnetic resonance imaging, older people

INTRODUCTION

Non-pharmacological approaches are expected to delay cognitive decline and reduce the risk of dementia. Leisure activity (LA), which refers to activities that "individuals engage in for enjoyment or well-being that are independent of activities of daily living" (Leung et al., 2011) is one of the methods included in non-pharmacological approaches. Previous studies have reported that engaging in LA in later life maintains cognitive function and reduces the risk of dementia (Verghese et al., 2003, 2006; Fallahpour et al., 2016; Yates et al., 2016). The underlying mechanism is considered to be related to the accumulation of cognitive reserves (Stern, 2002, 2009, 2012).

There is another concept called brain reserve, which explains why individuals differ in their susceptibility to cognitive aging and the conditions associated with Alzheimer's disease (Fratiglioni and Wang, 2007; Valenzuela, 2008; Stern, 2012). Brain volume, which is a typical index of brain reserve, is regarded as a correlate of cognitive function and the risk of dementia (Katzman et al., 1988; Fratiglioni and Wang, 2007; Valenzuela, 2008; Stern, 2012). Several studies have shown that larger hippocampal and gray matter volumes are associated with higher cognitive function and a lower risk of dementia (MacLullich et al., 2002; Fotenos et al., 2005; Brickman et al., 2007; Taki et al., 2011; Teipel et al., 2013; Vaughan et al., 2014; Hilal et al., 2015). However, the relationship between LA and brain volume has not been examined among older adults.

Engaging in a broad (rather than a narrow) range of LAs may strongly affect brain volume as it may lead to strong stimulation of the brain and enhance neuroplasticity. Several studies have found that engaging in a broader range of LAs lowers the risk of dementia (Leung et al., 2011; Kozono et al., 2016; Ling et al., 2020), and broader LA contents are associated with higher cognitive test scores (Ihle et al., 2015). Moreover, in Japan, it has been found that engaging in a broader range of LAs promotes stability, improves mental health (e.g., higher life satisfaction called ikigai) (Haraoka, 2004), increases resilience (Matsunaka et al., 2019), and reduces the risk of frailty (Fushiki et al., 2012). Thus, engaging in a broader range of LAs has a positive effect on health; therefore, we hypothesized that this may also hold true for brain volume.

Accordingly, we examined the association between LA variety and brain volume with a focus on the hippocampus and gray matter among community-dwelling older adults in Japan.

MATERIALS AND METHODS

Study Sample and Data Collection

Data were obtained from the baseline survey of the Neuron to Environmental Impact across Generations (NEIGE) study conducted in Tokamachi City, Niigata, Japan, in 2017. Tokamachi City is a rural area located approximately 180 km northwest of Tokyo. The population of the city was 51,964, and the proportion of older adults was 36.9% as of January 31, 2020. Of all those aged 65–84 years who were living in Tokamachi City, 1346 individuals who were not recipients of long-term care insurance and were not admitted to a hospital or nursing home were randomly selected from a resident registry. A total of 527 individuals, who agreed to participate in the NEIGE study, were enrolled in the survey. A detailed profile of this study (study concept, design, and sample) is elsewhere (Shobugawa et al., 2020).

Ethical Approval

The study protocol was approved by The University Ethics Committee (Niigata University and Tokyo Medical University; approval number: 2666 and 3921). We explained the purpose, methods, and ethical considerations of this study and obtained written informed consent from all participants based on the Declaration of Helsinki before enrolment.

Measures

Leisure Activity Variety

We developed original questions about LA. First, the participants responded with either "yes" or "no" to indicate whether they were currently engaged in LA. If the participant's response was "yes," they were further asked to indicate whether they engaged in any of the following 20 activities: grand golf, golf, pachinko (Typical Japanese gambling device resembling slot machine), gymnastics or tai chi, walking or jogging, computer use, reading books, playing board games, painting, fishing, karaoke, dancing, craftwork, calligraphy, tea ceremony or flower arrangement, crop work, gardening, photography, traveling, and others. These activities are regarded as popular LAs in Japan based on previous studies and literatures (Kozono et al., 2016; Iwasa and Yoshida, 2018; Japan Productivity Centre, 2019). Participants who chose the "Others" option were asked to specifically describe the activities in which they engaged. The information about LA was collected with a self-reported questionnaire.

After data were collected, we classified the items (including "Others" responses) into the following 10 categories of LAs: (1) physical activities (walking, jogging, gymnastics, tai chi, dancing, fishing, golf, ground golf, climbing, skiing, swimming, tennis, table tennis, volleyball, baseball, and cycling); (2) gaming (board games, crossword puzzles, and billiards); (3) traveling (traveling and driving); (4) creative activities (painting, craftwork, collecting stamps, and carpentry); (5) cultural activities (flower arrangement, tea ceremony, calligraphy, and poetry, including Japanese haiku, tanka, and shigin); (6) developmental activities (reading books, reading aloud, studying history, and attending public lectures); (7) agricultural activities (crop work and gardening); (8) singing (chorus and karaoke); (9) gambling (pachinko and stock investment); and (10) technology use (computer use and photography). We developed these categories based on a review of previous studies conducted in Japan (Kozono et al., 2016; Iwasa and Yoshida, 2018). Finally, we counted the number of categories of LAs reported by each participant, and divided them into quartiles [0 type (i.e., = no activity), 1 type, 2 types, or $\geq$ 3 types out of 10].

Brain Volume

Each participant underwent magnetic resonance imaging (MRI) at the Niigata Prefectural Tokamachi Hospital. We used a 1.5

Tesla scanner (MAGNETOM Avanto fit, Siemens, Germany) in three-dimensional mode with the following parameters: repetition time = 1,700 ms; echo time = 4.31 ms; inversion time = 800 ms; flip angle = 15°; slice thickness = 1.25 mm; field of view = 230 × 230; matrix size = 256 × 256; and number of slices = 144. Segmentation and volume calculations were undertaken using FreeSurfer Version 6.0[1].

For this procedure, we removed non-brain tissue (e.g., brain skull), normalized the voxel intensities, and labeled the volumes of each segmentation using FreeSurfer. Hippocampal volume, total gray matter volume, and intracranial volume were automatically derived and labeled. Hippocampal volume was separately determined for the left and right hemispheres, and the total volume of the left and right hippocampus (total hippocampal volume) was used in the analysis.

Covariates

Sociodemographic factors, health conditions, physical activity, and social interaction served as covariates. The information regarding the covariates was collected with a self-reported questionnaire and interviews conducted by trained staff. The assessed sociodemographic factors included age, sex, years of education ($\leq$ 9 years or $\geq$ 10 years), annual household income ($<$ 2.5 million yen, 2.5–3.9 million yen, 4.0–6.9 million yen, or $\geq$ 7.0 million yen), current occupational status (employed or unemployed).

The assessed health conditions included comorbidities and depressive mood. Information on comorbidities was obtained through interviews conducted by medical doctors or nurses. Hypertension, diabetes, cardiovascular disease, cerebrovascular disease, and neuropsychiatric disorders served as covariates. Depressive mood was assessed using the Japanese version of the Geriatric Depression Scale (GDS): Short Form (Sheikh and Yesavage, 1986; Sugishita and Asada, 2009). The GDS consisted of 15 items, and respondents answered dichotomous questions. The responses were summed; total scores can range from 0 to 15. The Cronbach's alpha of this scale was 0.77 in this study. We used a cut-off point of $\geq$ 6, which indicated a depressive mood (Sugishita and Asada, 2009).

Physical activity was assessed using an accelerometer, namely, the Active style Pro HJA-750C (Omron Healthcare, Kyoto, Japan). The participants were asked to wear the accelerometer over their waist on an elasticated belt for seven consecutive days while awake, and average daily amount of moderate-to-vigorous (i.e., $\geq$ 3.0 metabolic equivalents) physical activity served as covariates. Participants who did not have valid data for more than 4 days were excluded. A more detailed description of the accelerometer is available elsewhere (Oshima et al., 2010; Ohkawara et al., 2011; Park et al., 2017).

Social interaction was assessed based on the frequency of meeting friends and acquaintances. The frequency of meeting friends and acquaintances was enquired with a question comprising six categories ($\geq$ 4 days/week, 2–3 days/week, 1 day/week, 1–3 days/month, several times/year, and none). We divided the participants based on this frequency into two groups: $<$ 1 day/week and $\geq$ 1 day/week.

In addition to these covariates, we assessed the participants' cognitive status using the Mini-Mental State Examination-Japanese version (MMSE-J) (Sugishita et al., 2016). The MMSE-J consists of 11 questions, and total scores can range from 0 to 30. We used the MMSE-J scores to examine participant characteristics, but this variable was not included in the regression model.

Statistical Analysis

Participant's characteristics by categories of LAs were compared using one-way analysis of variance for continuous variables and chi-square test for categorical variables.

We conducted multiple linear regression analysis to examine the association between LA variety and brain volume. We separately entered hippocampal and gray matter volumes as dependent variables; the different categories of LAs (divided into quartiles) served as the independent variable. The LA categories were entered into the regression models as dummy variables, and the no-activity group (i.e., 0 types) served as the reference. Model 1 was adjusted for age, sex, and years of education, which are generally included as covariates in studies on LA, and intracranial volume. Model 2 was additionally adjusted for annual household income, occupational status, comorbidities, GDS score, physical activity, and social interaction which are potential confounding factors. Further, to examine sex differences, the data were stratified by sex, and the analysis was separately conducted for males and females.

For reference, we conducted the following two analyses: (1) stratification by left and right hippocampus as some studies indicated differential effect of health behaviors on brain volume by the brain side (Firth et al., 2018; Machida et al., 2021; Vujic et al., 2021) and (2) adding an interaction term between LA variety and comorbidities/mental health on brain volume to consider the possibility that the relationship between LA variety and brain volume varies by disease and mental health condition because chronic disease and mental health can be possible confounders (Campbell et al., 2004; Firbank et al., 2007; Callisaya et al., 2019).

The associations were examined by computing regression coefficients (b) and 95% confidence intervals (CIs). All analyses were conducted using IBM Statistical Package for the Social Sciences version 23 (IBM Inc., Chicago, IL, United States).

RESULTS

Of the 527 participants, we excluded 27 individuals whose MRI data were not of sufficient quality and 18 others with missing data for any of the covariates. Thus, the data of 482 participants were analyzed.

Participant characteristics are presented in **Table 1**. Their average age was 73.2 years (standard deviation = 5.4), and 47.3% of them were males. With regard to years of education, 37.1% had received less than 9 years of education. Approximately half of the participants had hypertension (52.9%), and 18.0% of them

[1]http://surfer.nmr.mgh.harvard.edu

TABLE 1 | Participant characteristics ($N = 482$).

Variable	Category	Mean (SD)	*n*	%
Age (years)		73.2 (5.4)		
Sex	Males		228	47.3
	Females		254	52.7
Years of education	≤9		179	37.1
	≥10		303	62.9
Annual household income (million yen)	<2.5		135	28.0
	2.5–3.9		127	26.3
	4.0–6.9		122	25.3
	≥7.0		98	20.3
Current occupational status	Employed		201	41.7
	Unemployed		281	58.3
Comorbidities				
Hypertension	Having		255	52.9
	Not having		227	47.1
Diabetes	Having		87	18.0
	Not having		395	82.0
Cardiovascular disease	Having		93	19.3
	Not having		389	80.7
Cerebrovascular disease	Having		35	7.3
	Not having		447	92.7
Neuropsychiatric disorder	Having		21	4.4
	Not having		461	95.6
GDS score	≤5		404	83.8
	≥ 6		78	18.0
Physical activity[a] (METs-hours per day)		3.0 (2.3)		
MMSE-J score		27.1 (2.5)		
Social interaction	<1 day/week		202	41.9
	≥1 day/week		280	58.1
Leisure activity variety (type)[b]	0		73	15.1
	1		121	25.1
	2		127	26.3
	≥3		161	33.4
Brain volume (mm^3)				
Intracranial volume		1433189.2 (152127.6)		
Total hippocampal volume		7213.2 (775.7)		
Gray matter volume		569911.0 (46847.1)		

GDS, Japanese version of the Geriatric Depression Scale: Short Form; METs, Metabolic equivalents; MMSE-J, Mini-Mental State Examination-Japanese version; SD, standard deviation.
[a] *Level of physical activity ≥ 3.0 METs.*
[b] *Number of categories of leisure activities.*

obtained scores ≥ 6 on the GDS. The average MMSE-J score was 27.1 (standard deviation = 2.5), and three participants reported that they had been diagnosed with dementia. The percentages of individuals with 0, 1, 2, and ≥ 3 types of LAs were 15.1, 25.1, 26.3, and 33.4%, respectively.

Table 2 shows a comparison between the participant's characteristics. There were significant differences among years of education, number of participants who had neuropsychiatric disorder, GDS score, MMSE-J score, and social interaction between categories of LAs (all $p < 0.05$).

Table 3 presents the association between LA variety and brain volume. Participants with ≥ 3 types of LAs had significantly greater total hippocampal and gray matter volumes than their no-activity counterparts, when age, sex, and years of education were controlled for in Model 1 (b [95% CI] = 217.3 [46.3–388.4] for total hippocampal volume and 7954.6 [1197.0–14712.1] for total gray matter volume). This association remained significant even after the model was additionally adjusted for sociodemographic factors, health conditions, physical activity, and social interaction (Model 2; 216.8 [39.1–394.5] for total hippocampal volume, and 7466.4 [490.3–14442.5] for total gray matter volume).

Further, participants who engaged in one type of LA had greater total hippocampal volumes than their no-activity counterparts in both Models 1 (213.5 [34.3–392.8]) and 2 (205.9 [23.8–388.1]).

We separately conducted multiple regression analysis using data collected from males and females (**Table 4**). There were sex differences in the emergent associations. Males who engaged in ≥ 3 types of LAs and one type of LA had greater total hippocampal volume in Models 1 (≥ 3 types: 329.3 [61.3–597.4]; one type: 352.4 [57.1–647.7]) and 2 (≥ 3 types: 319.0 [38.3–599.8]; one type: 320.6 [12.8–628.4]). However, there were no significant associations among females. In addition, stratified analysis revealed that there was no significant association between LA variety and total gray matter volume among either males or females.

For reference, the results of a separate analysis conducted for the left and right hippocampal volumes are present in **Supplementary Material A**. Participants with ≥ 3 types of LAs had a significantly greater right and left hippocampal volumes than their no-activity counterparts. The participants engaged in one LA type had an enlarged hippocampal volume only on the left side. In addition, the interaction of diabetes × LA variety was robust (**Supplementary Material B**), and the association between LA variety and brain volume was stronger in participants with diabetes.

These results did not change significantly when we excluded the three participants who had been diagnosed with dementia (mean age = 69 years; two males and one female) from the analysis due to concerns about recall bias (**Supplementary Materials C, D**).

DISCUSSION

This study examined the association between LA variety and brain volume, with a focus on the hippocampus and gray matter, among community-dwelling Japanese older adults. The results showed that hippocampal and gray matter volumes were significantly greater among those who engaged in ≥ 3 types of LAs than those who engaged in no such activity. Moreover, total hippocampal volumes were greater among those who engaged

TABLE 2 | The comparison of the participant's characteristics by categories of leisure activity ($N = 482$).

Variable		Leisure activity variety				p^a
		0 type	1 type	2 types	≥ 3 types	
Age (years)	Mean (SD)	72.6 (5.4)	73.9 (6.0)	73.7 (5.5)	72.6 (5.0)	0.126
Sex (males)	%	43.8	39.6	50.3	52.1	0.158
Years of education (≤ 9 years)	%	46.5	43.8	33.0	31.0	0.036
Annual household income (< 2.5 million yen)	%	26.0	30.5	26.7	27.9	0.912
Current occupational status (Employed)	%	35.6	42.1	39.3	45.9	0.456
Comorbidities (Having)						
Hypertension	%	53.4	53.7	45.6	57.7	0.237
Diabetes	%	17.8	23.1	13.3	18.0	0.262
Cardiovascular disease	%	15.0	19.0	22.0	19.2	0.691
Cerebrovascular disease	%	5.4	6.6	4.7	10.5	0.237
Neuropsychiatric disorder	%	6.8	3.3	7.8	1.2	0.030
GDS score (≥ 6)	%	28.7	18.1	18.8	6.8	<0.001
Physical activity (METs-hours per day)	Mean (SD)	3.2 (2.2)	3.1 (2.8)	2.6 (2.0)	3.2 (2.1)	0.134
Social interaction (≥ 1 day/week)	%	53.4	52.8	53.5	67.7	0.027
MMSE-J score	Mean (SD)	26.3 (3.0)	27.0 (2.3)	27.0 (2.6)	27.4 (2.2)	0.012
Brain volume						
Total hippocampal volume (mm^3)	Mean (SD)	7054.1 (806.9)	7187.1 (832.7)	7203.6 (726.2)	7312.5 (747.4)	0.118
Gray matter volume (mm^3)	Mean (SD)	563118.5 (47214.4)	562766.8 (46939.9)	574726.9 (41974.8)	574561.3 (49544.9)	0.063

GDS, Japanese version of the Geriatric Depression Scale short-form; MMSE-J, Mini-Mental State Examination, Japanese version; SD, Standard deviation.
[a]p-values indicate the results of one-way analysis of variance for continuous variables and chi-square test for categorical variables.

TABLE 3 | Association between leisure activity variety and brain volume: Results of multiple regression analysis.

Model	Leisure activity variety	Total hippocampal volume		Gray matter volume	
		b	95% CI	b	95% CI
Model 1	0 type	Ref.		Ref.	
	1 type	213.5	(34.3, 392.8)	3431.5	(−3649.7, 10512.8)
	2 types	86.2	(−92.8, 265.2)	1176.9	(−5897.9, 8251.8)
	≥ 3 types	217.3	(46.3, 388.4)	7954.6	(1197.0, 14712.1)
		p for trend = 0.085		p for trend = 0.027	
Model 2	0 type	Ref.		Ref.	
	1 type	205.9	(23.8, 388.1)	3321.0	(−3830.5, 10472.7)
	2 types	83.2	(−98.5, 264.9)	259.7	(−6876.4, 7396.0)
	≥ 3 types	216.8	(39.1, 394.5)	7466.4	(490.3, 14442.5)
		p for trend = 0.100		p for trend = 0.057	

CI, confidential interval; Ref., reference.
Model 1: adjusted for age, sex, years of education, and intracranial volume.
Model 2: additionally adjusted for current occupational status, annual household income, comorbidities (hypertension, diabetes, cardiovascular disease, cerebrovascular disease, and neuropsychiatric disorder), the Japanese version of the Geriatric Depression Scale: Short Form, physical activity, and social interaction.

in one type of LA than among those who engaged in no such activity. Furthermore, there was a sex difference in the association between LA variety and brain volume, which was more pronounced among males than among females.

Total hippocampal and gray matter volumes are associated with the risk of dementia (Du et al., 2001; Grundman et al., 2002; Cardenas et al., 2003; Taki et al., 2011; Teipel et al., 2013; Hilal et al., 2015). In this study, those who engaged in ≥ 3 types of LAs had significantly greater hippocampal and gray matter volumes than those who engaged in no such activity. Previous studies have reported that total hippocampal volume atrophies by approximately 0.98–1.12% annually and that total gray matter volume atrophies by approximately 0.30% because of natural aging (Taki et al., 2011; Fraser et al., 2015). In this study, those who engaged in ≥ 3 types of LAs had approximately 3.0% greater total hippocampal volume (217 mm^3/7213 mm^3) and approximately 1.3% greater total gray matter volume (7954 mm^3/569911 mm^3) than their no-activity counterparts. This indicates that there is a difference in the brain volume equivalent to 3–4 years of atrophy in those who engage in ≥ 3 types of LAs than those who engage in no such activity. According to the evidence for the basic biological consequences

TABLE 4 | Association between leisure activity variety and brain volume by sex.

Model	Leisure activity variety	Total hippocampal volume		Gray matter volume	
		b	95% CI	b	95% CI
Males					
Model 1	0 type	Ref.		Ref.	
	1 type	352.4	(57.1, 647.7)	4840.1	(−6749.6, 16426.9)
	2 types	279.9	(−3.2, 563.1)	3360.1	(−7750.5, 14470.7)
	≥ 3 types	329.3	(61.3, 597.4)	9575.7	(−942.0, 20093.6)
			p for trend = 0.083		*p* for trend = 0.077
Model 2	0 type	Ref.		Ref.	
	1 type	320.6	(12.8, 628.4)	5790.4	(−6236.4, 17817.3)
	2 types	266.8	(−28.0, 561.8)	1728.9	(−9795.8, 13253.7)
	≥ 3 types	319.0	(38.3, 599.8)	8438.9	(−2530.3, 19408.1)
			p for trend = 0.090		*p* for trend = 0.191
Females					
Model 1	0 type	Ref.		Ref.	
	1 type	117.8	(-105.9, 341.5)	2338.1	(−6667.8, 11344.0)
	2 types	−63.0	(-292.6, 166.6)	−395.7	(−9640.1, 8848.5)
	≥ 3 types	139.6	(-82.1, 361.4)	6533.1	(−2395.8, 15462.1)
			p for trend = 0.495		*p* for trend = 0.186
Model 2	0 type	Ref.		Ref.	
	1 type	101.1	(−126.4, 328.6)	1619.7	(−7482.0, 10721.5)
	2 types	−55.5	(−288.5, 177.4)	−963.9	(−10285.8, 8357.9)
	≥ 3 types	109.8	(−122.7, 342.5)	5656.3	(−3652.1, 14964.8)
			p for trend = 0.692		*p* for trend = 0.287

CI, confidential interval; Ref., reference.
Model 1: adjusted for age, sex, years of education, and intracranial volume.
Model 2: additionally adjusted for annual household income, current occupational status, comorbidities (hypertension, diabetes, cardiovascular disease, cerebrovascular disease, and neuropsychiatric disorder), the Japanese version of the Geriatric Depression Scale: Short Form, physical activity, and social interaction.

of environmental enrichment, more complex and stimulating environments induce neural and synaptic structural changes, such as dendritic arborization and synaptogenesis (West and Greenough, 1972; Kempermann et al., 1997; Nithianantharajah and Hannan, 2006), and this principle can be extended to human life itself (Queen et al., 2020). As a mechanism to promote synaptogenesis, an enriched environment increases brain-derived neurotrophic factor (BDNF) and binds it to receptors (TrkB) in the hippocampus and cerebral cortex, resulting in long-term potentiation and promoting neurogenesis (Kempermann et al., 2002; Rossi et al., 2006). It is regarded as a phenomenon that applies to humans as well, since previous studies have shown that exercise, certain types of games, and social activities increase BDNF and maintain the hippocampal volume and gray matter volume (Erickson et al., 2011; Carlson et al., 2015; Lin et al., 2015). Engagement in a wide range of LAs involves exposure to more stimulating and complex environments; in this regard, the present findings can be considered logically reasonable.

There was a similar association between LA variety and hippocampal volumes in males; however, it was not significant among females. In Japan, older females tend to have strong social relationships and actively engage not only in LAs but also other activities such as socializing with neighbors and friends and housework than older males (Hatanaka and Tanaka, 1999; Hirai et al., 2005). Therefore, LA may have had a relatively small effect and may not have been associated with brain volume among females.

There were no significant differences in the brain volumes of participants who engaged in 2 types of LAs and their no-activity counterparts. However, participants who engaged in one type of LA had greater total hippocampal volumes than those who engaged in no such activity. This was an unexpected finding as it was unlikely to be a matter of statistical power, such as sample size. In an intervention study involving cognitive activities, it was found that focusing on one type of intervention (photography) rather than a combination of 2 types of interventions (photography and craftwork) was more effective in improving episodic memory (Park et al., 2014). Those who participated in only one type of intervention may have focused on their activities more keenly, and this may have had a greater effect on episodic memory than participation in 2 types of intervention. Similarly, even in this study, those who engaged in one type of LA may have done so more intensively than those who engaged in 2 types of LAs; this may have affected their hippocampal volume. Conversely, people who engaged in ≥ 3 types of LAs may show a greater effect on the total hippocampal and gray matter volumes as they have engaged in LAs more intensively or frequently and have received more stimulation than those who engaged in 1 or 2 types of LAs. However, it is not possible to reach a complete conclusion. It is also possible that there is a sample bias, such as the presence of some special characteristics in those who engaged in 2 types of LAs. Therefore, further examination is required to reveal the mechanisms in the future.

This study yielded novel findings about the association between LA variety and brain volume; however, this study also has some limitations. First, we did not assess LAs in great detail. Indeed, the effect of LA on brain volume may differ depending on LA frequency, intensity, location, and group members. Such information should be collected in future studies. In addition, although we focused on LA variety and classified LAs into 10 categories on the basis of the types of LA, there is diversity even within the same type of LA when examined in detail. Therefore, not only the LA variety but also the number of LAs is important. We intend to investigate the relationship between the number of each LA and brain volume in a future study. Second, this study was conducted in a rural area; therefore, care should be taken while generalizing the findings. Third, the fact that the association between LA and hippocampal volume was different in the left and right sides, and the association was stronger in people with diabetes needs to be investigated in future studies. Finally, because this study adopted a cross-sectional design, we could not determine if LA variety results in greater brain volume or if people with greater brain volumes engage in a broader range of LAs. Therefore, future studies should examine the association between LA and brain volume longitudinally.

CONCLUSION

The present findings suggest that engaging in a wide range of LAs is related to greater total hippocampal and gray matter volumes among community-dwelling older adults. Moreover, there was a sex difference in the association between LA variety and brain volume. Further research is needed to longitudinally examine the causal relationship between LA variety and brain volume.

DATA AVAILABILITY STATEMENT

The raw data supporting the conclusions of this article will be made available by the authors, without undue reservation.

ETHICS STATEMENT

The studies involving human participants were reviewed and approved by the Niigata University and Tokyo Medical University. The patients/participants provided their written informed consent to participate in this study.

AUTHOR CONTRIBUTIONS

AI and HM: conceptualization, formal analysis, and methodology. MM, SA, SI, TF, and YS: data curation and project administration. HM, MM, SA, SI, TF, and YS: investigation. YS: supervision. AI and YS: writing–original draft. All authors have read and approved the published version of the manuscript.

FUNDING

This work was supported by a grant from the Policy Research Institute, Ministry of Agriculture, Forestry and Fisheries, the Pfizer Health Research Foundation, and JSPS KAKENHI (16H03249, 17K19794, 18K10829, 19H03910, and 20K19580).

ACKNOWLEDGMENTS

We sincerely express our gratitude to all participants and collaborators of NEIGE study.

SUPPLEMENTARY MATERIAL

The Supplementary Material for this article can be found online at: https://www.frontiersin.org/articles/10.3389/fnagi.2021.758562/full#supplementary-material

REFERENCES

Brickman, A. M., Habeck, C., Zarahn, E., Flynn, J., and Stern, Y. (2007). Structural MRI covariance patterns associated with normal aging and neuropsychological functioning. *Neurobiol. Aging* 28, 284–295. doi: 10.1016/j.neurobiolaging.2005.12.016

Callisaya, M. L., Beare, R., Moran, C., Phan, T., Wang, W., and Srikanth, V. K. (2019). Type 2 diabetes mellitus, brain atrophy and cognitive decline in older people: a longitudinal study. *Diabetologia* 62, 448–458. doi: 10.1007/s00125-018-4778-9

Campbell, S., Marriott, M., Nahmias, C., and MacQueen, G. M. (2004). Lower hippocampal volume in patients suffering from depression: a meta-analysis. *Am. J. Psychiatry* 161, 598–607. doi: 10.1176/appi.ajp.161.4.598

Cardenas, V. A., Du, A. T., Hardin, D., Ezekiel, F., Weber, P., Jagust, W. J., et al. (2003). Comparison of methods for measuring longitudinal brain change in cognitive impairment and dementia. *Neurobiol. Aging* 24, 537–544. doi: 10.1016/S0197-4580(02)00130-6

Carlson, M. C., Kuo, J. H., Chuang, Y. F., Varma, V. R., Harris, G., Albert, M. S., et al. (2015). Impact of the baltimore experience corps trial on cortical and hippocampal volumes. *Alzheimers Dement.* 11, 1340–1348. doi: 10.1016/j.jalz.2014.12.005

Du, A. T., Schuff, N., Amend, D., Laakso, M. P., Hsu, Y. Y., Jagust, W. J., et al. (2001). Magnetic resonance imaging of the entorhinal cortex and hippocampus in mild cognitive impairment and Alzheimer's disease. *J. Neurol. Neurosurg. Psychiatry* 71, 441–447. doi: 10.1136/jnnp.71.4.441

Erickson, K. I., Voss, M. W., Prakash, R. S., Basak, C., Szabo, A., Chaddock, L., et al. (2011). Exercise training increases size of hippocampus and improves memory. *Proc. Natl. Acad. Sci. U.S.A.* 108, 3017–3022. doi: 10.1073/pnas.1015950108

Fallahpour, M., Borell, L., Luborsky, M., and Nygård, L. (2016). Leisure-activity participation to prevent later-life cognitive decline: a systematic review. *Scand. J. Occup. Ther.* 23, 162–197. doi: 10.3109/11038128.2015.1102320

Firbank, M. J., Wiseman, R. M., Burton, E. J., Saxby, B. K., O'Brien, J. T., and Ford, G. A. (2007). Brain atrophy and white matter hyperintensity change in older adults and relationship to blood pressure. Brain atrophy, WMH change and blood pressure. *J. Neurol.* 254, 713–721. doi: 10.1007/s00415-006-0238-4

Firth, J., Stubbs, B., Vancampfort, D., Schuch, F., Lagopoulos, J., Rosenbaum, S., et al. (2018). Effect of aerobic exercise on hippocampal volume in humans: a systematic review and meta-analysis. *Neuroimage* 166, 230–238. doi: 10.1016/j.neuroimage.2017.11.007

Fotenos, A. F., Snyder, A. Z., Girton, L. E., Morris, J. C., and Buckner, R. L. (2005). Normative estimates of cross-sectional and longitudinal brain volume decline in aging and AD. *Neurology* 64, 1032–1039. doi: 10.1212/01.WNL.0000154530.72969.11

Fraser, M. A., Shaw, M. E., and Cherbuin, N. (2015). A systematic review and meta-analysis of longitudinal hippocampal atrophy in healthy human ageing. *Neuroimage* 15, 364–374. doi: 10.1016/j.neuroimage.2015.03.035

Fratiglioni, L., and Wang, H. X. (2007). Brain reserve hypothesis in dementia. *J. Alzheimers Dis.* 12, 11–22. doi: 10.3233/JAD-2007-12103

Fushiki, Y., Ohnishi, H., Sakauchi, F., Oura, A., and Mori, M. (2012). Relationship of hobby activities with mortality and frailty among community-dwelling elderly adults: results of a follow-up study in Japan. *J. Epidemiol.* 22, 340–347. doi: 10.2188/jea.JE20110057

Grundman, M., Sencakova, D., Jack, C. R. Jr., Petersen, R. C., Kim, H. T., Schultz, A., et al. (2002). Brain MRI hippocampal volume and prediction of clinical status in a mild cognitive impairment trial. *J. Mol. Neurosci.* 19, 23–27. doi: 10.1007/s12031-002-0006-6

Haraoka, K. (2004). [Relation between prevention of intellectual decrease and way of life on senior citizens –From the investigation results in fiscal year 2002- (in Japanese)]. *Psychol. Res.* 3, 33–60. doi: 10.11477/mf.1662902025

Hatanaka, Y., and Tanaka, H. (1999). [Chiiki Hitori Gurashi Koureisya no tojikomori no jittai to seikatujoukyou (in Japanese)]. *Hokenfuzasshi* 55, 664–669.

Hilal, S., Amin, S. M., Venketasubramanian, N., Niessen, W. J., Vrooman, H., Wong, T. Y., et al. (2015). Subcortical atrophy in cognitive impairment and dementia. *J. Alzheimers Dis.* 48, 813–823. doi: 10.3233/JAD-150473

Hirai, H., Kondo, K., and Yukida, Y. (2005). [Koureisya no tojikomori (in Japanese)]. *Kosyueisei* 69, 485–489. doi: 10.11477/mf.1401100110

Ihle, A., Oris, M., Fagot, D., Baeriswyl, M., Guichard, E., and Kliegel, M. (2015). The association of leisure activities in middle adulthood with cognitive performance in old age: the moderating role of educational level. *Gerontology* 61, 543–550. doi: 10.1037/pne0000146

Iwasa, H., and Yoshida, Y. (2018). Actual conditions of leisure activity among older community-dwelling japanese adults. *Gerontol. Geriatr. Med.* 13:2333721418781677.

Japan Productivity Centre (2019). *[Leisure Hakusyo 2019 (in Japanese)]*. Tokyo: Japan Productivity Centre.

Katzman, R., Terry, R., DeTeresa, R., Brown, T., Davies, P., Fuld, P., et al. (1988). Clinical, pathological, and neurochemical changes in dementia: a subgroup with preserved mental status and numerous neocortical plaques. *Ann. Neurol.* 23, 138–144. doi: 10.1002/ana.410230206

Kempermann, G., Gast, D., and Gage, F. H. (2002). Neuroplasticity in old age: sustained fivefold induction of hippocampal neurogenesis by long-term environmental enrichment. *Ann. Neurol.* 52, 135–143. doi: 10.1002/ana.10262

Kempermann, G., Kuhn, H., and Gage, F. (1997). More hippocampal neurons in adult mice living in an enriched environment. *Nature* 386, 493–495. doi: 10.1038/386493a0

Kozono, M., Gondo, Y., Ogawa, M., Ishioka, Y. L., Masui, Y., Nakagawa, T., et al. (2016). [The relationship between leisure activities and cognitive function in community dwelling older adults (in Japanese)]. *Japanese J. Gerontol.* 38, 32–44. doi: 10.34393/rousha.38.1_32

Leung, G. T., Leung, K. F., and Lam, L. C. (2011). Classification of late-life leisure activities among elderly Chinese in Hong Kong. *East Asian Arch. Psychiatry* 21, 123–127.

Lin, Q., Cao, Y., and Gao, J. (2015). The impacts of a GO-game (Chinese chess) intervention on Alzheimer disease in a Northeast Chinese population. *Front. Aging Neurosci.* 25:163. doi: 10.3389/fnagi.2015.00163

Ling, L., Tsuji, T., Nagamine, Y., Miyaguni, Y., and Kondo, K. (2020). [Types and number of hobbies and incidence of dementia among older adults: a six-year longitudinal study from the Japan Gerontological Evaluation Study (JAGES) (in Japanese)]. *Nihon Koshu Eisei Zasshi* 67, 800–810. doi: 10.11236/jph.67.11_800

Machida, M., Takamiya, T., Amagasa, S., Murayama, H., Fujiwara, T., Odagiri, Y., et al. (2021). Objectively measured intensity-specific physical activity and hippocampal volume among community-dwelling older adults. *J. Epidemiol.* [Epub ahead of print]. doi: 10.2188/jea.JE20200534

MacLullich, A. M., Ferguson, K. J., Deary, I. J., Seckl, J. R., Starr, J. M., and Wardlaw, J. M. (2002). Intracranial capacity and brain volumes are associated with cognition in healthy elderly men. *Neurology* 23, 169–174. doi: 10.1212/WNL.59.2.169

Matsunaka, K., Okawa, N., and Kuratsune, H. (2019). Relationship between leisure activities and resilience in school teachers. *J. Health Psychol. Res.* 31, 101–111. doi: 10.11560/jhpr.160330083

Nithianantharajah, J., and Hannan, A. J. (2006). Enriched environments, experience-dependent plasticity and disorders of the nervous system. *Nat. Rev. Neurosci.* 7, 697–709. doi: 10.1038/nrn1970

Ohkawara, K., Oshima, Y., Hikihara, Y., Ishikawa-Takata, K., and Tabata, I. (2011). Real-time estimation of daily physical activity intensity by a triaxial accelerometer and a gravity-removal classification algorithm. *Br. J. Nutr.* 105, 1681–1691. doi: 10.1017/S0007114510005441

Oshima, Y., Kawaguchi, K., Tanaka, S., Ohkawara, K., Hikihara, Y., Ishikawa-Takata, K., et al. (2010). Classifying household and locomotive activities using a triaxial accelerometer. *Gait Posture* 31, 370–374. doi: 10.1016/j.gaitpost.2010.01.005

Park, D. C., Lodi-Smith, J., Drew, L., Haber, S., Hebrank, A., Bischof, G. N., et al. (2014). The impact of sustained engagement on cognitive function in older adults: the Synapse Project. *Psychol. Sci.* 25, 103–112. doi: 10.1177/09567976134

Park, J., Ishikawa-Takata, K., Tanaka, S., Bessyo, K., Tanaka, S., and Kimura, T. (2017). Accuracy of estimating step counts and intensity using accelerometers in older people with or without assistive devices. *J. Aging Phys. Act.* 25, 41–50. doi: 10.1123/japa.2015-0201

Queen, N. J., Hassan, Q. N. II, and Cao, L. (2020). Improvements to healthspan through environmental enrichment and lifestyle interventions: where are we now? *Front. Neurosci.* 14:605. doi: 10.3389/fnins.2020.00605

Rossi, C., Angelucci, A., Costantin, L., Braschi, C., Mazzantini, M., Babbini, F., et al. (2006). Brain-derived neurotrophic factor (BDNF) is required for the enhancement of hippocampal neurogenesis following environmental enrichment. *Eur. J. Neurosci.* 24, 1850–1856. doi: 10.1111/j.1460-9568.2006.05059.x

Sheikh, J. I., and Yesavage, J. A. (1986). "Geriatric Depression Scale (GDS) Recent evidence and development of a shorter version," in *Clinical Gerontology : A Guide to Assessment and Intervention*, ed. T. L. Brink (New York, NY: The Haworth Press), 165–173. doi: 10.3109/09638288.2010.503835

Shobugawa, Y., Murayama, H., Fujiwara, T., and Inoue, S. (2020). Cohort profile of the NEIGE Study in Tokamachi City, Japan. *J. Epidemiol.* 7, 281–287. doi: 10.2188/jea.JE20190036

Stern, Y. (2002). What is cognitive reserve? Theory and research application of the reserve concept. *J. Int. Neuropsychol. Soc.* 8, 448–460. doi: 10.1017/S1355617702813248

Stern, Y. (2009). Cognitive reserve. *Neuropsychologia* 47, 2015–2028. doi: 10.1016/j.neuropsychologia.2009.03.004

Stern, Y. (2012). Cognitive reserve in ageing and Alzheimer's disease. *Lancet Neurol.* 11, 1006–1012. doi: 10.1016/S1474-4422(12)70191-6

Sugishita, M., and Asada, T. (2009). [Geriatric Depression Scale-Short Version Japanese, GDS-S-J No Sakusei ni tsuite (in Japanese)]. *Ninchi Shinkei Kagaku* 11, 87–90. doi: 10.11253/ninchishinkeikagaku.11.87

Sugishita, M., Hemmi, I., and Takeuchi, T. (2016). Reexamination of the validity and reliability of the Japanese version of the Mini-Mental State Examination (MMSE-J). *Jpn. J. Cogn. Neurosci.* 18, 168–183. doi: 10.11253/ninchishinkeikagaku.18.168

Taki, Y., Kinomura, S., Sato, K., Goto, R., Wu, K., Kawashima, R., et al. (2011). Correlation between baseline regional gray matter volume and global gray matter volume decline rate. *Neuroimage* 54:743749. doi: 10.1016/j.neuroimage.2010.09.071

Teipel, S. J., Grothe, M., Lista, S., Toschi, N., Garaci, F. G., and Hampel, H. (2013). Relevance of magnetic resonance imaging for early detection and diagnosis of Alzheimer disease. *Med. Clin. North Am.* 97, 399–424. doi: 10.1016/j.mcna.2012.12.013

Valenzuela, M. J. (2008). Brain reserve and the prevention of dementia. *Curr. Opin. Psychiatry* 21, 296–302. doi: 10.1097/YCO.0b013e3282f97b1f

Vaughan, L., Erickson, K. I., Espeland, M. A., Smith, J. C., Tindle, H. A., and Rapp, S. R. (2014). Concurrent and longitudinal relationships between

cognitive activity, cognitive performance, and brain volume in older adult women. *J. Gerontol. B Psychol. Sci. Soc. Sci.* 69, 826–836. doi: 10.1093/geronb/gbu109

Verghese, J., LeValley, A., Derby, C., Kuslansky, G., Katz, M., Hall, C., et al. (2006). Leisure activities and the risk of amnestic mild cognitive impairment in the elderly. *Neurology* 66, 821–827. doi: 10.1212/01.wnl.0000202520.68987.48

Verghese, J., Lipton, R. B., Katz, M. J., Hall, C. B., Derby, C. A., Kuslansky, G., et al. (2003). Leisure activities and the risk of dementia in the elderly. *N. Engl. J. Med.* 348, 2508–2516. doi: 10.1056/NEJMoa022252

Vujic, A., Mowszowski, L., Meares, S., Duffy, S., Batchelor, J., and Naismith, S. L. (2021). Engagement in cognitively stimulating activities in individuals with Mild Cognitive Impairment: relationships with neuropsychological domains and hippocampal volume. *Neuropsychol. Dev. Cogn. B Aging Neuropsychol. Cogn.* 30, 1–22. doi: 10.1080/13825585.2021.1955822

West, R. W., and Greenough, W. T. (1972). Effect of environmental complexity on cortical synapses of rats: preliminary results. *Behav. Biol.* 7, 279–284. doi: 10.1016/S0091-6773(72)80207-4

Yates, L. A., Ziser, S., Spector, A., and Orrell, M. (2016). Cognitive leisure activities and future risk of cognitive impairment and dementia: systematic review and meta-analysis. *Int. Psychogeriatr.* 28, 1791–1806. doi: 10.1017/S1041610216001137

Conflict of Interest: This study received funding from the Pfizer Health Research Foundation. The funder was not involved in the study design, collection, analysis, interpretation of data, the writing of this article or the decision to submit it for publication.

The authors declare that the research was conducted in the absence of any commercial or financial relationships that could be construed as a potential conflict of interest.

frontiers in Aging Neuroscience

ORIGINAL RESEARCH
published: 07 February 2022
doi: 10.3389/fnagi.2021.784054

Effects of Cognitive Reserve in Alzheimer's Disease and Cognitively Unimpaired Individuals

Dong Hyuk Lee[1,2,3], Sang Won Seo[4], Jee Hoon Roh[5,6], Minyoung Oh[7], Jungsu S. Oh[7], Seung Jun Oh[7], Jae Seung Kim[7] and Yong Jeong[1,8,9] for the Alzheimer's Disease Neuroimaging Initiative (ADNI)†*

[1] Graduate School of Medical Science and Engineering, Korea Advanced Institute of Science and Technology, Daejeon, South Korea, [2] College of Korean Medicine, Sangji University, Wonju, South Korea, [3] Research Institute of Korean Medicine, Sangji University, Wonju, South Korea, [4] Department of Neurology, Samsung Medical Center, Sungkyunkwan University School of Medicine, Seoul, South Korea, [5] Department of Physiology, Korea University College of Medicine, Seoul, South Korea, [6] Neuroscience Research Institute, Korea University College of Medicine, Seoul, South Korea, [7] Department of Nuclear Medicine, Asan Medical Center, University of Ulsan College of Medicine, Seoul, South Korea, [8] Department of Bio and Brain Engineering, Korea Advanced Institute of Science and Technology, Daejeon, South Korea, [9] KI for Health Science and Technology, Korea Advanced Institute of Science and Technology, Daejeon, South Korea

The concept of cognitive reserve (CR) has been proposed as a protective factor that modifies the effect of brain pathology on cognitive performance. It has been characterized through CR proxies; however, they have intrinsic limitations. In this study, we utilized two different datasets containing tau, amyloid PET, and T1 magnetic resonance imaging. First, 91 Alzheimer's disease (AD) continuum subjects were included from Alzheimer's Disease Neuroimaging Initiative 3. CR was conceptualized as the residual between actual cognition and estimated cognition based on amyloid, tau, and neurodegeneration. The proposed marker was tested by the correlation with CR proxy and modulation of brain pathology effects on cognitive function. Second, longitudinal data of baseline 53 AD spectrum and 34 cognitively unimpaired (CU) participants in the MEMORI dataset were analyzed. CR marker was evaluated for the association with disease conversion rate and clinical progression. Applying our multimodal CR model, this study demonstrates the differential effect of CR on clinical progression according to the disease status and the modulating effect on the relationship between brain pathology and cognition. The proposed marker was associated with years of education and modulated the effect of pathological burden on cognitive performance in the AD spectrum. Longitudinally, higher CR marker was associated with lower disease conversion rate among prodromal AD and CU individuals. Higher CR marker was related to exacerbated cognitive decline in the AD spectrum; however, it was associated with a mitigated decline in CU individuals. These results provide evidence that CR may affect the clinical progression differentially depending on the disease status.

Keywords: cognitive reserve, Alzheimer's disease, AD spectrum, cognitive aging, multimodal neuroimaging

OPEN ACCESS

Edited by:
Kenji Toba,
Tokyo Metropolitan Institute of Gerontology, Japan

Reviewed by:
Takeshi Iwatsubo,
The University of Tokyo, Japan
Paul Newhouse,
Vanderbilt University, United States

****Correspondence:***
Yong Jeong
yong@kaist.ac.kr

†Data used in the preparation of this manuscript were obtained from the Alzheimer's Disease Neuroimaging Initiative (ADNI) database (http://adni.loni.usc.edu). As such, the investigators within the ADNI contributed to the design and implementation of ADNI and/or provided data but did not participate in the analysis or writing of this manuscript. A complete listing of ADNI investigators can be found in the coinvestigators list at http://adni.loni.usc.edu/wp-content/uploads/how_to_apply/ADNI_Authorship_List.pdf

Specialty section:
This article was submitted to Neurocognitive Aging and Behavior, a section of the journal Frontiers in Aging Neuroscience

Received: *27 September 2021*
Accepted: *28 December 2021*
Published: *07 February 2022*

Citation:
Lee DH, Seo SW, Roh JH, Oh M, Oh JS, Oh SJ, Kim JS and Jeong Y (2022) Effects of Cognitive Reserve in Alzheimer's Disease and Cognitively Unimpaired Individuals. Front. Aging Neurosci. 13:784054. doi: 10.3389/fnagi.2021.784054

INTRODUCTION

The neuropathological hallmarks of Alzheimer's disease (AD) are intracellular neurofibrillary tangles of hyper-phosphorylated tau protein and extracellular depositions of β-amyloid as the main component of senile plaque (Serrano-Pozo et al., 2011). The National Institute on Aging and Alzheimer's Association (NIA-AA) recently announced a new research framework for the biological definition of AD, which focused on the diagnosis of AD with three biomarkers (Jack et al., 2018). The biomarkers were grouped into β-amyloid, tau protein, and neurodegeneration (A/T/N), capturing the overall neuropathology of AD.

Cognitive reserve (CR) stems from the discrepancy between the degree of brain pathology and its clinical manifestations (Katzman et al., 1988). The reserve concept accounts for individual susceptibility to age-related brain changes or AD-related brain neuropathology (Stern, 2012). CR is measured using surrogate markers of lifestyle, although they have several innate shortcomings (Zahodne et al., 2013). We previously demonstrated that the model reflecting overall AD neuropathology (A-T-N) could capture the properties of CR in a cross-sectional study (Lee et al., 2019).

The association between CR and clinical progression remains controversial. Several studies have reported that CR is associated with clinical progression (Bracco et al., 2007; Reed et al., 2010; Myung et al., 2017; Robitaille et al., 2018), but others did not detect an association (Singh-Manoux et al., 2011; Cadar et al., 2015; Reijs et al., 2017). These conflicting results may be due to the usage of erratic CR proxies, misdiagnosis of pure AD without AD biomarkers, and mixture of disease and unimpaired groups in the analysis.

Thus, in this study, we examined the effect of CR on the relationship between brain pathology and cognitive function and on the clinical progression over time by (1) applying a CR model capturing overall AD neuropathology, (2) selecting amyloid-positive subjects, and (3) subdividing subjects based on the disease status. We hypothesized that CR would modulate the association between brain pathology and cognition and differentially influence the clinical progression according to the disease status.

MATERIALS AND METHODS

Participants

First, participants were recruited within the Alzheimer's Disease Neuroimaging Initiative (ADNI 3, ClinicalTrials.gov ID: NCT02854033). Inclusion criteria for AD, amnestic mild cognitive impairment (aMCI), and cognitively unimpaired subjects (CU) followed the protocol of ADNI 3 (Number: ATRI-001). We only included amyloid-positive subjects who had all three imaging modalities [tau (^{18}F-AV-1451 PET), amyloid PET (^{18}F-AV-45 or ^{18}F-florbetaben PET), and T1-weighted magnetic resonance imaging (MRI)]. Amyloid (Aβ) status was determined by the global standard uptake value ratio (SUVR) $>$ 1.11 (^{18}F-AV-45) or $>$ 1.08 (^{18}F-florbetaben). At baseline, the final participants comprised 25 AD, 42 prodromal AD [Aβ (+) aMCI], and 24 preclinical AD [Aβ (+) CU]. Subsequently, 77 subjects (19 AD, 36 MCI, and 22 CU) were available in the longitudinal analysis.

Second, subjects were recruited at the memory disorder clinic in the Department of Neurology at the Asan Medical Center (AMC) and the Samsung Medical Center (SMC) in Seoul, South Korea. We obtained all three modalities for each subject at baseline (tau PET [^{18}THK-5351], Aβ PET [^{18}F-florbetaben], and T1 MRI). All AD subjects fulfilled the clinical diagnostic criteria for AD according to the NINCDS/ADRDA, and those with aMCI met the Petersen's criteria. Subjects with AD and aMCI were Aβ-positive as determined by brain amyloid plaque load (BAPL score) $\geq$ 2. CU was defined as being elderly and free of neurological disease, Clinical Dementia Rating (CDR) 0 and Mini-Mental State Examination (MMSE) $>$ 27. At baseline, 87 participants [21 AD, 32 prodromal AD, and 34 Aβ (-) CU] were included. At 4-year follow-up, 61 and 43 subjects had available longitudinal data for the MMSE and other cognitive scores, respectively.

For dataset 1, ethics approval was obtained by the ADNI investigators. All study participants provided written informed consent. ADNI 3 is listed in the ClinicalTrials.gov registry (identifier: NCT02854033). For dataset 2, the Institutional Review Board of both hospitals approved the study, and all subjects provided written informed consent.

Neuropsychological Assessment and Cognitive Reserve Surrogate Marker

In dataset 1, we utilized composite scores of memory (ADNI-MEM), executive function (ADNI-EF), language function (ADNI-LAN), and visuospatial function (ADNI-VIS) in ADNI 3 to construct CR marker. These were composite *z*-scores from the ADNI neuropsychological battery of test. We applied the total summation of four domain scores as a global cognitive composite score. Other cognitive measures, including the Alzheimer's Disease Assessment Scale-Cognitive Subscale (ADAS-cog) 11 and MMSE, were used for further validation. In dataset 2, we measured the global composite score for the CR marker based on previous studies (Jahng et al., 2015; Lee et al., 2019). The global composite score was obtained from the average of five domains containing 14 neuropsychological tests (e.g., attention, visuospatial, language, executive, and memory function). The tests were composed of Seoul Verbal Learning Test (SVLT-E) and Rey Complex Figure Test (RCFT) in memory domain contrasting program, Go-No-Go test and Controlled Oral Ward Association Test (COWAT) in executive function, forward and backward Digit Span Test (DST) in Attention, RCFT copying task in Visuospatial function, and Korean-Boston Naming Test (K-BNT) in language function.

We used years of education as a CR proxy. In dataset 1, we correlated the CR marker with years of education. To further validate our CR marker, education was applied to identify CR-related regions in Aβ pathology and neurodegeneration.

Image Acquisition

In ADNI dataset, MRI scans were acquired on scanners from different manufacturers (Philips, Best, Netherlands; GE, Cleveland, OH; and Siemens, Malvern, PA, United States)

using harmonized protocols. We obtained 3D T1-weighted magnetization-prepared rapid gradient echo (MPRAGE) sequence, with 1 mm isotropic voxel resolution and repetition time (TR) = 2,300 ms. Aβ PET scans were recorded for 20 min at 50 min after 370 MBq ± 10% injection (^{18}F-AV-45) or 90 min after 300 MBq ± 10% injection (^{18}F-florbetaben) of the tracer. Tau PET scans were acquired for 30 min at 75–105 min after 370 MBq ± 10% tracer injection. In dataset 2, we obtained 3D T1-weighted MPRAGE with voxel size (AMC: 1.11 × 1.11 × 1.2 mm^3, SMC: 1.0 × 1.0 × 0.5 mm^3) and a TR (AMC: 6.8 ms, SMC: 9.9 ms) from the manufacturer Philips (Eindhoven, Netherlands). Tau PET scans were acquired for 20 min, commencing 50 min after the injection of 185 MBq ± 10% of ^{18}F-THK5351. Aβ PET scans were acquired for 20 min, commencing 90 min after the injection of 300 MBq ± 10% of the tracer. Hoffman phantom-based PET harmonization was applied in datasets 1 and 2.

Data Preprocessing

In both datasets, individual tau and Aβ PET scans were co-registered onto the individual T1 image and normalized into Montreal Neurological Institute (MNI) standard space. Preprocessed images were smoothed (6 mm). SUVR images were calculated for all individuals using the cerebellar gray matter as a reference. All preprocessing was conducted using SPM12 (Wellcome Trust Centre for Neuroimaging, University College London) and MATLAB R2014b (The Mathworks, Natick, MA, United States). For cortical thickness, T1-weighted images underwent preprocessing steps with Freesurfer 6.0[1]. The total intracranial volume (TIV) was obtained by summing the volumes of gray matter, white matter, and CSF.

Calculation of the Cognitive Reserve Marker

We conceptualized CR as the residual of actual cognitive performance and estimated performance; the latter was estimated from AD neuropathology, demographics, a genetic factor (ApoE ε4), and TIV. The "residual" concept for quantifying CR has been applied previously (Reed et al., 2010; Habeck et al., 2017; van Loenhoud et al., 2017). While these studies captured only the structural aspects, our method had an advantage in that the overall AD neuropathology was reflected in the model as follows (A-T-N: primary components of AD biomarkers):

$$\text{Cognitive function}_{\text{estimated}} = \beta_0 + \beta_1 \times X_{\text{Tau}} + \beta_2 \times X_{\text{A}\beta} + \beta_3 \times X_{\text{Thickness}} + \beta_4 \times X_{Age} + \beta_5 \times X_{\text{Sex}} + \beta_6 \times X_{\text{ApoE } \varepsilon 4} + \beta_7 \times X_{\text{TIV}}$$

$(+ \beta_8 \times X_{\text{A}\beta\ \text{tracertype}}$: In dataset 1, Aβ tracer type was included; X_{Tau}, $X_{\text{A}\beta}$, and $X_{\text{Thickness}}$: Global value obtained from each imaging modality)

Cognitive function: Cognitive composite score using multiple domains

Cognitive reserve (CR) = $\text{Cognitive function}_{\text{observed}}$ − $\text{Cognitive function}_{\text{estimated}}$

As a global value for each AD pathology, we extracted the global extent of tau, Aβ, and cortical thickness per subject using multimodal imaging. In tau PET, we obtained images with GM probability > 0.5 and calculated the average tau SUVR value per subject in Braak regions of interest (ROIs) (Hoenig et al., 2017). To avoid off-target effects of the tracer, we excluded ROIs in the basal ganglia and thalamus (Harada et al., 2016). In Aβ PET, we obtained images with GM probability > 0.5 and extracted a global Aβ SUVR value in combined ROIs (Jack et al., 2010). Similarly, we measured the average thickness value among 68 Desikan ROIs. Age (Guerreiro and Bras, 2015) and sex (Mielke, 2018) are demographic risk factors for AD, and ApoE allele 4 (Liu et al., 2013; Safieh et al., 2019) is considered a representative genetic factor of AD. TIV was added as a covariate for thickness and an estimate of brain reserve (Tate et al., 2011). We subsequently performed multiple linear regression with the dependent variable of cognitive function; predictors of global tau, Aβ deposition, and thickness (AD neuropathology); and covariates of age, sex, ApoE ε4 status, and TIV. The beta coefficients of these variables were applied to estimate the cognitive function. Finally, we calculated the CR marker as the residual between the actual and estimated score. According to the equation, higher CR marker value denoted greater CR as it indicated that relatively high cognitive function was maintained at a given level of AD neuropathology in the population.

Effect of the Cognitive Reserve Marker on the Relationship Between Pathological Burden and Cognition

For dataset 1, we calculated Pearson's correlation between the CR marker and a conventional CR proxy, years of education. We also performed multiple linear regression using education as an outcome; CR marker as a predictor; and age, sex, and TIV as covariates.

Fundamentally, we investigated whether the CR marker could modulate the effect of brain pathology on cognitive function across the AD spectrum. To identify regions for which greater education enabled subjects to tolerate greater Aβ burden (CR-related regions), we first performed voxel-wise multiple linear regression of Aβ SUVR with education as the predictor, adjusting for age, sex, Aβ scanner type, and MMSE. The resulting t map was thresholded at the voxel level at $\alpha = 0.01$ and corrected at the cluster level at FWE $\alpha < 0.05$. We then extracted the average Aβ SUVR within the CR-related regions for each subject. Finally, we tested the interaction of the CR marker × Aβ SUVR on cognition, controlling for age and sex across the AD spectrum. We conducted similar procedures with cortical thickness in ROI-wise, adjusting for age, sex, MMSE, and TIV among the AD spectrum (FDR $p < 0.05$). We measured the atrophy value as the reciprocal of thickness value within significant regions. We tested the interaction of the CR marker × atrophy value on cognitive function, controlling for age, sex, and TIV across the AD spectrum.

Effect of the Cognitive Reserve Marker on Clinical Progression

For dataset 2, we performed longitudinal analysis to verify the effect of the CR marker on clinical progression. For a 4-year

[1]https://surfer.nmr.mgh.harvard.edu

period, we examined the conversion rate and change in cognitive scores and disease severity across the entire group. We performed Cox-proportional hazard regression among prodromal AD (n = 32) and CU (n = 34) to investigate the relationship between the CR marker and disease conversion. In this case, we calculated the CR marker without AD subjects at baseline. Diagnostic changes to more severe stages were only considered as a disease conversion. The model contained conversion with time as an outcome measure; CR marker (continuous or binary) as a predictor; and age, sex, ApoE, and TIV as covariates. We validated the effect of the CR marker by confirming hazard ratio (HR), p-value, and 95% confidence intervals (CIs) of HR in the model. Finally, we conducted a likelihood ratio test to evaluate the goodness of model fit between two competing models with and without the CR marker, respectively. We also assessed the Akaike Information Criterion (AIC) to estimate the relative quality of statistical models for a given data. AIC deals with the tradeoff between the goodness of model fit and complexity of the data; smaller AIC indicates higher quality (Vrieze, 2012).

We conducted linear mixed models with cognitive composite score, memory score, and MMSE as outcomes; the CR marker at baseline, time, and CR marker × time as predictors; and adjusted for age, sex, ApoE, and TIV. We repeated a linear mixed model with CDR-SB as an outcome with the same predictors and covariates. Our interest was the interaction of the CR marker and time, as this referred to the effect of the CR marker on clinical progression.

These analyses were divided into AD spectrum and CU groups, as CR behavioral pattern would exert differently according to the disease status. The 95% CIs of beta coefficient of the CR marker, time, and their interaction were estimated. Finally, we performed a likelihood ratio test and AIC to estimate the additional value of the model with the interaction.

In order to estimate more reliable CIs for beta values of the interaction in clinical progression, semi-parametric bootstrapping of the linear mixed model was performed. For this process, we made 1,000 bootstrap samples by resampling the original data with replacement and calculated 95% CIs of the bootstrapped coefficients.

For dataset 1, we repeated linear mixed models with ADAS-cog 11 as outcomes; the CR marker at baseline, time, and CR marker × time as predictors; and adjusted for age, sex, ApoE, and TIV. The analyses were also divided into AD spectrum and CU groups. We conducted a likelihood ratio test and AIC to estimate the additional value of the model with the interaction.

Sensitivity Analysis

In a longitudinal analysis of dataset 2, to figure out the difference between using continuous Aβ SUVR value and using visual diagnosis of Aβ, first we applied binary value (positivity, negativity) instead of continuous value in the calculation of the CR marker. Then, we repeated linear mixed model analysis and compared the results with the model constructed from continuous Aβ SUVR.

Second, we investigated the effect of education on clinical progression in dataset 2. Therefore, we conducted linear mixed model analysis by replacing the CR marker with education into the model.

Finally, we added the global pathological burden (global tau, Aβ, and thickness value) in the linear mixed model as covariates to partly account for the explanation that the CR marker is only a derivative of pathological measurement in relation to cognitive function.

Statistical Analysis

Statistical analyses were conducted in SPSS 18 (Chicago, IL, United States). To compare participant characteristics, chi-square tests and ANOVA tests were performed. In the longitudinal analysis, linear mixed model analysis and semi-parametric bootstrapping were conducted using R[2].

RESULTS

Participant Characteristics

As shown in **Table 1**, we observed significant differences among the three groups in global tau, Aβ deposition, cortical thickness, and cognitive scores. In dataset 1, we investigated the A/T/N classification status using CSF information. Among the 91 subjects, 62 subjects (16 AD, 26 MCI, 20 CU) have baseline CSF information of p-tau181 and t-tau. Unlike the pathological burden obtained from imaging modalities, CSF levels of p-tau and t-tau did not differ significantly among the three groups (**Table 1**). Abnormal levels of CSF biomarkers were defined as p-tau > 27 pg/ml (T +) and t-tau > 300 pg/ml (N +) (Blennow et al., 2019). In the AD subjects, A/T/N (+/+/+) group accounted for 68.8% (11/16) and A/T/N (+/−/−) group accounted for the rest. Among the MCI subjects, A/T/N (+/+/+) group accounted for 42.3% (11/26), A/T/N (+/−/−) group accounted for 50% (13/26), and A/T/N (+/+/−) group accounted for the rest. In the CU subjects, each A/T/N (+/+/+) and A/T/N (+/−/−) group accounted for 45% of the total, and A/T/N (+/+/−) group accounted for the rest (10%). Therefore, it was confirmed that the AD group showed a relatively large distribution of A/T/N (+/+/+). The average follow-up period was 26 months. In total, 77 subjects (19 AD, 36 MCI, and 22 CU) were available in the longitudinal analysis.

In dataset 2, the mean age was lower in the AD group than that in the prodromal AD and CU groups, attributing to the inclusion of 15 early-onset AD. The portion of ApoE ε4 carriers was higher in the AD spectrum than that in the CU. We could not investigate the A/T/N classification of the respective group because the dataset did not contain CSF information. The average follow-up period was 27 months. A total of 61 participants (18 AD, 28 prodromal AD, and 15 CU) had longitudinal MMSE, and 43 subjects (11 AD, 20 prodromal AD, and 12 CU) had follow-up composite score, memory score, and CDR-SB. The total incidence of diagnostic conversion was 28.8%. The conversion rate of prodromal to AD was 53.1%, and the conversion rate of CU to prodromal or CU to AD was 2.9%, respectively.

[2]www.r-project.org

TABLE 1 | Baseline characteristics of dataset 1 (ADNI) and dataset 2.

Dataset 1 (ADNI 3)	**AD (*n* = 25)**	**aMCI (*n* = 42)**	**CU (*n* = 24)**
Demographics			
Age	73.4 (9.0)	73.2 (7.3)	72.3 (5.6)
Sex, F[a] (%)	9 (36.0)	20 (47.6)	17 (70.8)
Education	15.9 (2.4)	16.1 (2.5)	17.0 (1.9)
ApoE ϵ4 (%)	19 (76.0)	30 (71.4)	14 (58.3)
TIV	1.57 (0.21)	1.54 (0.16)	1.51 (0.12)
Pathologic burden			
Tau deposition (SUVR)[b]	1.30 (0.38)	1.12 (0.20)	1.08 (0.15)
Aß deposition (SUVR)[c]	1.45 (0.20)	1.38 (0.19)	1.21 (0.18)
Cortical thickness (mm)[c]	2.37 (0.11)	2.48 (0.08)	2.51 (0.11)
CSF p-tau (pg/ml)	34.5 (12.7)	36.1 (19.9)	26.9 (12.9)
CSF t-tau (pg/ml)	343.6 (104.3)	341.0 (150.4)	277.7 (97.7)
Cognitive function			
MMSE[c]	22.0 (3.2)	27.3 (2.3)	29.1 (1.4)
Composite (*z*-scores)[c]	−3.67 (3.02)	0.99 (2.25)	2.92 (1.65)
ADNI-MEM (*z*-scores)[c]	−0.90 (0.52)	0.14 (0.55)	1.02 (0.50)
ADNI-EF (*z*-scores)[c]	−1.03 (1.15)	0.34 (0.89)	0.91 (0.73)
ADNI-LAN (*z*-scores)[c]	−0.67 (0.92)	0.40 (0.86)	0.81 (0.62)
ADNI-VS (*z*-scores)[c]	−1.12 (1.12)	0.13 (0.65)	0.19 (0.71)
ADAS-cog 11 (baseline)[c]	21.1 (6.7)	10.2 (4.3)	5.0 (2.6)
ADAS-cog 11 (follow-up)[c]	29.5 (11.3)	13.2 (7.0)	5.5 (2.4)
Dataset 2	**AD (*n* = 21)**	**aMCI (*n* = 32)**	**CU (*n* = 34)**
Demographics			
Age[a]	63.2 (11.3)	69.2 (7.2)	68.7 (6.8)
Sex, F (%)	14 (66.7)	23 (71.9)	22 (64.7)
Education	11.6 (4.4)	11.0 (4.3)	10.6 (4.8)
ApoE ϵ4[b] (%)	9 (42.9)	17 (53.1)	6 (17.6)
TIV	1.35 (0.12)	1.33 (0.13)	1.37 (0.13)
CDR-SB[c]	6.39 (3.98)	1.90 (0.96)	0.31 (0.43)
Pathologic burden			
Tau deposition (SUVR)[c]	1.39 (0.09)	1.32 (0.11)	1.20 (0.10)
Aß deposition (SUVR)[c]	1.44 (0.15)	1.50 (0.14)	1.10 (0.07)
Cortical thickness (mm)[c]	2.29 (0.13)	2.39 (0.11)	2.45 (0.12)
Cognitive function			
MMSE[c]	19.4 (5.0)	24.3 (3.6)	28.6 (1.2)
Composite[c]	31.5 (11.1)	42.8 (9.5)	61.0 (7.1)
Memory[c]	46.1 (13.3)	61.6 (14.6)	107.9 (15.2)
Executive[c]	56.0 (29.8)	75.5 (24.9)	102.3 (17.5)
Language[c]	34.1 (13.8)	37.6 (13.4)	50.8 (5.4)
Attention[b]	8.6 (2.3)	9.3 (2.6)	11.1 (2.8)
Visuospatial[c]	12.8 (11.9)	30.2 (6.2)	33.0 (4.5)
Clinical progression			
Follow-up (month)	25.8 (12.3)	29.1 (9.0)	23.3 (9.1)
Conversion to AD, n (%)	–	17 (53.1)	1 (2.9)
Conversion to aMCI, n (%)	–	–	1 (2.9)

Values are mean (standard deviation) or number (%). [a]$p < 0.05$; [b]$p < 0.01$; [c]$p < 0.001$, significant between groups.

AD, Alzheimer's disease; aMCI, amnestic mild cognitive impairment; CU, cognitively unimpaired; ApoE ϵ4, apolipoprotein ϵ4 allele; TIV, total intracranial volume; SUVR, standardized uptake value ratio; p-tau, phosphorylated tau; t-tau, total tau; MMSE, Mini-Mental State Examination; ADAS-cog 11, Alzheimer's Disease Assessment Scale-Cognitive Subscale 11; Composite score, the average score of five domains; CDR-SB, Clinical Dementia Rating Scale-Sum of Boxes.

Model Construction

In dataset 1, we confirmed the relationship between cognitive performance and each predictor *via* beta values. The linear regression model revealed that composite score was negatively associated with global tau ($\beta_{tau} = -6.35$) and Aβ deposition ($\beta_{A\beta} = -1.80$). The composite score was positively associated with the global cortical thickness ($\beta_{thickness} = 12.85$). The R^2 of the model was 0.52 (F-test, $p = 1.49^{*}e^{-10}$, adjusted $R^2 = 0.48$). There was no multicollinearity among variables (maximum VIF < 1.85). As a result, the estimated composite z-scores were significantly correlated with the actual composite z-scores using Pearson's correlation ($r = 0.72$, $p = 6.51^{*}e^{-16}$). Then, we dichotomized the actual z-score using median value (median = 0.819) and investigated whether the estimated z-scores predicted actual z-scores well. In a discrete ROC curve analysis, the estimated composite z-score classified high and low actual z-scores well (AUC = 0.83, 95% CI = 0.75–0.92, accuracy = 0.77, sensitivity = 0.83, specificity = 0.71). Through this analysis, we can conclude that the estimated cognitive function from the biological markers, demographics, and genetic factors would be a reasonable estimate of the actual cognitive function. Finally, we calculated the CR marker using the differences between the actual and estimated composite scores.

Using dataset 2, we already validated the suitability of the model (Lee et al., 2019). In brief, the constructed model demonstrated that the composite score was significantly associated with each global AD neuropathology ($\beta_{tau} = -18.86$, $\beta_{A\beta} = -32.05$, and $\beta_{thickness} = 34.11$). The R^2 of the model was 0.57 (F-test, $p < 0.00001$). There was no multicollinearity within variables (maximum VIF < 1.9). Estimated composite scores were significantly correlated with actual composite scores ($r = 0.76$, $p = 2.21^{*}e^{-17}$). Also, we dichotomized the actual composite score using median value (median = 47.2) and investigated whether the estimated composite scores predicted high and low composite scores well. In a discrete ROC curve analysis, the estimated composite score classified high and low actual composite scores reasonably well (AUC = 0.92, 95% CI = 0.87–0.98, accuracy = 0.82, sensitivity = 0.77, specificity = 0.86). Then, we calculated the CR marker from the residuals between the actual and estimated composite scores.

Effect of the Cognitive Reserve Marker on the Relationship Between Pathological Burden and Cognition

In dataset 1, the CR marker was significantly correlated with years of education ($r = 0.29$, $p = 0.005$). Subjects with more years of education had greater CR than individuals with fewer years of education. The positive association between the CR marker and years of education remained even after adjusting for age, sex, and TIV ($t = 2.94$, $p = 0.004$).

Fundamentally, we tested whether the CR marker could modulate the association between AD pathological burden and cognitive function across the AD spectrum. In **Figures 1A,B**, for Aβ pathology, higher level of education was associated with greater Aβ deposition within the left superior and middle frontal

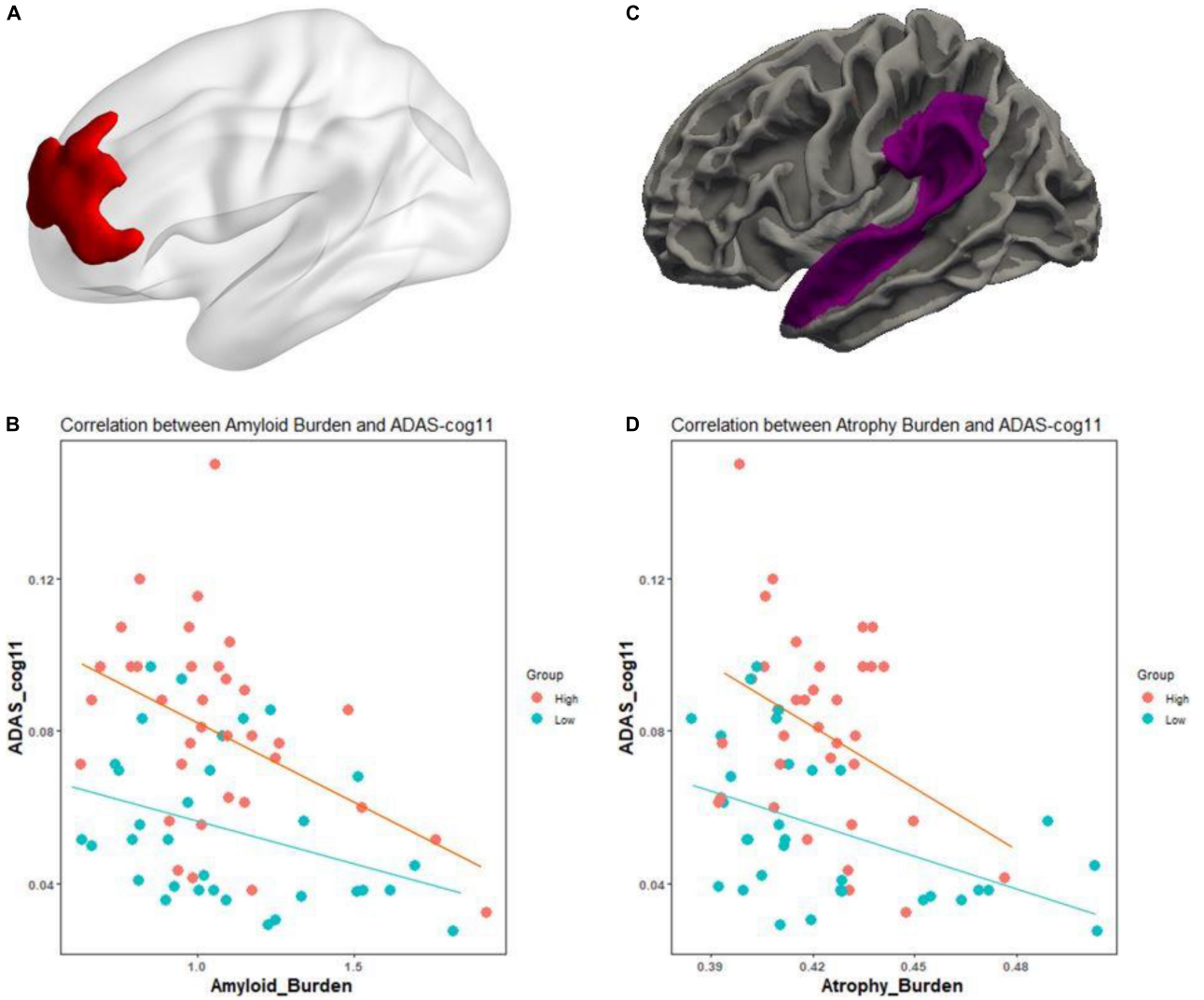

FIGURE 1 | Effect of the CR marker on the relationship between pathological burden and cognitive functions in AD spectrum. **(A)** CR-related regions in amyloid burden using education as a CR proxy (left frontal region). **(B)** Scatterplot for the interaction of the CR marker × left frontal Aβ SUVR on reciprocal of the Alzheimer's Disease Assessment Scale-Cognitive Subscale 11 (ADAS-cog 11). **(C)** CR-related regions in thickness using education as a CR proxy (left temporoparietal region). **(D)** Scatterplot for the interaction of the CR marker × left temporoparietal atrophy on the reciprocal of the Alzheimer's Disease Assessment Scale-Cognitive Subscale 11 (ADAS-cog 11). To better represent the effect of CR marker, ADAS-cog 11 score was expressed as reciprocal. For illustration, groups of high and low CR markers (*via* median value) are plotted separately.

regions, after adjusting for age, sex, Aβ scanner type, and MMSE (t = 2.37, p < 0.01). We examined whether the CR marker modified the effect of left frontal Aβ burden on cognition in the AD spectrum, controlling for age, sex, and ApoE. There was a significant interaction effect of the CR marker × left frontal Aβ SUVR on ADAS-cog 11 (t-stat = 2.17, p = 0.034). The interaction effect of CR marker × left frontal Aβ SUVR on MMSE was marginal (t-stat = −1.93, p = 0.058). As shown in **Figures 1C,D**, higher education was associated with greater cortical atrophy within the left superior temporal gyrus and supramarginal gyrus after controlling for age, sex, MMSE, and TIV. The interaction effect of the CR marker × left temporoparietal atrophy on ADAS-cog 11 was confirmed to be significant (t-stat = 2.29, p = 0.026).

Effect of the Cognitive Reserve Marker on Clinical Progression

Cox regression analysis revealed that in prodromal AD and CU groups, the CR marker was negatively associated with conversion rate, indicating that higher CR was related to lower conversion risk (continuous: HR = 0.57, 95% CI: 0.34 ∼ 0.97, β = −0.56, p = 0.037; binary: HR = 0.33, 95% CI: 0.11∼0.97, β = −1.10, p = 0.044). The model with the CR marker showed a better model fit than that of the model without the CR marker in a likelihood ratio test (continuous: p = 0.031; binary: p = 0.037). The model with the CR marker had lower AIC value than that of the model without the CR marker [without CR marker: 115.75, with CR marker: 113.12 (continuous)/113.40 (binary)].

In the analysis of cognitive decline among AD spectrum, clear cognitive decline was observed across time in all cognitive scores. Particularly, higher CR marker was related to more exacerbated decline in cognitive performance in the AD spectrum (MMSE: $p = 0.026$, composite score: $p = 0.045$, memory score: $p = 0.036$) throughout **Table 2** and **Figure 2**. In CU, cognitive scores decreased over time, with the exception of MMSE. The CR marker also modified the relationship between cognitive function and time. However, the pattern modulated by the CR marker was different from that of the AD spectrum, such that subjects with high CR exhibited attenuated cognitive decline (MMSE: $p = 0.017$, composite score: $p < 0.001$, memory score: $p = 0.003$) throughout **Table 2** and **Figure 2**. The likelihood ratio test revealed that the model with the interaction showed a better model fit than that of the model without interaction in all cognitive scores among CU and AD spectrum. In the aspects of AIC, the model with interaction also had lower AIC values in both AD spectrum and CU as shown in **Table 3**. AD spectrum participants with high CR exhibited more drastic alterations in disease severity in **Table 2**. The model with the interaction showed a better model fit than that of the model without interaction among AD spectrum in **Table 3**.

More reliable results were obtained from 95% CIs derived from bootstrapping, indicating that the behavioral pattern of CR differed depending on disease stage and was related to accelerated cognitive decline in AD spectrum subjects but with alleviated cognitive decline in CU subjects as shown in **Table 4**.

In the analysis of ADAS-cog 11 among AD spectrum in dataset 1, the CR marker modified the relationship between cognitive decline and time, such that subjects with higher CR marker exhibited worse cognitive decline ($\beta = 0.07$; $p = 0.026$; **Supplementary Table 1**). Since the higher score in ADAS-cog 11 indicates greater cognitive impairment, AD spectrum subjects with higher CR marker showed more steeper increase in the score. However, in the CU group, the CR marker showed a tendency to modulate the relationship between cognitive function and time, but did not reach a significant level ($\beta = -0.02$; $p = 0.20$; **Supplementary Table 1**). The likelihood ratio test also revealed that the model with the interaction showed a better model fit than that of the model without the interaction in the AD spectrum (**Supplementary Table 1**).

Sensitivity Analysis

The constructed model using visual diagnosis of Aβ demonstrated that the composite score was significantly associated with each global AD neuropathology ($\beta_{tau} = -18.36$, $\beta_{A\beta} = -17.42$, $\beta_{thickness} = 22.41$). The R^2 of the model was 0.62 (F-test, $p < 0.00001$, adjusted $R^2 = 0.59$). We calculated the CR marker from the residuals between the actual and estimated composite scores. The CR marker correlated well with years of education ($r = 0.49$, $p < 0.00001$). In the analysis of cognitive decline among AD spectrum, the CR marker showed a tendency to modulate the relationship between cognitive function and time, but did not reach a significant level (MMSE: $p = 0.08$, composite score: $p = 0.13$, memory score: $p = 0.26$, **Supplementary Table 2**). However, subjects with high CR exhibited more drastic alterations in disease severity (CDR-SB: $p = 0.046$). In the longitudinal analysis of CU subjects, the CR marker modulated the association between cognitive performance and time (MMSE: $p = 0.001$, composite score: $p < 0.001$, memory score: $p = 0.027$, **Supplementary Table 2**). In case of CDR-SB, CU subjects with high CR

TABLE 2 | Effect of the CR marker on cognitive decline and disease severity in AD spectrum and cognitively unimpaired group.

	AD spectrum			CU		
	β	CI	*P*-value	β	CI	*P*-value
MMSE						
CR marker	1.39	−0.17 ∼ 2.97	0.084	0.89	0.15 ∼ 1.62	0.026
Time	−0.12	−0.16 ∼ −0.08	<0.001	−0.02	−0.05 ∼ 0.01	0.26
CR marker × Time	−0.04	−0.08 ∼ −0.01	0.026	0.04	0.01 ∼ 0.07	0.017
Composite score						
CR marker	5.19	2.20 ∼ 8.21	0.001	5.47	3.25 ∼ 7.65	<0.001
Time	−0.20	−0.28 ∼ −0.12	<0.001	−0.18	−0.27 ∼ −0.08	0.001
CR marker × Time	−0.08	−0.15 ∼ −0.003	0.045	0.20	0.12 ∼ 0.28	<0.001
Memory score						
CR marker	7.81	0.35 ∼ 15.32	0.018	8.78	3.91 ∼13.65	0.001
Time	−0.24	−0.37 ∼ −0.11	<0.001	−0.47	−0.76 ∼ −0.18	0.003
CR marker × Time	−0.14	−0.26 ∼ −0.01	0.036	0.39	0.15 ∼ 0.64	0.003
CDR-SB						
CR marker	−0.68	−1.58 ∼ 0.22	0.14	−0.10	−0.64 ∼ 0.44	0.72
Time	0.07	0.04 ∼ 0.10	<0.001	0.02	−0.01 ∼ 0.06	0.15
CR marker × Time	0.03	0.01 ∼ 0.06	0.04	−0.02	−0.04 ∼ 0.01	0.23

AD spectrum, Alzheimer's disease spectrum; CU, cognitively unimpaired group; MMSE, Mini-Mental State Examination; Composite score, the average score of five domains; CDR-SB, Clinical Dementia Rating Scale-Sum of Boxes; β, Beta coefficient of each variable; CI, 95% confidence interval of the beta coefficient; P-value, p-value of each variable in the linear mixed model.

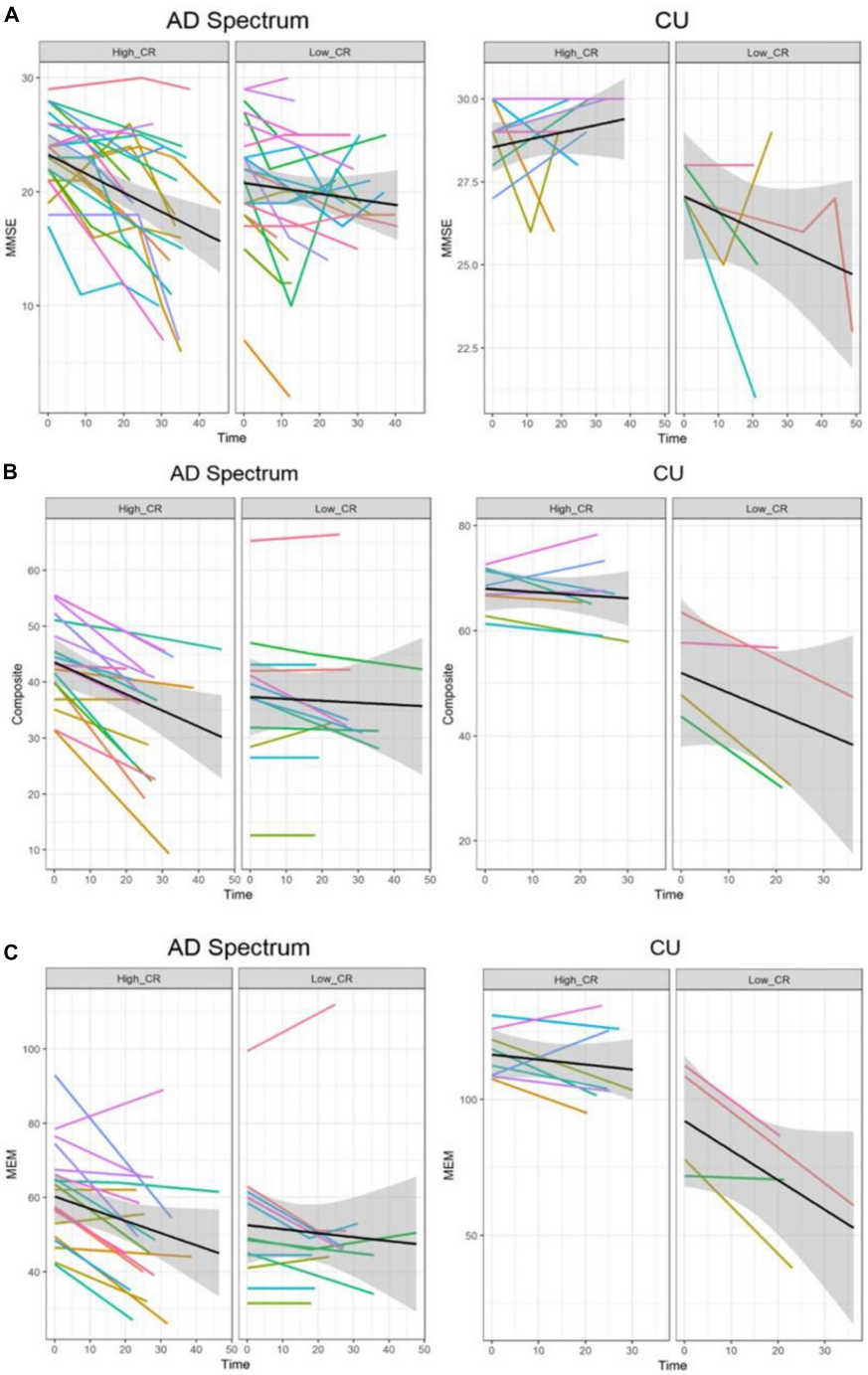

FIGURE 2 | Trajectories of cognitive decline according to the CR marker in AD spectrum and cognitively unimpaired group. Panels **(A–C)** represent the different cognitive scores. In each plot, *X*-axis: Time (month), *Y*-axis: each cognitive score, Left panel: high CR group, Right panel: low CR group. **(A)** Trajectories of MMSE according to the CR marker. **(B)** Trajectories of composite score according to the CR marker. **(C)** Trajectories of memory score according to the CR marker. In the AD spectrum, individuals with high CR showed a steeper decline than the low CR group. In contrast, individuals with high CR showed a attenuated decline than the low CR among the cognitively unimpaired group. Shadows in each plot indicate 95% confidence intervals. CU, cognitively unimpaired group; MMSE, Mini-Mental State Examination; Composite, cognitive composite score; MEM, memory function score.

showed more delayed alterations in disease severity (CDR-SB: p = 0.024). Therefore, it was found that although the CR marker using binarization of amyloid PET tended to modulate the relationship between cognition and time to some extent, the CR marker using continuous SUVR value reflects the properties of CR better.

TABLE 3 | Goodness of fit in models with the interaction between the CR marker and time on cognitive trajectories among AD spectrum and cognitively unimpaired group.

	AD spectrum			CU		
Model	**AIC**	**Log likelihood**	***P*-value**	**AIC**	**Log likelihood**	***P*-value**
MMSE						
w/o the interaction	792.07	−385.04	–	147.12	−62.56	–
with the interaction	789.12	−382.56	0.026	143.94	−59.97	0.023
Composite score						
w/o the interaction	458.11	−218.05	–	158.54	−70.27	–
with the interaction	456.11	−216.06	0.046	146.99	−63.49	0.0002
Memory score						
w/o the interaction	523.29	−250.65	–	198.40	−90.20	–
with the interaction	520.86	−248.43	0.035	191.53	−85.77	0.003
CDR-SB						
w/o the interaction	313.04	−145.52	–	87.57	−34.79	–
with the interaction	310.76	−143.38	0.039	88.09	−34.05	0.22

AD spectrum, Alzheimer's disease spectrum; CU, cognitively unimpaired groups; AIC, Akaike Information Criterion; Interaction, interaction of the CR marker with time; w/o, without; MMSE, Mini-Mental State Examination; Composite score, the average score of five domains; CDR-SB, Clinical Dementia Rating Scale-Sum of Boxes.

In case of education, years of education was not associated with accelerated cognitive decline (memory score: $p = 0.12$, MMSE: $p = 0.19$, composite score: $p = 0.78$). In the CU group, education modified the relationship between cognitive function and time, such that subjects with higher education exhibited attenuated cognitive decline (memory score: $p = 0.003$, MMSE: $p = 0.004$, composite score: $p < 0.001$, **Supplementary Table 3**).

We verified whether the CR marker had an independent effect on clinical progression by adjusting global pathological burden as covariates. Even though the values of global pathology were added as covariates, the CR marker still had an effect on clinical progression among AD spectrum in MMSE, memory score, but not composite score (MMSE: $p = 0.023$, memory score: $p = 0.047$, composite score: $p = 0.06$, **Supplementary Table 4**). The subjects with high CR showed more exacerbated cognitive decline in the AD spectrum. In the analysis of CU subjects, the CR marker also affected the relationship between cognitive function and time (MMSE: $p = 0.006$, memory score: $p = 0.003$, composite score: $p < 0.001$, **Supplementary Table 4**). In case of CDR-SB, CU subjects with high CR showed more delayed alterations in disease severity (CDR-SB: $p = 0.047$). Through this subsequent analysis, it was determined at least in part that the CR marker could have an additional effect on clinical progression, not simply a derivative of global pathology.

DISCUSSION

Our major findings were that CR, defined as the difference between actual and estimated cognitive function from overall AD neuropathology, modulated the effect of AD pathological burden on cognition and differentially affected clinical progression depending on the disease status. We demonstrated that the slope of cognitive decline against AD pathological burden was steeper in those with high CR among AD spectrum. We observed that CR affected clinical progression as AD spectrum with high CR exhibited aggravated cognitive decline and disease severity. In contrast, CR was related to mitigated cognitive decline in the CU. These results represent the phenomenon of CR well (Stern, 2009).

Specifically, among CU participants, CR exhibited a protective effect that delayed the onset of cognitive impairment. However, once cognitive decline had commenced, CR was associated with accelerated cognitive deterioration. We can argue this phenomenon as follows (Stern, 2012): Individuals

TABLE 4 | Effect of the CR marker on cognitive decline and disease severity (95% confidence intervals from bootstrapping).

	AD spectrum	CU
	95% CIs of β values	**95% CIs of β values**
MMSE		
CR marker	−0.17 ∼ 3.01	0.17 ∼ 1.67
Time	−0.16 ∼ −0.08	−0.05 ∼ 0.01
CR marker × Time	−0.08 ∼ −0.006	0.01 ∼ 0.07
Composite score		
CR marker	2.00 ∼ 8.50	3.47 ∼ 7.47
Time	−0.28 ∼ −0.12	−0.26 ∼ −0.09
CR marker × Time	−0.15 ∼ −0.007	0.13 ∼ 0.27
Memory score		
CR marker	1.23 ∼ 14.39	4.31 ∼ 13.79
Time	−0.38 ∼ −0.11	−0.75 ∼ −0.22
CR marker × Time	−0.27 ∼ −0.01	0.14 ∼ 0.62
CDR-SB		
CR marker	−1.64 ∼ 0.27	−0.64 ∼ 0.42
Time	0.04 ∼ 0.10	−0.01 ∼ 0.06
CR marker × Time	0.003 ∼ 0.06	−0.05 ∼ 0.01

AD spectrum, Alzheimer's disease spectrum; CU, cognitively unimpaired group; MMSE, Mini-Mental State Examination; Composite score, the average score of five domains; CDR-SB, Clinical Dementia Rating Scale-Sum of Boxes; β, beta coefficient of each variable; CI, 95% confidence interval of the beta coefficient.

with higher CR may tolerate greater AD neuropathology burden; thus, the point at which cognitive function begins to deteriorate would be delayed relative to those with lower CR. However, there is a certain level (threshold) where the pathological burden is so severe that cognitive function cannot be maintained. Based on this presumption, individuals with higher CR will experience cognitive decline when pathology has progressed to a greater degree and have less time to the end point where pathology defeats cognitive function. This would induce a steeper rate of cognitive decline once it has begun.

Although definitive conclusions on the differential effects of CR depending on disease status have yet to be drawn, multiple studies have reproduced this pattern using various methods to quantify CR. In disease stage showing CR-related accelerated progression, education (Andel et al., 2006; Scarmeas et al., 2006; Hall et al., 2007), occupational complexity (Andel et al., 2006; Boots et al., 2015), IQ (Pavlik et al., 2006; Bracco et al., 2007), and W-score method (van Loenhoud et al., 2019) have been used to identify CR. The literature has reported CR-related attenuated cognitive decline in early stages of AD and CU groups using education (Allegri et al., 2010; Clouston et al., 2019), occupational complexity (Andel et al., 2005; Smart et al., 2014), composite scores (Pettigrew et al., 2017; Soldan et al., 2017), and latent variable method (Reed et al., 2010; Zahodne et al., 2013) to measure CR. However, relatively few studies have been conducted to verify the longitudinal effects of CR on clinical progression across CU and AD spectrum. Most studies have only addressed one specific stage of the disease or unimpaired groups. Moreover, the inclusion of participants was often dependent on clinical entities without AD biomarkers, and results may be misleading. In contrast, our study demonstrated cross-sectional and longitudinal effects of CR on cognitive function in both CU and AD spectrum using an identical method with AD biomarkers.

The underlying mechanism linking CR, AD neuropathology, and cognitive function remains unclear. One tentative theoretical model that integrates CR-related researches has been proposed (Arenaza-Urquijo et al., 2015), whereby neuroprotective and compensatory mechanisms coexist and play differential roles in disease, with neuroprotective mechanisms playing a major role in early stages and compensatory mechanisms coming into play in more advanced disease stages. The concept of neuroprotection in early stages is supported by animal and intervention studies. Animal studies have demonstrated reduced Aβ levels or increased Aβ clearance in mouse with environmental enrichment or voluntary wheel running (Lazarov et al., 2005; Costa et al., 2007). Intervention studies have reported increased perfusion and hippocampal size with exercise and biochemical changes in the hippocampus after cognitive training in the normal elderly people (Valenzuela et al., 2003; Burdette et al., 2010; Erickson et al., 2011). Compensatory mechanisms have been supported by epidemiological, neuroimaging, and autopsy studies (Bennett et al., 2003; Mortimer et al., 2005), showing modulatory effects of CR on the relationship between Aβ pathology and cognition. This differential mechanism of CR is in line with our findings.

Our approach to quantify CR has several strengths over CR proxies. We first attempted to reflect overall AD neuropathology using multimodal neuroimaging, similar to previous residual models, in that CR is defined as a residual. However, our model focused on both structural aspect (neurodegeneration) and proteinopathies (Amyloid and tau). This concept is in line with the latest NIA-AA research framework on the biological definition of AD. Second, our model mirrored the "present" state of CR, unlike one static value of CR proxy for life. As CR is considered an active construct developing from continuous cognitive exposure, our model can be applied dynamically according to the disease stage. Third, we distinguished CR itself from CR proxies, as the latter have inherent limitations such as inter-correlations, static value, and possible mechanisms other than CR, by exhibiting direct impact on the neuropathological process. We believe that the conceptualization of CR without CR proxies can help to avoid these drawbacks.

Understanding the role of CR on the clinical progression in AD has important implications in the clinical and research fields. Despite persistent efforts, disease-modifying treatments have failed for more than three decades. Alternative strategies have been suggested to overcome the failures in disease-modifying therapies for AD. CR may contribute to the development of non-pharmacological approaches for delaying AD onset or promoting AD prevention. Moreover, the concept of CR is closely associated with precision or personalized medicine, an emerging strategy for disease treatment and prevention that takes into account individual variability in genes, environments, and lifestyles. Precision medicine aims to optimize the effectiveness of disease treatment and prevention by considering biological components that may influence disease heterogeneity (Hahn and Lee, 2019). Therefore, considering CR in the clinical environment may provide a basis for accurate prognosis of patients and facilitate an integrated approach. Finally, the genuine effects of an intervention may be identified by categorizing individual patients based on CR levels in clinical trials. Results of the trials may thus be interpreted correctly through the adjustment of baseline differences in CR between groups. Our approach for measuring CR will facilitate understanding of the cognitive trajectory of aging and AD, clarify individuals with susceptibility or resistance to AD pathology, and characterize patients for successful clinical trials.

Our study has some limitations. First, we recognize that our CR model is a relatively simple linear model. We assumed a simple linear relationship between cognitive function and brain pathology and did not consider possible interactions between AD biomarkers or other contributing factors such as white matter hyperintensity or vascular components. In this study, we attempted to extend the validity of our CR model based on primary AD biomarkers (A-T-N) through longitudinal and cross-sectional analysis, rather than aiming to capture the full complexity of CR. Second, the sample size of the longitudinal study was relatively small, and the results may be preliminary. If we applied CSF information rather than PET imaging, it might be possible to obtain a larger size of samples. However, we initially intended to utilize the topological information of amyloid and tau that CSF information cannot provide. Finally, two datasets have

heterogeneity in the amyloid positivity of CU individuals. Dataset 2 only contains amyloid-negative subjects due to the scarcity of amyloid positivity in unimpaired states. In Dataset 1 (ADNI), we can utilize amyloid positivity participants in CU individuals. Although the two datasets have heterogeneous characteristics, we considered this to be somewhat meaningful in terms of the opportunity to test the applicability of our methodology.

DATA AVAILABILITY STATEMENT

The datasets presented in this study can be found in online repositories. The names of the repository/repositories and accession number(s) can be found in the article/**Supplementary Material**. The ADNI data are accessible from adni.loni.usc.edu/data-samples/access-data.

ETHICS STATEMENT

The studies involving human participants were reviewed and approved by Institutional Review Board of Asan Medical Center and Samsung Medical Center. For ADNI data, ethics approval was obtained by the ADNI investigators. The patients/participants provided their written informed consent to participate in this study. Written informed consent was obtained from the individual(s) for the publication of any potentially identifiable images or data included in this article.

AUTHOR CONTRIBUTIONS

DL conceptualized the study, analyzed and interpreted the data, and drafted the manuscript. SS, JR, MO, JO, SO, and JK contributed to the acquisition, processing, and analysis of the data. YJ supervised the study, interpreted the data, and revised the manuscript. All authors contributed to the article and approved the submitted version.

FUNDING

This research was supported by the grant HI14C2768 from the Korea Health Technology Research and Development Project through the Korea Health Industry Development Institute, funded by the Ministry of Health and Welfare, South Korea.

ACKNOWLEDGMENTS

Data collection and sharing for this project was funded by the Alzheimer's Disease Neuroimaging Initiative (ADNI) (NIH grant U01 AG024904) and DOD ADNI (Department of Defense award number W81XWH-12-2-0012). ADNI was funded by the National Institute on Aging and the National Institute of Biomedical Imaging and Bioengineering, and was contributed by the following: AbbVie; Alzheimer's Association; Alzheimer's Drug Discovery Foundation; Araclon Biotech; BioClinica; Biogen; Bristol-Myers Squibb Company; CereSpin; Cogstate; Eisai; Elan Pharmaceuticals; Eli Lilly and Company; EuroImmun; F. Hoffmann-La Roche and its affiliated company Genentech.; Fujirebio; GE Healthcare; IXICO; Janssen Alzheimer Immunotherapy Research and Development; Johnson & Johnson Pharmaceutical Research and Development; Lumosity; Lundbeck; Merck and Co.; Meso Scale Diagnostics; NeuroRx Research; Neurotrack Technologies; Novartis Pharmaceuticals Corporation; Pfizer; Piramal Imaging; Servier; Takeda Pharmaceutical Company; and Transition Therapeutics. The Canadian Institutes of Health Research has provided funds to support ADNI clinical sites in Canada. Private sector contributions were facilitated by the Foundation for the NIH (fnih.org). The grantee organization is the Northern California Institute for Research and Education, and the study was coordinated by the Alzheimer's Therapeutic Research Institute at the University of Southern California. ADNI data were disseminated by the Laboratory for NeuroImaging at the University of Southern California.

SUPPLEMENTARY MATERIAL

The Supplementary Material for this article can be found online at: https://www.frontiersin.org/articles/10.3389/fnagi.2021.784054/full#supplementary-material

REFERENCES

Allegri, R. F., Taragano, F. E., Krupitzki, H., Serrano, C. M., Dillon, C., Sarasola, D., et al. (2010). Role of cognitive reserve in progression from mild cognitive impairment to dementia. *Dement. Neuropsychol.* 4, 28–34. doi: 10.1590/S1980-57642010DN40100005

Andel, R., Crowe, M., Pedersen, N. L., Mortimer, J., Crimmins, E., Johansson, B., et al. (2005). Complexity of work and risk of Alzheimer's disease: a population-based study of Swedish twins. *J. Gerontol. B Psychol. Sci. Soc. Sci.* 60, 251–258. doi: 10.1093/geronb/60.5.p251

Andel, R., Vigen, C., Mack, W. J., Clark, L. J., and Gatz, M. (2006). The effect of education and occupational complexity on rate of cognitive decline in Alzheimer's patients. *J. Int. Neuropsychol. Soc.* 12, 147–152. doi: 10.1017/S1355617706060206

Arenaza-Urquijo, E. M., Wirth, M., and Chetelat, G. (2015). Cognitive reserve and lifestyle: moving towards preclinical Alzheimer's disease. *Front. Aging Neurosci.* 7:134. doi: 10.3389/fnagi.2015.00134

Bennett, D. A., Wilson, R. S., Schneider, J. A., Evans, D. A., Mendes De Leon, C. F., Arnold, S. E., et al. (2003). Education modifies the relation of AD pathology to level of cognitive function in older persons. *Neurology* 60, 1909–1915. doi: 10.1212/01.wnl.0000069923.64550.9f

Blennow, K., Shaw, L. M., Stomrud, E., Mattsson, N., Toledo, J. B., Buck, K., et al. (2019). Predicting clinical decline and conversion to Alzheimer's disease or dementia using novel Elecsys Abeta(1-42), pTau and tTau CSF immunoassays. *Sci. Rep.* 9:19024. doi: 10.1038/s41598-019-54204-z

Boots, E. A., Schultz, S. A., Almeida, R. P., Oh, J. M., Koscik, R. L., Dowling, M. N., et al. (2015). Occupational complexity and cognitive reserve in a middle-aged

cohort at risk for Alzheimer's disease. *Arch. Clin. Neuropsychol.* 30, 634–642. doi: 10.1093/arclin/acv041

Bracco, L., Piccini, C., Baccini, M., Bessi, V., Biancucci, F., Nacmias, B., et al. (2007). Pattern and progression of cognitive decline in Alzheimer's disease: role of premorbid intelligence and ApoE genotype. *Dement. Geriatr. Cogn. Disord.* 24, 483–491. doi: 10.1159/000111081

Burdette, J. H., Laurienti, P. J., Espeland, M. A., Morgan, A., Telesford, Q., Vechlekar, C. D., et al. (2010). Using network science to evaluate exercise-associated brain changes in older adults. *Front. Aging Neurosci.* 2:23. doi: 10.3389/fnagi.2010.00023

Cadar, D., Stephan, B. C. M., Jagger, C., Sharma, N., Dufouil, C., Den Elzen, W. P. J., et al. (2015). Is education a demographic dividend? The role of cognitive reserve in dementia-related cognitive decline: a comparison of six longitudinal studies of ageing. *Lancet* 386, S25–S25.

Clouston, S. A. P., Smith, D. M., Mukherjee, S., Zhang, Y., Hou, W., Link, B. G., et al. (2019). Education and cognitive decline: an integrative analysis of global longitudinal studies of cognitive aging. *J. Gerontol. B Psychol. Sci. Soc. Sci.* 75, e151–e160. doi: 10.1093/geronb/gbz053

Costa, D. A., Craechiolo, J. R., Bachstetter, A. D., Hughes, T. F., Bales, K. R., Paul, S. M., et al. (2007). Enrichment improves cognition in AD mice by amyloid-related and unrelated mechanisms. *Neurobiol. Aging* 28, 831–844. doi: 10.1016/j.neurobiolaging.2006.04.009

Erickson, K. I., Voss, M. W., Prakash, R. S., Basak, C., Szabo, A., Chaddock, L., et al. (2011). Exercise training increases size of hippocampus and improves memory. *Proc. Natl. Acad. Sci. U.S.A.* 108, 3017–3022. doi: 10.1073/pnas.1015950108

Guerreiro, R., and Bras, J. (2015). The age factor in Alzheimer's disease. *Genome Med.* 7:106. doi: 10.1186/s13073-015-0232-5

Habeck, C., Razlighi, Q., Gazes, Y., Barulli, D., Steffener, J., and Stern, Y. (2017). Cognitive reserve and brain maintenance: orthogonal concepts in theory and practice. *Cereb. Cortex* 27, 3962–3969. doi: 10.1093/cercor/bhw208

Hahn, C., and Lee, C. U. (2019). A brief review of paradigm shifts in prevention of Alzheimer's disease: from cognitive reserve to precision medicine. *Front. Psychiatry* 10:786. doi: 10.3389/fpsyt.2019.00786

Hall, C. B., Derby, C., Levalley, A., Katz, M. J., Verghese, J., and Lipton, R. B. (2007). Education delays accelerated decline on a memory test in persons who develop dementia. *Neurology* 69, 1657–1664. doi: 10.1212/01.wnl.0000278163.82636.30

Harada, R., Okamura, N., Furumoto, S., Furukawa, K., Ishiki, A., Tomita, N., et al. (2016). 18F-THK5351: a novel PET radiotracer for imaging neurofibrillary pathology in Alzheimer disease. *J. Nucl. Med.* 57, 208–214. doi: 10.2967/jnumed.115.164848

Hoenig, M. C., Bischof, G. N., Hammes, J., Faber, J., Fliessbach, K., Van Eimeren, T., et al. (2017). Tau pathology and cognitive reserve in Alzheimer's disease. *Neurobiol. Aging* 57, 1–7. doi: 10.1016/j.neurobiolaging.2017.05.004

Jack, C. R. Jr., Bennett, D. A., Blennow, K., Carrillo, M. C., Dunn, B., Haeberlein, S. B., et al. (2018). NIA-AA research framework: toward a biological definition of Alzheimer's disease. *Alzheimers Dement.* 14, 535–562. doi: 10.1016/j.jalz.2018.02.018

Jack, C. R. Jr., Wiste, H. J., Vemuri, P., Weigand, S. D., Senjem, M. L., Zeng, G., et al. (2010). Brain beta-amyloid measures and magnetic resonance imaging atrophy both predict time-to-progression from mild cognitive impairment to Alzheimer's disease. *Brain* 133, 3336–3348. doi: 10.1093/brain/awq277

Jahng, S., Na, D. L., and Kang, Y. (2015). Constructing a composite score for the seoul neuropsychological screening battery-core. *Dement. Neurocogn. Disord.* 14, 137–142. doi: 10.1212/WNL.0000000000010347

Katzman, R., Terry, R., Deteresa, R., Brown, T., Davies, P., Fuld, P., et al. (1988). Clinical, pathological, and neurochemical changes in dementia: a subgroup with preserved mental status and numerous neocortical plaques. *Ann. Neurol.* 23, 138–144. doi: 10.1002/ana.410230206

Lazarov, O., Robinson, J., Tang, Y. P., Hairston, I. S., Korade-Mirnics, Z., Lee, V. M., et al. (2005). Environmental enrichment reduces Abeta levels and amyloid deposition in transgenic mice. *Cell* 120, 701–713. doi: 10.1016/j.cell.2005.01.015

Lee, D. H., Lee, P., Seo, S. W., Roh, J. H., Oh, M., Oh, J. S., et al. (2019). Neural substrates of cognitive reserve in Alzheimer's disease spectrum and normal aging. *Neuroimage* 186, 690–702. doi: 10.1016/j.neuroimage.2018.11.053

Liu, C. C., Liu, C. C., Kanekiyo, T., Xu, H., and Bu, G. (2013). Apolipoprotein E and Alzheimer disease: risk, mechanisms and therapy. *Nat. Rev. Neurol.* 9, 106–118. doi: 10.1038/nrneurol.2012.263

Mielke, M. M. (2018). Sex and gender differences in Alzheimer's disease dementia. *Psychiatr. Times* 35, 14–17.

Mortimer, J. A., Borenstein, A. R., Gosche, K. M., and Snowdon, D. A. (2005). Very early detection of Alzheimer neuropathology and the role of brain reserve in modifying its clinical expression. *J. Geriatr. Psychiatry Neurol.* 18, 218–223. doi: 10.1177/0891988705281869

Myung, W., Lee, C., Park, J. H., Woo, S. Y., Kim, S., Kim, S., et al. (2017). Occupational attainment as risk factor for progression from mild cognitive impairment to Alzheimer's disease: a CREDOS study. *J. Alzheimers Dis.* 55, 283–292. doi: 10.3233/JAD-160257

Pavlik, V. N., Doody, R. S., Massman, P. J., and Chan, W. (2006). Influence of premorbid IQ and education on progression of Alzheimer's disease. *Dement. Geriatr. Cogn. Disord.* 22, 367–377. doi: 10.1159/000095640

Pettigrew, C., Soldan, A., Zhu, Y., Wang, M. C., Brown, T., Miller, M., et al. (2017). Cognitive reserve and cortical thickness in preclinical Alzheimer's disease. *Brain Imaging Behav.* 11, 357–367. doi: 10.1007/s11682-016-9581-y

Reed, B. R., Mungas, D., Farias, S. T., Harvey, D., Beckett, L., Widaman, K., et al. (2010). Measuring cognitive reserve based on the decomposition of episodic memory variance. *Brain* 133, 2196–2209. doi: 10.1093/brain/awq154

Reijs, B. L. R., Vos, S. J. B., Soininen, H., Lotjonen, J., Koikkalainen, J., Pikkarainen, M., et al. (2017). Association between later life lifestyle factors and Alzheimer's disease biomarkers in non-demented individuals: a longitudinal descriptive cohort study. *J. Alzheimers Dis.* 60, 1387–1395. doi: 10.3233/JAD-170039

Robitaille, A., Van Den Hout, A., Machado, R. J. M., Bennett, D. A., Cukic, I., Deary, I. J., et al. (2018). Transitions across cognitive states and death among older adults in relation to education: A multistate survival model using data from six longitudinal studies. *Alzheimers Dement.* 14, 462–472. doi: 10.1016/j.jalz.2017.10.003

Safieh, M., Korczyn, A. D., and Michaelson, D. M. (2019). ApoE4: an emerging therapeutic target for Alzheimer's disease. *BMC Med.* 17:64. doi: 10.1186/s12916-019-1299-4

Scarmeas, N., Albert, S. M., Manly, J. J., and Stern, Y. (2006). Education and rates of cognitive decline in incident Alzheimer's disease. *J. Neurol. Neurosurg. Psychiatry* 77, 308–316. doi: 10.1136/jnnp.2005.072306

Serrano-Pozo, A., Frosch, M. P., Masliah, E., and Hyman, B. T. (2011). Neuropathological alterations in Alzheimer disease. *Cold Spring Harb. Perspect. Med.* 1:a006189.

Singh-Manoux, A., Marmot, M. G., Glymour, M., Sabia, S., Kivimaki, M., and Dugravot, A. (2011). Does cognitive reserve shape cognitive decline? *Ann. Neurol.* 70, 296–304. doi: 10.1002/ana.22391

Smart, E. L., Gow, A. J., and Deary, I. J. (2014). Occupational complexity and lifetime cognitive abilities. *Neurology* 83, 2285–2291.

Soldan, A., Pettigrew, C., Cai, Q., Wang, J., Wang, M. C., Moghekar, A., et al. (2017). Cognitive reserve and long-term change in cognition in aging and preclinical Alzheimer's disease. *Neurobiol. Aging* 60, 164–172. doi: 10.1016/j.neurobiolaging.2017.09.002

Stern, Y. (2009). Cognitive reserve. *Neuropsychologia* 47, 2015–2028.

Stern, Y. (2012). Cognitive reserve in ageing and Alzheimer's disease. *Lancet Neurol.* 11, 1006–1012. doi: 10.1016/s1474-4422(12)70191-6

Tate, D. F., Neeley, E. S., Norton, M. C., Tschanz, J. T., Miller, M. J., Wolfson, L., et al. (2011). Intracranial volume and dementia: some evidence in support of the cerebral reserve hypothesis. *Brain Res.* 1385, 151–162. doi: 10.1016/j.brainres.2010.12.038

Valenzuela, M. J., Jones, M., Wen, W., Rae, C., Graham, S., Shnier, R., et al. (2003). Memory training alters hippocampal neurochemistry in healthy elderly. *Neuroreport* 14, 1333–1337. doi: 10.1097/01.wnr.0000077548.91466.05

van Loenhoud, A. C., Van Der Flier, W. M., Wink, A. M., Dicks, E., Groot, C., Twisk, J., et al. (2019). Cognitive reserve and clinical progression in Alzheimer disease: a paradoxical relationship. *Neurology* 93, e334–e346. doi: 10.1212/WNL.0000000000007821

van Loenhoud, A. C., Wink, A. M., Groot, C., Verfaillie, S. C. J., Twisk, J., Barkhof, F., et al. (2017). A neuroimaging approach to capture cognitive reserve: application to Alzheimer's disease. *Hum. Brain Mapp.* 38, 4703–4715. doi: 10.1002/hbm.23695

Vrieze, S. I. (2012). Model selection and psychological theory: a discussion of the differences between the Akaike information criterion (AIC) and the Bayesian information criterion (BIC). *Psychol. Methods* 17, 228–243. doi: 10.1037/a0027127

Zahodne, L. B., Manly, J. J., Brickman, A. M., Siedlecki, K. L., Decarli, C., and Stern, Y. (2013). Quantifying cognitive reserve in older adults by decomposing episodic memory variance: replication and extension. *J. Int. Neuropsychol. Soc.* 19, 854–862. doi: 10.1017/S1355617713000738

Conflict of Interest: The authors declare that the research was conducted in the absence of any commercial or financial relationships that could be construed as a potential conflict of interest.

Publisher's Note: All claims expressed in this article are solely those of the authors and do not necessarily represent those of their affiliated organizations, or those of the publisher, the editors and the reviewers. Any product that may be evaluated in this article, or claim that may be made by its manufacturer, is not guaranteed or endorsed by the publisher.

frontiers | Frontiers in Aging Neuroscience

ORIGINAL RESEARCH
published: 19 April 2022
doi: 10.3389/fnagi.2022.847094

Possibility of Enlargement in Left Medial Temporal Areas Against Cerebral Amyloid Deposition Observed During Preclinical Stage

Etsuko Imabayashi[1,2], Kenji Ishii[1], Jun Toyohara[1], Kei Wagatsuma[1,3], Muneyuki Sakata[1], Tetsuro Tago[1], Kenji Ishibashi[1], Narumi Kojima[4], Noriyuki Kohda[5], Aya M. Tokumaru[6] and Hunkyung Kim[4]*

[1] Research Team for Neuroimaging, Tokyo Metropolitan Institute of Gerontology, Tokyo, Japan, [2] Diagnostic and Therapeutic Nuclear Medicine Group, Department of Molecular Imaging and Theranostics, Quantum Life and Medical Science Directorate, Institute for Quantum Medical Science, National Institutes for Quantum and Radiological Science and Technology, Chiba, Japan, [3] School of Allied Health Sciences, Kitasato University, Sagamihara, Japan, [4] Research Team for Promoting Independence and Mental Health, Tokyo Metropolitan Institute of Gerontology, Tokyo, Japan, [5] Nutraceuticals Division, Otsu Nutraceuticals Research Institute, Otsuka Pharmaceutical Co., Ltd., Tokyo, Japan, [6] Department of Radiology, Tokyo Metropolitan Institute of Gerontology, Tokyo, Japan

OPEN ACCESS

Edited by:
Chu-Chung Huang,
East China Normal University, China

Reviewed by:
Pei-Lin Lee,
National Yang-Ming University, Taiwan
Melissa Edler,
Kent State University, United States

***Correspondence:**
Etsuko Imabayashi
imabayashi@pet.tmig.or.jp;
imabayashi.etsuko@qst.go.jp

Specialty section:
This article was submitted to Alzheimer's Disease and Related Dementias, a section of the journal Frontiers in Aging Neuroscience

Received: *01 January 2022*
Accepted: *18 March 2022*
Published: *19 April 2022*

Citation:
Imabayashi E, Ishii K, Toyohara J, Wagatsuma K, Sakata M, Tago T, Ishibashi K, Kojima N, Kohda N, Tokumaru AM and Kim H (2022) Possibility of Enlargement in Left Medial Temporal Areas Against Cerebral Amyloid Deposition Observed During Preclinical Stage. Front. Aging Neurosci. 14:847094. doi: 10.3389/fnagi.2022.847094

Neurodegenerative changes in the preclinical stage of Alzheimer's disease (AD) have recently been the focus of attention because they may present a range of treatment opportunities. A total of 134 elderly volunteers who lived in a local community were investigated and grouped into preclinical and mild cognitive impairment stages according to the Clinical Dementia Rating test; we also estimated amyloid deposition in the brain using positron emission tomography (PET). A significant interaction between clinical stage and amyloid PET positivity on cerebral atrophy was observed in the bilateral parietal lobe, parahippocampal gyri, hippocampus, fusiform gyrus, and right superior and middle temporal gyri, as previously reported. Early AD-specific voxel of interest (VOI) analysis was also applied and averaged Z-scores in the right, left, bilateral, and right minus left medial temporal early AD specific area were computed. We defined these averaged Z-scores in the right, left, bilateral, and right minus left early AD specific VOI in medial temporal area as R-MedT-Atrophy-score, L-MedT-Atrophy-score, Bil-MedT-Atrophy-score, and R_L-MedT-Atrophy-score, respectively. It revealed that the R_L-MedT-Atrophy-scores were significantly larger in the amyloid-positive than in the amyloid-negative cognitively normal (CN) elderly group, that is, the right medial temporal areas were smaller than left in amyloid positive CN group and these left-right differences were significantly larger in amyloid positive than amyloid negative CN elderly group. The L-MedT-Atrophy-score was slightly larger (p = 0.073), that is, the left medial temporal area was smaller in the amyloid-negative CN group than in the amyloid-positive CN group. Conclusively, the left medial temporal area could be larger in CN participants with amyloid deposition than in those without amyloid deposition. The area under the receiver operating characteristic curve for differentiating amyloid positivity among CN participants using the R_L-MedT-Atrophy-scores was 0.73; the sensitivity and specificity were 0.828

and 0.606, respectively. Although not significant, a negative correlation was observed between the composite cerebral standardized uptake value ratio in amyloid PET images and L-MedT-Atrophy-score in CN group. The left medial temporal volume might become enlarged because of compensatory effects against AD pathology occurring at the beginning of the amyloid deposition.

Keywords: Alzheimer's disease, compensation, voxel-based morphometry, MRI, amyloid, preclinical, MCI

INTRODUCTION

Alzheimer's disease (AD) is a progressive neurodegenerative disease that is histopathologically characterized by an accumulation of senile plaques consists of amyloid beta and neurofibrillary tangles consist of tau. According to the criteria published by the National Institute on Aging – Alzheimer's Association (NIA-AA) in 2011, the concept of clinical stages of AD; preclinical AD, MCI due to AD, and AD dementia, are adopted as pathophysiological continuum with a temporal order of biomarker changes for amyloid beta and neurodegeneration. In 2018, NIA-AA updated and unified this guideline and labeled it as research framework (Jack et al., 2018). Within this research framework, tau was defined as an independent biomarker, and the diagnosis of AD was totally based on the biomarkers for amyloid beta, tau and neurodegeneration, but not on the stage of clinical symptoms. In this study, we studied the relationship between amyloid deposition measured with positron emission tomography (PET) and neurodegeneration as atrophy evaluated by magnetic resonance imaging (MRI). Amyloid deposition starts years before objective clinical cognitive impairment, continuous morphological medial temporal atrophy is reportedly appeared on MRI mainly with comparison in mild cognitive impairment (MCI) stage to cognitively normal controls (Zhang et al., 2021).

In the late 1980s, morphometry for AD was first attempted with manual tracing on MRI (Seab et al., 1988), followed by voxel-based volumetric analysis at the beginning of this century (Ohnishi et al., 2001). An automated voxel-based morphometry procedure was then developed around the same time as the first effective symptomatic treatment; since then, clinically automated procedures for medial temporal atrophy evaluation have progressed (Matsuda et al., 2012). In the early clinical stage of AD, atrophy begins in the medial temporal area, trans-entorhinal region, entorhinal cortex, and hippocampus (Arnsten et al., 2021). Atrophy in these areas can be automatically detected using Z-score analysis, which compares each individual image with healthy images from a database (Matsuda et al., 2012). We used the Voxel-based Specific Regional Analysis System for Alzheimer's Disease (VSRAD®), which is Japanese-approved software using Statistical Parametric Mapping (SPM) 8 and the Diffeomorphic Anatomical Registration using Exponentiated Lie Algebra (DARTEL) algorithm for tissue segmentation and spatial normalization. VSRAD produces Z-score map after comparison to normal database preinstalled in the software and then calculates the mean Z-score within the bilateral, left, right, and right-minus-left early AD–specific voxel of interest (VOI). These disease-specific VOIs are the areas with statistically significant volume change between the early clinical stage of AD and normal control demarcated on the t-map obtained from group comparison, that is, data-driven optimized VOI. Analyses using these statistical masks are better than anatomical VOI at differentiating disease condition from disease-free condition because they reflect pathological condition (Herholz et al., 2002; Hirata et al., 2005).

Recently, neuromorphological changes associated with cognitive changes in the preclinical stages of AD have been investigated with amyloid positron emission tomography (PET) data. Amyloid deposition has been shown to occur more than 10 years before symptom onset, and these preclinical stages may provide a more effective opportunity for therapy (Sperling et al., 2011).

In this study, to evaluate volume change within the preclinical stage of AD influenced by amyloid deposition, voxel-based comparison of tissue-segmented MR images using volumetric methods was performed among four groups [amyloid-negative cognitively normal (CN), amyloid-positive CN, amyloid-negative with MCI, and amyloid-positive with MCI] to confirm the regional distribution of atrophy. Then, early AD-specific VOI analyses were performed on MRI data to mainly evaluate whether any early volume change could be detected even among CN participants at the preclinical stage within the area known to shrink during the early stage of symptomatic AD.

MATERIALS AND METHODS

Participants

This was a prospective single-cohort study of volunteers who lived in Itabashi-ku, Tokyo. A total of 136 participants were recruited, all of whom lived independently. The Clinical Dementia Rating (CDR) and Mini Mental State Examination (MMSE) scales were administered, education duration was determined, and brain scans were performed for all participants. MRI scans were performed for screening and volumetry, and amyloid PET using ^{18}F-flutemetamol was used to determine amyloid accumulation in the brain and to quantify the degree of amyloid accumulation.

Image Scanning

Screening and volumetric MRIs were performed using Achieva 1.5T (Philips Healthcare, Andover, MA, United States). T1-weighted 3D turbo field echo SENSE1 sequence was used for volumetric MRI.

^{18}F-Flutemetamol PET images were acquired using Discovery MI (GE Healthcare, Milwaukee, WI, United States) as a 30-min scan starting 90 min after injection of approximately 185 MBq of ^{18}F-flutemetamol. Images were reconstructed using a 3D-ordered subset expectation maximization method with a time-of-flight procedure.

Visual Interpretation of Amyloid Positron Emission Tomography Images

Two experts with more than 7 years of experience in visual interpretation of amyloid PET images interpreted the images according to the procedure approved by the US Food and Drug Administration[1]: The brightness of the pons was adjusted to 90% of the maximum intensity of the color scale, and the accumulation of flutemetamol in five regions (frontal lobes, posterior cingulate and precuneus, lateral temporal lobes, inferolateral parietal lobes, and striatum) was evaluated. A scan was judged as positive if at least one region has gray matter radioactivity that is as intense as or exceeds the intensity of the adjacent white matter. Both experts were blinded to the participants' information. When judgments were conflicting, both positive and negative, the final judgment was reached by consensus.

Quantification of Amyloid Positron Emission Tomography Images

The CortexID Suite[2] is a fully automated quantification method reported to agree well with the histopathologic classification of neuritic plaque density and has a strong concordance with visual read results (Thurfjell et al., 2014). The reference region was the pons, and the average standardized uptake value ratio (SUVR) within the composite VOIs was fully automatically computed from SUVR images that were spatially normalized to the Montreal Neurological Institute (MNI) template space (Thurfjell et al., 2014) as CortexID composite SUVR images ($SUVR_{CortexID}$).

Voxel-Based Morphometry

For voxel-based morphometry, the Computational Anatomy Toolbox 12 (CAT12)[3] was used for image processing. The tissue segmentation procedure was initialized using standard tissue probability maps in SPM12[4] and the DARTEL algorithm (Ashburner, 2007) was used.

Statistical Analyses

Voxel-Based Analysis

A full factorial design was applied for voxel-based analysis using SPM12. A two-way factorial design with two factors was used: clinical stage (CN or MCI) and visual interpretation of amyloid PET accumulation (positive or negative). The interaction between clinical stage and amyloid PET positivity with the regional cortex volume variable was measured. Age and sex were removed from the comparison as nuisance variables, and total intracranial volume (TIV) was measured by summation of the brain cortex, white matter, and cerebrospinal fluid (CSF) space and used to correct inter-subject size variation through voxel-based analyses (Malone et al., 2015).

Voxel of Interest-Based *Z*-Score Analysis

Z-score analysis using a voxel-based specific regional analysis system for AD (VSRAD; Japanese Medical Device approval number 30200BZX00060000) was applied to 3D volumetric MR images. The operation achieved by VSRAD automatically is as follows: first, volumetry was performed using SPM8 and DARTEL, including tissue segmentation, spatial normalization, and smoothing. Second, the Z-score was calculated within each voxel compared with the normal database preinstalled within this software (Matsuda et al., 2012). Z-scores were calculated for each voxel using the following formula:

$$Z\ \text{score} = \frac{\text{mean voxel value of normal database} - \text{subject's voxel value}}{\text{standard deviation of normal database}},$$

Where large Z-scores mean both smaller volume and severe atrophy.

Third, using specific VOIs for early AD in the medial temporal area in the MNI space, the VSRAD program automatically computed the averaged positive *Z*-score values within the right, left, bilateral and right-minus-left VOI values (Matsuda et al., 2012). In **Figure 1**, the VOIs for early AD in VSRAD are shown in red superimposed on the cortex in the MNI space. We defined averaged Z-score in this specific VOIs for early AD in the medial temporal area as MedT-Atrophy-score. The interaction between clinical stage and amyloid positivity on the averaged *Z*-score value in the right-specific VOI; R-MedT-Atrophy-scores, left-specific VOI; L-MedT-Atrophy-scores, bilateral-specific VOI; Bil-MedT-Atrophy-scores, and right-minus-left VOI; R_L-MedT-Atrophy-scores was statistically examined using EZR software (Saitama Medical Center, Jichi Medical University, Tochigi, Japan)[5], which is a graphical user interface for R version 4.0.3 (The R Foundation for Statistical Computing, Vienna, Austria). More precisely, it is a modified version of R commander version 2.7–1 designed to add statistical functions frequently used in biostatistics (Kanda, 2013). All *p*-values were two-sided, with p-value ≤ 0.05 considered statistically significant. One-way analysis of variance and multiple comparisons were applied based on whether participants in each group (CN or MCI) were visually amyloid-positive or amyloid-negative and the *post hoc* test was applied with R software with age, sex and TIV as nuisance covariates. For the four groups (amyloid-positive CN, amyloid-positive MCI, amyloid-negative CN,

[1]https://www.accessdata.fda.gov/drugsatfda_docs/label/2017/203137s008lbl.pdf
[2]https://www.gehealthcare.co.uk/-/media/13c81ada33df479ebb5e45f450f13c1b.pdf
[3]http://www.neuro.uni-jena.de/cat/
[4]https://www.fil.ion.ucl.ac.uk/spm/software/spm12/
[5]https://www.jichi.ac.jp/saitama-sct/SaitamaHP.files/statmedEN.html

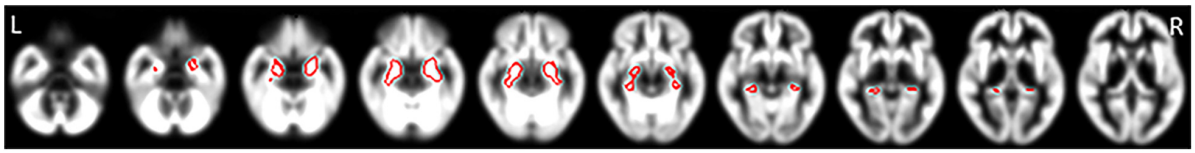

FIGURE 1 | Specific VOIs for early AD in the medial temporal area of the brain cortex in the MNI space preinstalled in the VSRAD program. VOIs for early AD are drawn in red superimposed on segmented cortical T1-weighted MR images in the MNI space. Averaged positive *Z*-score values within each right, left, and bilateral VOI and the right-minus-left values were computed (Matsuda et al., 2012). We defined these *Z*-scores as R-MedT-Atrophy-score, L-MedT-Atrophy-score, Bil-MedT-Atrophy-score, and R_L-MedT-Atrophy-score, respectively. VOI, voxel of interest; AD, Alzheimer's disease; MNI, Montreal Neurological Institute; VSRAD, Voxel-based Specific Regional Analysis System for Alzheimer's Disease; MRI, magnetic resonance imaging.

TABLE 1 | Participants' demographic characteristics.

	Total (*n* = 134)	**Visually amyloid-positive**		**Visually amyloid-negative**	
		CN stage (CDR 0) (*n* = 29)	**MCI (CDR 0.5–1) (*n* = 18)**	**CN stage (CDR 0) (*n* = 70)**	**MCI (CDR 0.5–1) (*n* = 17)**
Age (years)	79.18 ± 4.03	79.4 ± 4.66 (68–86)	80.3 ± 2.80$^{\blacklozenge}$ (75–86)	79.2 ± 4.10 (68–86)	77.6 ± 3.50$^{\blacklozenge}$ (69–84)
Female/male ratio	95:39	26:3	14:4	50:20	8:9
MMSE	27.80 ± 2.16	27.9 ± 2.17* (24–30)	26.1 ± 2.33* (22–30)	28.4 ± 1.63† (24–30)	26.9 ± 2.80† (22–30)
		27.2 ± 2.39*		28.1 ± 1.99*	
$SUVR_{CortexID}$	0.517 ± 0.130	0.652 ± 0.115**	0.678 ± 0.119§	0.435 ± 0.0357$^{\divideontimes}$**	0.456 ± 0.0449$^{\divideontimes\S}$
Education (years)	12.9 ± 2.51	12.6 ± 2.06	11.4 ± 2.62	13.4 ± 2.46	13.2 ± 2.81
		12.1 ± 2.34***		13.4 ± 2.34***	
TIV (mL)		1381 ± 134.9$^{\Phi}$	1385 ± 122.2¶	1446 ± 133.9$^{\Phi}$	1510 ± 142.1¶

Values are presented as mean ± standard deviation (range) or ratio.
*Comparison between $^{\blacklozenge}$amyloid-positive vs. amyloid-negative MCI, p = 0.0192. *Amyloid-positive CN vs. MCI, p = 0.00865. †Amyloid-negative CN vs. MCI, p = 0.00449. *Amyloid-positive CN and MCI vs. amyloid-negative CN and MCI, p = 0.0300. **Amyloid-positive vs. amyloid-negative CN, p < 0.0001. §Amyloid-positive and amyloid-negative MCI, p < 0.0001. ¶Amyloid-positive and amyloid-negative MCI, p = 0.00865. $^{\divideontimes}$Amyloid-negative CN vs. MCI, p = 0.0378. ***Amyloid-positive vs. amyloid-negative CN and MCI, p = 0.00749. $^{\Phi}$Amyloid-positive vs. amyloid-negative CN, p = 0.0309.*
CN, cognitively normal; MCI, mild cognitive impairment; CDR, Clinical Dementia Rating; MMSE, Mini Mental State Examination; SUVR, standardized uptake value ratio; TIV, total intracranial volume.

and amyloid-negative MCI) in which significant differences in MedT-Atrophy-scores were observed even at the preclinical stage, the receiver operating characteristic (ROC) curve was plotted to estimate the clinical ability to differentiate amyloid positivity.

The Pearson product-moment correlation coefficients of $SUVR_{CortexID}$ and MedT-Atrophy-scores and of education duration and MedT-Atrophy-scores were also computed using EZR. *p*-values ≤ 0.05 were considered statistically significant.

RESULTS

The MRI scans for screening and volumetry as well as amyloid PET scans were examined in 136 participants (female/male ratio, 96/40; mean age, 79.2 ± 4.0 years). Two participants, one whose volumetric MRI scan could not be segmented and another who had sequelae from a contusion in the temporal lobes, were excluded. The demographics of the remaining 134 participants are presented in **Table 1**. The global CDR score was used to determine the CN preclinical (CDR 0) or MCI stage (CDR 0.5 or 1.0) of AD. Among the 99 participants in the preclinical stage, 29 had positive amyloid PET scans and 70 had negative scans in the visual read. Among the 35 participants in the MCI group, 18 had positive scans and 17 had negative scans in the visual interpretation of amyloid PET images.

Participants with MCI with visually interpreted amyloid PET positivity were significantly older than amyloid-negative participants with MCI. The MMSE scores were significantly lower in the MCI stage than in the preclinical stage for the amyloid-positive and amyloid-negative groups. However, the MMSE scores were not significantly different between patients in the amyloid-negative and amyloid-positive CN groups or between the amyloid-negative and amyloid-positive MCI groups. $SUVR_{CortexID}$ was significantly higher in the visually amyloid-positive group. Within the amyloid-positive group, no significant difference in $SUVR_{CortexID}$ was observed between the preclinical and MCI stages. Within the amyloid-negative group, those with MCI showed a significantly higher $SUVR_{CortexID}$ than those at a preclinical stage. The visually amyloid-negative group had significantly more years of education than the amyloid-positive group. However, no significant differences were observed between the preclinical and MCI groups in this variable. The TIV, which consisted of the brain cortex, white matter, and CSF space, was significantly smaller in the visually amyloid-positive group than in the amyloid-negative group at both the preclinical and MCI stages. Accordingly, the TIV was measured and used to correct for different brain sizes and volumes.

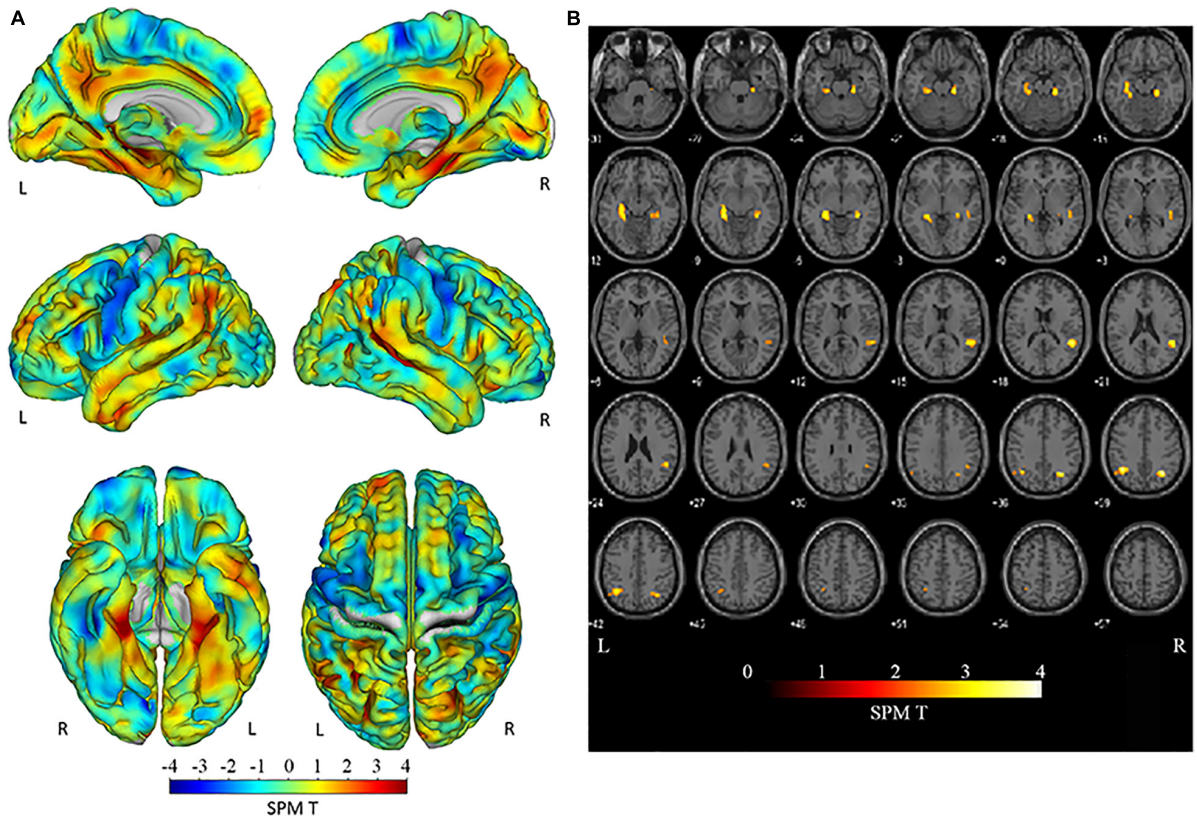

FIGURE 2 | Negative interaction between clinical stages and amyloid positivity on brain cortex atrophy. **(A)** The SPM T map superimposed on the surface MR image in the MNI space showing atrophied areas both with clinical stage progression and amyloid positivity. Atrophy was observed in the parietal lobe, from the posterior cingulate to the precunei, from the middle to the posterior medial temporal area, and the left temporal tip. **(B)** Regions with statistically significant ($p < 0.01$; extent threshold, 300 voxels) atrophy in **(A)** superimposed on the template brain T1-weighted MR image in the MNI space. The anatomical labels of these statistically significantly atrophied areas, including the bilateral parietal lobe, parahippocampal gyri, hippocampus, fusiform, and right superior and middle temporal gyri, are presented in **Table 2**. Atrophy from the precuneus to the PCC and left temporal gyri was also observed but without significant differences. SPM, Statistical Parametric Mapping; MNI, Montreal Neurological Institute; PCC, posterior cingulate cortex.

Figure 2A shows the interaction between clinical stages and amyloid positivity in atrophy of the brain cortex. **Figure 2B** shows statistically significant ($p < 0.01$, extent threshold 300 voxels without multiple comparison) atrophied regions within **Figure 2A** superimposed on the template brain T1-weighted MR image in the MNI space. The anatomical labels of these statistically significantly atrophied areas are presented in **Table 2** and include the bilateral parietal lobe, parahippocampal gyri, hippocampus, fusiform, and right superior and middle temporal gyri. Non-significant atrophy from the precuneus to the posterior cingulate cortex (PCC) and left temporal gyri was observed. No significant positive interaction was observed in the cerebral cortex; a significant positive interaction was observed only in the cerebellum.

The results of MedT-Atrophy-score analysis are shown in **Figure 3**. Interactions were observed among the L-MedT-Atrophy-scores ($p = 0.0022$), Bil-MedT-Atrophy-scores ($p = 0.013$), and R_L-MedT-Atrophy-scores ($p = 0.019$). Though any significant influence of age, sex, and TIV were not observed, we added them as nuisance variables and the *post hoc* test revealed significantly more severe atrophy in the amyloid-positive group than in the amyloid-negative group within the MCI stage on the L-MedT-Atrophy-scores ($p = 0.034$) and Bil-MedT-Atrophy-score ($p = 0.018$) as well as a significant

TABLE 2 | Areas of significant negative interaction between clinical stages and amyloid positivity on brain cortex atrophy observed in **Figure 2A**.

T-value	Size	*x*, *y*, and *z* (mm)	Area
4.34	358	33, −60, 38	Right angular gyrus
			Right superior and middle occipital
4.02	552	−39, −56, 39	Left angular gyrus
			Left superior and inferior parietal lobule
3.85	907	35, −36, −8	Right parahippocampal gyrus
			Right hippocampus
			Right fusiform
3.77	1152	54, −45, 18	Right superior and middle temporal gyrus
			Right angular gyrus
3.57	1556	−27, −36, −9	Left hippocampus
			Left parahippocampal gyrus
			Left fusiform

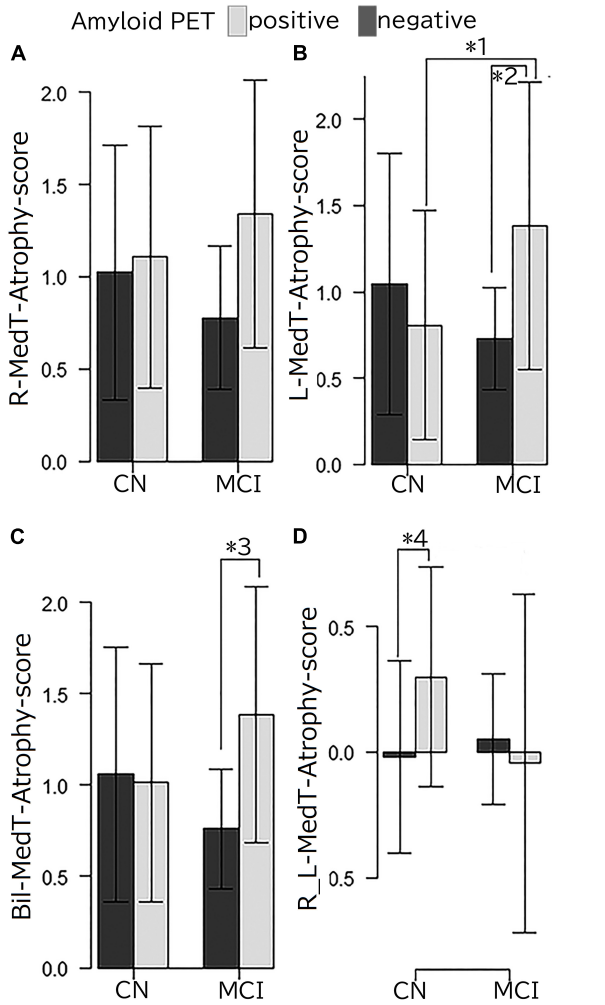

FIGURE 3 | (A) R-MedT-Atrophy-scores, **(B)** L-MedT-Atrophy-scores, **(C)** Bil-MedT-Atrophy-scores, and **(D)** R_L-MedT-Atrophy-scores R, right; L, left; Bil, bilateral; R_L, right minus left; MedT-Atrophy-score, averaged *Z*-score values in early AD-specific medial temporal VOIs preinstalled in the Voxel-based Specific Regional Analysis System for Alzheimer's Disease. Interaction of clinical stage and amyloid positivity in the mean *Z*-score value in the right-specific, left-specific, bilateral-specific, and R_L VOIs ($p = 0.081$, $p = 0.0022$, $p = 0.013$, and $p = 0.019$, respectively). Multiple comparison analysis after one-way analysis of variance using the Turkey-Kramer method with age, sex and TIV as nuisance variables had the following results: *1, $p = 0.016$; *2, $p = 0.034$; *3, $p = 0.018$; *4, $p = 0.0013$. Among the clinically normal participants, the L-MedT-Atrophy-scores were smaller in the amyloid-negative participants than in amyloid-positive ones, but the difference was not significant; the R_L-MedT-Atrophy-scores were significantly larger in the amyloid-positive participants than in the amyloid-negative participants.

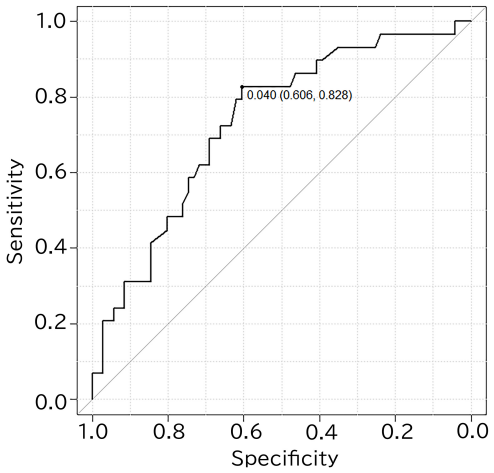

FIGURE 4 | ROC curve for differentiating amyloid positivity in cognitively normal participants using the R_L-MedT-Atrophy-scores. The area under the curve, sensitivity, specificity and accuracy were 0.733 (95% confidence interval, 0.626–0.84) (DeLong et al., 1988), 0.828, 0.606, and 0.666, respectively. ROC, receiver operating curve; VOI, voxel of interest; R_L, right minus left; MedT-Atrophy-score, averaged *Z*-score values in early AD-specific medial temporal VOIs preinstalled in the Voxel-based Specific Regional Analysis System for Alzheimer's Disease.

difference between amyloid-positive and amyloid-negative groups within the preclinical stage on R_L-MedT-Atrophy-score ($p = 0.0013$). This significant laterality disappeared in the MCI group. Within the amyloid-positive group between CN and MCI, other significant differences were observed on the L-MedT-Atrophy-score ($p = 0.016$) and slight difference were observed on the R_L-MedT-Atrophy-score ($p = 0.051$).

The performance for predicting visual amyloid positivity or negativity using R_L-MedT-Atrophy-score was quantified using an ROC curve. The area under the curve, sensitivity, specificity, and accuracy were 0.733 [95% confidence interval (CI), 0.626–0.84] (DeLong et al., 1988), 0.828, 0.606, and 0.666, respectively (**Figure 4**).

The correlation coefficients of $SUVR_{CortexID}$ and MedT-Atrophy-scores were only significant in the R_L-MedT-Atrophy-score in the preclinical stage ($p = 0.00865$). The Pearson product-moment correlation coefficient was 0.261 (95% CI, 0.0683–0.435) (**Figure 5**). Furthermore, a slight negative correlation was observed in the L-MedT-Atrophy-scores in the preclinical stage ($p = 0.143$). The Pearson product-moment correlation coefficient was −0.148 (95% CI, −0.334–0.0503) (**Supplementary Figure 1**).

The correlation coefficients of education duration and MedT-Atrophy-scores were only significant in the R-MedT-Atrophy-score in the MCI stage ($p = 0.0196$). The Pearson product-moment correlation coefficient was 0.544 (95% CI, 0.103–0.806) (**Figure 6**).

DISCUSSION

This cohort study evaluated volume change within the preclinical stage of AD influenced by amyloid deposition through ^{18}F-flutemetamol amyloid PET and volumetric MRI on elderly participants living an ordinary life in a downtown area of Tokyo. In the voxel-based group analysis, significant atrophy in the medial temporal and lateral parietal was observed due to the interaction of stages and visually interpreted amyloid PET

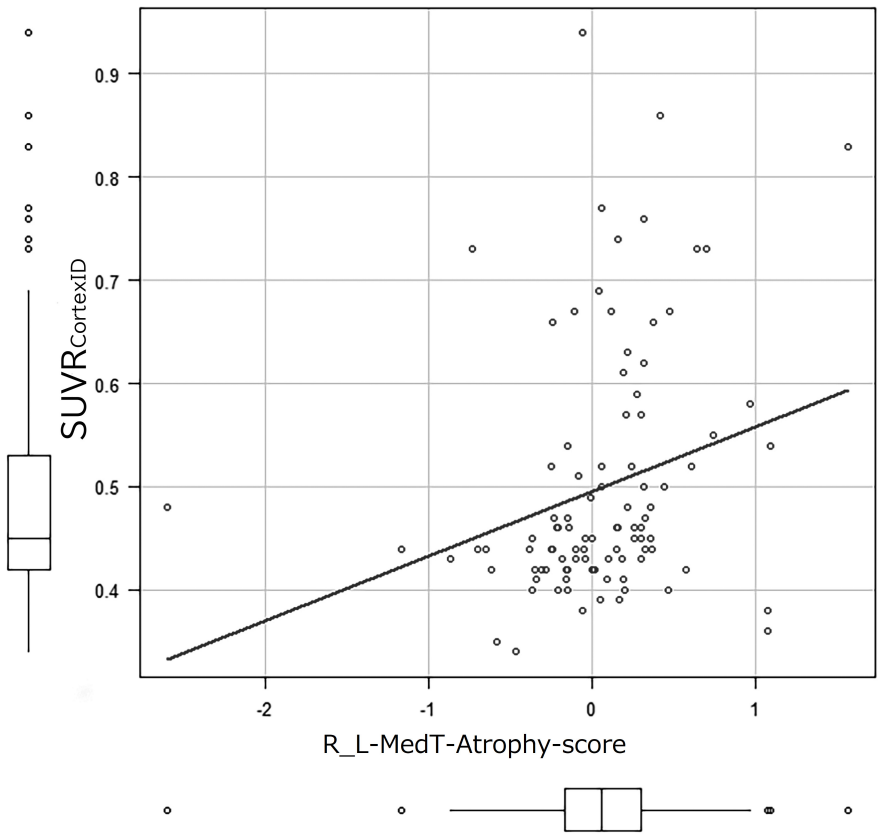

FIGURE 5 | Correlation coefficient between $SUVR_{CortexID}$ and MedT-Atrophy-score. A significant correlation was observed only in the R_L-MedT-Atrophy-scores at the preclinical stage (p = 0.00865). The Pearson's product-moment correlation coefficient was 0.261 (95% confidence interval, 0.0683–0.435). R_L, right minus left; MedT-Atrophy-score, averaged Z-score values in early AD-specific medial temporal VOIs preinstalled in the Voxel-based Specific Regional Analysis System for Alzheimer's Disease; $SUVR_{CortexID}$, average standardized uptake value ratio within the composite VOIs in the Montreal Neurological Institute space obtained with the CortexID Suite.

positivity. In the individual early AD-specific VOI analysis, a significant difference in R_L-MedT-Atrophy score was observed between the amyloid-positive and amyloid-negative participants, even in the CN stage.

In this study, the participants in the visually amyloid-positive MCI group were significantly older than those in the visually amyloid-negative MCI group. Younger elderly patients with MCI due to non-AD or older elderly patients with MCI due to AD might be easily included in this cohort study. On the contrary, older elderly patients with MCI due to non-AD or younger elderly patients with MCI due to AD might mainly refuse to participate in this study. Younger patients with MCI due to AD (i.e., early-onset AD) usually have more severe or progressive symptoms; thus, they might hesitate or refuse to attend a study recruiting normal participants. Alternatively, perhaps due to their heightened awareness of the disease, they might choose to go to the hospital rather than attend a study. Age and sex were removed from comparison as nuisance variables. The TIV was significantly smaller in the amyloid-positive group than in the amyloid-negative group at both preclinical and MCI stages. The TIV was used to correct for different brain sizes and volumes.

Brain atrophy was investigated cross-sectionally in the amyloid-negative and amyloid-positive groups during preclinical and MCI stages. Atrophy in the hippocampus and parahippocampal gyrus is a well-established finding in patients with MCI due to AD (Matsuda et al., 2012) and even in patients with early MCI (Grothe et al., 2016), which is consistent with our study. Only a loose criterion without multiple comparison could be used in our study, which we considered to be due to the inclusion of preclinical cases. Except for these regions, the lateral temporal areas showed atrophy in those with late MCI in the Alzheimer's Disease Neuroimaging Initiative (ADNI) cohort (Grothe et al., 2016). In our study, except for the medial temporal area, atrophy in the lateral parietal regions was observed across the CN to the MCI stage according to the status of amyloid PET positivity or negativity (**Figure 2B** and **Table 2**). This difference might be attributed to the difference in the patients' age between studies; participants in our study were older than those in the ADNI cohort (Grothe et al., 2016). Furthermore, cognitive reserve and education duration may have also resulted in bias. Baukneht et al. (2018) reported hypometabolism in the parietal area in the highly educated group. The education duration in our

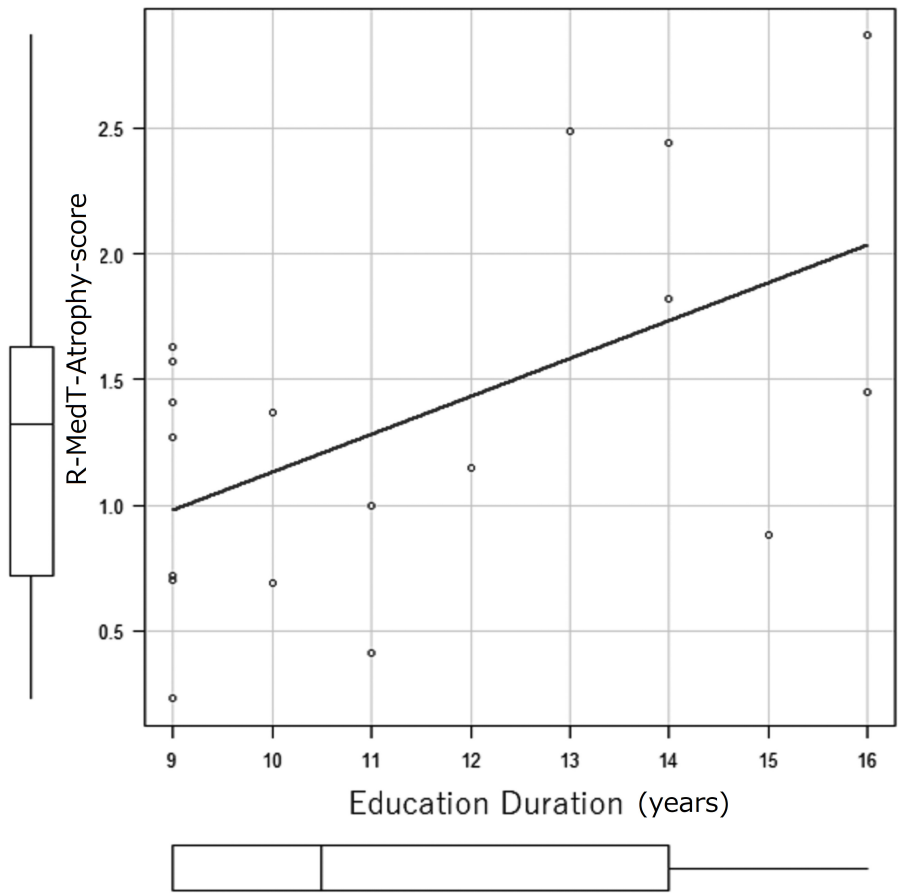

FIGURE 6 | Correlation coefficient between education duration (years) and MedT-Atrophy-score. A significant correlation was observed only in the R-MedT-Atrophy-scores at the CN stage (p = 0.0196). The Pearson's product-moment correlation coefficient was 0.544 (95% confidence interval, 0.103–0.806). R, right; MedT-Atrophy-score, averaged Z-score values in early AD-specific medial temporal VOIs preinstalled in the Voxel-based Specific Regional Analysis System for Alzheimer's Disease.

study was shorter than that in the ADNI cohort but longer than that in the study of Bauckneht et al. (2018); furthermore, participants in our study showed more atrophy in the parietal area than those in the study of Bauckneht et al. (2018). Thus, depending on education and age, cognitive reserve might affect the distribution of atrophy.

Conclusively, medial temporal atrophy was observed in those with amyloid-positive MCI in this study. In a previous report, the medial temporal areas showed atrophy in patient with MCI due to AD with only clinical diagnosis and without amyloid confirmation (Matsuda et al., 2012). However, we confirmed this shrinkage in a more posterior lesion of the medial temporal area than those shown in a previous report (Matsuda et al., 2012) of amyloid deposition at an earlier stage.

MedT-Atrophy-scores were also computed in our study; data of participants in this study were compared with normal data set preinstalled in VSRAD using early AD-specific VOIs, which were also preinstalled in VSRAD. In the amyloid-positive group, the L-MedT-Atrophy-scores was significantly larger; that is, the medial temporal areas were significantly smaller or more atrophied in the MCI group than in the preclinical CN group. Concerning the size differences between the right and left medial temporal volumes in the preclinical stage, the R_L-MedT-Atrophy-scores were significantly larger in amyloid-positive than in amyloid-negative participants. This significant difference of R_L-MedT-Atrophy-scores between amyloid-positive and amyloid-negative groups in the preclinical CN stage was not observed in the MCI stage; moreover, the R_L-MedT-Atrophy-scores were slightly smaller in the amyloid-positive group at the MCI stage than in the group at the CN stage (p = 0.051). Furthermore, an additional ROC curve showed significant discrimination between amyloid-positive and amyloid-negative participants even in the preclinical stage using these R_L-MedT-Atrophy-scores (area under the curve, 0.733) (**Figure 4**). Larger R_L-MedT-Atrophy-scores indicated small L-MedT-Atrophy-scores or large R-MedT-Atrophy-scores. Thus, there can be two presumptions: either the left medial temporal volumes were larger in the amyloid-positive CN participants than in amyloid-negative CN ones or the right medial temporal volumes were smaller in the amyloid-positive CN participants than in amyloid-negative CN ones. According to **Figures 3A,B**,

although the L-MedT-Atrophy-scores tended to be smaller in the amyloid-positive CN participants than in the amyloid-negative CN ones, and because significant results were observed only in the R_L-MedT-Atrophy-scores, both these factors could be related.

We assumed that a compensatory mechanism is involved in increasing the temporal volume. Medial temporal structures reportedly show increased perfusion (Alsop et al., 2008) or lesser atrophy than that observed in very mild to moderate AD (Matsuda et al., 2002; Guedj et al., 2009). Choi et al. (2021) reported that increased hippocampal glucose uptake was associated with the metabolic reconfiguration of microglia; they measured the triggering receptor expressed on myeloid cells 2 in the CSF. Furthermore, Fox et al. (2005) reported that Aβ immunization responders showed the whole brain and hippocampal volume reduction after 12 months of follow-up; however, the results were not significant and did not reflect worsening cognitive performance. According to these observations, not only medial temporal metabolism and perfusion but also volume change could be induced by immunization in the medial temporal area, and the volume could vary depending on function and inflammation. Regarding the core neuronal part of adult hippocampal neurogenesis (AHN), adult neurogenesis persists throughout adulthood in humans and decreases with age (Babcock et al., 2021), except for a niche part of AHN that includes characteristic extracellular matrix components, distinct vasculature structures, a host of secreted factors, and factors derived by microglia and astrocytes (Araki et al., 2021). AHN also decreases in patients with AD (Li Puma et al., 2020). Neurogenesis that contributes to the addition of new granule to the dentate gyri throughout the lifespan (although the efficiency decreases with age and in AD patients) has been observed in patients with AD as old as 90 years (Tobin et al., 2019). Furthermore, overexpression of human tau in mice reportedly induced AHN deficits but increased astrogenesis, which is associated with a downregulation of gamma-amino butyric acid in mice (Zheng et al., 2020). Hence, an observed increase in the left medial temporal volume could result from an increase in the niche of vascular and glial factors of AHN. This increase in the vascular factor may be attributed to glial cell activity, which may be essential for compensation and form the cognitive reserve.

Concerning the decrease in the right medial temporal volume, a pathology other than amyloid β, especially argyrophilic grain disease, could be considered. Adachi et al. (2010) reported that, in patients with argyrophilic grain stage 3 and CDR as 0, the right medial temporal volume was smaller; additionally, more pathologically extensive argyrophilic grains were observed predominantly in the right side. The mean age of their participants was 81 years. Contrarily, those with argyrophilic grain stage 3 and CDR > 0.5 had a dominant left side. Accordingly, those whose CDR was 0 and amyloid-positive participants in our cohort may have had such right-side dominant degenerative disease in the preclinical stage.

When the atrophy within the early AD-specific VOI of each case was individually compared with a normal database preinstalled in VSRAD using R_L-MedT-Atrophy-scores, we observed a significant difference between the amyloid-positive and amyloid-negative participants, even within the CN groups. Furthermore, when applying this R_L-MedT-Atrophy-scores as thresholds in the preclinical stage, the area under the curve for retrospective discrimination of amyloid positivity and negativity was 0.733. Supposedly, this value was sufficiently high to discriminate amyloid positivity and negativity using only volumetric MRI within the CN stage. We also found a significant correlation between R_L-MedT-Atrophy-scores and composite SUVR calculated with CortexID ($SUVR_{CortexID}$). Accordingly, left medial temporal lesions were suspected to be enlarged due to the compensatory mechanism of the AHN.

Regarding the correlation between education duration and MedT-Atrophy-scores we hypothesized that if the right medial temporal area is more vulnerable and more atrophied for amyloid deposition than the left medial temporal area, the cognitive reserve in participants with long duration of education might maintain them in the MCI stage clinically, despite progression of shrinkage.

There is evidence of laterality in volume preservation in the medial temporal area that might correlate with compensation and cognitive reserve; however, this study has some limitations. The results were from only one cohort; hence, another cohort is needed to ensure such volume preservation and discuss compensation. Furthermore, in terms of brain and sex difference, our study included more women than men; thus, our result might be mostly representative of female sex. As the cohort in the present study was very small to compare female and male, comparison between male and female should be performed in a study with a larger cohort.

DATA AVAILABILITY STATEMENT

The original contributions presented in the study are included in the article/**Supplementary Material**, further inquiries can be directed to the corresponding author/s.

ETHICS STATEMENT

The studies involving human participants were reviewed and approved by the Ethical Committee of the Tokyo Metropolitan Institute of Gerontology. The patients/participants provided their written informed consent to participate in this study.

AUTHOR CONTRIBUTIONS

HK designed and coordinated the study. NoK coordinated the study. EI performed the neuroimaging analysis, interpreted the neuroimaging data, and drafted the manuscript. KIi interpreted the imaging data and drafted the manuscript. AT clinically interpreted the neuroimaging data, designed the neuroimaging protocols, and reviewed the manuscript. JT and TT produced and qualified the tracer. KW performed and

qualified the PET imaging data. MS performed the statistical analysis and reviewed the manuscript. KIb and NaK performed cognitive assessments and reviewed the manuscript. All authors contributed to the article and approved the submitted version.

FUNDING

This research was supported by the Japan Agency for Medical Research and Development (AMED) under grant numbers JP20dk0207051 and JP21ae0101077. This study received funding from Otsuka Pharmaceutical Co., Ltd. The funder was not involved in the study design, collection, analysis, interpretation of data, writing of the article, or decision to submit it for publication.

ACKNOWLEDGMENTS

We would like to thank Editage (www.editage.com) for English language editing.

SUPPLEMENTARY MATERIAL

The Supplementary Material for this article can be found online at: https://www.frontiersin.org/articles/10.3389/fnagi.2022.847094/full#supplementary-material

Supplementary Figure 1 | Correlation coefficient between $SUVR_{CortexID}$ and MedT-Atrophy-score. A non-significant negative correlation was observed in the L-MedT-Atrophy-score in the preclinical stage ($p = 0.143$). The Pearson's product-moment correlation coefficient was −0.148 (95% confidence interval, −0.334–0.0503). L, left; MedT-Atrophy-score, averaged *Z*-score values in early AD-specific medial temporal VOIs preinstalled in the Voxel-based Specific Regional Analysis System for Alzheimer's Disease; $SUVR_{CortexID}$, average standardized uptake value ratio within the composite VOIs in the Montreal Neurological Institute space obtained with the CortexID Suite.

Supplementary Figure 2 | The images to show representations of visually amyloid-negative **(A)** and visually amyloid-positive **(B)**. **(A)** This negative scan shows lower intensity in cortical gray matter than in white matter, creating clear gray-white matter contrast. **(B)** This positive scan have five cortical regions (frontal lobes, lateral temporal lobes, inferolateral parietal lobes, posterior cingulate and precuneus and striatum) in which gray matter signal is as intense or exceeds the intensity in adjacent white matter.

REFERENCES

Adachi, T., Saito, Y., Hatsuta, H., Funabe, S., Tokumaru, A. M., Ishii, K., et al. (2010). Neuropathological asymmetry in argyrophilic grain disease. *J. Neuropathol. Exp. Neurol.* 69, 737–744. doi: 10.1097/NEN.0b013e3181e5ae5c

Alsop, D. C., Casement, M., de Bazelaire, C., Fong, T., and Press, D. Z. (2008). Hippocampal hyperperfusion in Alzheimer's disease. *Neuroimage.* 42, 1267–1274. doi: 10.1016/j.neuroimage.2008.06.006

Araki, T., Ikegaya, Y., and Koyama, R. (2021). The effects of microglia- and astrocyte-derived factors on neurogenesis in health and disease. *Eur. J. Neurosci.* 54, 5880–5901. doi: 10.1111/ejn.14969

Arnsten, A. F. T., Datta, D., Del Tredici, K., and Braak, H. (2021). Hypothesis: tau pathology is an initiating factor in sporadic Alzheimer's disease. *Alzheimers Dement.* 17, 115–124. doi: 10.1002/alz.12192

Ashburner, J. (2007). A fast diffeomorphic image registration algorithm. *Neuroimage* 38, 95–113. doi: 10.1016/j.neuroimage.2007.07.007

Babcock, K. R., Page, J. S., Fallon, J. R., and Webb, A. E. (2021). Adult hippocampal neurogenesis in aging and Alzheimer's disease. *Stem Cell Rep.* 16, 681–693. doi: 10.1016/j.stemcr.2021.01.019

Bauckneht, M., Chincarini, A., Piva, R., Arnaldi, D., Girtler, N., Massa, F., et al. (2018). Metabolic correlates of reserve and resilience in MCI due to Alzheimer's disease (AD). *Alzheimers Res. Ther.* 10:35. doi: 10.1186/s13195-018-0366-y

Choi, H., Choi, Y., Lee, E. J., Kim, H., Lee, Y., Kwon, S., et al. (2021). Hippocampal glucose uptake as a surrogate of metabolic change of microglia in Alzheimer's disease. *J. Neuroinflammation.* 18:190. doi: 10.1186/s12974-021-02244-6

DeLong, E. R., DeLong, D. M., and Clarke-Pearson, D. L. (1988). Comparing the areas under two or more correlated receiver operating characteristic curves: a nonparametric approach. *Biometrics* 44, 837–845. doi: 10.2307/2531595

Fox, N. C., Black, R. S., Gilman, S., Rossor, M. N., Griffith, S. G., Jenkins, L., et al. (2005). Effects of Abeta immunization (AN1792) on MRI measures of cerebral volume in Alzheimer disease. *Neurology* 64, 1563–1572. doi: 10.1212/01.WNL.0000159743.08996.99

Grothe, M. J., Teipel, S. J., Alzheimer's Disease, and Neuroimaging Initiative. (2016). Spatial patterns of atrophy, hypometabolism, and amyloid deposition in Alzheimer's disease correspond to dissociable functional brain networks. *Hum. Brain Mapp.* 37, 35–53. doi: 10.1002/hbm.23018

Guedj, E., Barbeau, E. J., Didic, M., Felician, O., de Laforte, C., Ranjeva, J. P., et al. (2009). Effects of medial temporal lobe degeneration on brain perfusion in amnestic MCI of AD type: deafferentation and functional compensation? *Eur. J. Nucl. Med. Mol. Imaging* 36, 1101–1112. doi: 10.1007/s00259-009-1060-x

Herholz, K., Salmon, E., Perani, D., Baron, J. C., Holthoff, V., Frölich, L., et al. (2002). Discrimination between Alzheimer dementia and controls by automated analysis of multicenter FDG PET. *Neuroimage* 17, 302–316. doi: 10.1006/nimg.2002.1208

Hirata, Y., Matsuda, H., Nemoto, K., Ohnishi, T., Hirao, K., Yamashita, F., et al. (2005). Voxel-based morphometry to discriminate early Alzheimer's disease from controls. *Neurosci. Lett.* 382, 269–274. doi: 10.1016/j.neulet.2005.03.038

Jack, C. R. Jr., Bennett, D. A., Blennow, K., Carrillo, M. C., Dunn, B., Haeberlein, S. B., et al. (2018). NIA-AA Research Framework: Toward a biological definition of Alzheimer's disease. *Alzheimers Dement* 14, 535–562. doi: 10.1016/j.jalz.2018.02.018

Kanda, Y. (2013). Investigation of the freely available easy-to-use software 'EZR' for medical statistics. *Bone Marrow Transplant.* 48, 452–458. doi: 10.1038/bmt.2012.244

Li Puma, D. D., Piacentini, R., and Grassi, C. (2020). Does impairment of adult neurogenesis contribute to pathophysiology of Alzheimer's disease? A still open question. *Front. Mol. Neurosci.* 13:578211. doi: 10.3389/fnmol.2020.578211

Malone, I. B., Leung, K. K., Clegg, S., Barnes, J., Whitwell, J. L., Ashburner, J., et al. (2015). Accurate automatic estimation of total intracranial volume: a nuisance variable with less nuisance. *Neuroimage* 104, 366–372. doi: 10.1016/j.neuroimage.2014.09.034

Matsuda, H., Kitayama, N., Ohnishi, T., Asada, T., Nakano, S., Sakamoto, S., et al. (2002). Longitudinal evaluation of both morphologic and functional changes in the same individuals with Alzheimer's disease. *J. Nucl. Med.* 43, 304–311.

Matsuda, H., Mizumura, S., Nemoto, K., Yamashita, F., Imabayashi, E., Sato, N., et al. (2012). Automatic voxel-based morphometry of structural MRI by SPM8 plus diffeomorphic anatomic registration through exponentiated lie algebra improves the diagnosis of probable Alzheimer disease. *AJNR Am. J. Neuroradiol.* 33, 1109–1114. doi: 10.3174/ajnr.A2935

Ohnishi, T., Matsuda, H., Tabira, T., Asada, T., and Uno, M. (2001). Changes in brain morphology in Alzheimer disease and normal aging: is Alzheimer disease an exaggerated aging process? *AJNR Am. J. Neuroradiol.* 22, 1680–1685.

Seab, J. P., Jagust, W. J., Wong, S. T., Roos, M. S., Reed, B. R., and Budinger, T. F. (1988). Quantitative NMR measurements of hippocampal atrophy in Alzheimer's disease. *Magn. Reson. Med.* 8, 200–208. doi: 10.1002/mrm.1910080210

Sperling, R. A., Aisen, P. S., Beckett, L. A., Bennett, D. A., Craft, S., Fagan, A. M., et al. (2011). Toward defining the preclinical stages of

Alzheimer's disease: recommendations from the National Institute on Aging-Alzheimer's Association workgroups on diagnostic guidelines for Alzheimer's disease. *Alzheimers Dement.* 7, 280–292. doi: 10.1016/j.jalz.2011.03.003

Thurfjell, L., Lilja, J., Lundqvist, R., Buckley, C., Smith, A., Vandenberghe, R., et al. (2014). Automated quantification of 18F-flutemetamol PET activity for categorizing scans as negative or positive for brain amyloid: concordance with visual image reads. *J. Nucl. Med.* 55, 1623–1628. doi: 10.2967/jnumed.114.142109

Tobin, M. K., Musaraca, K., Disouky, A., Shetti, A., Bheri, A., Honer, W. G., et al. (2019). Human hippocampal neurogenesis persists in aged adults and Alzheimer's disease patients. *Cell Stem Cell* 24, 974.e–982.e. doi: 10.1016/j.stem.2019.05.003

Zhang, J., Liu, Y., Lan, K., Huang, X., He, Y., Yang, F., et al. (2021). Gray matter atrophy in amnestic mild cognitive impairment: A voxel-based meta-analysis. *Front. Aging Neurosci.* 13:627919. doi: 10.3389/fnagi.2021.627919

Zheng, J., Li, H. L., Tian, N., Liu, F., Wang, L., Yin, Y., et al. (2020). Interneuron accumulation of phosphorylated tau impairs adult hippocampal neurogenesis by suppressing GABAergic transmission. *Cell Stem Cell* 26, 331–345.e6. doi: 10.1016/j.stem.2019.12.015

Conflict of Interest: NoK was a permanent employee of Otsuka Pharmaceutical Co., Ltd.

The remaining authors declare that the research was conducted in the absence of any commercial or financial relationships that could be construed as a potential conflict of interest.

Publisher's Note: All claims expressed in this article are solely those of the authors and do not necessarily represent those of their affiliated organizations, or those of the publisher, the editors and the reviewers. Any product that may be evaluated in this article, or claim that may be made by its manufacturer, is not guaranteed or endorsed by the publisher.

frontiers | Frontiers in Aging Neuroscience

ORIGINAL RESEARCH
published: 26 April 2022
doi: 10.3389/fnagi.2022.850655

Potential Diffusion Tensor Imaging Biomarkers for Elucidating Intra-Individual Age-Related Changes in Cognitive Control and Processing Speed

Shulan Hsieh[1,2,3]* *and Meng-Heng Yang*[1]

[1] *Cognitive Electrophysiology Laboratory: Control, Aging, Sleep, and Emotion, Department of Psychology, National Cheng Kung University, Tainan, Taiwan,* [2] *Institute of Allied Health Sciences, National Cheng Kung University, Tainan, Taiwan,* [3] *Department of Public Health, National Cheng Kung University, Tainan, Taiwan*

Cognitive aging, especially cognitive control, and processing speed aging have been well-documented in the literature. Most of the evidence was reported based on cross-sectional data, in which inter-individual age effects were shown. However, there have been some studies pointing out the possibility of overlooking intra-individual changes in cognitive aging. To systematically examine whether age-related differences and age-related changes might yield distinctive patterns, this study directly compared cognitive control function and processing speed between different cohorts versus follow-up changes across the adult lifespan. Moreover, considering that cognitive aging has been attributed to brain disconnection in white matter (WM) integrity, this study focused on WM integrity via acquiring diffusion-weighted imaging data with an MRI instrument that are further fitted to a diffusion tensor model (i.e., DTI) to detect water diffusion directionality (i.e., fractional anisotropy, FA; mean diffusivity, MD; radial diffusivity, RD; axial diffusivity, AxD). Following data preprocessing, 114 participants remained for further analyses in which they completed the two follow-up sessions (with a range of 1–2 years) containing a series of neuropsychology instruments and computerized cognitive control tasks. The results show that many significant correlations between age and cognitive control functions originally shown on cross-sectional data no longer exist on the longitudinal data. The current longitudinal data show that MD, RD, and AxD (especially in the association fibers of anterior thalamic radiation) are more strongly correlated to follow-up aging processes, suggesting that axonal/myelin damage is a more robust phenomenon for observing intra-individual aging processes. Moreover, processing speed appears to be the most prominent cognitive function to reflect DTI-related ***age*** (cross-sectional) and ***aging*** (longitudinal) effects. Finally, converging the results from regression analyses and mediation models, MD, RD, and AxD appear to be the representative DTI measures to reveal age-related changes in processing speed. To conclude, the current results provide new insights to which indicator of WM integrity and which type of cognitive changes are most representative (i.e., potentially to be neuroimaging biomarkers) to reflect intra-individual cognitive aging processes.

Keywords: white matter integrity, DTI, FA, MD, RD, AxD, cognitive control, processing speed

OPEN ACCESS

Edited by:
Chu-Chung Huang,
East China Normal University, China

Reviewed by:
Mustapha Bouhrara,
National Institute on Aging (NIH), United States
Sindhuja T. Govindarajan,
University of Pennsylvania, United States

***Correspondence:**
Shulan Hsieh
psyhsl@mail.ncku.edu.tw

Specialty section:
This article was submitted to Neurocognitive Aging and Behavior, a section of the journal Frontiers in Aging Neuroscience

Received: *08 January 2022*
Accepted: *24 March 2022*
Published: *26 April 2022*

Citation:
Hsieh S and Yang M-H (2022) Potential Diffusion Tensor Imaging Biomarkers for Elucidating Intra-Individual Age-Related Changes in Cognitive Control and Processing Speed. Front. Aging Neurosci. 14:850655. doi: 10.3389/fnagi.2022.850655

INTRODUCTION

Cognitive aging has been extensively investigated over the past two decades. One of the critical reasons for this research trend is due to the crisis of population aging which encourages researchers paying attention to evaluate the trajectories of cognitive function decline across chronical age to help people age gracefully. One pronounced diagram showing behavioral performance on measures of processing speed, working memory, long-term memory, and world knowledge was first reported by Park et al. (2002), in which while many cognitive functions, such as speed, spatial orientation, problem solving, numerical ability, verbal memory were significantly declined with age, whereas verbal ability (e.g., vocabulary) did not show decline with age. However, these trajectories of functional decline with age was based on the cross-sectional aging data (Light, 1991; Park, 2002; Park et al., 2002; Salthouse, 2004), it is still unclear whether similar results could also be seen in longitudinal (or follow-up) data. Literature has highlighted an important distinction between ***age*** effects and ***aging*** effects (see Rugg, 2017). An ***age*** effect refers to a scenario in which a dependent variable differs between groups of individuals with different mean ages (such as contrasting a younger group with an older group)—this is known as a cross-sectional design. Whereas an ***aging*** effect refers to a scenario in which we observe an individual's performance changes over time—this is known as a longitudinal or follow-up design. Rugg (2017) has indicated several inferring limitations regarding age-related cognitive aging using a cross-sectional design. Some studies have also provided evidence in showing discrepant results coming from cross-sectional versus longitudinal data, hence highlighting the importance of longitudinal evidence to reveal actual aging effect in cognition (Hedden and Gabrieli, 2004; Hsieh and Yang, 2021).

Brain Structural Connectivity and Cognitive Control in Age/Aging

Cognitive aging has been attributed to brain disconnection in white matter integrity, in which a disruption of communication between cortical regions can result in cognitive dysfunction (O'Sullivan et al., 2001; Bartzokis, 2004; Andrews-Hanna et al., 2007; Fjell et al., 2016; Madden et al., 2017). For human studies, white matter (WM) integrity can be measured via acquiring diffusion-weighted imaging (DWI) data with a magnetic resonance imaging (MRI) instrument that are further fitted to a diffusion tensor model (i.e., diffusion tensor imaging; DTI) to detect water diffusion directionality, which in turn shows the microstructural architecture of tissue. Through DTI fitting model (Behrens et al., 2003), one can derive some indicators reflecting the degree of tissue integrity, such as fractional anisotropy (FA), mean diffusivity (MD), radial diffusivity (RD), and axial diffusivity (AxD). DTI can detect microstructural WM abnormalities preceding the lesions (de Groot et al., 2013; Maillard et al., 2014), and further reveal the neurobiological mechanism(s) of axonal fiber damage (Le Bihan et al., 2001; Vernooij et al., 2009). Specifically, it has been shown that lower FA and higher MD indicate the overall reduction in WM fiber integrity (Le Bihan et al., 2001), and elevated RD and AxD may, at least in part, reflect axonal demyelination and/or degeneration (Song et al., 2003; Klawiter et al., 2011). By means of these indicators, literature has shown a decrease in FA and increase in MD with increasing age, suggesting a decreased WM integrity with age (Salat et al., 2005; Yap et al., 2013; Lebel et al., 2012; Sexton et al., 2014; de Groot et al., 2015; de Lange et al., 2016; Marques et al., 2016). In addition, literature has also shown a significant relationship between WM integrity and cognitive performance in older adults (Bennett and Madden, 2014; see Madden et al., 2012 for a review). Although these previous studies have reported the association between WM integrity and age, and between WM integrity and cognitive performance, most studies used a cross-sectional design and did not provide direct evidence showing whether WM integrity plays a mediation role in the association between age/aging and cognitive performance. Furthermore, some existing longitudinal studies focused on specific WM tracts rather than a whole brain WM integrity. Therefore, the primary aim of this study was to fill the research gap by incorporating both cross-sectional (***age***) and follow-up (***aging***) designs to examine the relationship among age/aging, WM integrity measured by DTI metrics (e.g., FA, RD, MD, and AxD), and cognitive performance. We hypothesized that the results for age-related differences might be different from age-related changes due to cohort and other factors (Hedden and Gabrieli, 2004; Rugg, 2017; Hsieh and Yang, 2021).

For cognitive performance, in this study, we focused on processing speed and cognitive control abilities. This is because the prominent cognitive aging manifests in general slowing (Madden and Allen, 1995) and cognitive control dysfunction (Craik and Byrd, 1982). Furthermore, the age-related deterioration of WM integrity has been observed to be particularly vulnerable to frontal regions (Davis et al., 2009; Bennett et al., 2010; Burzynska et al., 2010). Therefore, we hypothesized that WM integrity should be related to age-related cognitive control changes. To directly test this hypothesis, we also employed a mediation model for longitudinal data to see if WM integrity mediates age-related changes in processing speed and/or cognitive control. Cognitive control function is a broad term. In this study, we adapted the definition by Miyake et al. (2000) which suggests components of inhibition (e.g., measured by a stop-signal task; to note, the inhibition component was later-on modified as a common component), updating (e.g., working memory measured by a n-back task), and shifting (e.g., measured by a paper-and-pencil Trail Making Test (TMT) and a computerized task-switching paradigm) components. As for measuring processing speed, we used a commonly used neuropsychological test, Grooved Pegboard Test (GPT) to collect visuo-motor action speed. In addition, we derived some basic processing speed indicators from TMT form A, and from some computerized cognitive control task in which the basic processing conditions are included (e.g., go trials' reaction time in a stop-signal task; repeat trials' reaction time in a task-switching paradigm). We used both original task's performance indexes and the transformed indexes suggested by Miyake et al. (2000), please see detail in the "Materials and Methods" Section.

Using the definitions of cognitive control based on Miyake's model, some specific issues could be addressed in this study. First, regarding the association between age/aging and cognitive control (including processing speed), we would like to know what type of cognitive control functions are more closely related to age/aging. Second, regarding the association between age/aging and DTI measures, we would like to examine which WM tracts and which WM integrity's indicators (i.e., FA, MD, RD, and AxD) would be more closely related to age/aging. Third, regarding the association between cognitive control functions (including processing speed) and DTI measures, we would like to examine which cognitive performance is more closely related to which WM integrity's indicator. Fourth, whether age-related changes in WM integrity would mediate the association between aging and cognitive performance. Since these four issues have not been directly explored previously, we did not set up any specific predictions, but simply hypothesized that there should be different patterns among different types of cognitive control functions and among different DTI metrics with age/aging effects.

TABLE 1 | Participants' demographic information and DTI measures for time point 1 (TP1) and time point 2 (TP2) and their corresponding paired *t*-tests.

	TP1	TP2	Paired *t*-test (*p-values*)
N	114	114	N/A
Age	48.72 (±16.54) range: 20.25∼77.92	50.49 (±16.64) range: 21.92∼79.83	**0.000**
Gender (F%)	60.53%	60.53%	N/A
Education (Y)	15.02 (±2.65)	15.02 (±2.65)	N/A
BDI-II	4.97 (±4.18)	5.39 (±6.06)	0.440
MoCA	27.63 (±1.86)	28.97 (±1.25)	**0.000**
FA	0.4387 (±0.01593)	0.4389 (±0.01606)	0.624
MD	$0.760*10^{-3}$ ($\pm0.022*10^{-3}$)	$0.763*10^{-3}$ ($\pm0.023*10^{-3}$)	**0.000**
RD	$0.560*10^{-3}$ ($\pm0.025*10^{-3}$)	$0.563*10^{-3}$ ($\pm0.026*10^{-3}$)	**0.003**
AxD	$1.159*10^{-3}$ ($\pm0.020*10^{-3}$)	$1.166*10^{-3}$ ($\pm0.021*10^{-3}$)	**0.000**

p-values marked in bold are those also passing the Bonferroni correction method. BDI-II, Beck Depression Inventory; MoCA, Montreal Cognitive Assessment; FA, fractional anisotropy; MD, mean diffusivity; RD, radial diffusivity; AxD, axial diffusivity.

MATERIALS AND METHODS

Participants

We used advertisements on the Internet and bulletin boards to recruit hundreds of right-handed participants from southern Taiwan. Participants' medical information including neurological history and mental health status were collected via a self-report. The participants included in this study all reported no history of any psychiatric or neurological disorders and they also past the screening criteria of the two neuropsychological tests, including the Montreal Cognitive Assessment (MoCA) to screen for cognitive impairment if the scores were ≤25 (Nasreddine et al., 2005; Chinese Version: Tsai et al., 2012), and the Beck Depression Inventory-II (BDI-II; Beck et al., 1996; Chinese version published by Chinese Behavioral Science Corporation) to screen for depression if the scores were ≥14. A total of 121 qualified participants completed the two follow-up sessions (with a range of 1–2 years). In each session, participants completed the questionnaire of demographic information, computerized cognitive tasks, neuropsychological tests for measuring cognitive control and processing speed, and magnetic resonance imaging (MRI) acquisitions. Four participants were excluded because of technical problems with MRI or incomplete data. Three participants were further excluded because their DTI's measures >5 standard deviations. Furthermore, all remaining 114 participants' images passed quality control. We also visually inspected all images after normalization and co-registration steps. This ensures that there is no serious warping. The mean age of the remaining 114 participants (females' ratio = 60.53%) was 48.72 ± 16.54 years [timepoint 1 (TP1); 20.25–77.92 years] and 50.49 ± 16.64 years [timepoint 2 (TP2); range 21.92–79.83 years]. See **Table 1** for the participants' age range distribution and demographic information.

The study was carried out in accordance with the Declaration of Helsinki and the study protocol was approved by Ethical Committee at the National Cheng Kung University (reference number #104-004). Participants received monetary compensation for their participation after the completion of all assessments (NTD$1,500 per session).

Computerized Cognitive Tasks for Measuring Cognitive Control Performance and Processing Speed

General Instruments for Visual Presentation

The visual stimuli used in the following computerized tasks were programmed using Presentation software, and were displayed on a 17-inch monitor with 1024*768 resolution.

Stop-signal task

The stop-signal task was a modified version of Logan's paradigm (Logan et al., 2014). Participants were asked to fixate at the visual stimulus on the screen and use their index fingers of both hands to press either the "z" or "/" stroke on the keyboard when target "O" or "X" was presented. Participants were told to react to the stimulus as quickly and accurately as possible. On some occasions, a "beep" sound with a duration of 100 ms which served as a "stop" signal might be delivered following a target with a delay (i.e., stop-signal delay; SSD) initially set at 150 or 350 ms, and adjusted with a staircase tracking procedure (i.e., decreased by 50 ms following a failure stop and increased by 50 ms following a successful stop). Participants were informed to ignore this sound in the first practice session, so that they could be familiar with quickly responding to the stimuli. In the second practice session, participants were told to immediately stop their intended action once they heard the "beep" sound. We reminded participants with the instruction of "Do not hold your responses while waiting for a beep sound." Following the two practice sessions, there were four experimental blocks which contained randomly intermixed 40 stop trials (i.e., trials followed

by a stop sound) and 100 go trials without a stop signal. The whole duration for this task was about half an hour.

The stop-signal reaction time (SSRT) indexing the stopping efficiency was calculated by subtracting the median SSD from the median RT of the go trials. The larger the SSRT indicates the worse stopping efficiency.

Task-switching paradigm

Task-switching abilities were measured by a modified paradigm from Karayanidis et al.'s (2003) study. Each trial contained a cue (non-informative or informative) with a duration of 600 ms, and followed by a target display with an interval of 1,000 ms (i.e., cue-target interval, CTI). An informative cue was a colored cross with either a warm color (red or orange) or a cold color (green or blue) indicating which is the forthcoming task: a letter classification or a number classification task. A non-informative cue was colored in gray, which provided no information about the forthcoming task type. The target display contained a pair of two stimuli, in which there were two different pair types: an incongruent pair and a neutral pair (50% each in a mixed task block). An incongruent pair contained a Chinese letter and an Arabic number, and a neutral pair only contained one of them and paired with a symbol sign (e.g.,%, #, @, or $). The Chinese letter was one of eight Chinese letters which were retrieved from the Ten Celestial Stem system (i.e., Tiangan). Participants were asked to respond to the stimulus display using either their right or left index finger that was mapped to the first-half/second-half or odd/even for Chinese-letter and Arabic-number tasks, respectively.

All participants practiced six blocks before the experiment. The experiment contained 12 blocks: (1) two single-task blocks which contained only Arabic numbers (i.e., a neutral pair) for a sequence of 70 trials per block; (2) two single-task blocks which contained only Chinese letters (i.e., a neutral pair) for a sequence of 70 trials per block; (3) four mixed informative task blocks of 70 trials per block (with a switch rate around 33.3%); and (4) four mixed non-informative task blocks of 70 trials per block (with a switch rate around 33.3%). The entire experiment lasted for about 35∼40 min.

We calculated the switch cost by subtracting the average RT of the repeat trials in the mixed-task blocks from the average RT of the switch trials in the mixed-task blocks.

Spatial n-back task

In this study, we adapted a spatial version of 1-back and 2-back tasks to measure working memory updating function. The spatial n-back is a single n-back task based on spatial locations as the stimuli stream. For example, in this study, the stimuli were presented within a 3-by-3 grid in each trial. One of the grid squares was randomly assigned to be filled with blue. In a 1-back task, participants were asked to continuously memorize the position of the blue grid square shown in the previous trial and to match it to the current trial's position of the blue grid square. In a 2-back task, participants were asked to continuously memorize the position of the blue grid square in the previous two trials and to compare it to the current trial's position of the blue grid square. If the blue grid square appeared in the same location as instructed (either matched to the previous one trial's grid position in a 1-back task or the previous two trial's grid position in a 2-back task), participants pressed the "F" button using their left index finger. If the blue grid square appeared in a different location, participants pressed the "J" button using their right index finger. Each grid stimulus appeared for 500 ms followed by an interstimulus interval (ISI) of 2,000 ms. Participants completed one practice block with performance feedback, and three experimental blocks which contained 21 trials per block. This entire experiment lasted for 30 to 40 min.

We calculated performance sensitivity (d') as a working memory updating index, which was based on the hit rate (H) and false-alarm (F) rate. We first transformed the raw data into z scores. The formula is as follows: $d' = Z(\mathrm{H}) - Z(\mathrm{F})$ (Z denotes the z score of the normal distribution). The larger values of the d' indicates higher working memory updating ability. Therefore, the direction of the d' value is the opposite to the other indexes, such as inhibition and shifting. Therefore, to equalize the direction of the performance for these three types of cognitive control indexes, we transformed d' into negative values, so that the higher d' value (i.e., less negative) would indicate worse updating performance which yields a similar performance direction for SSRT, switch costs, and d'.

Computing Common and Specific Executive Function Components – Miyake's Definition

The performance on each of the three tasks (switch cost in a task-switching paradigm, SSRT in a stop-signal task, and d' in a n-back task) were calculated into z value. Following Miyake and Friedman's procedures, we averaged these three z scores to make a composite score reflecting common EF for every participant. We regressed SSRT and n-back d', and used the residuals as a shifting EF component. We regressed d' against SSRT and switching cost, and used the residuals as an updating EF component.

Neuropsychological Tests for Measuring Cognitive Control Performance and Processing Speed

Trail Making Test

In this study, we used the Chinese version of the Trail Making Test (TMT), which consisted of two forms (A and B) of task conditions. The reliability of the Chinese version of the TMT has been reported by Wang et al. (2018). Form A consisted of numbers from "1" to "25" and was displayed randomly on an A4 sheet of paper. Form B consisted of digit numbers from "1" to "12" and Chinese zodiac letters ("rat" to "pig") were shown. Participants drew a line connecting these items during a sequence of "1"–"2"–"3"–. . ."25" in form A and an alternating sequence of "1"–"rat"–"2"–"ox"–. . ."12"–"pig" in form B. The time to finish the form (TMT-A, TMT-B) was recorded as a performance index. TMT-A is considered as a metric reflecting processing speed, while TMT-B is a metric of switching proficiency plus processing speed.

Grooved Pegboard Test

Participants were asked to insert cylindrical metal pegs into 25 holes of a pegboard as fast as possible. Left- and right-handed

performances were tested separately. The test began with the self-identified dominant hand (i.e., the right hand in this study), followed by the non-dominant hand. Participants were asked to insert pegs in the standardized order (from left to right for all rows when using the right hand and from right to left for all rows when using the left hand) and to use just one hand at a time. The whole time to finish the test was recorded as an index of processing speed for each hand, respectively (GPT_R; GPT_L).

Cognitive Performance Indexes for Cognitive Control and Processing Speed

The performance indexes (all transformed into *z* scores) collected from the above series of cognitive tasks and neuropsychological tests are summarized in **Table 2**, in which TMT-A, GPT_R/L, go RT in a stop-signal task are considered as indexes for processing speed, switch cost (informative and non-informative), TMT-B is considered as indexes of shifting, SSRT is an inhibition index, whereas mixing cost derived from task-switching paradigm, and 1-/2-back *d*' are considered as indexes of working memory. In addition, as aforementioned, we also calculated common and specific EF components (i.e., common, shifting, updating) derived from the three computerized cognitive control tasks based on Miyake's model (see **Table 2**).

Neuroimaging Acquisition and Analysis

Image Acquisition

All brain images in this research were acquired using a GE MR750 3T scanner (GE Healthcare, Waukesha, WI, United States) installed in the Mind Research and Imaging Center at National Cheng Kung University (NCKU).

High-spatial-resolution T1-weighted images were acquired with fast spoiled gradient echo (fast-SPGR) (TR/TE: 7.6 ms/3.3 ms; flip angle: 12°; FOV: 22.4*22.4 cm^2; thickness: 1 mm; matrices: 224*224). A total of 166 axial slices was acquired during a scan time of 218 s.

Diffusion tensor imaging was acquired using a spin-echo echo-planar imaging sequence with the acquisition parameters: TR/TE = 5500 ms/62∼64 ms, 50 directions with b = 1000 s/mm^2, 100 × 100 matrices, slice thickness = 2.5 mm, voxel size = 2.5 × 2.5 × 2.5 mm, number of slices = 50, FOV = 25 cm, NEX = 3. The total scan time for the DTI acquisition was 924 seconds. A reversed-phase-encoding DTI was also acquired for off-line top-up corrections in the DTI preprocessing. The acquisition parameters for the reversed-phase-encoding DTI were identical to the DTI, with the only difference being the number of directions as six. The total scan time for the reversed-phase-encoding DTI was 198 seconds. The reason for choosing fewer numbers of reversed-phase-encoded directions was to avoid motion artifacts due to long scanning times.

Diffusion Tensor Imaging Processing

We used the FMRIB software Library (FSL v5.0.9[1]; Smith et al., 2004) for all diffusion-weighted imaging (DWI) data processing.

[1]www.fmrib.ox.ac.uk/fsl

The preprocessing steps were identical to those of earlier work (for details, refer to Yang et al., 2019). DWI data processing as follows: (1) estimating and correcting susceptibility induced distortions using "*topup*" tool, (2) correcting slice-to-volume movement using "*eddy_correct,*" (3) fitting a diffusion tensor model to the images using "*dtifit*" to obtain scalar DTI maps, in which each voxel was assigned with three eigenvalue (principal diffusivities: λ1, λ2, λ3) and three eigenvector (principal directions: v1, v2, v3), describing the water diffusion within the voxel., and (4) performing voxel-wise statistical analyses of the fractional anisotropy (FA) data by using tract-based spatial statistics (*TBSS*; Scahill et al., 2003) to register and normalize all participants' FA images to the MNI standard space. This process was then repeated for MD and RD images using the tbss_non_FA function.

Subsequently, for tract-of-interest (TOI) analyses, TBSS-skeleton binary masks were overlaid with atlas binary masks which were created with a threshold of 5% based on the probabilistic Johns Hopkins University (JHU) white-matter tractography atlas in FSL (provided by the ICBM DTI workgroup). We chose anterior thalamic radiation (ATR) left (L) and right (R) hemisphere, cingulum/cingulate gyrus (CG) L/R, cingulum/hippocampus (CH) L/R, corticospinal tract (CST) L/R, forceps major (Fmaj), forceps minor (Fmin), inferior fronto-occipital fasciculus (IFF) L/R, inferior longitudinal fasciculus (ILF) L/R, superior longitudinal fasciculus (SLF) L/R, and uncinate fasciculus (UF) L/R as TOIs. Fmin is the commissural fibers of the anterior corpus callosum, whereas Fmaj is the commissural fibers of the posterior corpus callosum. Then we used these masks to mask the FA/MD/RD/AxD map which produced from the TBSS step for each participant. The average FA/MD/RD/AxD values were computed and used in the following analysis.

Statistical Analyses

To evaluate the relationship between age, FA/MD/RD/AxD and cognitive performance. In the first part, we tested cross-sectional correlations between (1) age and cognitive performance, (2) age and FA/MD/RD/AxD, and (3) cognitive performance and FA/MD/RD/AxD. For all these three sets of Pearson *r* correlation analyses, we used gender, education and BDI-II as covariates. In addition, for cross-sectional data, we also tested the quadratic effects of age (i.e., age^2).

In the second part, we used longitudinal data to calculate changes in DTI measures and changes in cognitive performance by subtracting DTI (or cognitive performance score) at time 1 (TP1) from time 2 (TP2) and dividing by the exact number of years between scans adjusted to 2 years. In addition, we considered participants' baseline scores of TP1 by adding a denominator of TP1 measure into the formula to form percentage change scores (e.g., Simmonds et al., 2014 on early life changes). Furthermore, the time between scans was adjusted to 2 years as the average time between the two acquisitions for the cohort was 1.77 years (e.g., Breukelaar et al., 2017).

TABLE 2 | The significant Pearson correlation *r* values for age (cross-sectional) and aging (longitudinal) effects in percentage changes of cognitive control and processing speed.

	Cross-sectional cognitive performance (TP1) correlation with age (TP1)	Longitudinal Δ cognitive performance correlation with age (TP1)	Domain
TMT-A	**0.544**	–	Speed
TMT-B	**0.384**	–	Shift
GPT_L	**0.560**	**0.288**	Speed
GPT_R	**0.494**	–	Speed
SSRT	**0.312**	–	Inhibition
goRT	**0.369**	–	Speed
infSWIcost	−0.167	–	Shift
non-infSWIcost	–	–	Shift
MIXcost	–	–	WM updating
2-back *d′*	**0.367**	–	WM updating
1-back *d′*	–	–	WM updating
Common EF	**0.272**	–	Inhibition
Shifting EF	0.156	–	Shift
Updating EF	**0.257**	–	WM

The r value denoted in the table represents its p value passing the bootstrap criteria (i.e., upper and lower bound do not pass 0). r value marked in bold indicates its p value also passing the Bonferroni correction criteria ($p < 0.0004$). '–' denotes non-significance. TMT, Trail Making Test; GPT, Grooved Pegboard Test (L, left hand; R, right hand); SSRT, stop signal reaction time; infSWIcost, inform condition's switch cost; non-infSWIcost, non-inform condition's switch cost; MIXcost, mixing cost; EF, executive function; WM, working memory.

The formula is shown below:

$$[(\text{Measure}_{\text{TP2}} - \text{Measure}_{\text{TP1}})/\text{Measure}_{\text{TP1}}]$$
$$\text{x}\left(\frac{2}{TP2-TP1}\right) = \Delta\text{Measure}$$

Please note, percentage change scores (i.e., ratio scores) will be denoted as ΔMeasure for brevity throughout the manuscript. We tested longitudinal correlations between (1) age (at TP1) and Δcognitive performance, (2) age (at TP1) and ΔFA/MD/RD/AxD, and (3) Δcognitive performance and ΔFA/MD/RD/AxD. We used gender, education and BDI-II as covariates in all Pearson *r* correlation analyses. All data were transformed into *z* score before analyses in this study.

All analyses with multiple comparisons were corrected using the Bootstrap method in which we ran 1,000 iterations to calculate the bias-corrected and accelerated (BCa) bootstrap interval (upper and lower bond). We also used a conventional Bonferroni correction method for multiple comparisons, that is, we used a critical value of $r > 0.271$, $p < 0.004$ for examining significant correlations of cognitive performance in relation to age, and a critical value of $r > 0.279$, $p < 0.003$ for DTI in relation to age and to cognitive performance. However, here we interpreted the results based on the Bootstrap method because it has the advantage of taking into account the dependence structure of *p* values (Vilar-Fernández et al., 2007).

Mediation Analysis

For the mediation analysis, we used Mplus version 8 to build a mediation path model with latent DTI variables. The latent DTI variables (FA, MD, RD, AxD separately) were defined by the tract which was significantly correlated with cognitive measurement. This estimated both the direct and indirect effects on all cognitive measurement. The model was estimated using maximum likelihood estimation. The significance of indirect effects was assessed with a 95% confidence interval calculated by the Bootstrap method. To estimate confidence intervals, we used a bias-corrected method with the percentile bootstrap estimation approach, which ran 5,000 bootstrap iterations that were implemented. We rejected the null hypothesis if the interval didn't include zero.

RESULTS

Participants' demographic information and DTI measures for TP1 and TP2 and their statistical tests are shown in **Table 1**. The results show that age, MoCA, MD, RD, and AxD, but not BDI-II and FA scores, are significantly different between TP1 and TP2. Please note, for each of the cognitive performance index and for each WM tract of the DTI measures between TP1 and TP2, the mean scores and respective paired *t*-tests results are shown in the **Supplementary Tables 1**, **2**.

To address the issues set out in this study, we report the results as follows:

Associations Between Age/Aging and Cognitive Control (Including Processing Speed)

Cross-sectional result (***age*** effect): **Table 2**'s left column shows linear correlation between age and cognitive performance at TP1. It can be found that age was significant correlated with processing speed (include TMT-A, GPT_L, GPT_R, and goRT), inhibition (SSRT, common EF), shifting (TMT-B,

infSWIcost, and shifting EF component), and updating (2-back d', updating EF component).

Longitudinal result (***aging*** effect): **Table 2**'s right column shows correlation between age (at TP1) and follow-up percentage changes in cognitive performance. There was only one significance remaining on the follow-up data, i.e., between age (at TP1) and speed changes (Δ GPT_L).

Associations Between Age/Aging and Diffusion Tensor Imaging

Cross-sectional result (***age*** effect): **Table 3**'s left columns show Pearson correlation *r* values between age and DTI (FA, MD, RD, and AxD) at TP1. The results show that FA, MD, and RD were all correlated with the age effect, except a few WM tracts such as CG_R, CH_L/R, CST_R in FA, and CG_R, CH_L in MD/RD. Whereas AxD showed fewer WM tracts significantly correlated with the age effect, that is, only ATR_L/R, CH_R, and Fmin were significantly correlated with age at TP1.

As mentioned, we also ran a set of non-linear analyses for the age effect on DTI (see **Figure 1**). Most of the WM tracts in the quadratic age effects retained the same patterns as those for the linear age effect. r^2 values in CG_L, Fmin, IFF, ILF, SLF and UF remained to be between 0.07 and 0.26. We found that MD and RD had the highest quadratic age effect in ATR L/R ($r^2 > 0.4$), whereas FA had the highest quadratic age effect in Fmin ($r^2 > 0.4$). As similar as the linear age effect, the quadratic age effects of FA in CG_R, CH, and CST were not significant ($r^2 < 0.03$), yet although the indicator of MD for CH_L tract didn't have a linear effect, it does have a quadratic effect ($r^2 = 0.115$). Conversely, compared to the linear correlation results, AxD now showed many more WM tracts (except CG, ILF_R, Fmaj) that were significantly associated with age, suggesting that AxD is better interpreted non-linearly for the cross-sectional data.

Longitudinal result (***aging*** effect): **Table 3**'s right columns show correlations between age (at TP1) and DTI percentage changes from TP1 to TP2 (i.e., ΔFA, ΔMD, ΔRD, ΔAxD). We found that although at cross-sectional data showing FA, MD, and RD were mostly correlated with the age effect, but in the longitudinal data, FA changes (ΔFA) paradoxically showed very few WM tract's significances with age (at TP1) except that CH_L/R and CST_L tracts were significant. Conversely, although AxD showed fewer WM tracts significantly linearly correlated with age cross-sectionally, its changes (ΔAxD) on many WM tracts showed significantly correlated with age (at TP1), suggesting that AxD index is closely related to intra-individual aging changes. As for MD and RD changes (i.e., ΔMD and ΔRD), they were mostly still significantly correlated with age (at TP1) except a few tracts (e.g., ΔMD: CG_R, CH_R, CST_L/R, Fmaj, & Fmin; ΔRD: CG_R, CH_L/R, ILF_L, SLF_L, CST_L/R, Fmaj, Fmin; see **Table 3** for details), suggesting that MD and RD indexes are more representative for both ***age*** and ***aging*** effects, whereas FA seems to be only sensitive to the age effect (i.e., cross-sectional), but not aging effect.

TABLE 3 | The significant Pearson correlation r values for age and DTI (cross-sectional and longitudinal ratio scores).

	Cross-sectional DTI (TP1) correlation with age				Longitudinal DTI correlation with age			
	FA	**MD**	**RD**	**AxD**	**FA**	**MD**	**RD**	**AxD**
Association fiber								
ATR_L	**−0.504**	**0.562**	**0.600**	**0.409**	–	**0.293**	0.251	**0.319**
ATR_R	**−0.474**	**0.570**	**0.599**	**0.434**	–	**0.284**	0.242	**0.344**
CG_L	**−0.436**	0.219	**0.349**	–	–	**0.318**	0.231	**0.377**
CG_R	–	–	–	–	–	–	–	–
CH_L	–	–	–	–	0.199	0.213	–	0.271
CH_R	–	0.267	0.238	0.238	0.193	–	–	–
IFF_L	**−0.531**	**0.319**	**0.430**	–	–	**0.295**	0.224	**0.344**
IFF_R	**−0.477**	**0.323**	**0.407**	–	–	**0.353**	0.251	**0.418**
ILF_L	**−0.481**	0.271	**0.373**	–	–	0.199		0.230
ILF_R	**−0.480**	0.251	**0.360**	–	–	**0.336**	0.243	**0.398**
SLF_L	**−0.429**	0.219	**0.324**	–	–	0.207		0.251
SLF_R	**−0.421**	0.223	**0.321**	–	–	0.256	0.194	**0.314**
UF_L	**−0.450**	0.258	**0.354**	–	–	**0.327**	**0.279**	**0.377**
UF_R	**−0.352**	0.204	**0.285**	–	–	**0.403**	**0.340**	**0.453**
Projection fiber								
CST_L	–0.248	0.195	0.255	–	0.215	–	–	0.209
CST_R	–	0.212	0.238	–	–	–	–	0.255
Commissural fiber								
Fmaj	**−0.507**	**0.285**	**0.430**	–	–	–	–	–
Fmin	**−0.637**	0.255	**0.465**	**−0.280**	–	–	–	–

The r value denoted in the table represents its p value passing the bootstrap criteria (i.e., upper and lower bound do not pass 0).; r value marked in ***bold*** *indicates its p value also passing the Bonferroni correction criteria (p < .0003). '–' denotes non-significance.*

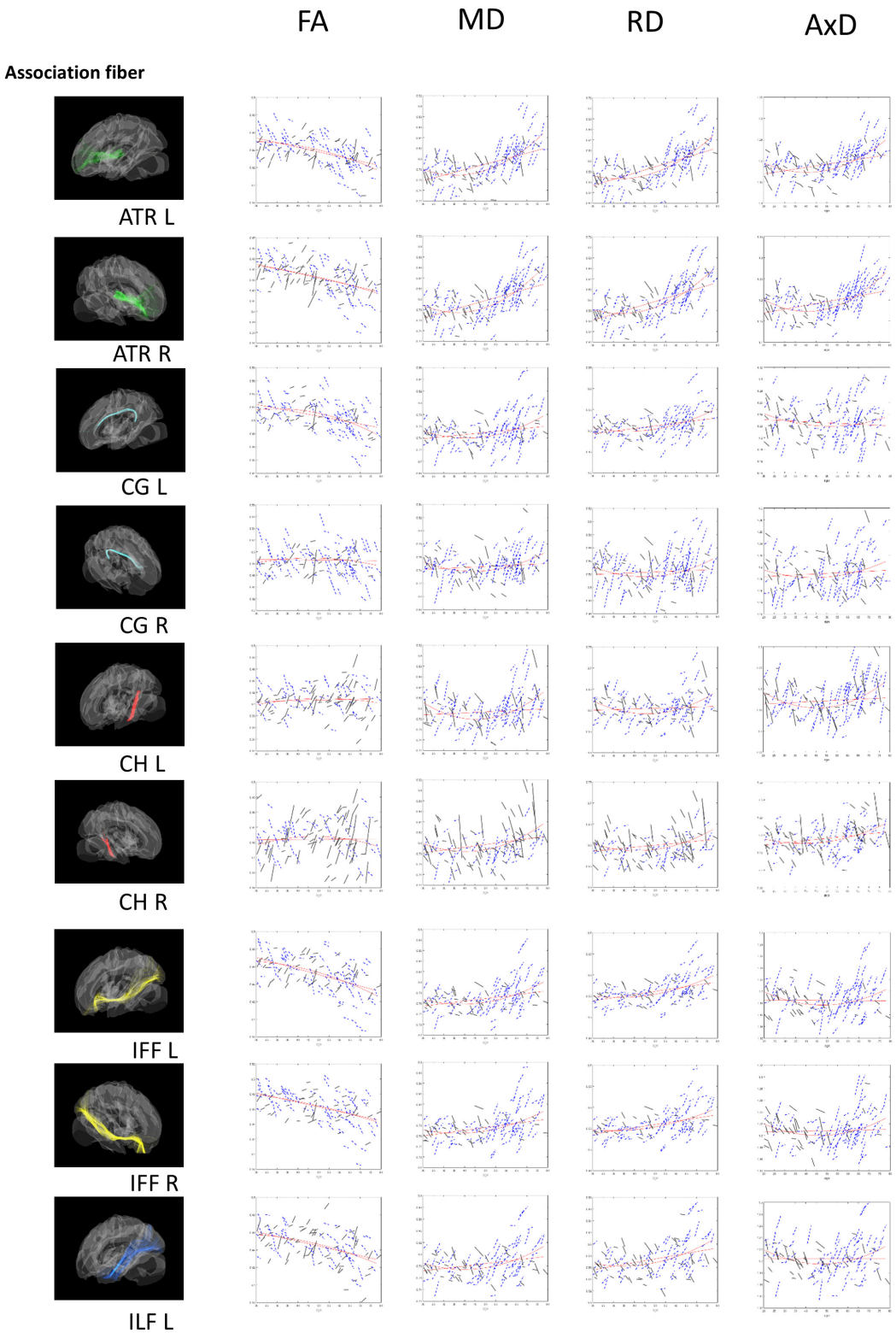

FIGURE 1 | (Continued)

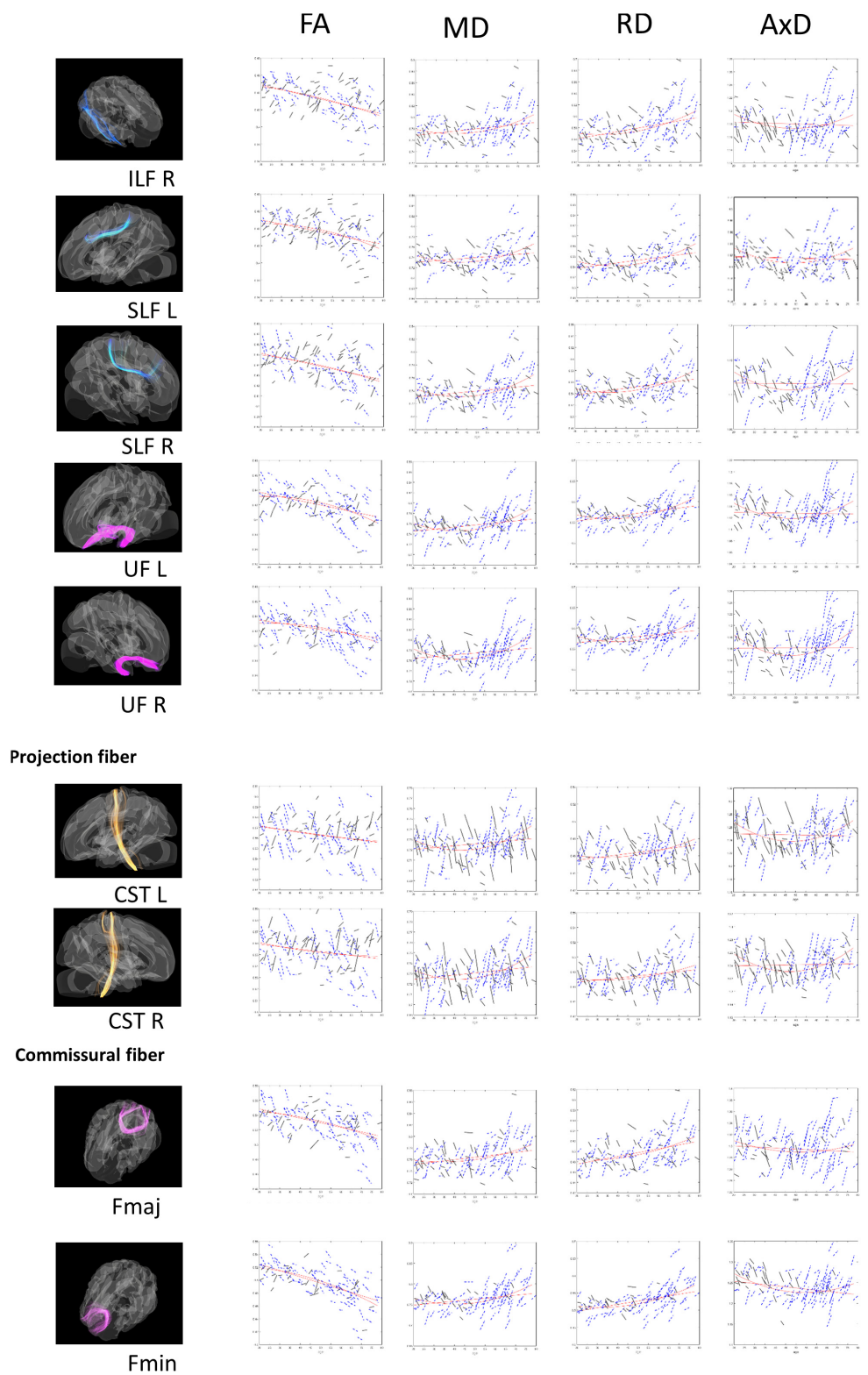

FIGURE 1 | Tract-of-Interest for DTI (FA, MD, RD, and AxD) and their relationships with age. The spaghetti plot that connects the repeated measurements for time point 1 (TP1) and time point 2 (TP2). Tract-of-Interest for DTI measures (FA, MD, RD, and AxD) and their relationships with age is shown in the figure, respectively. Black solid lines denote the better white matter integrity for TP2 than TP1. Conversely, blue dashed lines denote worse white matter integrity for TP2 than TP1. Red lines denote best fitting linear and non-linear regression lines for cross-sectional data on TP1.

Cognitive Control (Including Processing Speed) and Diffusion Tensor Imaging

Processing Speed and Diffusion Tensor Imaging

Cross-sectional result (***age*** effect): **Table 4** left columns show significant correlations between processing speed and FA/MD/RD/AxD measures for the cross-sectional data (TP1). We can find there were many significant correlations between processing speed and DTI measures, with FA being as negative correlations, and MD and RD being as positive correlations. AxD showed relatively fewer significant positive correlations in WM tracts (only in ATR_L/R and CH_L tracts) with processing speed.

Longitudinal result (***aging*** effect): **Table 4** right columns show significant correlations between Δprocessing speed and ΔFA/MD/RD/AxD measures. Contrary to the cross-sectional result, there were relatively fewer significant correlations between Δprocessing speed and ΔDTI for the follow-up data. These include negative correlations between processing speed and nine tracts in FA, and positive correlations between processing speed and five tracts in MD, five tracts in RD, and four tracts in AxD (see **Table 4** for details).

Common/Inhibition Component and Diffusion Tensor Imaging

Cross-sectional result (***age*** effect): **Table 5** left columns show significant correlations between the common/inhibition component and FA/MD/RD/AxD measures for the cross-sectional data (TP1). We can find there were many significant correlations between the common/inhibition component and DTI metrics, with FA being as negative correlations, and MD and RD being as positive correlations. Yet, AxD showed relatively fewer significant positive correlations in WM tracts (only in Fmin tract) with the common/inhibition component.

Longitudinal result (***aging*** effect): **Table 5** right columns show significant correlations between the Δcommon/inhibition component and percentage changes in DTI measures. Contrary to the cross-sectional result, there were no significant correlations between the Δcommon/inhibition and ΔDTI measures for the follow-up data.

Shifting Component and Diffusion Tensor Imaging

Cross-sectional result (***age*** effect): **Table 6** left columns show significant correlations between the shifting component and DTI measures for the cross-sectional data (TP1). We can find there were a few significant correlations between the shifting component and FA/MD/RD measures, with FA being as negative correlations, and MD/RD being as positive correlations. AxD showed relatively fewer significant positive correlations in WM tracts (only in ATR_R and ILF_L tracts) with the shifting component (see **Table 6** for details).

Longitudinal result (***aging*** effect): **Table 6** right columns show significant correlations between the Δshifting component and ΔFA/MD/RD/AxD. Contrary to the cross-sectional result, there were much fewer significant correlations between Δshifting and ΔFA/MD/RD/AxD in WM tracts (**FA:** ATR_R, CG_L; **MD:** CG_L, Fmaj, Fmin; **RD:** CH_L; **AxD:** SLF_R, Fmaj) for the follow-up data.

Working Memory/Updating Component and Diffusion Tensor Imaging

Cross-sectional result (***age*** effect): **Table 7** left columns show significant correlations between the working memory/updating component and DTI measures for the cross-sectional data (TP1). We can find there were a few significant correlations between the working memory/updating component and DTI measures, with FA being as negative correlations, and MD/RD/AxD being as positive correlations (see **Table 7** for details).

Longitudinal result (***aging*** effect): **Table 7** right columns show significant correlations between the Δworking memory/updating component and percentage changes in DTI measures. Contrary to the cross-sectional result, there were much fewer significant correlations between Δworking memory/updating and ΔFA/MD/RD/AxD in WM tracts (**FA:** CH_L/R, ILF_R; **RD:** CST_L; **AxD:** CG_R, Fmaj) for the follow-up data.

Mediation Model Among Age (Timepoint 1), Diffusion Tensor Imaging Changes, and Processing Speed Changes

To directly test the idea if changes in MD (ΔMD), RD (ΔRD), and/or AxD (ΔAxD) mediated the relationship between age (at TP1) and changes in cognitive performance, especially ***processing speed***, we ran a series of mediation models. The results of model fittings showed that two models on ΔMD yielded good model fits. One model showed an indirect effect between age (at TP1) and changes in the neuropsychological task of GPT_L (an index of processing speed) with the latent variable of changes in MD (ΔMD) in WM tracts of CG_L, CH_L, and ILF_L as mediators (RMSEA < 0.06; chi square $p = 0.188$; CFI = 0.97) (see **Figure 2A**). The other model showed an indirect effect between age (at TP1) and changes in the neuropsychological task of GPT_R (an index of processing speed) with the latent variable of changes in MD (ΔMD) in WM tracts of IFF_L/R (RMSEA < 0.001; chi square $p = 0.931$; CFI = 1.00) (see **Figure 2B**). In addition, there was one good model fit on ΔRD showing that the latent variable of changes in WM tracts of CG_L, IFF_L/R, and UF_L mediated the relationship between age and the neuropsychological task of GPT_R (an index of processing speed) (RMSEA < 0.001; chi square $p = 0.977$; CFI = 1.00). A fourth good model fit is on ΔAxD, showing that the changes in AxD (ΔAxD) in WM tract of SLF_L mediated the relationship between age and changes in go RT (an index of processing speed).

DISCUSSION

This study aimed to provide longitudinal data to compare with cross-sectional data, in which we were interested in examining if age-related differences (cross-sectional) in WM tracts and cognitive control functions can be also observed in age-related changes data with a follow-up interval of 2 years (longitudinal).

Regarding the first issue of the relationship between age and cognitive control function (including processing speed) cross-sectionally and longitudinally, we observed that while there were several significant age-related differences in processing speed, common (inhibition), shifting, and working memory

TABLE 4 | The significant Pearson correlation *r* values for processing speed in relation to DTI measures (FA, MD, RD, and AxD) for cross-sectional and longitudinal ratio scores.

	Behavior (covariate: gender, edu, BDI-II)							
	Cross-sectional and processing speed				Longitudinal and processing speed			
	FA	**MD**	**RD**	**AxD**	**FA**	**MD**	**RD**	**AxD**
Association fiber								
ATR_L	**−0.400 (TMT-A)** **−0.337 (GPT_L)** **−0.381 (GPT_R)**	**0.442 (TMT-A)** **0.371 (GPT_L)** **0.318 (GPT_R)** 0.223 (goRT)	**0.464 (TMT-A)** **0.394 (GPT_L)** **0.361 (GPT_R)** 0.225 (goRT)	**0.342 (TMT-A)** 0.277 (GPT_L) 0.199 (goRT)	−0.274 (GPT_R)	–	–	–
ATR_R	**−0.348 (TMT-A)** **−0.311 (GPT_L)** **−0.364 (GPT_R)**	**0.418 (TMT-A)** **0.375 (GPT_L)** **0.345 (GPT_R)** 0.241 (goRT)	**0.430 (TMT-A)** **0.394 (GPT_L)** **0.375 (GPT_R)** 0.230 (goRT)	**0.346 (TMT-A)** **0.292 (GPT_L)** 0.243 (GPT_R) 0.228 (goRT)	–	–	–	–
CG_L	**−0.341 (TMT-A)** **−0.294 (GPT_L)** **−0.291 (GPT_R)**	0.220 (TMT-A) 0.221 (GPT_R)	**0.296 (TMT-A)** 0.263 (GPT_L) **0.279 (GPT_R)**	–	−0.230 (GPT_R)	0.213 (GPT_L)	0.235 (GPT_R)	–
CG_R	–	–	–	–	−0.216 (GPT_R)	–	–	–
CH_L	–	0.263 (TMT-A)	0.222 (TMT-A)	0.263 (TMT-A)	–	**0.304 (GPT_L)**	–	**0.312 (GPT_L)**
CH_R	–	0.270 (TMT-A)	0.277 (TMT-A) 0.175 (GPT_R)	–	–	–	–	–
IFF_L	**−0.385 (TMT-A)** **−0.346 (GPT_L)** **−0.375 (GPT_R)**	**0.315 (TMT-A)** 0.277 (GPT_L) **0.307 (GPT_R)**	**0.365 (TMT-A)** **0.322 (GPT_L)** **0.357 (GPT_R)**	–	**−0.284 (GPT_R)**	0.199 (GPT_R)	0.242 (GPT_R)	0.236 (GPT_L)
IFF_R	**−0.357 (TMT-A)** **−0.314 (GPT_L)** **−0.363 (GPT_R)**	**0.329 (TMT-A)** 0.251 (GPT_L) **0.307 (GPT_R)**	**0.362 (TMT-A)** **0.295 (GPT_L)** **0.352 (GPT_R)**	–	–	0.216 (GPT_R)	0.237 (GPT_R)	–
ILF_L	**−0.376 (TMT-A)** **−0.309 (GPT_L)** **−0.340 (GPT_R)**	**0.311 (TMT-A)** 0.254 (GPT_L) **0.289 (GPT_R)**	**0.357 (TMT-A)** **0.290 (GPT_L)** **0.330 (GPT_R)**	–	−0.226 (GPT_R)	0.226 (GPT_L)	–	0.242 (GPT_L)
ILF_R	**−0.370 (TMT-A)** **−0.314 (GPT_L)** **−0.349 (GPT_R)**	**0.291 (TMT-A**) 0.226 (GPT_L) 0.276 (GPT_R)	**0.343 (TMT-A)** 0.276 (GPT_L) **0.321 (GPT_R)**	–	–	–	–	–

(Continued)

TABLE 4 | (Continued)

	Behavior (covariate: gender, edu, BDI-II)							
	Cross-sectional and processing speed				Longitudinal and processing speed			
	FA	**MD**	**RD**	**AxD**	**FA**	**MD**	**RD**	**AxD**
SLF_L	**−0.308 (TMT-A)** **−0.283 (GPT_L)** **−0.328 (GPT_R)**	0.245 (TMT-A) 0.256 (GPT_R)	**0.291 (TMT-A)** 0.232 (GPT_L) **0.300 (GPT_R)**	–	–	–	–	−0.227 (goRT)
SLF_R	**−0.298 (TMT-A)** −0.270 (GPT_L) −0.283 (GPT_R)	0.248 (TMT-A)	**0.290 (TMT-A)** 0.225 (GPT_L) 0.252 (GPT_R)	–	–	–	–	–
UF_L	−**0.342 (TMT-A)** **−0.321 (GPT_L)** **−0.322 (GPT_R)**	**0.296 (TMT-A)** 0.240 (GPT_L) 0.261 (GPT_R)	**0.335 (TMT-A)** **0.289 (GPT_L)** **0.305 (GPT_R)**	–	**−0.344 (GPT_R)**	–	0.225 (GPT_R)	–
UF_R	**−0.281 (TMT-A)** −0.258 (GPT_L) −0.253 (GPT_R)	**0.291 (TMT-A)** 0.199 (GPT_L) 0.225 (GPT_R)	**0.315 (TMT-A)** 0.242 (GPT_L) 0.259 (GPT_R)	–	−0.210 (GPT_R)	–	–	–
Projection fiber								
CST_L	**−0.293 (TMT-A)** −0.202 (GPT_R)	0.221 (TMT-A)	**0.302 (TMT-A)** 0.185 (GPT_R)	–	–	–	–	–
CST_R	−0.237 (TMT-A)	0.213 (TMT-A)	0.260 (TMT-A)	–	–	–	–	–
Commissural fiber								
Fmaj	**−0.379 (TMT-A)** **−0.393 (GPT_L)** **−0.428 (GPT_R)**	**0.286 (TMT-A)** 0.232 (GPT_L) **0.287 (GPT_R)**	**0.363 (TMT-A)** **0.341 (GPT_L)** **0.388 (GPT_R)**	–	−0.243 (GPT_R)	–	–	–
Fmin	**−0.430 (TMT-A)** **−0.400 (GPT_L)** **−0.355 (GPT_R)** −0.243 (goRT)	0.234 (TMT-A) 0.248 (GPT_L) 0.250 (GPT_R)	**0.349 (TMT-A)** **0.348 (GPT_L)** **0.323 (GPT_R)**	–	**−0.311 (GPT_R)**	–	0.269 (GPT_R)	–

The ratio score's formula: [(Measure$_{TP2}$ − Measure$_{TP1}$)/Measure$_{TP1}$] × [2/(TP2 − TP1)]. The r value denoted in the table represents its p value passing the bootstrap criteria (i.e., upper and lower bound do not pass 0). r value marked in bold indicates its p value also passing the Bonferroni correction criteria ($p < 0.0003$). '–' denotes non-significance.

TABLE 5 | The significant Pearson correlation *r* values for the common/inhibition component in relation to DTI measures (FA, MD, RD, and AxD) for cross-sectional and longitudinal ratio scores.

	Behavior (covariate: gender, edu, BDI-II)							
	Cross-sectional and common/inhibition				**Longitudinal and common/inhibition**			
	FA	**MD**	**RD**	**AxD**	**FA**	**MD**	**RD**	**AxD**
Association fiber								
ATR_L	–	0.217 (commonEF)	0.222 (commonEF)	–	–	–	–	–
ATR_R	–	–	0.223 (SSRT) 0.227 (commonEF)	–	–	–	–	–
CG_L	−0.264 (SSRT)	–	0.206 (SSRT)	–	–	–	–	–
CG_R	–	–	–	–	–	–	–	–
CH_L	–	–	–	–	–	–	–	–
CH_R	–	–	–	–	–	–	–	–
IFF_L	−0.255 (SSRT) −0.240 (commonEF)	0.216 (commonEF)	0.212 (SSRT) 0.239 (commonEF)	–	–	–	–	–
IFF_R	−0.252 (SSRT) −0.245 (commonEF)	–	0.211 (SSRT) 0.232 (commonEF)	–	–	–	–	–
ILF_L	−0.278 (SSRT) **−0.279 (commonEF)**	0.216 (commonEF)	0.222 (SSRT) 0.254 (commonEF)	–	–	–	–	–
ILF_R	−0.267 (SSRT) −0.267 (commonEF)	0.187 (commonEF)	0.203 (SSRT) 0.235 (commonEF)	–	–	–	–	–
SLF_L	−0.254 (SSRT) −0.217 (commonEF)	0.199 (commonEF)	0.206 (SSRT) 0.219 (commonEF)	–	–	–	–	–
SLF_R	−0.240 (SSRT)	0.200 (commonEF)	0.212 (SSRT) 0.222 (commonEF)	–	–	–	–	–
UF_L	–	–	0.213 (commonEF)	–	–	–	–	–
UF_R	−0.249 (SSRT)	–	0.211 (commonEF)	–	–	–	–	–
Projection fiber								
CST_L	–	–	–	–	–	–	–	–
CST_R	–	–	–	–	–	–	–	–
Commissural fiber								
Fmaj	−0.210 (SSRT) −0.221 (commonEF)	–	0.203 (commonEF)	–	–	–	–	–
Fmin	**−0.319 (SSRT)** −0.278 (commonEF)	–	0.225 (SSRT) 0.220 (commonEF)	−0.172 (SSRT)	–	–	–	–

The ratio score's formula: [(Measure$_{TP2}$ − Measure$_{TP1}$)/Measure$_{TP1}$] × [2/(TP2 − TP1)]. The r value denoted in the table represents its p value passing the bootstrap criteria (i.e., upper and lower bound do not pass 0). r value marked in bold indicates its p value also passing the Bonferroni correction criteria ($p < 0.0003$). '–' denotes non-significance.

TABLE 6 | The significant Pearson correlation *r* values for the shifting component in relation to DTI measures (FA, MD, RD, and AxD) for cross-sectional and longitudinal ratio scores.

	Behavior (covariate: gender, edu, BDI-II)							
	Cross-sectional and shifting				**Longitudinal and shifting**			
	FA	**MD**	**RD**	**AxD**	**FA**	**MD**	**RD**	**AxD**
Association fiber								
ATR_L	–	0.226 (TMT-B)	0.223 (TMT-B)	–	–	–	–	–
ATR_R	–	0.214 (TMT-B)	0.194 (TMT-B)	0.233 (TMT-B)	−0.176 (non-infSWI)	–	–	–
CG_L	–	–	–	–	0.164 (SWI)	−0.122 (SWI)	–	–
CG_R	–	–	–	–	–	–	–	–
CH_L	–	–	0.200 (non-infSWI)	–	–	–	0.214 (non-infSWI)	–
CH_R	–	–	–	–	–	–	–	–
IFF_L	−0.214 (non-iSWI)	0.216 (TMT-B) –	0.230 (non-iSWI)	–	–	–	–	–
IFF_R	−0.223 (non-iSWI)	0.195 (TMT-B)	0.221 (non-iSWI)	–	–	–	–	–
ILF_L	−0.267 (non-infSWI)	0.201 (TMT-B) 0.213 (non-infSWI)	0.251 (non-infSWI)	0.208 (TMT-B)	–	–	–	–
ILF_R	−0.260 (non-infSWI)	0.176 (TMT-B) 0.213 (non-infSWI)	0.255 (non-infSWI)	–	–	–	–	–
SLF_L	–	–	–	–	–	–	–	–
SLF_R	–	–	–	–	–	–	–	−0.203 (TMT-B)
UF_L	–	–	0.207 (non-infSWI)	–	–	–	–	–
UF_R	–	–	–	–	–	–	–	–
Projection fiber								
CST_L	–	–	–	–	–	–	–	–
CST_R	–	–	–	–	–	–	–	–
Commissural fiber								
Fmaj	−0.260 (non-iSWI) −0.190 (TMT-B)	0.216 (non-iSWI) 0.186 (TMT-B)	0.257 (non-iSWI)	–	–	0.166 (SWI)	–	0.163 (SWI)
Fmin	−0.208 (TMT-B)	–	–	–	–	0.166 (SWI)	–	–

The ratio score's formula: [(Measure$_{TP2}$ − Measure$_{TP1}$)/Measure$_{TP1}$] × [2/(TP2 − TP1)]. The r value denoted in the table represents its p value passing the bootstrap criteria (i.e., upper and lower bound do not pass 0). r value marked in bold indicates its p value also passing the Bonferroni correction criteria ($p < 0.0003$). '–' denotes non-significance.

TABLE 7 | The significant Pearson correlation *r* values for the working memory/updating component and DTI measures (FA, MD, RD, and AxD for cross-sectional and longitudinal ratio scores.

	Behavior (covariate: gender, edu, BDI-II)							
	Cross-sectional and working memory/updating				**Longitudinal and working memory/updating**			
	FA	**MD**	**RD**	**AxD**	**FA**	**MD**	**RD**	**AxD**
Association fiber								
ATR_L	–	0.206 (2back)	0.209 (2back)	–	–	–	–	–
ATR_R	–	0.215 (2back)	0.224 (2back)	0.175 (2back)	–	–	–	–
CG_L	–	–	–	–	–	–	–	–
CG_R	–	–	–	0.206 (updating)	–	–	–	0.193 (1back)
CH_L	–	–	–	–	−0.183 (MIX) −0.256 (2back)	–	–	–
CH_R	–	–	–	–	**−0.372 (2back)**	–	–	–
IFF_L	−0.194 (2back)	0.238 (2back) 0.198 (updating)	0.236 (2back) 0.175 (updating)	0.182 (2back) 0.198 (updating)	–	–	–	–
IFF_R	–	0.214 (2back)	0.211 (2back)	–	–	–	–	–
ILF_L	−0.208 (2back)	0.213 (2back)	0.223 (2back)	–	–	–	–	–
ILF_R	–	–	–	−0.202 (MIX)	−0.210 (2back)	–	–	–
SLF_L	–	–	–	–	–	–	–	–
SLF_R	–	–	–	–	–	–	–	–
UF_L	–	–	–	–	–	–	–	–
UF_R	–	–	–	–	–	–	–	–
Projection fiber								
CST_L	–	–	–	–	–	–	0.191 (1back *d'*)	–
CST_R	–	–	–	–	–	–	–	–
Commissural fiber								
Fmaj	−0.188 (2back)	–	0.192 (2back)	–	–	–	–	0.177 (2back)
Fmin	−0.227 (2back)	–	0.199 (2back)	–	–	–	–	–

The ratio score's formula: [(Measure$_{TP2}$ − Measure$_{TP1}$)/Measure$_{TP1}$] × [2/(TP2 − TP1)]. The r value denoted in the table represents its p value passing the bootstrap criteria (i.e., upper and lower bound do not pass 0). r value marked in bold indicates its p value also passing the Bonferroni correction criteria ($p < 0.0003$). '–' denotes non-significance.

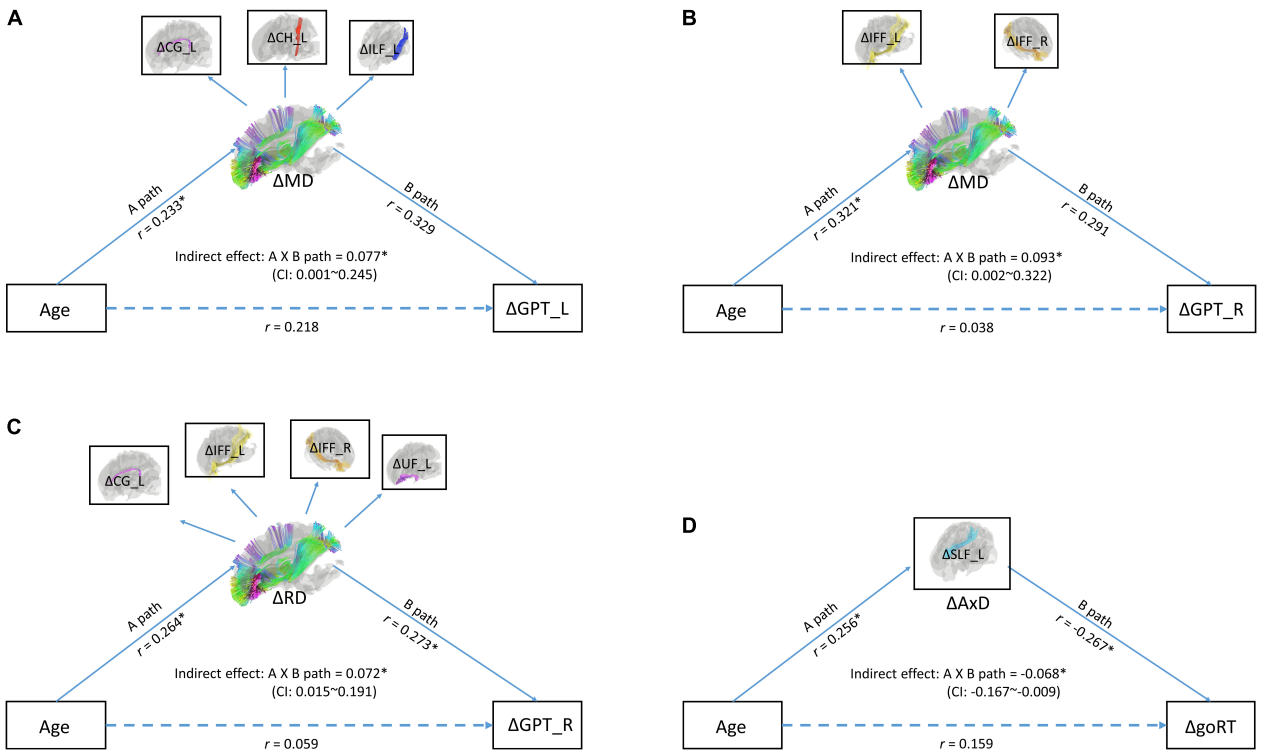

FIGURE 2 | (A) A mediation model with latent variables for age (at time point 1), ΔMD (changes in mean diffusivity), and ΔGPT_L (changes in processing speed). **(B)** A mediation model with latent variables for age (at time point 1), ΔMD (changes in mean diffusivity), and GPT_R (changes in processing speed). **(C)** A mediation model with age (at time point 1), ΔRD, and GPT_R. **(D)** A mediation model with age (at time point 1), ΔAxD, and goRT (changes in processing speed). In these models, observed variables (shown in boxes) serve as independent variables and indicators of latent variables (shown in ellipses). Indirect effect between age and mixing cost was tested by the bootstrap method. Upper and lower bound of the 95% confidence interval was marked in the center of the model. GPT_L, Grooved Pegboard Test with the left hand; GPT_R, Grooved Pegboard Test with the right hand.

updating, there were no significant correlations for age-related changes in cognitive control functions. Only changes in processing speed from TP1 to TP2 reflected on GPT_L were significantly related to age (at TP1). The results suggest that many significant correlations between age and cognitive control functions originally shown on cross-sectional data no longer exist on the longitudinal data, except that the relationship with age for ***processing speed*** was still retained even in the longitudinal data.

The current findings bring our attention in the fact that although we could observe age-related cognitive control deficits which are typically reported in most literature using cross-sectional approach (e.g., less working memory capacity – Salthouse, 1994; West, 1996; Grady and Craik, 2000; a deficit in inhibitory processing – Hasher and Zacks, 1988; Kramer et al., 1994; a lack of cognitive flexibility – Kramer et al., 1999; Mayr, 2001), when we followed up these individuals across the adult lifespan over an average of 2 years, we did not see many differences (except ***processing speed*** reflected on the left hand's movement) in their changing trajectories. Literature has also indicated a similar finding in that age did not significantly correlate with working memory changes over a period of 2 years (Charlton et al., 2010; Lövdén et al., 2014). Therefore, we should not overlook the possibility that ***aging*** processing in cognitive control functions likewise occurs for younger adults. ***That is, the aging process in cognitive control functions may not be older-age specific, but more generally occur across lifespan.***

Regarding the second issue of the relationship between age and DTI measures (FA, MD, RD, AxD), we observed that FA indexes in many WM tracts at TP1 were sensitive to ***age*** effect (cross-sectional data: all tracts except CG_R, CH_L, CH_R, and CST_R). In particular, Fmin has the strongest age effect reflected on FA, which is in line with the findings in the literature either using a longitudinal or cross-sectional approach (e.g., longitudinal approach: Barrick et al., 2010; cross-sectional approach: Salat et al., 1997; Vernooij et al., 2008; Sullivan et al., 2010; Jolly et al., 2016; Zavaliangos-Petropulu et al., 2019; Hsieh et al., 2020). Conversely, the FA index's changes from TP1 to TP2 were **much less** correlated to the ***aging*** effect (i.e., follow-up data). The result suggests that FA might ***not*** be a robust index when examining the ***aging*** effect. On the other hand, both MD and RD at TP1 and their changes from TP1 to TP2 showed relatively similar relationships with age (except CST_L/R, Fmaj, and Fmin tracts)[2] Although AxD showed a different pattern from other DTI measures in relation to age on the cross-sectional data

[2]In the current study, we further found that there was a non-linear aging trajectory for MD and RD showing a knob transition occurred around 50 years old for cross-sectional data at TP1 (see **Figure 2**).

(e.g., they were more non-linearly correlated with age compared to other DTI metrics), its changes somehow showed similar patterns as MD and RD changes in the follow-up results, in which several WM tracts were significantly correlated with aging (except Fmaj and Fmin tracts). Although previously based on the cross-sectional data, even our lab also claimed that FA might play a more important role than MD, RD, or AxD in reflecting the age effect (Hsieh et al., 2020), the current results based on both cross-sectional and longitudinal data conversely suggest that MD, RD, and AxD indexes in WM tracts might be more representative than FA when examining both ***age*** and ***aging*** effects with DTI (note: AxD yielded more non-linear correlations with age cross-sectionally). FA is a ratio value reflecting the directional consistency of diffusion, with higher values indicating that diffusion within a voxel is primarily restricted to one direction (O'Donnell and Westin, 2011), conversely, MD refers to the average amount of diffusion occurring within an image voxel, RD is calculated as the amount of diffusion perpendicular to the main directional axis of fibers, and AxD refers to the magnitude of diffusivity parallel to fiber tracts. Early studies of optic nerve fiber damage (Song et al., 2003, 2005) indicated that increases in RD values are associated with axonal demyelination (Wheeler-Kingshott and Cercignani, 2009), whereas lower AxD may reflect axonal injury, reduced axonal caliber, or less coherent orientation axons. Literature has shown a negative correlation between age and FA, suggesting that in older individuals the diffusion tensor is less fractionally anisotropic than in relatively younger individuals (e.g., a cross-sectional study by Boekel and Hsieh, 2018). In addition, literature using a cross-sectional approach also often report a positive correlation between MD, RD, or AxD and age (e.g., Sullivan et al., 2001; Pfefferbaum and Sullivan, 2003; Abe et al., 2008; Westlye et al., 2009; Burzynska et al., 2010; Lebel et al., 2012). Since the current longitudinal data showed that MD, RD, and AxD changes are more closely related than FA changes to the aging process, we would suggest that axonal demyelination and/or axonal degeneration is a more robust phenomenon for observing intra-individual aging processes.

When we further compared age-related declines in different WM tracts, we found association fibers of CG_R and CH_L/R were less correlated to both ***age*** and ***aging*** effects when compared to other WM tracts. In addition, ATR_L/R, and Fmin tracts across FA/MD/RD/AxD appeared to be most correlated to the ***age*** effect (cross-sectional data), in which the findings are consistent with the suggestion of frontal and callosal areas being most affected by the ***age*** effect (e.g., cross-sectional studies: Zavaliangos-Petropulu et al., 2019; Hsieh et al., 2020; Behler et al., 2021).

However, the current longitudinal data showed that the commissural fiber of Fmin no longer yielded an ***aging*** effect, despite its strong relationship with the ***age*** effect cross-sectionally. On the other hand, although the frontal association fibers of ATR_L/R remain to be correlated with ***aging***, they were only present in MD/RD/AxD, but no in FA. ***Therefore, combining the cross-sectional and longitudinal results in the current study, we suggest that ATR tracts in MD/RD/AxD are the most representative when examining both age and aging effects.***

Turning to the third issue of the association between cognitive control functions (including processing speed) and DTI measures, we observed that ***processing speed*** and cognitive control functions (including common/inhibition, shifting, and working memory/updating) were related to DTI measures cross-sectionally, with ***processing speed*** showing the most correlations with WM tracts in FA/MD/RD. Literature using a cross-sectional approach has also shown that age-related WM decline may contribute to age-related cognitive control declines. For example, some studies have explored age-dependent relationships between white matter integrity and composite measures of cognitive control function (Kennedy and Raz, 2009; Vernooij et al., 2009; Zahr et al., 2009). Furthermore, some researchers have found that frontoparietal WM differences are linked to age-related differences in task-switching performance (Madden et al., 2009; Gold et al., 2010). Perry et al. (2009) using a cross-sectional approach also observed that advancing age was associated with declines in task-set shifting performance and with decreased FA in corpus callosum and in association tracts that connect the frontal cortex to more posterior brain regions. A more recent DTI study using a cross-sectional approach led by Karayanidis also demonstrated the role of WM microstructure in age-related cognitive decline (Jolly et al., 2013). Bucur et al. (2008) also using a cross-sectional approach observed that declines in FA in the pericallosal frontal region and in the genu of the corpus callosum, but not in other regions, mediated the relationship between perceptual speed and episodic retrieval reaction time. Hence, they suggested that WM integrity in prefrontal regions is one mechanism underlying the relationship between individual differences in perceptual speed and episodic retrieval (Bucur et al., 2008). Nevertheless, most of these studies cited above are cross-sectional results.

However, when we examined the longitudinal data in the current study, we observed that changes in ***processing speed*** as compared to changes in other cognitive control performance were more correlated to the changes in all DTI indexes. Therefore, ***processing speed*** appeared to be the function that was mostly related to WM integrity both cross-sectionally and longitudinally. Processing speed is a basic cognitive or brain process that subserves many other higher-order cognitive domains. One possibility is that over a short period of follow up, changes in processing speed would be more apparent than other cognitive control functions, thus would be easier to be observed to be related to changes in WM integrity. Future research with a longer period of follow up is needed to clarify the speculation.

Finally, to provide a more direct evidence in showing if changes in DTI mediated age-related changes in ***processing speed***, we tested a series of mediation models, and the result showed that four models yielded good model fits, in which ΔRD, ΔMD, and ΔAxD mediated age-related changes in ***processing speed***. Therefore, converging the regression results and mediation models, we could conclude that MD, RD, and AxD appear to be the most representative DTI measures to reveal age-related changes in ***processing speed***.

Some final remarks are worth mentioning before closing. First, in the current study, only a period of 1–2 years follow-up interval was performed, it is likely that the period is too short to be sensitive enough to reveal the aging process. For example, in the literature, Charlton et al. (2010) and Lövdén et al. (2014)

using a follow-up approach likewise did not find an aging effect on cognitive changes, but Vonk et al. (2020) found a linear aging effect in working memory and cognitive speed. The discrepant findings among these studies are likely due to their differences in the length of the follow-up interval. The follow-up interval between the two timepoints in Vonk et al.'s (2020) research was 4∼8 years, whereas in the other two research (i.e., Charlton et al., 2010; Lövdén et al., 2014), the age interval was about 2 years which is similar to the current study. Therefore, future studies with a longer follow-up interval or more times of follow-up are warranted. Second, while we examined the aging effect in relation to the changes in DTI from TP1 to TP2, we observed very few and even paradoxically positive correlations for three WM tracts (i.e., CH_L/R, CST_L) in FA. The finding was the opposite to the cross-sectional results reported by the prior and current research. One possibility is that the reduction rate for FA with aging was not as prominent as one could expect from other DTI indicators, and because this study only followed 1.77 years on average, thus very few significant changes could be observed for FA. However, why these three tracts (CH_L/R, CST_L) showed FA increases rather than decreases with aging remain puzzled. We suspected that individual differences might contribute to the paradoxical findings. One longitudinal study with 1-year follow up comparing healthy control and Alzheimer's disease also found that healthy controls did not demonstrate FA changes in the hippocampal cingulum (i.e., CH) as were observed in those with Alzheimer's disease (Mayo et al., 2017). The authors thus concluded that changes in microstructural integrity for the hippocampal cingulum over short time intervals (i.e., 1 year) may more specifically reflect ongoing degenerative processes due to Alzheimer's disease. Since the participants in the current study were all healthy controls, some of them might be even more reserved than middle-aged or young adults. Future research with a longer follow-up period and considering individual differences is needed to clarify the issue. Third, the participants' age range in this study covered a wide range of 20 to 80 years, it may be worth considering sub-groups of different ages rather than treat all participants as a single group (e.g., see Yap et al., 2013 and Lebel et al., 2019 for reviews of DTI findings related to development). Future studies with more numbers of participants are encouraged to split into subgroups with smaller age ranges (e.g., every 10 years old per group). Fourth, this study did not analyze myelin water fraction (MWF) which should not be overlooked and should be analyzed complementary to the conventional DTI metrics. A recent study (Kiely et al., 2022) has indicated that although DTI metrics (e.g., RD and FA – indices of myelin content) might be related to the age effect, they could not serve as specific metrics to myelin, so that further studies using more specific myelin measure, such as MWF relaxometry, are required. Fifth, in this study, we used the TBSS processing pipeline in the FSL, which was developed to reduce the effects of local mis-registrations by projecting all FA voxels onto the nearest location on a "skeleton" approximating WM tract centers (Smith et al., 2006). Some studies however pointed out that TBSS was designed to compensate for local registration errors, which might in return cause many more limitations due to over compromises (see Zalesky, 2011; Schwarz et al., 2014, for more examples). Despite the limitations outlined, TBSS remains a popular method for DTI analyses.

To conclude, the current results warrant the importance of longitudinal research for aging studies to elucidate actual *aging* processes on cognitive control function. More critically, the current results provide new insights to which indicator of WM integrity and which type of cognitive changes are most representative (i.e., potentially to be effective neuroimaging biomarkers) to reflect intra-individual cognitive aging processes.

DATA AVAILABILITY STATEMENT

The raw data supporting the conclusions of this article will be made available by the authors, without undue reservation.

ETHICS STATEMENT

The studies involving human participants were reviewed and approved by Research Ethics Committee of the National Cheng Kung University, Tainan, Taiwan (Contract No. 104–004). The patients/participants provided their written informed consent to participate in this study. Written informed consent was obtained from the individual(s) for the publication of any potentially identifiable images or data included in this article.

AUTHOR CONTRIBUTIONS

SH contributed to the grant resources, the design of the experiments, data processing, and preparation of the manuscript. M-HY contributed to the data collection and analysis, and preparation of figures and tables. Both authors contributed to the article and approved the submitted version.

ACKNOWLEDGMENTS

We would like to thank the Ministry of Science Technology (MOST) of the Republic of China, Taiwan for financially supporting this research (Contract Nos. 104-2410-H-006-021-MY2, 106-2410-H-006-031-MY2, 108-2321-B-006-022-MY2, 108-2410-H-006-038-MY3, 109-2923-H-006-002-MY3, 110-2321-B-006-004, and 111-2321-B-006-008). In addition, this research was, in part, supported by the Ministry of Education, Taiwan, Republic of China, the Aim for the Top University Project to the National Cheng Kung University (NCKU). We also wish to thank American Manuscript Editors (AmericanManuscriptEditors.com) for English proofreading.

SUPPLEMENTARY MATERIAL

The Supplementary Material for this article can be found online at: https://www.frontiersin.org/articles/10.3389/fnagi.2022.850655/full#supplementary-material

REFERENCES

Abe, O., Yamasue, H., Aoki, S., Suga, M., Yamada, H., Kasai, K., et al. (2008). Aging in the CNS: comparison of gray/white matter volume and diffusion tensor data. *Neurobiol. Aging* 29, 102–116. doi: 10.1016/j.neurobiolaging.2006.09.003

Andrews-Hanna, J. R., Snyder, A. Z., Vincent, J. L., Lustig, C., Head, D., Raichle, M. E., et al. (2007). Disruption of large-scale brain systems in advanced aging. *Neuron* 56, 924–935. doi: 10.1016/j.neuron.2007.10.038

Barrick, T. R., Charlton, R. A., Clark, C. A., and Markus, H. S. (2010). White matter structural decline in normal ageing: a prospective longitudinal study using tract-based spatial statistics. *Neuroimage* 51, 565–577. doi: 10.1016/j.neuroimage.2010.02.033

Bartzokis, G. (2004). Age-related myelin breakdown: a developmental model of cognitive decline and Alzheimer's disease. *Neurobiol. Aging* 25, 5–18. doi: 10.1016/j.neurobiolaging.2003.03.001

Beck, A. T., Steer, R. A., and Brown, G. K. (1996). *Manual for the Beck Depression Inventory-II*. San Antonio, TX: Psychological Corporation.

Behler, A., Kassubek, J., and Müller, H. P. (2021). Age-Related Alterations in DTI Metrics in the Human Brain—Consequences for Age Correction. *Front. Aging Neurosci.* 13:682109. doi: 10.3389/fnagi.2021.682109

Behrens, T. E., Woolrich, M. W., Jenkinson, M., Johansen-Berg, H., Nunes, R. G., Clare, S., et al. (2003). Characterization and propagation of uncertainty in diffusion-weighted MR imaging. *Mag. Reson. Med.* 50, 1077–1088. doi: 10.1002/mrm.10609

Bennett, I. J., and Madden, D. J. (2014). Disconnected aging: cerebral white matter integrity and age-related differences in cognition. *Neuroscience* 276, 187–205. doi: 10.1016/j.neuroscience.2013.11.026

Bennett, I. J., Madden, D. J., Vaidya, C. J., Howard, D. V., and Howard, J. H. Jr. (2010). Age-related differences in multiple measures of white matter integrity: A diffusion tensor imaging study of healthy aging. *Hum. Brain Mapp.* 31, 378–390. doi: 10.1002/hbm.20872

Boekel, W., and Hsieh, S. (2018). Cross-sectional white matter microstructure differences in age and trait mindfulness. *PloS One* 13:e0205718. doi: 10.1371/journal.pone.0205718

Breukelaar, I. A., Antees, C., Grieve, S. M., Foster, S. L., Gomes, L., Williams, L. M., et al. (2017). Cognitive control network anatomy correlates with neurocognitive behavior: a longitudinal study. *Hum. Brain Mapp.* 38, 631–643. doi: 10.1002/hbm.23401

Bucur, B., Madden, D. J., Spaniol, J., Provenzale, J. M., Cabeza, R., White, L. E., et al. (2008). Age-related slowing of memory retrieval: contributions of perceptual speed and cerebral white matter integrity. *Neurobiol. Aging* 29, 1070–1079. doi: 10.1016/j.neurobiolaging.2007.02.008

Burzynska, A. Z., Preuschhof, C., Bäckman, L., Nyberg, L., Li, S. C., Lindenberger, U., et al. (2010). Age-related differences in white matter microstructure: region-specific patterns of diffusivity. *Neuroimage* 49, 2104–2112. doi: 10.1016/j.neuroimage.2009.09.041

Charlton, R. A., Schiavone, F., Barrick, T. R., Morris, R. G., and Markus, H. S. (2010). Diffusion tensor imaging detects age related white matter change over a 2 year follow-up which is associated with working memory decline. *J. Neurol., Neurosurg. Psychiat.* 81, 13–19. doi: 10.1136/jnnp.2008.167288

Craik, F. I., and Byrd, M. (1982). "Aging and cognitive deficits," in *Aging and cognitive processes*, (Boston, MA: Springer), 191–211. doi: 10.1007/978-1-4684-4178-9_11

Davis, S. W., Dennis, N. A., Buchler, N. G., White, L. E., Madden, D. J., and Cabeza, R. (2009). Assessing the effects of age on long white matter tracts using diffusion tensor tractography. *Neuroimage* 46, 530–541. doi: 10.1016/j.neuroimage.2009.01.068

de Groot, M., Ikram, M. A., Akoudad, S., Krestin, G. P., Hofman, A., van der Lugt, A., et al. (2015). Tract-specific white matter degeneration in aging: the Rotterdam Study. *Alzheimers Dementia* 11, 321–330. doi: 10.1016/j.jalz.2014.06.011

de Groot, M., Verhaaren, B. F., de Boer, R., Klein, S., Hofman, A., van der Lugt, A., et al. (2013). Changes in normal-appearing white matter precede development of white matter lesions. *Stroke* 44, 1037–1042. doi: 10.1161/STROKEAHA.112.680223

de Lange, A. M. G., Bråthen, A. C. S., Grydeland, H., Sexton, C., Johansen-Berg, H., Andersson, J. L., et al. (2016). White matter integrity as a marker for cognitive plasticity in aging. *Neurobiol. Aging* 47, 74–82. doi: 10.1016/j.neurobiolaging.2016.07.007

Fjell, A. M., Sneve, M. H., Storsve, A. B., Grydeland, H., Yendiki, A., and Walhovd, K. B. (2016). Brain events underlying episodic memory changes in aging: a longitudinal investigation of structural and functional connectivity. *Cerebral Cortex* 26, 1272–1286. doi: 10.1093/cercor/bhv102

Gold, B. T., Powell, D. K., Xuan, L., Jicha, G. A., and Smith, C. D. (2010). Age-related slowing of task switching is associated with decreased integrity of frontoparietal white matter. *Neurobiol. Aging* 31, 512–522. doi: 10.1016/j.neurobiolaging.2008.04.005

Grady, C. L., and Craik, F. I. (2000). Changes in memory processing with age. *Curr. Opin. Neurobiol.* 10, 224–231. doi: 10.1016/s0959-4388(00)00073-8

Hasher, L., and Zacks, R. T. (1988). Working memory, comprehension, and aging: A review and a new view. *Psychol. Learn. Motivat.* 22, 193–225. doi: 10.1016/s0079-7421(08)60041-9

Hedden, T., and Gabrieli, J. D. (2004). Insights into the ageing mind: a view from cognitive neuroscience. *Nat. Rev. Neurosci.* 5, 87–96. doi: 10.1038/nrn1323

Hsieh, S., and Yang, M. H. (2021). Two-Year Follow-Up Study of the Relationship Between Brain Structure and Cognitive Control Function Across the Adult Lifespan. *Front. Aging Neurosci.* 13:655050. doi: 10.3389/fnagi.2021.655050

Hsieh, S., Yao, Z. F., Yang, M. H., Yang, C. T., and Wang, C. H. (2020). Diffusion tensor imaging revealing the relation of age-related differences in the corpus callosum with cognitive style. *Front. Hum. Neurosci.* 14:285. doi: 10.3389/fnhum.2020.00285

Jolly, T. A., Cooper, P. S., Wan Ahmadul, Badwi, S. A., Phillips, N. A., Rennie, J. L., et al. (2016). Microstructural white matter changes mediate age-related cognitive decline on the Montreal Cognitive Assessment (MoCA). *Psychophysiology* 53, 258–267. doi: 10.1111/psyp.12565

Jolly, T. A. D., Bateman, G. A., Levi, C. R., Parsons, M. W., Michie, P., and Karayanidis, F. (2013). Early detection of microstructural white matter changes associated with arterial pulsatility. *Front. Hum. Neurosci.* 7:782. doi: 10.3389/fnhum.2013.00782

Karayanidis, F., Coltheart, M., Michie, P. T., and Murphy, K. (2003). Electrophysiological correlates of anticipatory and poststimulus components of task switching. *Psychophysiology* 40, 329–348. doi: 10.1111/1469-8986.00037

Kennedy, K. M., and Raz, N. (2009). Aging white matter and cognition: differential effects of regional variations in diffusion properties on memory, executive functions, and speed. *Neuropsychologia* 47, 916–927. doi: 10.1016/j.neuropsychologia.2009.01.001

Kiely, M., Triebswetter, C., Cortina, L. E., Gong, Z., Alsameen, M. H., Spencer, R. G., et al. (2022). Insights into human cerebral white matter maturation and degeneration across the adult lifespan. *NeuroImage* 247:118727. doi: 10.1016/j.neuroimage.2021.118727

Klawiter, E. C., Schmidt, R. E., Trinkaus, K., Liang, H. F., Budde, M. D., Naismith, R. T., et al. (2011). Radial diffusivity predicts demyelination in ex vivo multiple sclerosis spinal cords. *Neuroimage* 55, 1454–1460. doi: 10.1016/j.neuroimage.2011.01.007

Kramer, A. F., Hahn, S., and Gopher, D. (1999). Task coordination and aging: Explorations of executive control processes in the task switching paradigm. *Acta Psychol.* 101, 339–378. doi: 10.1016/s0001-6918(99)00011-6

Kramer, A. F., Humphrey, D. G., Larish, J. F., and Logan, G. D. (1994). Aging and inhibition: beyond a unitary view of inhibitory processing in attention. *Psychol. Aging* 9:491. doi: 10.1037/0882-7974.9.4.491

Le Bihan, D., Mangin, J. F., Poupon, C., Clark, C. A., Pappata, S., and Molko, N. (2001). Diffusion tensor imaging: concepts and applications. *J. Mag. Reson. Imaging* 13, 534–546. doi: 10.1002/jmri.1076

Lebel, C., Gee, M., Camicioli, R., Wieler, M., Martin, W., and Beaulieu, C. (2012). Diffusion tensor imaging of white matter tract evolution over the lifespan. *Neuroimage* 60, 340–352. doi: 10.1016/j.neuroimage.2011.11.094

Lebel, C., Treit, S., and Beaulieu, C. (2019). A review of diffusion MRI of typical white matter development from early childhood to young adulthood. *NMR Biomed.* 32:e3778. doi: 10.1002/nbm.3778

Light, L. L. (1991). Memory and aging: Four hypotheses in search of data. *Ann. Rev. Psychol.* 42, 333–376. doi: 10.1146/annurev.ps.42.020191.002001

Logan, G. D., Van Zandt, T., Verbruggen, F., and Wagenmakers, E. J. (2014). On the ability to inhibit thought and action: general and special theories of an act of control. *Psychol. Rev.* 121:66. doi: 10.1037/a0035230

Lövdén, M., Köhncke, Y., Laukka, E. J., Kalpouzos, G., Salami, A., Li, T. Q., et al. (2014). Changes in perceptual speed and white matter microstructure in the corticospinal tract are associated in very old age. *Neuroimage* 102, 520–530. doi: 10.1016/j.neuroimage.2014.08.020

Madden, D. J., and Allen, P. A. (1995). Aging and the speed/accuracy relation in visual search: evidence for an accumulator model. *Optom. Vis. Sci.* 72, 210–216. doi: 10.1097/00006324-199503000-00010

Madden, D. J., Bennett, I. J., Burzynska, A., Potter, G. G., Chen, N. K., and Song, A. W. (2012). Diffusion tensor imaging of cerebral white matter integrity in cognitive aging. Biochimica et Biophysica Acta (BBA). *Mol. Basis Dis.* 1822, 386–400. doi: 10.1016/j.bbadis.2011.08.003

Madden, D. J., Bennett, I. J., and Song, A. W. (2009). Cerebral white matter integrity and cognitive aging: contributions from diffusion tensor imaging. *Neuropsychol. Rev.* 19:415. doi: 10.1007/s11065-009-9113-2

Madden, D. J., Parks, E. L., Tallman, C. W., Boylan, M. A., Hoagey, D. A., Cocjin, S. B., et al. (2017). Sources of disconnection in neurocognitive aging: cerebral white-matter integrity, resting-state functional connectivity, and white-matter hyperintensity volume. *Neurobiol. Aging* 54, 199–213. doi: 10.1016/j.neurobiolaging.2017.01.027

Maillard, P., Fletcher, E., Lockhart, S. N., Roach, A. E., Reed, B., Mungas, D., et al. (2014). White matter hyperintensities and their penumbra lie along a continuum of injury in the aging brain. *Stroke* 45, 1721–1726. doi: 10.1161/STROKEAHA.113.004084

Marques, P. C. G., Soares, J. M. M., da Silva, Magalhães, R. J., Santos, N. C., and Sousa, N. J. C. (2016). Macro-and micro-structural white matter differences correlate with cognitive performance in healthy aging. *Brain Imaging Behav.* 10, 168–181. doi: 10.1007/s11682-015-9378-4

Mayo, C. D., Mazerolle, E. L., Ritchie, L., Fisk, J. D., Gawryluk, J. R., Alzheimer's Disease, et al. (2017). Longitudinal changes in microstructural white matter metrics in Alzheimer's disease. *NeuroImage* 13, 330–338. doi: 10.1016/j.nicl.2016.12.012

Mayr, U. (2001). Age differences in the selection of mental sets: the role of inhibition, stimulus ambiguity, and response-set overlap. *Psychol. Aging* 16:96. doi: 10.1037/0882-7974.16.1.96

Miyake, A., Friedman, N. P., Emerson, M. J., Witzki, A. H., Howerter, A., and Wager, T. D. (2000). The unity and diversity of executive functions and their contributions to complex "frontal lobe" tasks: A latent variable analysis. *Cogn. Psychol.* 41, 49–100. doi: 10.1006/cogp.1999.0734

Nasreddine, Z. S., Phillips, N. A., Bédirian, V., Charbonneau, S., Whitehead, V., Collin, I., et al. (2005). The Montreal Cognitive Assessment, MoCA: a brief screening tool for mild cognitive impairment. *J. Am. Geriat. Soc.* 53, 695–699. doi: 10.1111/j.1532-5415.2005.53221.x

O'Donnell, L. J., and Westin, C. F. (2011). An introduction to diffusion tensor image analysis. *Neurosurg. Clin.* 22, 185–196. doi: 10.1016/j.nec.2010.12.004

O'Sullivan, M. R. C. P., Jones, D. K., Summers, P. E., Morris, R. G., Williams, S. C. R., and Markus, H. S. (2001). Evidence for cortical "disconnection" as a mechanism of age-related cognitive decline. *Neurology* 57, 632–638. doi: 10.1212/wnl.57.4.632

Park, D. C. (2002). Aging, cognition, and culture: a neuroscientific perspective. *Neurosci. Biobehav. Rev.* 26, 859–867. doi: 10.1016/s0149-7634(02)00072-6

Park, D. C., Lautenschlager, G., Hedden, T., Davidson, N. S., Smith, A. D., and Smith, P. K. (2002). Models of visuospatial and verbal memory across the adult life span. *Psychol. Aging* 17:299. doi: 10.1037/0882-7974.17.2.299

Perry, M. E., McDonald, C. R., Hagler, D. J. Jr., Gharapetian, L., Kuperman, J. M., Koyama, A. K., et al. (2009). White matter tracts associated with set-shifting in healthy aging. *Neuropsychologia* 47, 2835–2842. doi: 10.1016/j.neuropsychologia.2009.06.008

Pfefferbaum, A., and Sullivan, E. V. (2003). Increased brain white matter diffusivity in normal adult aging: relationship to anisotropy and partial voluming. *Magn. Reson. Med.* 49, 953–961. doi: 10.1002/mrm.10452

Rugg, M. D. (2017). "Interpreting age-related differences in memory-related neural activity," in *Cognitive neuroscience of aging: Linking cognitive and cerebral aging*, eds R. Cabeza, L. Nyberg, and D. C. Park (Oxford: Oxford University Press), 183–203. doi: 10.1093/acprof:oso/9780199372935.003.0008

Salat, D., Ward, A., Kaye, J. A., and Janowsky, J. S. (1997). Sex differences in the corpus callosum with aging. *Neurobiol. Aging* 18, 191–197. doi: 10.1016/s0197-4580(97)00014-6

Salat, D. H., Tuch, D. S., Greve, D. N., Van Der Kouwe, A. J. W., Hevelone, N. D., Zaleta, A. K., et al. (2005). Age-related alterations in white matter microstructure measured by diffusion tensor imaging. *Neurobiol. Aging* 26, 1215–1227. doi: 10.1016/j.neurobiolaging.2004.09.017

Salthouse, T. A. (1994). The aging of working memory. *Neuropsychology* 8, 535.

Salthouse, T. A. (2004). Localizing age-related individual differences in a hierarchical structure. *Intelligence* 32, 541–561. doi: 10.1016/j.intell.2004.07.003

Scahill, R. I., Frost, C., Jenkins, R., Whitwell, J. L., Rossor, M. N., and Fox, N. C. (2003). A longitudinal study of brain volume changes in normal aging using serial registered magnetic resonance imaging. *Arch. Neurol.* 60, 989–994. doi: 10.1001/archneur.60.7.989

Schwarz, C. G., Reid, R. I., Gunter, J. L., Senjem, M. L., Przybelski, S. A., Zuk, S. M., et al. (2014). Improved DTI registration allows voxel-based analysis that outperforms tract-based spatial statistics. *Neuroimage* 94, 65–78. doi: 10.1016/j.neuroimage.2014.03.026

Sexton, C. E., Walhovd, K. B., Storsve, A. B., Tamnes, C. K., Westlye, L. T., Johansen-Berg, H., et al. (2014). Accelerated changes in white matter microstructure during aging: a longitudinal diffusion tensor imaging study. *J. Neurosci.* 34, 15425–15436. doi: 10.1523/JNEUROSCI.0203-14.2014

Simmonds, D. J., Hallquist, M. N., Asato, M., and Luna, B. (2014). Developmental stages and sex differences of white matter and behavioral development through adolescence: a longitudinal diffusion tensor imaging (DTI) study. *Neuroimage* 92, 356–368. doi: 10.1016/j.neuroimage.2013.12.044

Smith, S. M., Jenkinson, M., Johansen-Berg, H., Rueckert, D., Nichols, T. E., Mackay, C. E., et al. (2006). Tract-based spatial statistics: voxelwise analysis of multi-subject diffusion data. *Neuroimage* 31, 1487–1505. doi: 10.1016/j.neuroimage.2006.02.024

Smith, S. M., Jenkinson, M., Woolrich, M. W., Beckmann, C. F., Behrens, T. E., Johansen-Berg, H., et al. (2004). Advances in functional and structural MR image analysis and implementation as FSL. *Neuroimage* 23, S208–S219. doi: 10.1016/j.neuroimage.2004.07.051

Song, S. K., Sun, S. W., Ju, W. K., Lin, S. J., Cross, A. H., and Neufeld, A. H. (2003). Diffusion tensor imaging detects and differentiates axon and myelin degeneration in mouse optic nerve after retinal ischemia. *Neuroimage* 20, 1714–1722. doi: 10.1016/j.neuroimage.2003.07.005

Song, S. K., Yoshino, J., Le, T. Q., Lin, S. J., Sun, S. W., Cross, A. H., et al. (2005). Demyelination increases radial diffusivity in corpus callosum of mouse brain. *Neuroimage* 26, 132–140. doi: 10.1016/j.neuroimage.2005.01.028

Sullivan, E. V., Adalsteinsson, E., Hedehus, M., Ju, C., Moseley, M., Lim, K. O., et al. (2001). Equivalent disruption of regional white matter microstructure in ageing healthy men and women. *Neuroreport* 12, 99–104. doi: 10.1097/00001756-200101220-00027

Sullivan, E. V., Zahr, N. M., Rohlfing, T., and Pfefferbaum, A. (2010). Fiber tracking functionally distinct components of the internal capsule. *Neuropsychologia* 48, 4155–4163. doi: 10.1016/j.neuropsychologia.2010.10.023

Tsai, C.-F., Lee, W.-J., Wang, S.-J., Shia, B.-C., Nasreddine, Z., and Fuh, J.-L. (2012). Psychometrics of the Montreal Cognitive Assessment (MOCA) and its subscales: validation of the Taiwanese version of the MOCA and an item response theory analysis. *Int. Psychogeriatr.* 24, 651–658. doi: 10.1017/S1041610211002298

Vernooij, M. W., Ikram, M. A., Vrooman, H. A., Wielopolski, P. A., Krestin, G. P., Hofman, A., et al. (2009). White matter microstructural integrity and cognitive function in a general elderly population. *Arch. Gen. Psychiat.* 66, 545–553. doi: 10.1001/archgenpsychiatry.2009.5

Vernooij, M. W., van der Lugt, A., Ikram, M. A., Wielopolski, P. A., Niessen, W. J., Hofman, A., et al. (2008). Prevalence and risk factors of cerebral microbleeds: the Rotterdam Scan Study. *Neurology* 70, 1208–1214. doi: 10.1212/01.wnl.0000307750.41970.d9

Vilar-Fernández, J. M., Vilar-Fernández, J. A., and González-Manteiga, W. (2007). Bootstrap tests for nonparametric comparison of regression curves with dependent errors. *Test* 16, 123–144. doi: 10.1016/j.jspi.2010.03.011

Vonk, J. M., Higby, E., Nikolaev, A., Cahana-Amitay, D., Spiro, A. III, Albert, M. L., et al. (2020). Demographic effects on longitudinal semantic processing, working memory, and cognitive speed. *J. Gerontol. Ser. B* 75, 1850–1862. doi: 10.1093/geronb/gbaa080

Wang, R. Y., Zhou, J. H., Huang, Y. C., and Yang, Y. R. (2018). Reliability of the Chinese version of the Trail Making Test and Stroop Color and Word Test among older adults. *Int. J. Gerontol.* 12, 336–339. doi: 10.1016/j.ijge.2018.06.003

West, R. L. (1996). An application of prefrontal cortex function theory to cognitive aging. *Psychol. Bull.* 120:272. doi: 10.1037/0033-2909.120.2.272

Westlye, L. T., Walhovd, K. B., Dale, A. M., Espeseth, T., Reinvang, I., Raz, N., et al. (2009). Increased sensitivity to effects of normal aging and Alzheimer's disease on cortical thickness by adjustment for local variability in gray/white contrast: a multi-sample MRI study. *Neuroimage* 47, 1545–1557. doi: 10.1016/j.neuroimage.2009.05.084

Westlye, L. T., Walhovd, K. B., Dale, A. M., Bjørnerud, A., Due-Tønnessen, P., Engvig, A., et al. (2010). Life-span changes of the human brain white matter: diffusion tensor imaging (DTI) and volumetry. *Cereb. Cortex* 20, 2055–2068. doi: 10.1093/cercor/bhp280

Wheeler-Kingshott, C. A., and Cercignani, M. (2009). About "axial" and "radial" diffusivities. *Magn. Reson. Med.* 61, 1255–1260. doi: 10.1002/mrm.21965

Yang, M. H., Yao, Z. F., and Hsieh, S. (2019). Multimodal neuroimaging analysis reveals age-associated common and discrete cognitive control constructs. *Hum. Brain Mapp.* 40, 2639–2661. doi: 10.1002/hbm.24550

Yap, Q. J., Teh, I., Fusar-Poli, P., Sum, M. Y., Kuswanto, C., and Sim, K. (2013). Tracking cerebral white matter changes across the lifespan: insights from diffusion tensor imaging studies. *J. Neural Transm.* 120, 1369–1395. doi: 10.1007/s00702-013-0971-7

Zahr, N. M., Rohlfing, T., Pfefferbaum, A., and Sullivan, E. V. (2009). Problem solving, working memory, and motor correlates of association and commissural fiber bundles in normal aging: a quantitative fiber tracking study. *Neuroimage* 44, 1050–1062. doi: 10.1016/j.neuroimage.2008.09.046

Zalesky, A. (2011). Moderating registration misalignment in voxelwise comparisons of DTI data: a performance evaluation of skeleton projection. *Mag. Reson. Imaging* 29, 111–125. doi: 10.1016/j.mri.2010.06.027

Zavaliangos-Petropulu, A., Nir, T. M., Thomopoulos, S. I., Reid, R. I., Bernstein, M. A., Borowski, B., et al. (2019). Diffusion MRI indices and their relation to cognitive impairment in brain aging: the updated multi-protocol approach in ADNI3. *Front. Neuroinform.* 13:2. doi: 10.3389/fninf.2019.00002

Conflict of Interest: The authors declare that the research was conducted in the absence of any commercial or financial relationships that could be construed as a potential conflict of interest.

frontiers | Frontiers in Aging Neuroscience

ORIGINAL RESEARCH
published: 18 May 2022
doi: 10.3389/fnagi.2022.757861

Mapping of Structure-Function Age-Related Connectivity Changes on Cognition Using Multimodal MRI

Daiana Roxana Pur[1], Maria Giulia Preti[2,3,4], Anik de Ribaupierre[5], Dimitri Van De Ville[2,3,4], Roy Eagleson[6,7], Nathalie Mella[5] and Sandrine de Ribaupierre[1,7,8]*

[1]Schulich School of Medicine & Dentistry, Western University, London, ON, Canada, [2]CIBM Center for Biomedical Imaging, Lausanne, Switzerland, [3]Institute of Bioengineering, Center for Neuroprosthetics, EPFL, Geneva, Switzerland, [4]Department of Radiology and Medical Informatics, University of Geneva (UNIGE), Geneva, Switzerland, [5]Department of Psychology, University of Geneva, Geneva, Switzerland, [6]Department of Electrical and Computer Engineering, Western University, London, ON, Canada, [7]The Brain and Mind Institute, Western University, London, ON, Canada, [8]Department of Clinical Neurological Sciences, Schulich School of Medicine, Western University, London, ON, Canada

OPEN ACCESS

Edited by:
Ching-Po Lin, National Yang-Ming University, Taiwan

Reviewed by:
Adriana L. Ruiz-Rizzo, Ludwig Maximilian University of Munich, Germany
Mario Torso, Oxford Brain Diagnostics Ltd, United Kingdom

***Correspondence:**
Daiana Roxana Pur
dpur@uwo.ca

Specialty section:
This article was submitted to Neurocognitive Aging and Behavior, a section of the journal Frontiers in Aging Neuroscience

Received: *12 August 2021*
Accepted: *21 April 2022*
Published: *18 May 2022*

Citation:
Pur DR, Preti MG, de Ribaupierre A, Van De Ville D, Eagleson R, Mella N and de Ribaupierre S (2022) Mapping of Structure-Function Age-Related Connectivity Changes on Cognition Using Multimodal MRI. Front. Aging Neurosci. 14:757861. doi: 10.3389/fnagi.2022.757861

The relationship between age-related changes in brain structural connectivity (SC) and functional connectivity (FC) with cognition is not well understood. Furthermore, it is not clear whether cognition is represented *via* a similar spatial pattern of FC and SC or instead is mapped by distinct sets of distributed connectivity patterns. To this end, we used a longitudinal, within-subject, multimodal approach aiming to combine brain data from diffusion-weighted MRI (DW-MRI), and functional MRI (fMRI) with behavioral evaluation, to better understand how changes in FC and SC correlate with changes in cognition in a sample of older adults. FC and SC measures were derived from the multimodal scans acquired at two time points. Change in FC and SC was correlated with 13 behavioral measures of cognitive function using Partial Least Squares Correlation (PLSC). Two of the measures indicate an age-related change in cognition and the rest indicate baseline cognitive performance. FC and SC—cognition correlations were expressed across several cognitive measures, and numerous structural and functional cortical connections, mainly cingulo-opercular, dorsolateral prefrontal, somatosensory and motor, and temporo-parieto-occipital, contributed both positively and negatively to the brain-behavior relationship. Whole-brain FC and SC captured distinct and independent connections related to the cognitive measures. Overall, we examined age-related function-structure associations of the brain in a comprehensive and integrated manner, using a multimodal approach. We pointed out the behavioral relevance of age-related changes in FC and SC. Taken together, our results highlight that the heterogeneity in distributed FC and SC connectivity patterns provide unique information about the variable nature of healthy cognitive aging.

Keywords: fMRI, functional connectivity, structural connectivity, healthy aging, variability, neuroimaging, structure-function coupling

INTRODUCTION

Aging is associated with heterogenous changes in cognition and in the structure and function of the brain (Kennedy and Raz, 2015; Damoiseaux, 2017). Research over the past decades has yet to elucidate the effect of age on the association between functional and structural brain networks. Various "disruptive" or "disconnection" theories suggest that cognitive decline in normal aging stems from alterations in the integration of functional properties of brain networks and/or from subtle anatomical disconnection between brain regions, possible due to microstructural white matter loss or demyelination (O'Sullivan et al., 2001; Salat et al., 2005; Andrews-Hanna et al., 2007).

Longitudinal studies of aging indicate that changes in cognition vary considerably across different cognitive domains and behavioral tasks (i.e., visuo-spatial abilities, reaction time, processing speed, planning, decision making) at the inter-individual and even intra-individual level (Kliegel and Sliwinski, 2004; Salthouse, 2009; Goh et al., 2013; Mella et al., 2015). For example, some individuals may experience a general cognitive decline across multiple behavioral tasks (i.e., homogenous decline), while others may decline in one cognitive ability but experience preservation or even improvement of others (i.e., heterogenous change). A hallmark of cognitive aging is decreased processing speed, or an inferior performance on perceptual, motor, and decision-making tasks (Salthouse, 2000). Processing speed involves coordinated activity across multiple neural networks, and so engages perception, decision making, planning, motor performance, and task evaluation (Salthouse, 1996; Eckert et al., 2010). Therefore, processing speed tasks could be evaluating any of these abilities.

The small number of longitudinal studies that investigated changes in functional connectivity (FC) in healthy older adults were inconsistent, some indicate stability (Persson et al., 2014), while others reported a decline in intra-network FC in the executive control network and default mode network (DMN) as well as an initial increase in inter-network FC between the executive control network and DMN followed by a subsequent decline with older age (Ng et al., 2016) On the other hand, some studies suggest a pattern of initial decrease and subsequent temporary increase in FC (Cao et al., 2014; Damoiseaux, 2017). These results are generally attributed to the variability of compensatory or over-recruitment mechanisms across different cognitive domains (reviewed by Betzel et al., 2014; Damoiseaux, 2017). For example, the initial increase in FC can be attributed to an attempt to compensate for declining function, a strategy that cannot be sustained over time. Studies on structural changes with aging are more consistent, with most results pointing to widespread decreases in fractional anisotropy, particularly in frontal brain regions (Betzel et al., 2014; Zhao et al., 2015; Damoiseaux, 2017).

Most studies on the topic of FC and SC changes in aging are cross-sectional, focusing on group mean differences rather than longitudinal individual-level age-related changes (i.e., the aging process itself; Damoiseaux, 2017). Zimmermann et al. (2016) examined the effect of age on the correlation of FC and structural connectivity (SC) in a small, adult lifespan sample, and found that age-related changes in FC and SC coupling are region-dependent.

The current study examined the effect of aging on the change in the structural and functional integrity of the brain while also considering individual differences in cognition. Specifically, the main objective of the present study was to investigate how changes in FC and SC derived from magnetic resonance imaging (MRI), over a span of 2 and a half years, correlate with changes in different cognitive measures using a multivariate framework. Partial least squares (PLS) were used to map orthogonal patterns of brain-cognition relationships (McIntosh and Lobaugh, 2004; Krishnan et al., 2011).

Overall, we expected FC and SC—cognition correlations to be captured by variations in the pattern and amplitude of change across various cognitive measures (i.e., heterogeneity and amplitude of change). Additionally, it was expected that the brain-behavior relationship was positively and negatively associated with numerous structural and functional connections, mainly relating to regions susceptible to age-related change such as cingulo-opercular, dorsolateral prefrontal, somatosensory and motor, and temporo-parieto-occipital. One of the novel aspects of the current study is the use of the measure of change in brain connectivity as well as of behavioral change, which should better reflect changes related to the aging process rather than just age-related differences.

MATERIALS AND METHODS

Participants

The participants of the current study came from the longitudinal Geneva Aging Study. They all provided written informed consent, and approval was obtained from the ethics committee of the Faculty of Psychology and Educational Sciences of the University of Geneva and the Swiss Ethics Committee.

Older subjects that underwent two T1-weighted structural images, diffusion-weighted images, and fMRI scans, as well as a battery of cognitive tests were selected from a larger pool of the Geneva Aging Study, a lifespan study of 219 older adults (Fagot et al., 2018). The current analyses focused on a subset of individuals that completed longitudinal follow-up at ∼2.5 years including behavioral testing and scanning. Subjects missing any one of the behavioral tests or scans were not included. At this stage, 31 subjects were selected. Two subjects were excluded due to additional missing behavioral data and one because of a lesion on the anatomical MRI. The final sample included 28 older subjects (mean age at first scan = 72 ± 6 years, mean age at second scan = 74 ± 6 years; eight males). Their demographic information is presented in **Table 1**. Participants were screened for health problems with a health questionnaire and their structural MRIs were inspected by a neurosurgeon with significant experience evaluating MRIs (SR) to rule out abnormalities. The battery of the behavioral tests was systematically administered before the scanning sessions (mean interval between testing and MRI = 57 days, SD = 39). Image quality was additionally ensured

TABLE 1 | Participant demographic information.

Demographic	
Age at first scan (years)	72 ± 6
Age at second scan (years)	74 ± 6
Sex	20 females/8 males
Education (years)	12.34 ± 2.76
Handedness	26 R, 1L, 1A

Abbreviations: R, right-handed; L, left-handed; A, ambidextrous.

by examining head motion: absolute head motion at a single time point >2 mm and relative head motion >2.5 mm were criteria for participant removal. No participants were removed.

Behavioral Measures

Participants underwent a battery of cognitive tests including 11 different measures which are briefly synthesized in **Table 2** and reported in detail in other manuscripts (Mella et al., 2013, 2015; Fagot et al., 2018). Two of the measures, heterogeneity and amplitude of change, indicate an age-related change in cognition and the rest indicate baseline cognitive performance (i.e., measured at one timepoint). These measures are a composite score summarizing spatial and spatial-verbal working memory scores (Mat_span, MDA), crystallized abilities (MH), fluid intelligence (Raven), cognitive inhibition (Stroop), as well as mean performance and intraindividual variability in three reaction time tasks (a simple reaction time task, SRT) and a two-conditions complex processing speed task (CL6 and CL9). Intraindividual variability and mean performance have been shown to reflect different cognitive processes, intraindividual variability being linked to sustained attention abilities, while mean performance reflects the general level of processing speed. The composite scores of amplitude and heterogeneity of change in cognitive abilities at the individual level have been computed using individual analyses of variance of all tasks assessing simple reaction times, complex processing speed, and inhibition. This allowed assessing both the general amplitude of change and the heterogeneity of individual change across these tasks independently of the sample characteristics (see Mella et al., 2018 for more details). Briefly, heterogeneity of change refers to variations in the patterns of change across various cognitive measures. The homogenous decline is said to reflect a global decline in attentional resources or of mental resources, while strong heterogeneity of change may indicate a decline in one ability but stability or improvement in another (i.e., heterogenous pattern). Mean amplitude of change refers to both the direction and amplitude of the change in performance across the tasks considered. A smaller, negative change does not necessarily indicate decline but rather stability or less improvement. The higher the absolute value the stronger the change (explained in detail in Mella et al., 2018).

The 11 single measures of cognition, as well as the general amplitude and heterogeneity of change were correlated with change in SC and FC (described below) using Partial Least Square Correlation (PLSC; Mella et al., 2013, 2015; Fagot et al., 2018).

MRI Acquisition and Preprocessing

Participants were scanned in a Siemens Trio 3T magnet. The following imaging sets were analyzed in the current study: resting-state functional MRI (fMRI), structural T1-weighted MR image (T1-w), and DWI sequences. Two sequences of 30 directions DWI were acquired (TR = 8,400 ms, TE = 88 ms, b value = 1,000 s/mm^2, and voxel size 2.0 mm^3). The two DWI acquisitions were concatenated using FSL 5.08[1] (Smith et al., 2004) to increase the signal-to-noise ratio during the postprocessing. Then, a structural T1-w MR image was acquired (TE = 2.27 ms, TR = 1,900 ms, FOV = 256 mm, voxel size 1.0 mm^3). Finally, the resting-state fMRI was obtained using an echo planar imaging acquisition (echo time, TE = 30 ms,

[1]http://www.fmrib.ox.ac.uk/fsl

TABLE 2 | Behavioral measures and corresponding cognitive function.

Behavioral task	Function	Mean (SD), range	Abbreviations
Single measures			
Mill Hill Vocabulary Test	Crystalized intelligence	28.06 (4.52), 14–33	MH_MRI1
Raven Progressive Matrices 38	Fluid Intelligence	41.07(8.75), 23–56	RAVEN_MRI1
Matrices task as position recall	Verbal spatial working memory	2.48 (0.82), 0.35–4.45	MDA_MRI1
Matrices task as word-position recall	Spatial working memory	4.48 (1.12), 3–7	MAT_MRI1_SPAN
Reaction time task (IIV)	Reaction time	0.22 (0.05), 0.12–0.32	SRT_MRI1CV
Reaction time tasks (mean)	reaction time	325.11 (62.43), 241.01–497.81	SRT_MRI1M
Letters Comparison task (6L, IIV)	Processing speed	0.22 (0.05), 0.12–0.38	CL6_MRI1CV
Letters Comparison task (9L, IIV)	Processing speed	0.18 (0.06), 0.11–040	CL9_MRI1CV
Letters Comparison task (6L, mean)	Processing speed	2,969.51 (735.24), 2,090.50–4,822.61	CL6_MRI1M
Letters Comparison task (9L, mean)	Processing speed	4,438.97 (935.65), 2,975.93–6,961.79	CL9_MRI1M
Color Stroop Task	Resistance to interference	0.22 (0.10), 0.03–0.53	STROOP_MRI1
Composite measures			
Heterogeneity of change in processing speed assessed in reaction time tasks of different complexity	Stability, improvement, or decline of performance across tasks	0.21 (0.01), 0.001–0.72	Heterogeneity
Amplitude of change (increase or decrease in performance)	Magnitude of the change	−0.044 (0,12), −0.34 to 0.21	Amplitude

Note: All measures of tasks are given at baseline. IIV, intraindividual variability; IIV in reaction time and processing speed tasks are estimated with coefficients of variation.

time repetition, TR = 2,100 ms, flip angle = 80°, field of view, FOV = 205 mm, voxel size = 3.2 mm^3, 140 volumes).

The diffusion data were corrected for eddy currents and movements using FSL (Andersson and Sotiropoulos, 2016). Structural T1-w MR images were preprocessed using Freesurfer version 6.0[2] (Fischl, 2012) with a standard automated preprocessing pipeline (i.e., "recon-all" with the default set of parameters). Tissue-segmented images were obtained (i.e., white matter, gray matter, and cerebrospinal fluid), and used at the diffusion data analysis stage. For each participant, the T1-w image was registered to the diffusion data with cross-modal registration (i.e., rigid with six degrees of freedom) using a boundary-based cost function (Greve and Fischl, 2009). The diffusion data were further processed using MRtrix3[3] (Tournier et al., 2019) following the following standard structural connectome construction steps. Briefly, to estimate white matter fiber orientation distributions the white matter response function was estimated and used to perform single-shell, single-tissue constrained spherical deconvolution (MRtrix command "dwi2 response Tournier"; Tournier et al., 2004, 2007, 2013). Whole-brain tractography was generated using anatomical-constrained tractography (MRtrix command "tckgen", 50 million streamlines, maximum tract length = 250, fractional anisotropy cutoff = 0.06; Smith et al., 2012). Spherical-deconvolution informed filtering of tractograms (SIFT2, command "tcksift2") algorithm was used to estimate structural connection density (Smith et al., 2015; Tournier et al., 2015). Finally, the structural connectome was produced by mapping a multi-modal parcellation atlas with 360 regions (180 per hemisphere) described in detail in Glasser et al. (2017), to the streamlines obtained from SIFT2. A 360 × 360 connectivity matrix was created, representing the number of white matter reconstructed pathways for each pair of regions, normalized by the sum of the volumes of the two regions.

Resting-state fMRI was preprocessed using SPM8[4] and functions of the data processing assistant for resting- state fMRI (Yan, 2010) and individual brain atlases using statistical parametric mapping (Alemán-Gómez, 2006) toolboxes. Standard preprocessing steps were followed: realignment of the functional scans, spatial smoothing with an isotropic Gaussian kernel of 5-mm full width at half maximum, co-registration of the T1-w image to the functional mean, and segmentation of the structural images (white matter, gray matter, cerebrospinal fluid). The average signal from cerebrospinal fluid and white matter then was regressed out from functional time courses, together with six motion parameters (translation and rotation along the three dimensions) and linear/quadratic trends. Next, Glasser's multimodal parcellation atlas (the same used for the structural connectome) was resliced to functional resolution and applied to the fMRI data to estimate regional average time courses. For each participant, functional connectivity was calculated as Pearson correlation between each pair of time series. These were then Fischer z-transformed and stored in a 360 × 360 FC matrix.

For each subject, the change in SC and FC was calculated as the difference in connectivity values between time 2 and time 1, after taking the absolute values of the matrices for FC. The absolute change in connectivity at the individual level, reflecting therefore a change in connectivity strength (regardless of the sign, for FC), was then stored as final connectivity difference matrices.

Age and gender were regressed from the SC and Fischer's z-transformed FC, and residuals were used for the PLSC analysis.

Statistical Analysis

The behavioral measures (n = 13) were correlated (Pearson's) with each other to better understand the relationships between them, resulting in a 13 × 13 cross-correlation matrix of correlation coefficients r. The p-values were corrected for multiple comparisons using a false discovery rate (FDR; Benjamini et al., 2006). MATLAB version 2019a[5] was used for all statistical analyses.

PLSC for neuroimaging (McIntosh and Lobaugh, 2004; Krishnan et al., 2011) was used to assess the multivariate patterns of correlations between behavioral variables (i.e., cognition) and SC and FC measures. The performed analysis relates to that described in Zimmermann et al. (2018). Briefly, the upper triangle of the symmetric connectivity difference matrices (360 × 360 regions of interest) was vectorized for each of the subjects. Structural connections that were 0 at both timepoints, for 66% of subjects or more, were excluded from the analysis to avoid issues with resampling statistics (Zimmermann et al., 2018). Vectorized brain connectomes were then stacked across subjects. The behavioral variables were stored in a matrix of subjects*13 behavioral measures. Next, to start the PLSC, we computed a correlation matrix between the brain and behavioral matrices (i.e., a cross-correlation matrix between two data matrices). The cross-correlation matrix representing the brain-behavior correlation was submitted to singular value decomposition (SVD), which yields orthogonal latent variables (LVs) that capture the covariance between the variables from the behavioral and brain datasets (McIntosh and Lobaugh, 2004; Ziegler et al., 2013). The significance of the LVs was determined *via* permutation tests (1,000 iterations) of the singular values from the SVD, and the stability of the brain and behavior weights (also called saliences) was assessed using bootstrapping (500 bootstrap samples). For each significant LV, bootstrap ratios (BSR) for brain and behavior weights were calculated as the ratio of the weight over its estimated standard error. The stability of each connection in brain weights and behavioral weights was assessed based on its BSR: a positive high BSR >2.5 contributed positively and reliably to the brain-cognition correlations while a negative high BSR <-2.5 contributed negatively and reliably to the brain-cognition correlations. The positive and negative dimensions reflect distributions of connections that covary in a similar pattern to one another. Therefore, a BSR with a larger magnitude indicates that the connection with which it is associated has a large singular vector weight (i.e., contributes

[2]http://surfer.nmr.mgh.harvard.edu/
[3]http://www.mrtrix.org/
[4]http://www.fil.ion.ucl.ac.uk/spm/
[5]https://www.mathworks.com/products/matlab.html

to the LV) and a small standard error (i.e., stable across participants).

To explore the contributions of each imaging modality to behavior, a matrix of the pairwise linear correlation coefficients (Pearson correlation coefficient) between each pair of regions was calculated. Next, each matrix was vectorized and correlated using Pearson correlation.

The PLSC analysis was conducted with the 13 cognitive measures (see **Table 2**) as behavioral variables and with SC and FC change as brain variables.

RESULTS

Cognitive Measures

The cognitive measures were mostly weakly correlated with each other. Only measures CL9 MRIM1 and CL6MRI1M, both measures of processing speed involving mean performance on letters comparison task with nine letters and six letters, respectively, were positively and significantly correlated after FDR correction (0.83, $p < 0.00001$; **Figure 1**).

Brain Connectivity and Behavioral Interpretation

The relationship between the change in FC and SC and cognitive function (resulting from the PLS analysis) was captured by one LV (17% of total covariance; singular value = 2,406.87; $p = 0.0070$), showing a significant contribution to the covariance. The LV revealed functional and structural correlations expressed across an array of behavioral measures, that optimally covaried with each other, and contributed negatively or positively to the FC and SC—cognition relationship. The contribution of the connections was expressed as BSRs, which indicates how robustly each connection contributed to the weighted pattern of the SC and FC—cognition matrix.

The two imaging modalities were overall weakly correlated (-0.072, $p < 0.0001$). The strength of correlations varied based on region as depicted in **Figure 2**. For example, regions in the posterior cortex (e.g., temporo-parieto-occipital junction, superior parietal, inferior parietal, posterior cingulate) were positively correlated with medial temporal and lateral temporal cortices. The anterior cortex and sensorimotor cortices largely showed negative correlations with the rest of the brain. Positive correlations indicate that both FC and SC change contribute in the same direction towards behavior, while negative correlations indicate that FC and SC change have opposite contributions.

The contributions to behavior can be better appreciated in **Figure 3**, which depicts the association of each region (i.e., node) to the brain-behavior relationship.

Specifically, several sets of functional and structural connections were found to have stable weights by bootstrapping (**Figure 4**). The behavioral weights corresponding to the significant LV are shown in **Figure 5**. In brief, **Figure 5** indicates the behavioral pattern determined by the LV. PLS selects patterns of connections whose signal change covaries with the behavioral pattern across subjects identified by the LV. Those behaviors with higher BSR are said to modulate or contribute to a greater extent to the functional or structural connections than behaviors with lower BSR. The behavioral interpretation is presented in the following subsections (i.e., "Structural connections", "Functional connections") in conjunction with the brain weights.

Several sets of overlapping and non-overlapping functional and structural connections, specified in detail in the following subsections, were found to uniquely and independently contribute both negatively and positively to the association between change in brain connectivity and cognition in aging.

To facilitate interpretation of the data, in each hemisphere the 180 regions were separated into 22 larger partitions or "cortices" based on their topological proximity, common properties, based on architecture, task-fMRI profiles, and/or FC. Therefore, each of the 360 regions occupies one of the 22 cortices. The assignment is described in detail in Supplementary Neuroanatomical Results in Glasser et al. (2017).

Structural Connections

Structural connections captured by the LV loaded mostly positively onto the brain-behavior relationship (**Figures 3**, **6**). Some notable exceptions were several interhemispheric connections, mainly between the prefrontal cortex and several other regions (i.e., anterior cingulate, inferior frontal cortex, etc.), that loaded negatively. Specifically, interhemispheric structural connections between right dorsolateral prefrontal cortex and several other regions: left anterior cingulate and medial prefrontal cortex (BSR = −5.01), left inferior frontal cortex (BSR = −4.32), left premotor cortex (BSR = −5.01), dorsal visual stream (BSR = −5.01), left dorsolateral prefrontal cortex (BSR = −5.00), and intra-hemispheric structural connections between right insular and frontal opercular cortex—right lateral temporal cortex (BSR = −4.128), left superior parietal cortex (including intra-parietal sulcus) and left premotor (BSR = −4.16), and right dorsal stream visual cortex and left temporo-parieto-occipital-junction (BSR = −3.46), etc. Parieto-occipital-junction was defined as a strip of cortex bounded by auditory, lateral temporal, inferior parietal, and occipital (visual MT+ complexes) regions (Glasser et al., 2017). Therefore, decreased SC between the above-mentioned regions was positively correlated with cognitive functioning (i.e., measured by heterogeneity and amplitude of change), and baseline performance on crystallized intelligence, verbal-spatial memory, and processing speed. Decreased SC was negatively correlated with baseline performance on spatial working memory, and fluid intelligence.

Functional Connections

There was variation in the contribution of FC connections to the brain-behavior relationship (**Figures 3**, **7**). Some connections showed a strong, positive contribution including left premotor cortex and right early visual cortex (BSR = 8.57), left lateral temporal cortex and left temporo-parieto-occipital junction (BSR = 8.60), somatosensory and motor—MT+ complex and neighboring visual areas (BSR = 5.13). Thus, increased FC in these regions was correlated with inferior baseline performance on crystallized intelligence, verbal-spatial memory, and processing speed. Increased FC was positively correlated

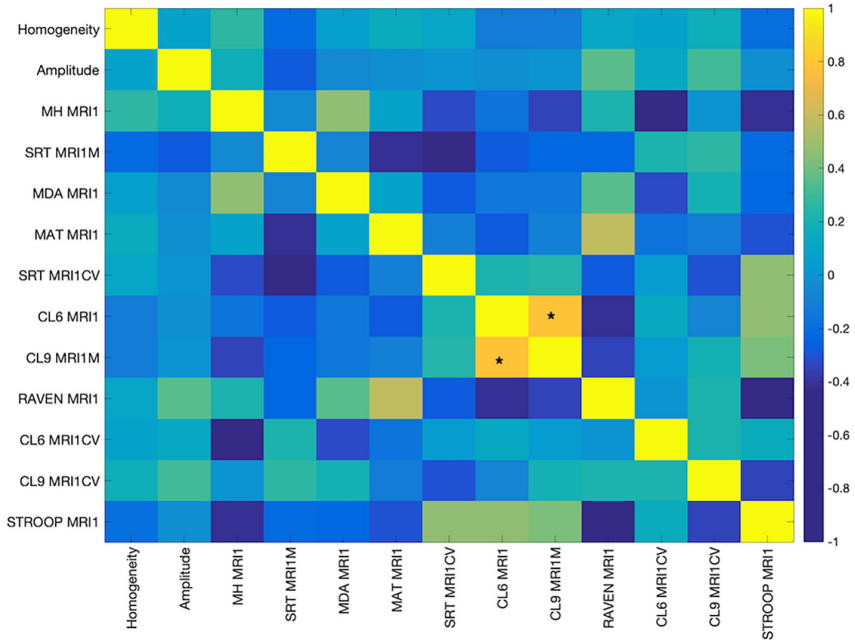

FIGURE 1 | Pearson's Correlation among the cognitive measures. The color bar indicates the strength of the correlation (r). Abbreviations: MH MR1, Mill Hill Vocabulary Test; SRT MRI1M, mean performance of Simple Reaction Time; MDA MRI1, Matrices Task with position recall; MAT MRI1, Matrices Task with word position recall; CL6 MRI1, mean performance on Letters Comparison Task with six letters; CL9 MRI1, mean performance on Letters Comparison task with nine letters; RAVEN MRI1, Raven Progressive Matrices 38; CL6 MRICV, Coefficient of variation of Letters Comparison task with six letters; CL9_MRI1CV, Coefficient of variation of letters comparison task with nine letters; Stroop MRI1, Color Stroop Task. *Indicates significance at $p < 0.00001$.

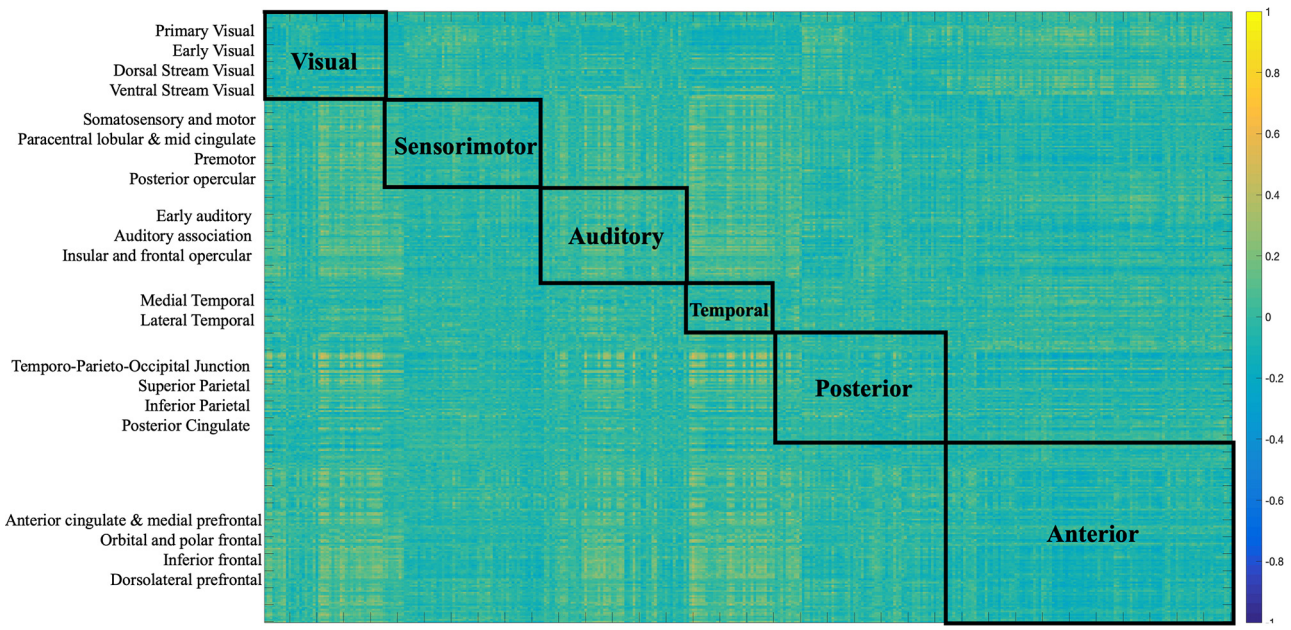

FIGURE 2 | Correlation matrix between SC and FC modalities. The first 180 regions pertain to the left hemisphere and the next 180 (i.e., 181–360) to the right hemisphere (i.e., homologs). Their full description can be found in Table 1 in Supplementary Neuroanatomical Results in Glasser et al. (2017). The color bar refers to the strength of the correlations.

with higher scores in baseline spatial working memory, and fluid intelligence.

Others showed a strong negative contribution, including interhemispheric functional connections between right

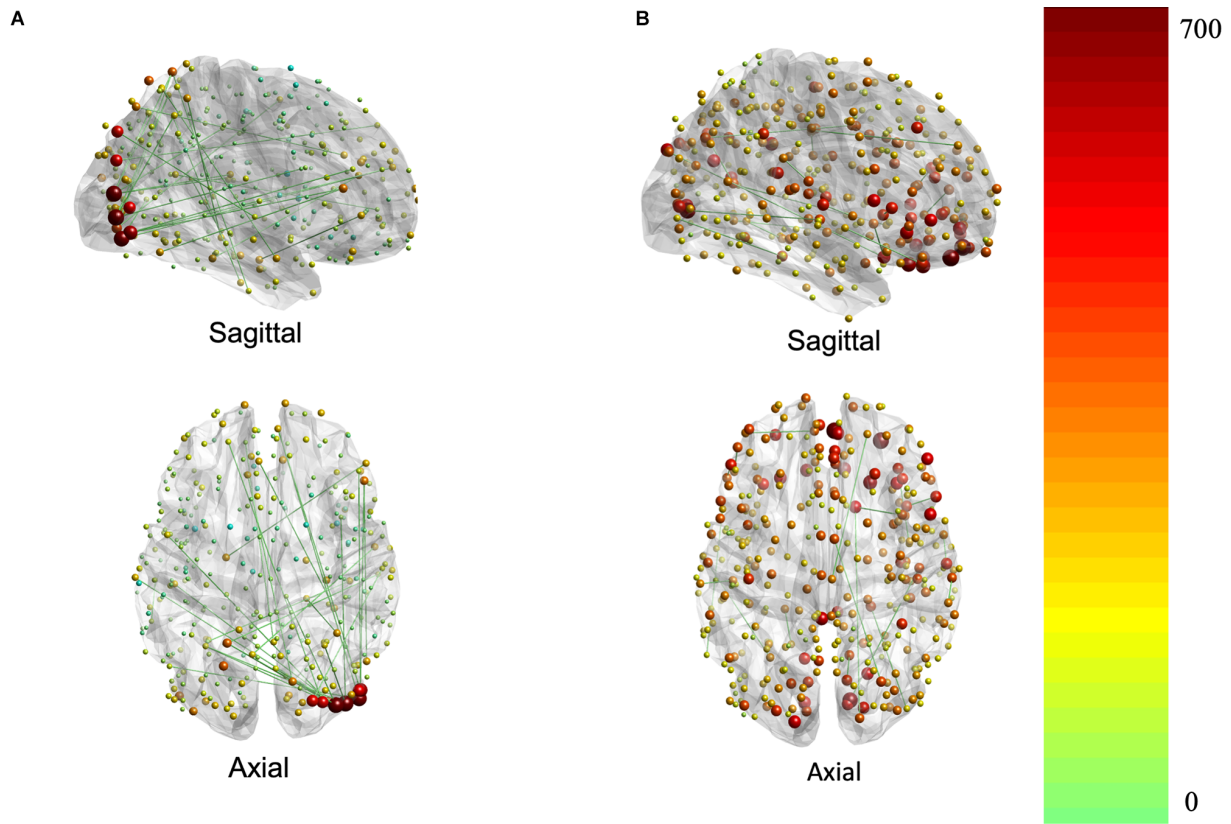

FIGURE 3 | Brain plots for FC **(A)** and SC **(B)** brain saliences. Brain regions are represented by nodes whose size and color code are proportional to their node strength. The node strength essentially represents the degree to which each connection contributes to the covariance pattern of behavior (red is higher strength while green is lower strength).

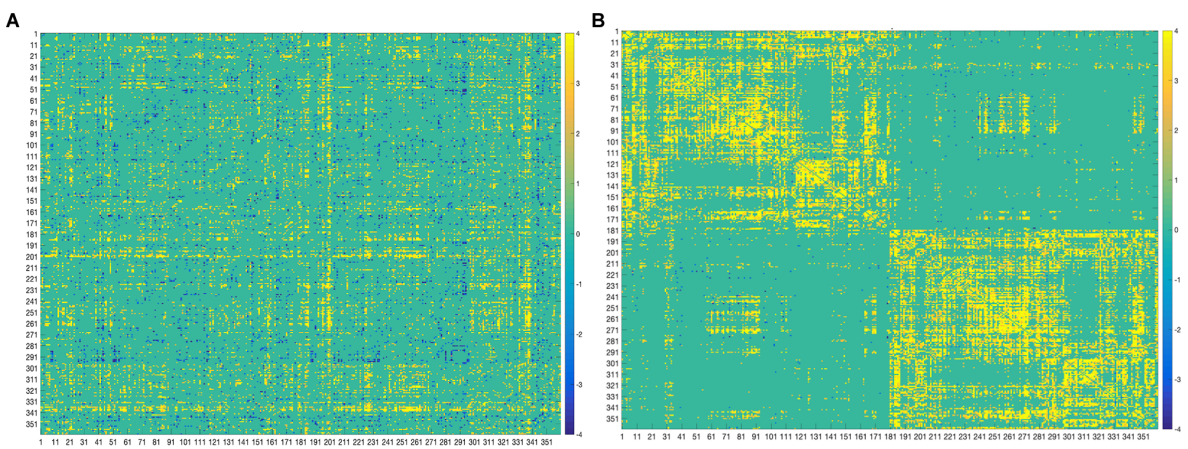

FIGURE 4 | Bootstrap connectivity weights for FC **(A)** and SC **(B)** change. The first 180 regions pertain to the left hemisphere and the next 180 (i.e., 181–360) to the right hemisphere (i.e., homologs). Their full description can be found in Table 1 in Supplementary Neuroanatomical Results in Glasser et al., 2017. The color bar refers to the bootstrap ratios. Connections with positive bootstrap ratios are positively associated with the FC or SC—cognition correlation, and negative bootstrap ratios are negatively associated with the FC or SC—cognition correlation.

insular and frontal opercular cortex and several other regions: left paracentral lobular and mid cingulate cortex (BSR = −5.47), left anterior cingulate and medial prefrontal cortex (BSR = −3.32), left inferior parietal cortex (BSR = −5.72),

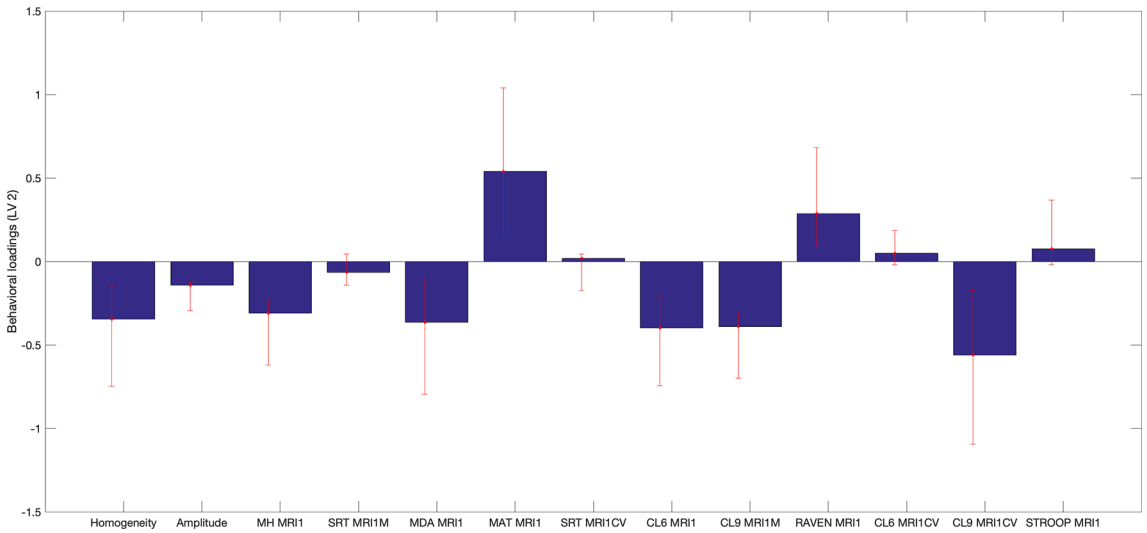

FIGURE 5 | Behavioral saliences, with confidence intervals from bootstrap resampling. Error bars indicate bootstrapping 5th to 95th percentiles. Abbreviations: MRI1, at first MRI scan; MH MR1, Mill Hill Vocabulary Test; SRT MRI1M, mean performance of Simple Reaction Time; MDA MRI1, Matrices Task with position recall; MAT MRI1, Matrices Task with word position recall; CL6 MRI1, mean performance on Letters Comparison Task with six letters; CL9 MRI1, mean performance on Letters Comparison Task with nine letters; RAVEN MRI1, Raven Progressive Matrices 38; CL6 MRICV, Coefficient of variation of Letters Comparison Task with six letters; CL9_MRI1CV, Coefficient of variation of letters comparison Task with nine letters; Stroop MRI1, Color Stroop Task.

FIGURE 6 | Bootstrap connectivity weights for SC change. Each of the 360 Glasser regions occupies one of the 22 cortices, which are listed on the y-axis. Each cortex was further labeled to a larger partition depicted on the matrix. The assignment is described in detail in Supplementary Neuroanatomical Results in Glasser et al. (2017).

posterior cingulate (BSR = −3.24), left somatosensory and motor cortex (BSR = −3.03), left superior parietal cortex and intra-parietal sulcus (BSR = −4.23). Also, intra-hemispheric functional connections between right between posterior opercular cortex and right posterior cingulate (BSR = −3.14), and right anterior cingulate and medial prefrontal cortex—insular and frontal opercular cortex (BSR = −4.23).

Therefore, decreased FC in these regions was positively correlated with cognitive functioning (i.e., measured by heterogeneity and amplitude of change), and baseline

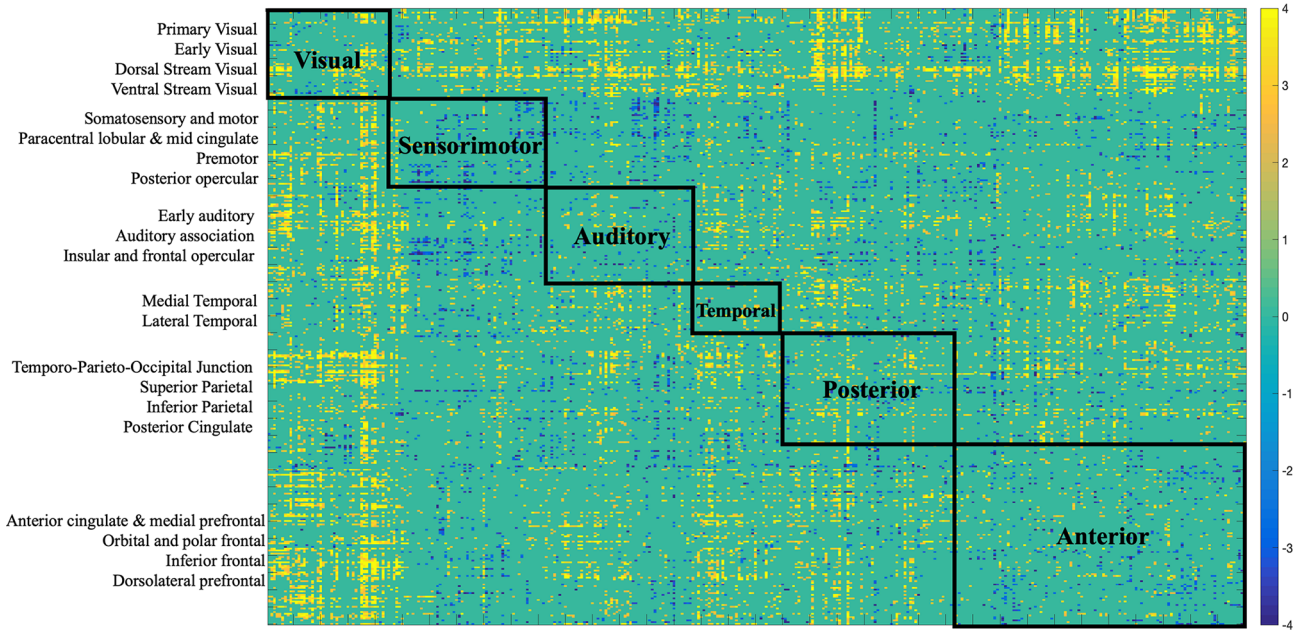

FIGURE 7 | Bootstrap connectivity weights for FC change. Each of the 360 Glasser regions occupies one of the 22 cortices, which are listed on the y-axis. Each cortex was further labeled to a larger partition depicted on the matrix. The assignment is described in detail in Supplementary Neuroanatomical Results in Glasser et al. (2017).

performance on crystallized intelligence, verbal-spatial memory, and processing speed. Decreased FC was negatively correlated with baseline spatial working memory and fluid intelligence.

DISCUSSION

In the current study, we characterized the mapping of age-related changes in FC and SC on 13 behavioral measures of cognitive function such as spatial working memory (MAT_MRI1_SPAN), crystallized intelligence (MH_MRI1), reaction time (SRT_MRI1M), and resistance to interference (i.e., STROOP_MRI1), in a sample of older adults.

We used PLSC, a multivariate method increasingly used for neuroimaging analysis (McIntosh and Lobaugh, 2004), to characterize brain-behavior relationships.

Structural and Functional Connections Vary in Their Contribution to the Brain-Behavior Relationship in Aging

Several distinct sets of functional and structural connections were identified and assigned to 22 larger partitions (see "Materials and Methods" Section). This can be visualized in **Figure 2**. Areas that contribute to behavior in the same way (either both negatively or both positively) are depicted in yellow (i.e., positive correlations), while areas that have opposing contributions are in dark blue. Visual, auditory, and temporal cortices mostly present positive correlations between FC and SC contributions indicating that in these areas FC and SC change contribute in the same direction to behavior. Anterior cortices had largely a negative correlation with other cortices. For example, FC change (**Figure 7**) indicates negative loading onto behavior while SC change (**Figure 6**) indicates positive loading. This indicates that there is preservation of structural connections but decline in functional ones.

The majority of the structural connections loaded positively onto the latent variables identified by PLSC, indicating stability or increased connectivity. Given the relatively short time of 2.5 years between the scans, and that our study sample is of healthy older adults we did not expect an accelerated global decrease in structural connectivity. Although the majority of structural connections contributed strongly and positively to the brain-behavior relationship, there were some exceptions with some areas contributing strongly and negatively (see **Figure 4**). Notably, interhemispheric structural connections between the right dorsolateral prefrontal cortex and several other regions (frontal, sensory, motor) in the left hemisphere: anterior cingulate and medial prefrontal cortex, inferior frontal, premotor, dorsal visual stream, and dorsolateral prefrontal cortex. The dorsal visual stream contains higher visual areas implicated in perceiving where visual stimuli are located and in planning visually guided actions (Ungerleider and Mishkin, 1982; Goodale and Milner, 1992). Other negatively contributing regions were left intra-hemispheric fronto-parietal and temporo-parieto-occipital structural connections. Decreased SC in these regions was associated with the decline in cognitive functioning (i.e., measured by heterogeneity and amplitude of change), and inferior baseline performance on crystallized intelligence, verbal-spatial memory, and processing speed. Our results are congruent

with other studies that indicate that normal aging involves decreasing myelination and reduced microstructural integrity of the white matter in the dorsolateral prefrontal cortex as well as in the corpus callosum (i.e., reduced interhemispheric connections), leading to reduced conduction of nerve fibers and cognitive decline (Peters and Sethares, 2002; Bowley et al., 2010; Kaller et al., 2015). Such changes are commonly seen in other prefrontal areas with aging and correlated with reduced cognitive ability especially involving processing speed, planning, and distractibility/inhibition (Eckert et al., 2010; Luebke et al., 2010; Kaller et al., 2015). Our measures of cognitive functioning, heterogeneity, and amplitude of change, were derived from tests assessing simple reaction times, complex processing speed, and inhibition. The findings of a decline in these measures correlating with decreased SC in prefrontal, motor, and sensory regions are in line with the existing literature. Studies indicate the decline in white matter fractional anisotropy is associated with lower processing speed, reflecting a regionally specific structural decline in attention-related regions in the prefrontal cortex, and a structural decline in the motor and sensory cortex, as these last are essential for performing processing speed tasks (Salthouse, 2000; Coffey et al., 2001; Charlton et al., 2006; Kennedy and Raz, 2009; Eckert et al., 2010).

There was variation in the contribution of functional connections to the brain-behavior relationship, which is in line with the existing literature, which indicates that age-related functional reorganization does not follow a global, whole-brain pattern rather is region-dependent (Goh et al., 2013; Cao et al., 2014; Zimmermann et al., 2016). Some connections showed a strong, positive contribution including somatosensory, motor, and temporo-occipital connections. Thus, preserved or increased FC in these regions was correlated with higher scores in baseline spatial working memory and fluid intelligence, decline in cognitive functioning, inferior baseline performance on crystallized intelligence, verbal-spatial memory, and processing speed. These observations are largely consistent with other studies reporting age-related increases in FC within motor cortices (Meier et al., 2012; Tomasi and Volkow, 2012), somato-motor connections (Betzel et al., 2014), and visual networks (Betzel et al., 2014; Geerligs et al., 2015).

Other functional connections showed a strong negative contribution to the brain-behavior relationship. Largely, these were composed of interhemispheric cingulo-opercular, and insular and opercular connections with parietal, paracentral lobule, medial prefrontal cortex, somatosensory, motor, anterior, mid, and posterior cingulate functional connections. To provide behavioral context to the above results, decreased FC in these regions was associated with the decline or less improvement in cognitive functioning (i.e., measured by heterogeneity and amplitude of change), inferior baseline performance on crystallized intelligence, verbal-spatial memory, processing speed, and higher scores in baseline spatial working memory, fluid intelligence.

Interestingly, decreased cingulo-opercular network (including the insula) FC has been reported to correlate with age-related reductions in visual processing speed (Ruiz-Rizzo et al., 2019), and so in our study, this may explain the lower scores on heterogeneity and amplitude of change since these were derived using processing speed tasks with visual stimuli. Some of the other functional connections mentioned (posterior cingulate, prefrontal, parietal cortex, etc.) are part of the default mode network (DMN; Alves et al., 2019), and lower DMN FC has been reported to be decreased in age-related decline in processed speed (Damoiseaux et al., 2008). We found that decreased FC between right insular and frontal opercular cortex and several other regions: left paracentral lobular and midcingulate cortex, left anterior cingulate and medial prefrontal cortex, left inferior parietal cortex, and posterior cingulate was associated with decreased cognitive functioning (i.e., measured by heterogeneity and amplitude of change), inferior baseline performance on crystallized intelligence, verbal-spatial memory, processing speed, and higher scores in baseline spatial working memory, fluid intelligence. Disruption of coordinated functional activity of key network regions such as the ones mentioned (posterior cingulate, prefrontal, parietal cortex), has been strongly linked to cognitive decline in advancing age without an overt disease (Andrews-Hanna et al., 2007). Some studies found that the relationship between decreased DMN and reduced processing speed is attenuated by controlling for whole-brain FC and white matter hyperintensities (Staffaroni et al., 2018) and reduced functional anisotropy between DMN areas (Andrews-Hanna et al., 2007). Therefore, there is a proposed vulnerability of these connections with cognitive aging. Similarly, reduced FC was reported for the insular and cingulated cortex with aging and cognitive decline (Onoda et al., 2012). Our study did not focus on within and between network analysis, however, that would be an interesting direction to explore. For example, the anticorrelation between the DMN and dorsal attention network is well-studied metric for cognitive functioning in aging. However, multi-modal longitudinal studies are limited in this area (Zhu et al., 2016).

Moreover, right intra-hemispheric functional connections involving cingulo-opercular, fronto-parietal, and prefrontal-opercular (including insula) connections, were also found to be negatively contributing to the brain-behavior relationship. In a comprehensive review by Robertson (2014), cognitive reserve (known to be protective in cognitive aging) is linked to the functional integrity of the frontoparietal connections in the right hemisphere, meaning that less FC in these regions may indicate a decline in cognitive functioning involving arousal, sustained attention, response to novelty, and awareness (Robertson, 2014; Haupt et al., 2019). Thereby, corroborating our results of decreased FC in these regions associated with a decline or less improvement in cognitive functioning.

Future Directions and Limitations

A significant strength of our study is our longitudinal design, as only longitudinal studies can measure change. It allowed the investigation of individual brain-behavior developmental trajectories in aging, rather than just general tendencies in age differences, an important approach considering that aging is a heterogenous process. The within-subject approach minimizes cohort and period effects typical of cross-sectional designs and may help disentangle to what degree change in FC and SC

ultimately drives aging-related changes in cognition, as well as investigate the behavioral relevance of FC and SC metrics.

Further longitudinal studies investigating age-related change in FC and SC while considering cognition are necessary to elucidate the underlying brain mechanisms behind cognitive decline in normal aging. It would be valuable to investigate the change in FC within and between brain networks (i.e., DMN, salience network, etc) and correlate it with white matter integrity and SC, with various brain parcellations, and across large longitudinal samples of healthy older adults and in different pathological states (i.e., Alzheimer's).

Some weaknesses of our study are our relatively small sample size (n = 28) and the small number of cognitive measures that represent change (i.e., heterogeneity and amplitude of change). We also had only two timepoints at a relatively short interval (2.5 years), which may limit the generalizability of our study to the lifespan scale. Additional time points and a larger time frame would allow a more robust assessment of where on the trajectory of age-related change an individual's brain is.

CONCLUSIONS

In summary, we have shown that age-related changes in the brain-behavior relationship are supported by distinct positive and negative contributions from structural and functional connections distributed across the brain. From a behavioral perspective, we found that subjects with a decline in cognitive functioning (as derived from processing speed tasks), had decreased SC in fronto-parietal, prefrontal, and frontal connections, and decreased FC in cingulo-opercular, and DMN associated regions. Globally, we found a tendency for whole-brain SC preservation and mixed FC changes.

DATA AVAILABILITY STATEMENT

The raw data supporting the conclusions of this article will be made available by the authors, without undue reservation.

ETHICS STATEMENT

The participants of the current study came from the longitudinal Geneva Aging Study. They all provided written informed consent, and approval was obtained from the ethics committee of the Faculty of Psychology and Educational Sciences of the University of Geneva and the Swiss Ethic Committee. The patients/participants provided their written informed consent to participate in this study.

AUTHOR CONTRIBUTIONS

All authors contributed to the design and implementation of the research, to the analysis of the results, and to the writing of the manuscripts. All authors contributed to the article and approved the submitted version.

FUNDING

This work was supported by the SNF (Swiss National Foundation, Grant Nos. 100014_135410, PMPDP1 171335, and PMPDP1 158319). Additionally, DP received funding from Mitacs Globalink Research Award while conducting the relevant research abroad. MP was supported by the CIBM Center for Biomedical Imaging, a Swiss research center of excellence founded and supported by Lausanne University Hospital (CHUV), University of Lausanne (UNIL), Ecole polytechnique fédérale de Lausanne (EPFL), University of Geneva (UNIGE), and Geneva University Hospitals (HUG).

ACKNOWLEDGMENTS

We thank the participants of the Geneva Aging Study. Thank you to the reviewers for their thorough read and edits, which have significantly improved the quality of the manuscript. Thank you to Renee-Marie Virginia Ragguett and Liam Emerson Bilbie for technical help with figures and matrices.

REFERENCES

Alemán-Gómez, Y. (2006). "IBASPM: toolbox for automatic parcellation of brain structures," in *12th Annual Meeting of the Organization for Human Brain Mapping* (Florence, Italy).

Alves, P. N., Chris, F., Vyacheslav, K., Danilo, B., Daniel, S. M., Emmanuelle, V., et al. (2019). An improved neuroanatomical model of the default-mode network reconciles previous neuroimaging and neuropathological findings. *Commun. Biol.* 2:370. doi: 10.1038/s42003-019-0611-3

Andersson, J. L. R., and Sotiropoulos, S. N. (2016). An integrated approach to correction for off-resonance effects and subject movement in diffusion MR imaging. *NeuroImage* 125, 1063–1078. doi: 10.1016/j.neuroimage.2015.10.019

Andrews-Hanna, J. R., Abraham, Z. S., Justin, L. V., Cindy, L., Denise, H., Marcus, E. E. R., et al. (2007). Disruption of large-scale brain systems in advanced aging. *Neuron* 56, 924–935. doi: 10.1016/j.neuron.2007.10.038

Benjamini, Y., Krieger, A. M., and Yekutieli, D. (2006). Adaptive linear step-up procedures that control the false discovery rate. *Biometrika* 93, 491–507. doi: 10.1093/biomet/93.3.491

Betzel, R. F., Lisa, B., Ye, H., Joaquín, G., Xi, N. Z., Olaf, S., et al. (2014). Changes in structural and functional connectivity among resting-state networks across the human lifespan. *NeuroImage* 102, 345–357. doi: 10.1016/j.neuroimage.2014.07.067

Bowley, M. P., Howard, C., Douglas, L. R., and Alan, P. (2010). Age changes in myelinated nerve fibers of the cingulate bundle and corpus callosum in the rhesus monkey. *J. Comp. Neurol.* 518, 3046–3064. doi: 10.1002/cne.22379

Cao, M., Jin, H. W., Zheng, J. D., Xiao, Y. C., Li, L. J., Feng, M. F., et al. (2014). Topological organization of the human brain functional connectome across the lifespan. *Dev. Cogn. Neurosci.* 7, 76–93. doi: 10.1016/j.dcn.2013.11.004

Charlton, R. A., Barrick, T. R., McIntyre, D. J., Shen, Y., O'Sullivan, M., Howe, F. A., et al. (2006). White matter damage on diffusion tensor imaging correlates with age-related cognitive decline. *Neurology* 66, 217–222. doi: 10.1212/01.wnl.0000194256.15247.83

Coffey, C. E., Ratcliff, G., Saxton, J. A., Bryan, R. N., Fried, L. P., Lucke, J. F., et al. (2001). Cognitive correlates of human brain aging: a quantitative magnetic resonance imaging investigation. *J. Neuropsychiatry Clin. Neurosci.* 13, 471–485. doi: 10.1176/jnp.13.4.471

Damoiseaux, J. S. (2017). Effects of aging on functional and structural brain connectivity. *NeuroImage* 160, 32–40. doi: 10.1016/j.neuroimage.2017.01.077

Damoiseaux, J. S., Beckmann, C. F., Sanz Arigita, E. J., Barkhof, F., Scheltens, P. H., Stam, C. J., et al. (2008). Reduced resting-state brain activity in the "default network" in normal aging. *Cereb. Cortex* 18, 1856–1864. doi: 10.1093/cercor/bhm207

Eckert, M. A., Noam, I. K., Donna, R. R., Vince, D. C., and Kelly, C. H. (2010). Age-related changes in processing speed: unique contributions of cerebellar and prefrontal cortex. *Front. Hum. Neurosci.* 4:10. doi: 10.3389/neuro.09.010.2010

Fagot, D., Nathalie, M., Erika, B., Paolo, G., Thierry, L., Anik, D. R., et al. (2018). Intra-individual variability from a lifespan perspective: a comparison of latency and accuracy measures. *J. Intell.* 6:16. doi: 10.3390/jintelligence6010016

Fischl, B. (2012). FreeSurfer. *NeuroImage* 62, 774–781. doi: 10.1016/j.neuroimage.2012.01.021

Geerligs, L., Remco, J. R., Emi, S., Natasha, M. M., and Monicque, M. L. (2015). A brain-wide study of age-related changes in functional connectivity. *Cereb. Cortex* 25, 1987–1999. doi: 10.1093/cercor/bhu012

Glasser, M. F., Timothy, S. C., Emma, C. R., Carl, D. H., Essa, Y., Kamil, U., et al. (2017). Europe pmc funders group europe pmc funders author manuscripts a multi-modal parcellation of human cerebral cortex. *Nature* 536, 171–178. doi: 10.1038/nature18933

Goh, J. O., Lori, L. B.-H., Yang, A., Michael, A. K., and Susan, M. R. (2013). Frontal function and executive processing in older adults: process and region specific age-related longitudinal functional changes. *NeuroImage* 69, 43–50. doi: 10.1016/j.neuroimage.2012.12.026

Goodale, M. A., and Milner, A. D. (1992). Separate visual pathways for perception and action. *Trends Neurosci.* 15, 20–25. doi: 10.1016/0166-2236(92)90344-8

Greve, D. N., and Fischl, B. (2009). Accurate and robust brain image alignment using boundary-based registration. *NeuroImage* 48, 63–72. doi: 10.1016/j.neuroimage.2009.06.060

Haupt, M., Adriana, L. R.-R., Christian, S., and Kathrin, F. (2019). Phasic alerting effects on visual processing speed are associated with intrinsic functional connectivity in the cingulo-opercular network. *NeuroImage* 196, 216–226. doi: 10.1016/j.neuroimage.2019.04.019

Kaller, C. P., Marco, R., Michael, K., Roza, U., Irina, M., Jürgen, H., et al. (2015). Predicting planning performance from structural connectivity between left and right mid-dorsolateral prefrontal cortex: moderating effects of age during postadolescence and midadulthood. *Cereb. Cortex* 25, 869–883. doi: 10.1093/cercor/bht276

Kennedy, K. M., and Raz, N. (2009). Aging white matter and cognition: differential effects of regional variations in diffusion properties on memory, executive functions and speed. *Neuropsychologia* 50, 39–43. doi: 10.1016/j.neuropsychologia.2009.01.001

Kennedy, K. M., and Raz, N. (2015). "Normal aging of the brain," in *Brain Mapping* (Elsevier), 603–617. doi: 10.1016/B978-0-12-397025-1.00068-3

Kliegel, M., and Sliwinski, M. (2004). MMSE cross-domain variability predicts cognitive decline in centenarians. *Gerontology* 50, 39–43. doi: 10.1159/000074388

Krishnan, A., Lynne, J. W., Anthony, R. M., and Hervé, A. (2011). Partial least squares (PLS) methods for neuroimaging: a tutorial and review. *NeuroImage* 56, 455–475. doi: 10.1016/j.neuroimage.2010.07.034

Luebke, J., Helen, B., and Alan, P. (2010). Effects of normal aging on prefrontal area 46 in the rhesus monkey. *Brain Res. Rev.* 62, 212–232. doi: 10.1016/j.brainresrev.2009.12.002

McIntosh, A. R., and Lobaugh, N. J. (2004). Partial least squares analysis of neuroimaging data: applications and advances. *NeuroImage* 23, 250–263. doi: 10.1016/j.neuroimage.2004.07.020

Meier, T. B., Alok, S. D., Svyatoslav, V., Veena, A. N., Jie, S., Bharat, B. B., et al. (2012). Support vector machine classification and characterization of age-related reorganization of functional brain networks. *NeuroImage* 60, 601–613. doi: 10.1016/j.neuroimage.2011.12.052

Mella, N., de Ribaupierre, S., Eagleson, R., and de Ribaupierre, A. (2013). Cognitive intraindividual variability and white matter integrity in aging. *ScientificWorldJournal* 2013:350623. doi: 10.1155/2013/350623

Mella, N., Fagot, D., Lecerf, T., and de Ribaupierre, A. (2015). Working memory and intraindividual variability in processing speed: a lifespan developmental and individual-differences study. *Mem. Cognit.* 43, 340–356. doi: 10.3758/s13421-014-0491-1

Mella, N., Fagot, D., Renaud, O., Kliegel, M., and De Ribaupierre, A. (2018). Individual differences in developmental change: quantifying the amplitude and heterogeneity in cognitive change across old age. *J. Intell.* 6:10. doi: 10.3390/jintelligence6010010

Ng, K. K., June, C. L., Joseph, K. W. L., Michael, W. L. C., and Juan, Z. (2016). Reduced functional segregation between the default mode network and the executive control network in healthy older adults: a longitudinal study. *NeuroImage* 133, 321–330. doi: 10.1016/j.neuroimage.2016.03.029

O'Sullivan, M., Jones, D. K., Summers, P. E., Morris, R. G., Williams, S. C. R., Markus, H. S., et al. (2001). Evidence for cortical "disconnection" as a mechanism of age-related cognitive decline. *Neurology* 57, 632–638. doi: 10.1212/wnl.57.4.632

Onoda, K., Masaki, I., and Shuhei, Y. (2012). Decreased functional connectivity by aging is associated with cognitive decline. *J. Cogn. Neurosci.* 24, 2186–2198. doi: 10.1162/jocn_a_00269

Persson, J., Sara, P., Lars-Göran, N., and Lars, N. (2014). Longitudinal assessment of default-mode brain function in aging. *Neurobiol. Aging* 35, 2107–2117. doi: 10.1016/j.neurobiolaging.2014.03.012

Peters, A., and Sethares, C. (2002). Aging and the myelinated fibers in prefrontal cortex and corpus callosum of the monkey. *J. Comp. Neurol.* 442, 277–291. doi: 10.1002/cne.10099

Robertson, I. H. (2014). A right hemisphere role in cognitive reserve. *Neurobiol. Aging* 35, 1375–1385. doi: 10.1016/j.neurobiolaging.2013.11.028

Ruiz-Rizzo, A. L., Christian, S., Natan, N., Julia, N., Aurore, M., Hermann, J. M., et al. (2019). Decreased cingulo-opercular network functional connectivity mediates the impact of aging on visual processing speed. *Neurobiol. Aging* 73, 50–60. doi: 10.1016/j.neurobiolaging.2018.09.014

Salat, D. H., Tuch, D. S., Greve, D. N., van der Kouwe, A. J., Hevelone, N. D., Zaleta, A. K., et al. (2005). Age-related alterations in white matter microstructure measured by diffusion tensor imaging. *Neurobiol. Aging* 26, 1215–1227. doi: 10.1016/j.neurobiolaging.2004.09.017

Salthouse, T. A. (1996). The processing-speed theory of adult age differences in cognition. *Psychol. Rev.* 103, 403–428. doi: 10.1037/0033-295x.103.3.403

Salthouse, T. A. (2000). Aging and measures of processing speed. *Biol. Psychol.* 54, 35–54. doi: 10.1016/s0301-0511(00)00052-1

Salthouse, T. A. (2009). Decomposing age correlations on neuropsychological and cognitive variables. *J. Int. Neuropsychol. Soc.* 15, 650–661. doi: 10.1017/S1355617709990385

Smith, R. E., Jacques, D. T., Fernando, C., and Alan, C. (2012). Anatomically-constrained tractography: improved diffusion mri streamlines tractography through effective use of anatomical information. *NeuroImage* 62, 1924–1938. doi: 10.1016/j.neuroimage.2012.06.005

Smith, S. M., Jenkinson, M., Woolrich, M. W., Beckmann, C. F., Behrens, T. E., Johansen-Berg, H., et al. (2004). Advances in functional and structural MR image analysis and implementation as FSL. *Neuroimage* 23, S208–S219. doi: 10.1016/j.neuroimage.2004.07.051

Smith, R. E., Tournier, J. D., Calamante, F., and Connelly, A. (2015). SIFT2: enabling dense quantitative assessment of brain white matter connectivity using streamlines tractography. *Neuroimage* 119, 338–351. doi: 10.1016/j.neuroimage.2015.06.092

Staffaroni, A. M., Jesse, A. B., Kaitlin, B. C., Fanny, M. E., Jersey, D., John, N., et al. (2018). The longitudinal trajectory of default mode network connectivity in healthy older adults varies as a function of age and is associated with changes in episodic memory and processing speed. *J. Neurosci.* 38, 2809–2817. doi: 10.1523/JNEUROSCI.3067-17.2018

Tomasi, D., and Volkow, N. D. (2012). Aging and functional brain networks. *Mol. Psychiatry* 17, 549–558. doi: 10.1038/mp.2011.81

Tournier, J. D., Fernando, C., and Alan, C. (2007). Robust determination of the fibre orientation distribution in diffusion mri: non-negativity constrained super-resolved spherical deconvolution. *Neuroimage* 35, 1459–1472. doi: 10.1016/j.neuroimage.2007.02.016

Tournier, J. D., Fernando, C., and Alan, C. (2013). Determination of the appropriate b value and number of gradient directions for high-angular-resolution diffusion-weighted imaging. *NMR Biomed.* 26, 1775–1786. doi: 10.1002/nbm.3017

Tournier, J. D., Fernando, C., and Alan, C. (2015). SIFT2: enabling dense quantitative assessment of brain white matter connectivity using streamlines tractography. *NeuroImage* 13, 612–632. doi: 10.1016/j.neuroimage.2015.06.092

Tournier, J. D., Fernando, C., David, G. G., and Alan, C. (2004). Direct estimation of the fiber orientation density function from diffusion-weighted MRI data using spherical deconvolution. *NeuroImage* 202:116137. doi: 10.1016/j.neuroimage.2004.07.037

Tournier, J. D., Robert, S., David, R., Rami, T., Thijs, D., Maximilian, P., et al. (2019). MRtrix3: a fast, flexible and open software framework for medical image processing and visualisation. *NeuroImage* 202:116137. doi: 10.1016/j.neuroimage.2019.116137

Ungerleider, L. G., and Mishkin, M. (1982). "Two cortical visual systems," in *Analysis of Visual Behavior*, eds D. J. Ingle, M. A. Goodale, and R. J. W. Mansfield (Cambridge: MIT Press), 549–586.

Yan, C. G. (2010). DPARSF: a matlab toolbox for "Pipeline" data analysis of resting-state FMRI. *Front. Syst. Neurosci.* 4:13. doi: 10.3389/fnsys.2010.00013

Zhao, T., Miao, C., Haijing, N., Xi, N. Z., Alan, E., Yong, H., et al. (2015). Age-related changes in the topological organization of the white matter structural connectome across the human lifespan. *Hum. Brain Mapp.* 36, 3777–3792. doi: 10.1002/hbm.22877

Zhu, H., Peng, Z., Sarael, A., Yuanyuan, C., Hongbao, C., Miao, T., et al. (2016). Changes of intranetwork and internetwork functional connectivity in Alzheimer's disease and mild cognitive impairment. *J. Neural Eng.* 13:46008. doi: 10.1088/1741-2560/13/4/046008

Ziegler, G., Dahnke, R., Winkler, A. D., and Gaser, C. (2013). Partial least squares correlation of multivariate cognitive abilities and local brain structure in children and adolescents. *NeuroImage* 82, 284–294. doi: 10.1016/j.neuroimage.2013.05.088

Zimmermann, J., John, D. G., and Anthony, R. M. (2018). Unique mapping of structural and functional connectivity on cognition. *J. Neurosci.* 38, 9658–9667. doi: 10.1523/JNEUROSCI.0900-18.2018

Zimmermann, J., Petra, R., Kelly, S., Simon, R., Michael, S., Anthony, R. M., et al. (2016). Structural architecture supports functional organization in the human aging brain at a regionwise and network level. *Hum. Brain Mapp.* 37, 2645–2661. doi: 10.1002/hbm.23200

Conflict of Interest: The authors declare that the research was conducted in the absence of any commercial or financial relationships that could be construed as a potential conflict of interest.

Publisher's Note: All claims expressed in this article are solely those of the authors and do not necessarily represent those of their affiliated organizations, or those of the publisher, the editors and the reviewers. Any product that may be evaluated in this article, or claim that may be made by its manufacturer, is not guaranteed or endorsed by the publisher.

frontiers | Frontiers in Aging Neuroscience

ORIGINAL RESEARCH
published: 25 May 2022
doi: 10.3389/fnagi.2022.865417

Age-Related Differences in the Neural Processing of Idioms: A Positive Perspective

Su-Ling Yeh[1,2,3,4], Shuo-Heng Li[1], Li Jingling[5], Joshua O. S. Goh[1,2,3,4,6], Yi-Ping Chao[7] and Arthur C. Tsai[8]*

[1] Department of Psychology, National Taiwan University, Taipei, Taiwan, [2] Graduate Institute of Brain and Mind Sciences, National Taiwan University, Taipei, Taiwan, [3] Neurobiology and Cognitive Science Center, National Taiwan University, Taipei, Taiwan, [4] Center for Artificial Intelligence and Advanced Robotics, National Taiwan University, Taipei, Taiwan, [5] Graduate Institute of Biomedical Sciences, China Medical University, Taichung, Taiwan, [6] Taiwan International Graduate Program, Interdisciplinary Neuroscience, Academia Sinica, Taipei, Taiwan, [7] Department of Computer Science and Information Engineering, Chang Gung University, Taoyuan, Taiwan, [8] Institute of Statistical Science, Academia Sinica, Taipei, Taiwan

We examined whether older adults benefit from a larger mental-lexicon size and world knowledge to process idioms, one of few abilities that do not stop developing until later adulthood. Participants viewed four-character sequences presented one at a time that combined to form (1) frequent idioms, (2) infrequent idioms, (3) random sequences, or (4) perceptual controls, and judged whether the four-character sequence was an idiom. Compared to their younger counterparts, older adults had higher accuracy for frequent idioms and equivalent accuracy for infrequent idioms. Compared to random sequences, when processing frequent and infrequent idioms, older adults showed higher activations in brain regions related to sematic representation than younger adults, suggesting that older adults devoted more cognitive resources to processing idioms. Also, higher activations in the articulation-related brain regions indicate that older adults adopted the thinking-aloud strategy in the idiom judgment task. These results suggest re-organized neural computational involvement in older adults' language representations due to life-long experiences. The current study provides evidence for the alternative view that aging may not necessarily be solely accompanied by decline.

Keywords: idiom, positive aspects of aging, language, experience, functional brain reorgization

OPEN ACCESS

Edited by:
Chu-Chung Huang,
East China Normal University, China

Reviewed by:
Sasa R. Filipovic,
University of Belgrade, Serbia
McNeel Gordon Jantzen,
Western Washington University, United States

****Correspondence:***
Su-Ling Yeh
suling@ntu.edu.tw

Specialty section:
This article was submitted to Neurocognitive Aging and Behavior, a section of the journal Frontiers in Aging Neuroscience

Received: *29 January 2022*
Accepted: *25 April 2022*
Published: *25 May 2022*

Citation:
Yeh S-L, Li S-H, Jingling L, Goh JOS, Chao Y-P and Tsai AC (2022) Age-Related Differences in the Neural Processing of Idioms: A Positive Perspective. Front. Aging Neurosci. 14:865417. doi: 10.3389/fnagi.2022.865417

INTRODUCTION

Aging has been portrayed as a process of deterioration. Like any developmental process, aging involves various aspects (physiological, cognitive, language, perceptual, motivational, and emotional) of changes. Physical deterioration seems inevitable with increased age from a biological perspective. Previous studies have illustrated age-related decline, including slower reaction time (Williamson et al., 2009), loss of muscular strength (Charlier et al., 2016), and lower cardiovascular efficiency (Freiheit et al., 2010). Thus, unsurprisingly, aging is often associated with frailty, characterized by multiple physiological impairments and dependency (Ferrucci et al., 2006; Kuh, 2007; Weiss et al., 2010).

Even if solely examining aging from a behavioral perspective, it also appears as if older adults always perform "worse" than younger adults, since it has been shown that the abilities gained throughout the first quarter of our lives will only decline in the latter part of development, including

sensation (Ulfhake et al., 2002), perception (Faubert, 2002), and cognition (Park et al., 2002). With such a negative societal view on aging, older adults may also acquire negative perspectives on their capabilities, which may prevent them from engaging in social and physical activities (Palacios et al., 2009) and living independently (Coudin and Alexopoulos, 2010). Indeed, many studies have demonstrated the detrimental effects of *ageism* on older adults' mental and physical health (Bryant et al., 2016). Moreover, Palacios et al. (2009) also suggested that older adults with less stereotypical views of aging were more likely to be socially and physically engaged. Thus, by changing perspectives on aging, or at least an aspect of the aging process, the whole society may benefit from enhanced older adults' overall well-being.

The current study aims to provide an alternative perspective and evidence that aging might not necessarily be solely accompanied by decay. Language is one of the functions that develop rapidly in childhood and remains relatively stable from adulthood to later life (Gaskell et al., 2009; Ramscar et al., 2013), especially in terms of lexicon size (Gaskell et al., 2009). However, some studies also suggest that language capacity becomes more limited with age due to sensory and cognitive decline [e.g., Burke and Shafto (2004)]. For instance, compared to younger adults, older adults produced fewer words, took a longer time, and made more errors when performing list generation tasks and object naming tasks (Goral, 2004; Goral et al., 2007). In addition, Chan and Poon (1999) have shown that older adults performed worse than younger adults in the category fluency task, suggesting an alternation of the semantic network in the process of aging (Tomer and Levin, 1993; Kozora and Cullum, 1995). A functional magnetic resonance imaging (fMRI) study also demonstrated that language lateralization toward the left hemisphere declined after age 25 (Szaflarski et al., 2006). Since language is a heavily lateralized function, such decline was interpreted as an explanation for less efficient communication in old age [but see Chen et al. (2019)].

However, older adults' decline in language functions can be interpreted differently. A well-researched language-related limitation in later life is the failure to retrieve appropriate words during conversations, known as the *tip-of-the-tongue* phenomenon (Juncos-Rabadán et al., 2010). Such a phenomenon of knowing a term but cannot immediately retrieve it from memory has been observed consistently when people age (Salthouse and Mandell, 2013). Burke et al. (1991) proposed that this phenomenon is due to infrequent word use, which leads to weaker connections between lexical and phonological nodes. However, Ramscar et al. (2013) proposed an alternative explanation. They interpreted this finding that older adults performed poorer on the pair association learning task was due to their larger lexicon size and more prosperous life experience. They suggested that existing knowledge of words might prevent older adults from forming new connections with previously unassociated words, implying that the tip-of-the-tongue phenomenon may also result from older adults' larger vocabulary size. Other studies have also supported the view of Ramscar and colleagues. For example, Bialystok and Luk (2012) found that older adults outperformed their younger peers on similar tasks due to their larger vocabulary size. Additionally, Fiez et al. (1999) also found that older adults know more rare words than younger adults. From this perspective, language-related knowledge increases with age rather than declines.

Here we examined whether and how older adults process idioms differently from younger adults from both behavioral and neural aspects. Idioms are commonly used in daily life, especially in Chinese, as they contain a rich cultural and historic background (Yang et al., 2016) with a stable structure (Liu et al., 2010), and their use is a form of language ability that we continue to acquire from adolescence through adulthood (Chan and Marinellie, 2008). As idioms work as large words or lexical units (Nippold et al., 2007; Conner et al., 2011), older adults should preserve the ability to process idioms with their stabilized or even increased lexicon size. Indeed, Hung and Nippold (2014) showed no age-related decline when tasked with explaining idioms, and 60–69 years old older adults reported greater familiarity and provided better explanations to idioms than 20–29 years old younger adults. Thus, the ability to process idioms varies between older and younger adults, depending on their familiarity with idioms. Despite that some studies have examined the effect of aging on idiom production [e.g., Qualls and Harris (2003) and Hung and Nippold (2014)], those studies might not be generalizable to the Chinese language, given that Chinese is relatively character-based processing, whereas, English idioms are relatively sentence-based. In addition, the Chinese writing system consists of characters taking up a square-shaped space with a nonlinear configuration varied in character structure (Yeh, 2000; Yeh and Li, 2002; Yeh et al., 2003), and the cognitive process underlying Chinese is different from that of English words (Tan et al., 2001). To date, no previous studies have investigated how aging might impact the processing of Chinese idioms, which is one of the novelties of the current study.

Chinese idioms require character processing that involves orthographic, phonological, and semantic processing (Wu et al., 2012). Using fMRI to directly examine which components might vary with age has several advantages to tackle how aging influences Chinese idiom processing. First, the task-based fMRI allows us to examine whether different neural substrates are in charge of the processing of idioms across different age groups, which can help us determine if older and younger adults recruit different brain areas in processing idioms; Second, fMRI allows us to investigate whether there is any re-organized neural processing in older adults' brain, where some brain regions might show more robust activation for older adults and positively correlate with behavioral performance. In comparison, the same pattern might be absent in younger adults.

MATERIALS AND METHODS

Participants

Since no previous studies have investigated age differences in processing Chinese idioms, we referenced a relevant study, Hung and Nippold (2014), to calculate the required sample size. In comparing familiarity with idioms across age groups, $\eta^2 = 0.29$ was found. According to G*Power ver. 3 (Faul et al., 2007), 34

participants (17 participants in each group) were required to detect age differences with power = 0.95. We recruited nearly 60% more participants than needed to verify our results to be more conservative. Hence, 28 older adults [mean age (SD) = 67.0 (4.96) years, age range 59–82 years old, male/female 9/18; mean years of education (SD) = 14.9 (3.21) years] and 30 younger adults [mean age (SD) = 23.2 (3.23) years, age range 19–31 years old, male/female 14/16; mean years of education (SD) = 15.9 (1.86) years] were recruited. All were right-handed Taiwanese with normal or corrected-to-normal vision and had Montreal Cognitive Assessment [MoCA; Nasreddine et al. (2005)] scores above or equal to 26 points. All participants gave written informed consent before participating. One older adult was excluded because of his excessive head movement in translation (>3 mm) during fMRI scanning, making the total number of older adults 27. This study was approved by the Research Ethics Committee at the National Taiwan University (201611HS004).

Stimuli and Procedure

Stimuli were presented using E-prime 2.0 (Psychology Software Toolbox, Sharpsburg, PA, United States) on a Windows PC. Participants viewed the stimuli *via* a head-mounted display in the scanner with 800 × 600 pixels resolution and 60 Hz refresh rate (Resonance Technology Inc., Northridge, CA, United States). Chinese idioms consisted of four characters (white, 4° × 4°) were presented serially one at a time at the center of a black background (**Figure 1**).

Four conditions were manipulated: frequent idiom, infrequent idiom, random, and perceptual control. Frequent and infrequent idioms were idioms of high and low frequency [mean (SD): 92.6 (49.66) vs. 6.84 (2.44) per million words; $t_{(24)}$ = 8.88, $p < 0.001$], respectively. There were 25 frequent and 25 infrequent idioms adapted from the materials used in Zhou et al. (2016). In the random condition, non-idiom four-character Chinese strings were generated randomly, and these characters did not overlap with the characters of frequent and infrequent idioms. In the perceptual control condition, non-word character stimuli were created by rearranging Chinese characters' strokes to form quartets of meaningless character-like stimuli. For the response cue display, a question mark (white, 4° × 2°) was presented at the same location as the Chinese characters.

There were 25 trials in each condition and 100 trials in total, equally distributed across five functional runs in this event-related fMRI experiment. There were five trials for each of the four conditions within a run, with the conditions presented in random order within each run. In each trial (**Figure 1**), during the target display, one of the characters of the four-character idiom was presented sequentially for 500 ms. After the quartet was completed, the response display with a question mark was presented for a maximum duration of 2,000 ms. Participants were instructed to judge whether the word sequence presented was an idiom or not during the response phase with assigned buttons as quickly and accurately as possible. After a response, the question mark would disappear, and a black background would appear until the entire 2000 ms period was over. A blank screen was then presented with the inter-trial interval (ITI) jittered between 3 and 4.5 s.

After the idiom judgment task, participants completed (1) the vocabulary test, the Wechsler Adult Intelligence Scale—Fourth Edition (WAIS-IV), and (2) the reading habits questionnaire based on Acheson et al. (2008). In the vocabulary test, 33 cards containing a Chinese two- or three-character word were shown to the participants, and they were asked to explain the meaning of each word. The reading habits questionnaire included author recognition and magazine recognition. Participants were asked to indicate from an author and magazine list the items they could recognize. The total score of these two tasks (author recognition and magazine recognition) indicates participants' reading habits.

fMRI Data Acquisition and Analysis

Scanning was conducted on a 3T Magnetom Prisma scanner (Siemens, Erlangen, Germany) with a 20-channel head coil at the Imaging Center for Integrated Body, Mind, and Culture Research of National Taiwan University, Taipei, Taiwan. For each participant, functional images were recorded using a gradient echo-planar imaging sequence with TR 2,000 ms, TE 32 ms, flip angle 87°, field of view 220 mm × 220 mm, voxel size 3.43 mm × 3.43 mm × 4.00 mm, 33 axial slices, and 390 scans. Axial slices were aligned parallel to the anterior-posterior commissural axis and placed for whole-brain coverage. We also acquired a T1-weighted Magnetization Prepared RApid Gradient Echo (MP-RAGE) sequence with TR 2,000 ms, TE 22.8 ms, flip angle 8°, field of view 256 mm × 256 mm, voxel size 1.00 mm isotropic, and 192 sagittal slices for registration and normalization to standardized template space.

Brain image data preprocessing and statistical analysis were performed using SPM12 (Wellcome Department of Imaging Neuroscience, London, United Kingdom). For each participant, functional volumes were realigned with unwarping to the first volume to correct for head motion and slice correction. Structural T1 images were then registered to the functional images and then segmented and normalized to the Montreal Neurological Institute (MNI) template space using the Diffeomorphic Anatomical Registration Through Exponentiated Lie algebra [DARTEL; Ashburner (2007)] procedure. T1 deformation parameters from the DARTEL procedure were then applied to the functional images with spatial smoothing using a 3D 8 mm Gaussian kernel.

First-level analysis of each participant's fMRI data was conducted using a General Linear Model (GLM) with canonical hemodynamic functions. The GLM included four predictors corresponding to the four conditions (frequent idioms, infrequent idioms, random, and perceptual control) in the idiom judgment task, and the six head movements of each run were added to the model as regressors. Thus, first-level GLMs yielded whole-brain voxel-wise estimates of each participant's neural responses to the four contrasts, including (1) idiom (frequent and infrequent idioms) vs. random, (2) frequent idiom vs. random, (3) infrequent idiom vs. random, and (4) idiom vs. perceptual control. These whole-brain neural response estimates were then submitted to second-level analysis.

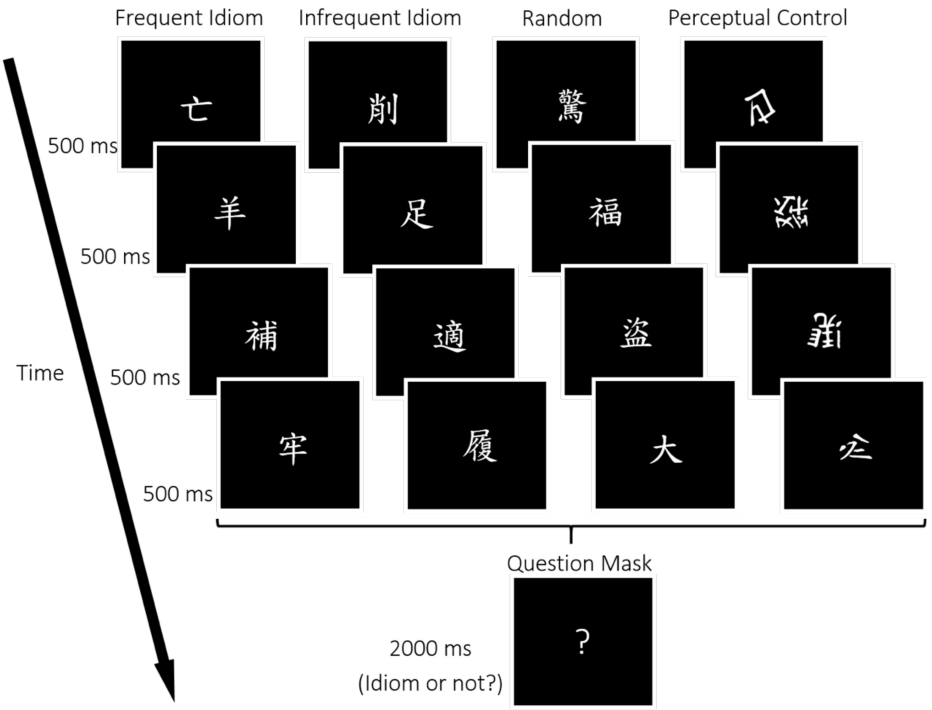

FIGURE 1 | Sample experimental stimuli of the idiom judgment task. Four conditions were used for the target phase in this study, including Frequent Idiom (e.g., "亡羊補牢" is translated as "When the sheep run away, then you mend the sheepfold," and means "To figure out a way to remedy the problem and prevent further loss"), Infrequent Idiom (e.g., "削足適履" is translated as "Cut off a piece of your feet to fit the size of the shoe" and means "To have inflexible thinking"), Random (character sequences with no meaning), and Perceptual Control (non-word sequences). For each trial, the four-character stimuli were presented sequentially after which a response display containing a question mark appeared, during which participants responded whether the quartets constituted an idiom or not.

Second-level analysis of the group-wise whole-brain neural response estimates was conducted using a two-sample t-test and multiple regressions to compare the contrast images of older and younger adults. The images were set at $p < 0.001$ (uncorrected) in all two-sample *t*-tests and multiple regression results. The cluster-wise correct False Discovery Rate (FDR) $q < 0.05$ was used in two-sample *t*-tests.

The Region Of Interest (ROI) mask was used in the multiple regression. The choice of ROIs was based on the overlapping brain regions between whole-brain neural results of idiom vs. random conditions and the semantically related areas (temporal and frontal regions) as suggested in the literature [e.g., Booth et al. (2002)]. The mask image of ROIs was produced by using XjView.[1]

RESULTS

Behavioral Performance

Age differences in demographics, results of the vocabulary test score, and reading habits questionnaire are shown in **Table 1**. Two younger and two older participants did not complete the post-test tasks (vocabulary test and reading habits questionnaires) and thus were not included for further post-test analysis, but their data for other analyses were included. As shown in **Table 1**, there were no significant differences in gender [$x^2(1, N = 57) = 1.05$, $p = 0.306$], education level [$t_{(55)} = 1.47$, $p = 0.148$], vocabulary test score [$t_{(51)} = -0.02$, $p = 0.986$], or reading habit score [$t_{(51)} = -0.83$, $p = 0.411$] for older and younger adults except for their difference in age [$t_{(55)} = -39.88$, $p < 0.001$].

TABLE 1 | Basic demographics and reading skills of younger and older participants (Standard deviations in parentheses).

	Younger	Older	*p*-value
Gender (Male: Female)	14:16	9:18	0.306[a]
Age in years	23.2 (3.23)	67.00 (4.96)	<0.001[b]
Education in years	15.93 (1.86)	14.93 (3.21)	0.148[b]
Vocabulary test score	52.54 (5.04)	52.56 (4.96)	0.986[b]
Reading habit score	36.39 (11.48)	39.36 (14.52)	0.411[b]

[a]*Chi-square test.* [b]*Two-sample t-test.*

Mean accuracies for the idiom judgment task are shown in **Figure 2**. Two types of trials were excluded from further analysis: trials in which participants responded before the response display and trials without responses. A two-way mixed repeated-measures analysis of variance (ANOVA) was applied on judgment responses with Age (younger and older) as the between-subjects variable and Condition (frequent, infrequent, random, and perceptual control) as

[1]www.alivelearn.net/xjview

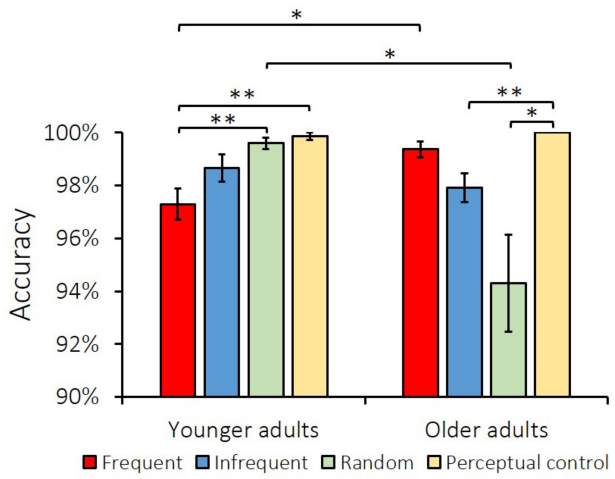

FIGURE 2 | Accuracy (including hits for frequent and infrequent idioms, and correct rejection for random and perceptual control) for younger and older adults in the idiom judgment task across four conditions. Error bars represent one standard error of the mean. Note that the standard error of older adults' perceptual control was zero. **denotes $p < 0.01$, and *denotes $p < 0.05$.

the within-subjects variable. The ANOVA revealed a main effect of Condition [$F_{(3,165)} = 6.04$, $MSE = 0.001$, $p = 0.001$, $\eta_p^2 = 0.099$] but not Age [$F_{(1,55)} = 3.43$, $MSE = 0.002$, $p = 0.069$, $\eta_p^2 = 0.059$]. *Post-hoc* pairwise comparisons corrected using the Šidák method showed that accuracy was higher for the perceptual control (99.9%) than the frequent (98.3%) [$t_{(56)} = 4.71$, $p < 0.001$], infrequent (98.3%) [$t_{(56)} = 4.18$, $p = 0.001$], and random (97.1%) [$t_{(56)} = 3.05$, $p = 0.007$] conditions.

The interaction effect of Age x Condition was significant [$F_{(3,165)} = 9.90$ $MSE = 0.001$, $p < 0.001$, $\eta_p^2 = 0.152$]. Simple main effect tests corrected by the Šidák method showed that older adults had higher accuracy for perceptual control than the infrequent idioms [100.0 vs. 97.9%, $t_{(26)} = 3.85$, $p = 0.004$] and random [100.0 vs. 94.3%, $t_{(26)} = 3.16$, $p = 0.024$] conditions. In contrast, younger adults showed lower accuracy for frequent idioms than the perceptual control [97.3 vs. 99.9%, $t_{(29)} = -4.56$, $p = 0.001$] and random conditions [97.3 vs. 99.6%, $t_{(29)} = -3.83$, $p = 0.004$]. These results indicate that for both age groups perceptual control (scrambled characters) could be correctly judged compared to other conditions consisting of characters. However, older adults tended to misjudge random sequences as idioms more often than younger adults, which was further confirmed by the result that accuracy for the random condition was lower for older adults than younger adults [94.3 vs. 99.6%, $t_{(55)} = -3.07$, $p = 0.012$]. Most important and relevant to our hypothesis was the result that accuracy for frequent idioms was higher for older adults than younger adults [99.4 vs. 97.3%, $t_{(55)} = 3.03$, $p = 0.016$]. No other contrasts achieved statistical significance ($ps < 0.05$).

We also calculated individual *d'* scores for the recognition of frequent and infrequent idioms. The *d'* scores were acquired by subtracting the Z scores of the false alarm rates from those of the hit rates. The estimation of the *d'* scores is as follows:

$$d' \; Z_{Accuracy_{idiom}} - Z_{(1-Accuracy_{random})} \quad (1)$$

Correct identification of the frequent idioms was used as the hit rate in the frequent idiom condition, and that of the infrequent idioms was used as the hit rate in the infrequent idiom condition. These two conditions shared the same false alarm rate from the erroneous identification as idioms when they were random sequences in the random condition.

Two-sample *t*-test comparisons of the mean *d'* scores across age groups yielded no significant difference between older and younger adults in the frequent idiom condition [4.09 vs. 4.25, $t_{(55)} = -1.17$, $p = 0.246$] but significantly lower *d'* for older than younger adults in the infrequent idiom condition [3.90 vs. 4.43, $t_{(55)} = -3.44$, $p = 0.001$]. In addition, we calculated individual β scores that indicate the bias to respond with one judgment more than the other. β larger than 1 indicates a tendency for "non-idiom" responses, whereas β smaller than 1 indicates a tendency for "idiom" responses. The calculation of β is as follows:

$$\beta = \exp\left\{d' \times -\frac{1}{2}\left[Z_{Accuracy_{idiom}} + Z_{\left(1-Accuracy_{random}\right)}\right]\right\} \quad (2)$$

Kolmogorov-Smirnov test showed that the distribution of β is not normally distributed (all *p*s < 0.001), so the non-parametric test was used. Mann-Whitney *U*-Tests showed lower β for older relative to younger adults in the frequent idiom condition [$z = 2.68$, $p = 0.007$], but no age difference for β in the infrequent idiom condition [$z = 1.65$, $p = 0.098$] (**Table 2**).

For reaction time (RT) data, trials that were two standard deviations above the mean RT and RTs of incorrect responses were excluded from the analysis. As above, we applied a two-way mixed repeated-measures ANOVA with Age (younger and older) and Condition (frequent, infrequent, random, and perceptual control) as independent variables. This analysis yielded main effects of Age [$F_{(1,55)} = 26.7$, $MSE = 42{,}061$, $p < 0.001$, $\eta_p^2 = 0.327$], Condition [$F_{(3,165)} = 31.0$, $MSE = 3{,}154$, $p < 0.001$, $\eta_p^2 = 0.361$], and Age by Condition interaction [$F_{(3,165)} = 3.51$, $MSE = 3{,}154$, $p = 0.017$, $\eta_p^2 = 0.060$]. *Post-hoc* pairwise analyses corrected by using the Šidák method revealed faster RTs in younger than older adults (340 vs. 480 ms), and RTs of both frequent (372 ms) and infrequent

TABLE 2 | Mean *d'* and β estimates of response biases in older and younger adults.

	Index	Young	Older	*p*-value
Frequent	*d'*	4.25	4.09	0.246[a]
	β	2.25	1.34	0.007[b]**
Infrequent	*d'*	4.43	3.9	0.001[a]**
	β	1.77	1.47	0.098[b]

*The calculations of the d' and β are based on Equations (1, 2), respectively. [a]Two-sample t-test. [b]Mann-Whitney U-test. ** denotes p < 0.001.*

(377 ms) conditions were faster than RTs of random (448 ms) and perceptual control (444 ms) conditions (all *p*s < 0.001). There were no differences between RTs for frequent and infrequent idioms, as well as random idioms and perceptual control non-words. For the interaction effect, younger adults had numerically faster RTs in the random condition than in the perceptual control condition [358 vs. 376 ms], and reversed result was found in older adults [539 vs. 512 ms]. However, the simple main effect test corrected by using the Šidák method could not obtain any statistically significant difference between the two conditions for either younger [$t_{(29)}$ = 2.20, p = 0.195] or older adults [$t_{(26)}$ = −0.92, p = 0.934].

Neuroimaging Data

We used whole-brain two-sample *t*-tests to evaluate brain areas in which older adults showed different contrast responses from younger adults across conditions (**Figure 3** and **Table 3**). For idioms (frequent and infrequent included), relative to random characters, older adults engaged higher neural responses than younger adults in the left superior temporal gyrus (STG), bilateral insula, right postcentral gyrus (PostCG), left superior frontal gyrus (SFG), and right middle temporal gyrus (MTG). Considering the two types of idioms separately, for frequent idioms relative to random characters, older adults showed higher activation than younger adults in the right supplementary motor area (SMA), left STG, and left paracentral lobule (PCL). For infrequent idioms relative to random characters, older adults showed higher activation than younger adults in the right MTG, left PostCG, and left STG. In addition, for random characters relative to non-word characters (perceptual control), older adults engaged higher neural responses in the left SFG. However, no higher activations across conditions were found in older compared to younger adults.

Based on the above whole-brain contrast of the idiom vs. random condition, ROIs were defined for the right MTG, left SFG, and left STG (see Materials and Methods). We then evaluated how ROI neural responses in younger and older adults were associated with behavioral performance during the idiom judgment task to see if there were compensatory activations or reorganization in older adults. Individual neural contrast response estimates were extracted from these ROIs and submitted to multiple regression analyses with *d'* scores, which shows the behavioral performance of the idiom judgment task without the response bias in the frequent and infrequent conditions with age groups as predictors. The idiom words (frequent or infrequent) relative to random characters and frequent idioms relative to infrequent idioms are included as contrast pairs in the multiple comparison corrections to clarify how the compensatory/reorganization system works on the language function of word regularity (idiom words vs. random characters) and the frequency of idioms (frequent vs. infrequent). The reported areas

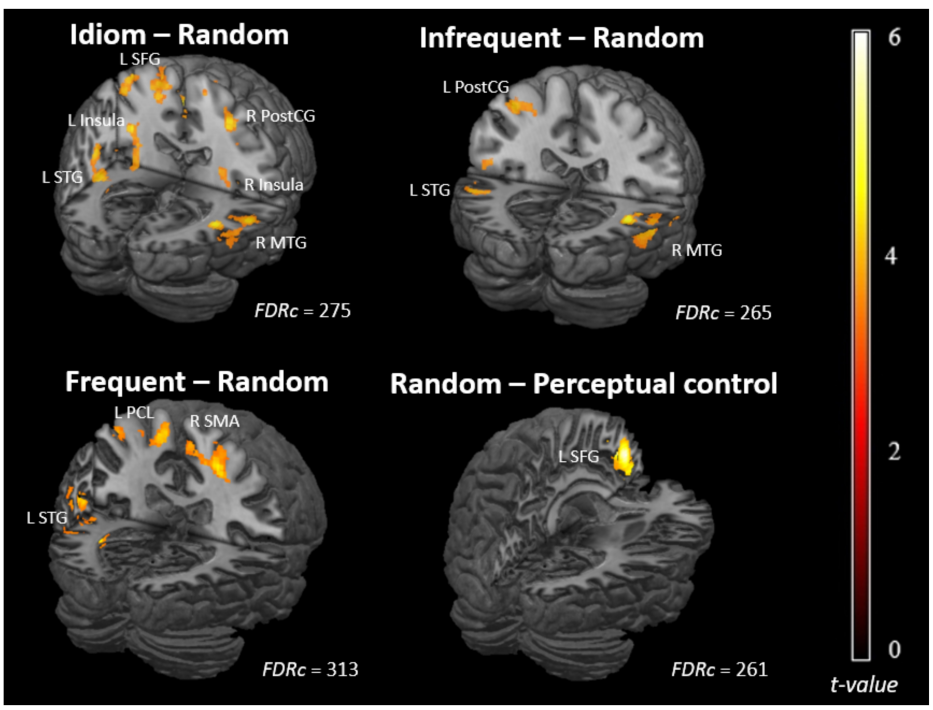

FIGURE 3 | Whole-brain statistical contrast maps overlaid on 3D rendered template brains. Contrast maps depict brain areas in which the contrast responses for older adults were higher than those for younger adults. Voxel-wise statistical significance was set at cluster-wise corrected q < 0.05 False Discovery Rate (FDR). L, left; R, right; FDRc, FDR-corrected cluster threshold; SFG, superior frontal gyrus; STG, superior temporal gyrus; MTG, middle temporal gyrus; SMA, supplementary motor area; PostCG, postcentral gyrus; PCL, paracentral lobule.

TABLE 3 | Peak activation details of brain areas with higher contrast responses in older than younger adults.

Brain region	# of voxels	$q_{FDR-corr}$	X	Y	Z	*t*-value
Idioms–random						
L superior temporal gyrus	866	< 0.001	−58	−12	−4	5.81
R insula	275	0.010	36	−2	16	5.79
L insula	301	0.008	−34	−8	16	4.42
R postcentral gyrus	484	0.001	44	−26	56	4.48
L superior frontal gyrus	1395	< 0.001	−22	−2	60	4.65
R middle temporal gyrus	408	0.002	58	−40	6	4.19
Frequent–random						
R supplementary motor area	330	0.016	8	−24	60	3.89
L superior temporal gyrus	313	0.016	−58	−36	18	4.17
L paracentral lobule	527	0.002	−12	−20	64	4.17
Infrequent–random						
R middle temporal gyrus	458	0.002	58	−50	4	4.14
L postcentral gyrus	274	0.017	−42	−28	58	4.26
L superior temporal gyrus	265	0.017	−50	−36	22	4.05
Random–perceptual control						
L superior frontal gyrus	261	0.010	−6	50	28	5.40

Whole-brain voxel-wise statistical significance was set at $p < 0.001$ (uncorrected) and cluster-wise corrected $q < 0.05$ False Discovery Rate (FDR). Coordinates of peak locations are in MNI space. L, Left; R, Right; # of voxels: Number of voxels in a cluster. $q_{FDR-corr}$, cluster-level correct q-values using FDR.

of activation of the ROI analysis were significant using $p < 0.05$ Familywise Error (*FWE*) correction with the three predefined ROIs.

Region of interest analysis showed correlation trends in which greater neural responses to infrequent idiom than random conditions correlated with higher *d'* scores in older adults. Specifically, a positive correlation between the brain activation in the infrequent condition (contrasting with the random condition) and *d'* was found in the left SFG ($P_{FWE-corr} = 0.011$, voxel size = 97) in older adults ($r = 0.747$, $p < 0.001$; shown in **Figure 4**), whereas no such correlation was found in younger adults ($r = 0.025$, $p = 0.895$). We further confirmed this by applying a regression analysis using age and *d'* as independent variables to predict the brain activation in the left SFG. A significant interaction of age and *d'* was found, $t_{(53)} = -2.11$, $p = 0.040$, verifying the greater brain-behavior associations in the left SFG for older than younger adults (**Figure 4**).

DISCUSSION

This study showed differences between older and younger participants in behavioral and imaging data. We discuss the implications of these differences below.

Behavioral Results of Idiom Processing

On the behavioral level, older adults showed higher accuracy for frequently seen idioms than younger adults. The results here thus indicate how experience benefits older adults, allowing them to be better than younger adults in making judgments on frequent idioms. No difference in the accuracy of infrequent idioms was found between older and younger adults, indicating the same level of performance in judging the less familiar idioms between the two age groups. Together, this supports our hypothesis that older adults preserve the language function in terms of idiom processing and can even perform better with frequent idioms than their younger counterparts.

However, by taking *d'* as the dependent variable, we found no age differences in the sensitivity of idiom judgment with frequent idioms and lower sensitivity for older adults with infrequent idioms. Closer scrutiny further indicates that the average *d'* for older adults (4.08 and 3.9 for frequent and infrequent idioms, respectively) was not low compared to the *d'* in younger adults (4.25 and 4.43 for frequent and infrequent idioms, respectively); this can further be verified by the similar accuracies (>97%) in infrequent idioms across age groups. It is to be noted that as the calculation of *d'* scores (of both frequent and infrequent idioms) involves the performance in random sequences (false alarm by mistaking these for idioms), how older and younger adults performed differently in this random condition is critical. Given that the *d'* measure depends on the responses to the random sequences which differed between older and younger adults, the accuracy of idiom judgment as mentioned above could better serve as a main behavioral proxy and the *d'* as an additional measure to reveal the results from different aspects.

It seems that older adults might not be able to correctly judge whether the random sequence was an idiom or not, as lower accuracy was found for older adults than younger ones. However, these results could also be due to older adults' better world knowledge (Spreng and Turner, 2019), which requires a serial search through memory to accumulate more evidence to reject the random sequence as an idiom. Lee et al. (2018) have suggested that answering "no" is more challenging to assess and that answering "no" may require much more evidence in comparison to answering "yes." Therefore, given older adults' higher world knowledge, the more accumulated evidence is needed to form a rejection, which could have caused performance accuracy to be lower in the random sequence than in younger adults.

The finding of higher response bias (β) for younger adults in the idiom judgment for frequent idioms suggests that younger adults were more conservative in making judgments regarding frequent idioms. The result here also indicates the benefit that older adults acquire because of their more considerable world knowledge, enabling them to make more liberal judgments of the frequent idioms than younger adults. Yet, the age difference in bias was absent in the infrequent idiom condition, indicating that both age groups had the same criterion for judging infrequent idioms.

Despite the differences in Chinese and English writing systems, the current results align with Hung and Nippold (2014), who did not find age-related declines in idiom processing of English. On the other hand, Hung and Nippold (2014) found better performance in explaining idioms in individuals over 60 years older than younger adults in

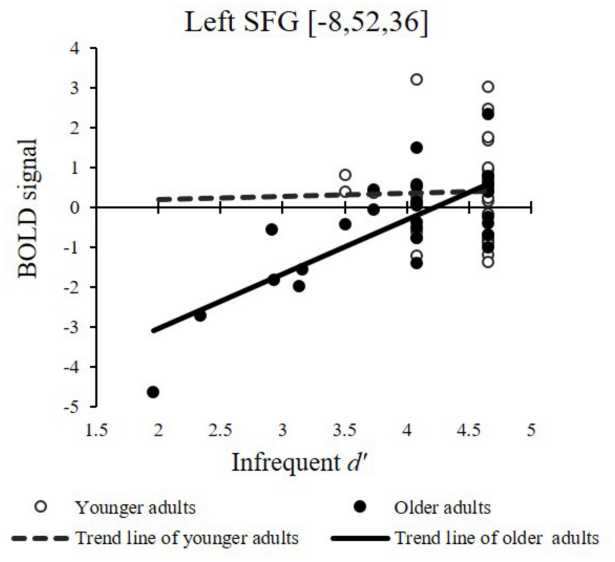

FIGURE 4 | Associations between individual infrequent *d'* scores in the infrequent idiom vs. random condition and brain contrast responses in younger and older adults in the left Superior Frontal Gyrus showed significant whole-brain age difference in the neural-behavior correlation.

their twenties. Additionally, Qualls and Harris (2003) also found better performances in idiom interpretation in African-American older adults than younger adults when controlling for working memory capacity and reading comprehension ability. Therefore, the superiority or maintenance of language functions in idiom processing for older adults is not only applied to the English language system but can also be generalized to Chinese and different ethnicities, as shown in the current study.

Higher Brain Activation in Older Adults Compared to Younger Adults

Compared to younger adults, older adults engaged in higher neural responses to idioms (both frequent and infrequent) relative to scrambled characters (i.e., the random condition) in the bilateral frontotemporal areas and the medial frontoparietal regions. This may indicate that older adults exert more cognitive resources in processing idioms than younger adults. For example, the SFG is in charge of working memory processing (Rypma et al., 1999). In addition, the STG is involved in the processing of tonal representations of Chinese characters (Tan et al., 2001) and is associated with the perception of intonation in speech prosody (Chang et al., 2010). The MTG is engaged in the extensive processing of spatial information in the Chinese language (Xiong et al., 2000) as a form of semantic representation (Booth et al., 2002, 2006). Higher activations in the insula and SMA were also found in older adults compared to younger adults. The activation in the SMA can be served as an index of motoric representation or articulatory rehearsal of vocally phonological information (Kuo et al., 2004) and the grapheme-to-phoneme conversion (Fiez et al., 1999). The insula has also been shown to mediate the motor aspect of speech production and articulatory control (Cereda et al., 2002; Oh et al., 2014). The higher activations in these brain regions suggest that older adults might recruit more resources to process idioms than younger adults. Older adults might also adopt the *thinking-aloud strategy* during the judgment of Chinese idioms as higher activations were found in several articulation-related areas, which might allow them to reduce cognitive load during the task (Smagorinsky, 1989). Together, we have shown that older adults adopted different strategies for judging Chinese idioms from a neuroimaging perspective.

We did not find higher activations in the fusiform gyrus (FG) and left inferior frontal gyrus (IFG) in older compared to younger adults. Both the FG and left IFG are highly associated with language processing, either in English or Chinese (Tan et al., 2005). In Chinese, the FG is related to the orthographic organization of Chinese (Bolger et al., 2005; Tan et al., 2005). As for the left IFG, previous studies have shown that the anterior and posterior part of the IFG is in charge of processing semantic and phonological information, respectively [see Wu et al. (2012) for review]. In addition, the IFG is associated with the processing of semantic integration in a sentence-level structure (Zhu et al., 2009). The absence of age differences in these two regions might indicate that older and younger adults recruited the same resources in processing orthographic organization and semantic integration across characters in the task. Although null results and inverse inference should be interpreted carefully, we consider this to be proper since the recognition of Chinese characters in skilled Chinese readers is based on orthographic constituents (Chen, 1996), which can easily be done by both younger and older adults in the current study. In addition, Atas et al. (2014) have shown that the temporal integration of symbols could be learned with trial-by-trial feedback. The learning of temporal regularity could even take place without visual awareness. Hence, with more experience in using idioms, older adults should have the ability to integrate temporal semantic information at the same level as younger adults.

When random vs. perceptual control conditions were compared, older participants recruited more high-level brain resources in the SFG than younger participants. No other brain regions showed significantly higher contrast responses in older than younger participants. These results are consistent with the behavior results: older adults made more effort during idiom processing, even with the random sequence characters. Moreover, a greater specific engagement of infrequent idioms relative to scrambled words across similar brain regions for semantic processing (left SFG) positively correlated with the task performance of older participants. These results suggest that when the brain regions correlated with idiom processing were active, older adults performed equally well as younger adults. Therefore, the activation in the SFG could be served as a form of compensatory mechanism (Cabeza et al., 2002), as the positive correlation between brain and performance was only found in older adults. Alternatively, given the higher accuracy of recognizing frequent idioms and higher brain activations for older adults than younger ones, this may

not just be a form of compensation (which would imply a presence of a deficit) but a reorganization with behavioral advantages. Future studies that more specifically distinguish linguistic operations involved in processing idioms, which arguably are quite complex, are required to better evaluate the roles of the above brain regions as reflecting compensatory or re-organized neuro-computational involvement in older adult language representations.

Current Views on Aging

By presenting the current study, we aim to combat the general stereotype regarding the decline of aging. While it is undeniable that certain capacity limitations are associated with the increase of age, there are potentially severe consequences when aging is evaluated solely from a negative perspective. With a view that aging is associated exclusively with deterioration, older adults may be perceived prejudicially and treated discriminatively even though most older adults do not experience frailty (McPherson, 2004). These negative beliefs from the public, the media, and policies seemed to influence older adults negatively. For example, age-related public policies, such as mandatory retirement age, can affect older adults' sense of self and how others regard them (Hendricks, 2004). Many studies [e.g., Hausdorff et al. (1999); Chrisler et al. (2016), and Ng et al. (2016)] demonstrated that older individuals' health and behaviors might be negatively affected in self-fulfilling ways as they embodied age-related stereotypes. Bai et al. (2016) also illustrated that those older adults with stronger beliefs about being a burden to their family have a higher risk of depression. Older individuals are affected physically and mentally by age-related negative stereotypes. They may require more social and healthcare support in a society where age is not respected, reinforcing the idea that older adults are weak or burdensome. This phenomenon was noted by Butler (2009), who coined the term *ageism* for negative stereotypes and discriminative acts against older adults. Older adults were greatly valued for their experience, knowledge, and institutional memory in the past. In Chinese culture, older adults have been regarded as the source of wisdom for their lifelong experiences. It has been considered virtuous for the younger generation to respect the older generation (Laidlaw et al., 2010).

Future Directions

We used Chinese idioms as the stimuli to tackle the issue of age-related differences in language processing as idiom processing is similar to regular phrases or short sentences (Liu et al., 2010). The extraction of a regular or consistent pattern from the environment to expect upcoming stimuli occurs as early as infancy when infants learn to segment sentences into words (Saffran et al., 1996), and prior experience is essential for statistical regularity (Samuelson, 2002; Lany and Gómez, 2008; Salvagio et al., 2015). Chinese idioms have a very high transitional probability between characters and words (e.g., in the idiom "亡羊補牢", the transitional probability between "亡羊" ("When the sheep run away") and "補牢" ("then you mend the sheepfold") is almost 100%). Such an ability to extract statistical regularity and expect upcoming events are crucial for daily lives. Future studies can examine other non-linguistic processing such as older adults' motion perception and dynamic emotional expression to see whether similar re-organization or compensation also occurs in the aging brain albeit in different neural networks. That is, whether older adults, with rich experience and knowledge, would have better statistical regularity in general, or idiom processing is a special case in language processing to counter the aging brain.

In addition to reading, previous studies on idiom processing in speech [e.g., Liu et al. (2020)] revealed a dynamic network among temporal-parietal-frontal regions and the crosstalk between the dual-stream systems, whereby the ventral system is for comprehension and the dorsal system for articulation in speech (Hickok and Poeppel, 2007). Fei et al. (2020) found reduced activity of STG and IFG in older adults than in younger adults and increased frontal-temporal-parietal functional connectivity that may work to help facilitate idiom processing in older adults. It is worth comparing the difference between the two forms (visual vs. auditory) of idiom processing within the same experimental framework to find the commonality and differences, especially regarding the preservation of performance and the brain's re-organization in older adults.

Finally, our finding that older adults could correctly judge frequent idioms better than younger adults and had the equivalent performance regarding infrequent idioms may be related to the expertise experience found previously in other domains. For example, experienced radiologists could recognize abnormal X-ray images better than novices, but not for normal X-ray images. Such a finding indicates that selective processing for distinguishable features increases with experience and this may hinder the detection of variations in normal images [Myles-Worsley et al. (1988), see also Evans et al. (2011)], an idea supported by eye-tracking results (Richter et al., 2020). It is likely that the older adults' higher accuracy for frequent idioms reflects their expertise performance in language processing due to their lifelong experiences. Whether the two have shared underlying mechanisms awaits future studies.

CONCLUSION

Compared to younger adults, we found better frequent-idiom recognition and higher neural activations in brain regions in charge of language processing and high-level functions for older adults. Older adults may benefit from experiences to help make judgments regarding Chinese idioms, which can be verified by their better (for frequent idioms) or similar performance (for infrequent idioms) in idiom judgments compared to younger adults. Despite previous studies investigating the deficits in semantic processing and reading in the aging population, this is the first study that directly examined the age effect on Chinese idiom processing with the measurement of neural correlates. This study provides another perspective on the aging process; namely, aging is not necessarily accompanied only by declines—instead, the experience accumulated across a lifespan with shifts in processing strategies.

DATA AVAILABILITY STATEMENT

The raw data supporting the conclusions of this article can be accessed on https://www.myqnapcloud.com/smartshare/608e947k4l6p7075v536a699_9g6igg0lklnq2p11q5v25723593e4h2g.

ETHICS STATEMENT

The studies involving human participants were reviewed and approved by the Research Ethic Committee at the National Taiwan University (201611HS004). The patients/participants provided their written informed consent to participate in this study.

AUTHOR CONTRIBUTIONS

S-LY: conceptualization, funding acquisition, and supervision. S-LY, JG, and S-HL: data curation. S-HL and JG: formal analysis. S-HL, JG, Y-PC, and S-LY: methodology. S-LY and S-HL: project administration and writing. S-LY, LJ, and AT: resources. S-HL: software. All authors: investigation and approved the submitted version.

FUNDING

This research was supported by grants from Taiwan's Ministry of Science and Technology awarded to S-LY (MOST106-2420-H-002-010-MY3, 110-2410-H-002-130-MY3, MOST110-2410-H-039-005, MOST110-2634-F-002-049, MOST110-2118-M-001-006-MY2, and MOST110-2221-E-182-009-MY2).

ACKNOWLEDGMENTS

We would like to thank the two reviewers for their constructive comments and suggestions, and the Imaging Center for Integrated Body, Mind, and Culture Research at National Taiwan University for providing the fMRI scanner. We also thank Chia-Lin Lee for her help in preparing and interpreting the questionnaires, Chii Shyang Kuo for his help in collecting data, and Hsin-Hao Lee for his help in interpreting part of the data.

REFERENCES

Acheson, D. J., Wells, J. B., and MacDonald, M. C. (2008). New and updated tests of print exposure and reading abilities in college students. *Behav. Res. Methods* 40, 278–289. doi: 10.3758/brm.40.1.278

Ashburner, J. (2007). A fast diffeomorphic image registration algorithm. *Neuroimage* 38, 95–113.

Atas, A., Faivre, N., Timmermans, B., Cleeremans, A., and Kouider, S. (2014). Nonconscious learning from crowded sequences. *Psychol. Sci.* 25, 113–119. doi: 10.1177/0956797613499591

Bai, X., Lai, D. W., and Guo, A. (2016). Ageism and depression: perceptions of older people as a burden in China. *J. Soc. Issues* 72, 26–46.

Bialystok, E., and Luk, G. (2012). Receptive vocabulary differences in monolingual and bilingual adults. *Bilingual. Lang. Cogn.* 15, 397–401.

Bolger, D. J., Perfetti, C. A., and Schneider, W. (2005). Cross-cultural effect on the brain revisited: universal structures plus writing system variation. *Human Brain Mapp.* 25, 92–104. doi: 10.1002/hbm.20124

Booth, J. R., Burman, D. D., Meyer, J. R., Gitelman, D. R., Parrish, T. B., and Mesulam, M. M. (2002). Modality independence of word comprehension. *Human Brain Mapp.* 16, 251–261. doi: 10.1002/hbm.10054

Booth, J. R., Lu, D., Burman, D. D., Chou, T.-L., Jin, Z., Peng, D.-L., et al. (2006). Specialization of phonological and semantic processing in Chinese word reading. *Brain Res.* 1071, 197–207. doi: 10.1016/j.brainres.2005.11.097

Bryant, C., Bei, B., Gilson, K.-M., Komiti, A., Jackson, H., and Judd, F. (2016). Antecedents of attitudes to aging: a study of the roles of personality and well-being. *Gerontologist* 56, 256–265. doi: 10.1093/geront/gnu041

Burke, D. M., and Shafto, M. A. (2004). Aging and language production. *Curr. Direct. Psychol. Sci.* 13, 21–24. doi: 10.1111/j.0963-7214.2004.01301006.x

Burke, D. M., MacKay, D. G., Worthley, J. S., and Wade, E. (1991). On the tip of the tongue: what causes word finding failures in young and older adults? *J. Memory Lang.* 30, 542–579. doi: 10.1016/0749-596x(91)90026-g

Butler, R. N. (2009). Combating ageism. *Int. Psychogeriat.* 21:211.

Cabeza, R., Anderson, N. D., Locantore, J. K., and McIntosh, A. R. (2002). Aging gracefully: compensatory brain activity in high-performing older adults. *Neuroimage* 17, 1394–1402. doi: 10.1006/nimg.2002.1280

Cereda, C., Ghika, J., Maeder, P., and Bogousslavsky, J. (2002). Strokes restricted to the insular cortex. *Neurology* 59, 1950–1955. doi: 10.1212/01.wnl.0000038905.75660.bd

Chan, A. S., and Poon, M. W. (1999). Performance of 7-to 95-year-old individuals in a Chinese version of the category fluency test. *J. Int. Neuropsychol. Soc.* 5, 525–533. doi: 10.1017/s135561779956606x

Chan, Y.-L., and Marinellie, S. A. (2008). Definitions of idioms in preadolescents, adolescents, and adults. *J. Psychol. Res.* 37, 1–20. doi: 10.1007/s10936-007-9056-9

Chang, E. F., Rieger, J. W., Johnson, K., Berger, M. S., Barbaro, N. M., and Knight, R. T. (2010). Categorical speech representation in human superior temporal gyrus. *Nat. Neurosci.* 13:1428.

Charlier, R., Knaeps, S., Mertens, E., Van Roie, E., Delecluse, C., Lefevre, J., et al. (2016). Age-related decline in muscle mass and muscle function in Flemish Caucasians: a 10-year follow-up. *Age* 38:36. doi: 10.1007/s11357-016-9900-7

Chen, P.-H., Wong, J.-S., Lin, W.-T., Tseng, W.-Y. I., Goh, J. O. S., and Lee, C. L. (2019). "Investigating the role of inter-hemispheric communication in age-related increase in right-hemisphere P600 grammaticality effect: a combined ERP and DTI study". *Poster presented at the Eleventh Annual Meeting of the Society for the Neurobiology of Language*. Helsinki: SNL.

Chen, Y.-P. (1996). What are the functional orthographic units in Chinese word recognition: the stroke or the stroke pattern? *Quart. J. Exp. Psychol. Sec. A* 49, 1024–1043.

Chrisler, J. C., Barney, A., and Palatino, B. (2016). Ageism can be hazardous to women's health: ageism, sexism, and stereotypes of older women in the healthcare system. *J. Soc. Issues* 72, 86–104.

Conner, P. S., Hyun, J., O'Connor Wells, B., Anema, I., Goral, M., Monereau-Merry, M.-M., et al. (2011). Age-related differences in idiom production in adulthood. *Clin. Linguist. Phonet.* 25, 899–912. doi: 10.3109/02699206.2011.584136

Coudin, G., and Alexopoulos, T. (2010). 'Help me! I'm old!'How negative aging stereotypes create dependency among older adults. *Aging ment. Health* 14, 516–523. doi: 10.1080/13607861003713182

Evans, K. K., Cohen, M. A., Tambouret, R., Horowitz, T., Kreindel, E., and Wolfe, J. M. (2011). Does visual expertise improve visual recognition memory? *Attent. Percep. Psychophys.* 73, 30–35. doi: 10.3758/s13414-010-0022-5

Faubert, J. (2002). Visual perception and aging. *Can. J. Exp. Psychol.* 56:164.

Faul, F., Erdfelder, E., Lang, A.-G., and Buchner, A. (2007). G* Power 3: A flexible statistical power analysis program for the social, behavioral, and biomedical sciences. *Behav. Res. Methods* 39, 175–191. doi: 10.3758/bf03193146

Fei, N., Ge, J., Wang, Y., and Gao, J.-H. (2020). Aging-related differences in the cortical network subserving intelligible speech. *Brain Lang.* 201:104713. doi: 10.1016/j.bandl.2019.104713

Ferrucci, L., Mahallati, A., and Simonsickm E. M. (2006). Frailty and the foolishness of Eos. *J. Gerontol. A Biol. Sci. Med. Sci.* 61, 260–261. doi: 10.1093/gerona/61.3.260

Fiez, J. A., Balota, D. A., Raichle, M. E., and Petersen, S. E. (1999). Effects of lexicality, frequency, and spelling-to-sound consistency on the functional anatomy of reading. *Neuron* 24, 205–218. doi: 10.1016/s0896-6273(00)80833-8

Freiheit, E. A., Hogan, D. B., Eliasziw, M., Meekes, M. F., Ghali, W. A., Partlo, L. A., et al. (2010). Development of a frailty index for patients with coronary artery disease. *J. Am. Geriat. Soc.* 58, 1526–1531. doi: 10.1111/j.1532-5415.2010.02961.x

Gaskell, M. G., and Ellis, A. W. (2009). Word learning and lexical development across the lifespan. *Philos. Trans. R. Soc. B Biol. Sci.* 364, 3607–3615. doi: 10.1098/rstb.2009.0213

Goral, M. (2004). First-language decline in healthy aging: implications for attrition in bilingualism. *J. Neurol.* 17, 31–52. doi: 10.1016/s0911-6044(03)00052-6

Goral, M., Spiro, A., Albert, M. L., Obler, L. K., and Connor, L. T. (2007). Change in lexical retrieval skills in adulthood. *Ment. Lexic.* 2, 215–238. doi: 10.1093/cercor/bhu120

Hausdorff, J. M., Levy, B. R., and Wei, J. Y. (1999). The power of ageism on physical function of older persons: reversibility of age-related gait changes. *J. Am. Geriat. Soc.* 47, 1346–1349. doi: 10.1111/j.1532-5415.1999.tb07437.x

Hendricks, J. (2004). Public policies and old age identity. *J. Aging Stud.* 18, 245–260. doi: 10.1016/j.jaging.2004.03.007

Hickok, G., and Poeppel, D. (2007). The cortical organization of speech processing. *Nat. Rev. Neurosci.* 8, 393–402. doi: 10.1038/nrn2113

Hung, P.-F., and Nippold, M. A. (2014). Idiom understanding in adulthood: examining age-related differences. *Clin. Linguist. Phonet.* 28, 208–221. doi: 10.3109/02699206.2013.850117

Juncos-Rabadán, O., Facal, D., Rodríguez, M. S., and Pereiro, A. X. (2010). Lexical knowledge and lexical retrieval in ageing: insights from a tip-of-the-tongue (TOT) study. *Lang. Cogn. Proc.* 25, 1301–1334.

Kozora, E., and Cullum, C. M. (1995). Generative naming in normal aging: total output and qualitative changes using phonemic and semantic constraints. *Clin. Neuropsychol.* 9, 313–320. doi: 10.1080/13854049508400495

Kuh, D. (2007). A life course approach to healthy aging, frailty, and capability. *J. Gerontol. Ser. Biol. Sci. Med. Sci.* 62, 717–721. doi: 10.1093/gerona/62.7.717

Kuo, W.-J., Yeh, T.-C., Lee, J.-R., Chen, L.-F., Lee, P.-L., Chen, S.-S., et al. (2004). Orthographic and phonological processing of Chinese characters: an fMRI study. *Neuroimage* 21, 1721–1731. doi: 10.1016/j.neuroimage.2003.12.007

Laidlaw, K., Wang, D., Coelho, C., and Power, M. (2010). Attitudes to ageing and expectations for filial piety across Chinese and British cultures: a pilot exploratory evaluation. *Aging Ment. Health* 14, 283–292. doi: 10.1080/13607860903483060

Lany, J., and Gómez, R. L. (2008). Twelve-month-old infants benefit from prior experience in statistical learning. *Psychol. Sci.* 19, 1247–1252. doi: 10.1111/j.1467-9280.2008.02233.x

Lee, A. L., Ruby, E., Giles, N., and Lau, H. (2018). Cross-domain association in metacognitive efficiency depends on first-order task types. *Front. Psychol.* 9:2464. doi: 10.3389/fpsyg.2018.02464

Liu, Y., Li, P., Shu, H., Zhang, Q., and Chen, L. (2010). Structure and meaning in Chinese: an ERP study of idioms. *J. Neurol.* 23, 615–630.

Liu, Z., Shu, S., Lu, L., Ge, J., and Gao, J.-H. (2020). Spatiotemporal dynamics of predictive. brain mechanisms during speech processing: an MEG study. *Brain Lang.* 203:104755. doi: 10.1016/j.bandl.2020.104755

McPherson, B. D. (2004). *Aging as a social process: Canadian perspectives*. Don Mills: Oxford University Press.

Myles-Worsley, M., Johnston, W. A., and Simons, M. A. (1988). The influence of expertise on X-ray image processing. *J. Exp. Psychol. Learn. Memory Cogn.* 14, 553–557.

Nasreddine, Z. S., Phillips, N. A., Bédirian, V., Charbonneau, S., Whitehead, V., Collin, I., et al. (2005). The montreal cognitive assessment, MoCA: a brief screening tool for mild cognitive impairment. *J. Am. Geriat. Soc.* 53, 695–699. doi: 10.1111/j.1532-5415.2005.53221.x

Ng, R., Allore, H. G., Monin, J. K., and Levy, B. R. (2016). Retirement as meaningful: positive retirement stereotypes associated with longevity. *J. Soc. Issues* 72, 69–85. doi: 10.1111/josi.12156

Nippold, M. A., Mansfield, T. C., and Billow, J. L. (2007). Peer conflict explanations in children, adolescents, and adults: examining the development of complex syntax. *Am. J. Speech Lang. Pathol.* 16, 179–188. doi: 10.1044/1058-0360(2007/022)

Oh, A., Duerden, E. G., and Pang, E. W. (2014). The role of the insula in speech and language processing. *Brain Lang.* 135, 96–103. doi: 10.1016/j.bandl.2014.06.003

Palacios, C. S., Torres, M. T., and Mena, M. B. (2009). Negative aging stereotypes and their relation with psychosocial variables in the elderly population. *Arch. Gerontol. Geriat.* 48, 385–390. doi: 10.1016/j.archger.2008.03.007

Park, D. C., Lautenschlager, G., Hedden, T., Davidson, N. S., Smith, A. D., and Smith, P. K. (2002). Models of visuospatial and verbal memory across the adult life span. *Psychol. Aging* 17:299.

Qualls, C. D., and Harris, J. L. (2003). Age, working memory, figurative language type, and reading ability. *Am. J. Speech-Lang. Pathol.* 12, 92–102. doi: 10.1044/1058-0360(2003/055)

Ramscar, M., Hendrix, P., Love, B., and Baayen, R. H. (2013). Learning is not decline: The mental lexicon as a window into cognition across the lifespan. *Ment. Lexic.* 8, 450–481.

Richter, J., Scheiter, K., Eder, T. F., Huettig, F., and Keutel, C. (2020). How massed practice improves visual expertise in reading panoramic radiographs in dental students: an eye tracking study. *PLoS One* 15:e0243060. doi: 10.1371/journal.pone.0243060

Rypma, B., Prabhakaran, V., Desmond, J. E., Glover, G. H., and Gabrieli, J. D. (1999). Load-dependent roles of frontal brain regions in the maintenance of working memory. *Neuroimage* 9, 216–226. doi: 10.1006/nimg.1998.0404

Saffran, J. R., Aslin, R. N., and Newport, E. L. (1996). Statistical learning by 8-month-old infants. *Science* 274, 1926–1928. doi: 10.1126/science.274.5294.1926

Salthouse, T. A., and Mandell, A. R. (2013). Do age-related increases in tip-of-the-tongue experiences signify episodic memory impairments? *Psychol. Sci.* 24, 2489–2497. doi: 10.1177/0956797613495881

Salvagio, E., Gomez, R., and Peterson, M. (2015). Is prior experience necessary for 5.5 month-old infants to use the statistical regularity of an unchanging object on an changing background for segmentation? *J. Vision* 15:338.

Samuelson, L. K. (2002). Statistical regularities in vocabulary guide language acquisition in connectionist models and 15-20-month-olds. *Dev. Psychol.* 38:1016. doi: 10.1037//0012-1649.38.6.1016

Smagorinsky, P. (1989). The reliability and validity of protocol analysis. *Writ. Commun.* 6, 463–479.

Spreng, R. N., and Turner, G. R. (2019). The shifting architecture of cognition and brain function in older adulthood. *Persp. Psychol. Sci.* 14, 523–542. doi: 10.1177/1745691619827511

Szaflarski, J. P., Holland, S. K., Schmithorst, V. J., and Byars, A. W. (2006). fMRI study of language lateralization in children and adults. *Human Brain Mapp.* 27, 202–212. doi: 10.1002/hbm.20177

Tan, L. H., Laird, A. R., Li, K., and Fox, P. T. (2005). Neuroanatomical correlates of phonological processing of Chinese characters and alphabetic words: a meta-analysis. *Human Brain Mapp.* 25, 83–91. doi: 10.1002/hbm.20134

Tan, L. H., Liu, H.-L., Perfetti, C. A., Spinks, J. A., Fox, P. T., and Gao, J.-H. (2001). The neural system underlying Chinese logograph reading. *Neuroimage* 13, 836–846. doi: 10.1006/nimg.2001.0749

Tomer, R., and Levin, B. E. (1993). Differential effects of aging on two verbal fluency tasks. *Percep. Motor Skills* 76, 465–466. doi: 10.2466/pms.1993.76.2.465

Ulfhake, B., Bergman, E., and Fundin, B. (2002). Impairment of peripheral sensory innervation in senescence. *Auton. Neurosci.* 96, 43–49. doi: 10.1016/s1566-0702(01)00368-x

Weiss, C. O., Hoenig, H. H., Varadhan, R., Simonsick, E. M., and Fried, L. P. (2010). Relationships of cardiac, pulmonary, and muscle reserves and frailty to exercise capacity in older women. *J. Gerontol. Ser. A Biomed. Sci. Med. Sci.* 65, 287–294. doi: 10.1093/gerona/glp147

Williamson, J. D., Espeland, M., Kritchevsky, S. B., Newman, A. B., King, A. C., Pahor, M., et al. (2009). Changes in cognitive function in a randomized trial of physical activity: results of the lifestyle interventions and independence for elders pilot study. *J. Gerontol. Ser. A Biomed. Sci. Med. Sci.* 64, 688–694. doi: 10.1093/gerona/glp014

Wu, C.-Y., Ho, M.-H. R., and Chen, S.-H. A. (2012). A meta-analysis of fMRI studies on Chinese orthographic, phonological, and semantic processing. *Neuroimage* 63, 381–391. doi: 10.1016/j.neuroimage.2012.06.047

Xiong, J., Rao, S., Jerabek, P., Zamarripa, F., Woldorff, M., Lancaster, J., et al. (2000). Intersubject variability in cortical activations during a complex language task. *Neuroimage* 12, 326–339. doi: 10.1006/nimg.2000.0621

Yang, J., Li, P., Fang, X., Shu, H., Liu, Y., and Chen, L. (2016). Hemispheric involvement in the processing of Chinese idioms: an fMRI study. *Neuropsychologia* 87, 12–24. doi: 10.1016/j.neuropsychologia.2016.04.029

Yeh, S. L. (2000). Structure detection of Chinese characters: Visual search slope as an index of similarity between different-structured characters. *Chin. J. Psychol.* 42, 191–216.

Yeh, S. L., and Li, J. L. (2002). Role of structure and component in judgments of visual similarity of Chinese characters. *J. Exp. Psychol. Human Percep. Perform.* 28:933. doi: 10.1037/0096-1523.28.4.933

Yeh, S. L., Li, J. L., Takeuchi, T., Sun, V., and Liu, W. R. (2003). The role of learning experience on the perceptual organization of Chinese characters. *Visual Cogn.* 10, 729–764.

Zhou, J., Lee, C.-L., Li, K.-A., Tien, Y.-H., and Yeh, S.-L. (2016). Does temporal integration occur for unrecognizable words in visual crowding? *PLoS One* 11:e0149355. doi: 10.1371/journal.pone.0149355

Zhu, Z., Zhang, J. X., Wang, S., Xiao, Z., Huang, J., and Chen, H.-C. (2009). Involvement of left inferior frontal gyrus in sentence-level semantic integration. *Neuroimage* 47, 756–763. doi: 10.1016/j.neuroimage.2009.04.086

Conflict of Interest: The authors declare that the research was conducted in the absence of any commercial or financial relationships that could be construed as a potential conflict of interest.

frontiers | Frontiers in Aging Neuroscience

ORIGINAL RESEARCH
published: 20 June 2022
doi: 10.3389/fnagi.2022.875589

Behavioral Reserve in Behavioral Variant Frontotemporal Dementia

Su Hong Kim[1,2], Yae Ji Kim[2,3], Byung Hwa Lee[4,5,6], Peter Lee[2], Ji Hyung Park[1], Sang Won Seo[4,5,6,7,8] and Yong Jeong[1,2,3,9]**

[1] Graduate School of Medical Science and Engineering, Korea Advanced Institute of Science and Technology, Daejeon, South Korea, [2] KAIST Institute for Health Science Technology, Korea Advanced Institute of Science and Technology, Daejeon, South Korea, [3] Program of Brain and Cognitive Engineering, Korea Advanced Institute of Science and Technology, Daejeon, South Korea, [4] Department of Neurology, Samsung Medical Center, Sungkyunkwan University, Seoul, South Korea, [5] Neuroscience Center, Samsung Medical Center, Seoul, South Korea, [6] Samsung Alzheimer Research Center, Samsung Medical Center, Seoul, South Korea, [7] Department of Health Science and Technology, Samsung Advanced Institute for Health Sciences and Technology (SAIHST), Sungkyunkwan University, Seoul, South Korea, [8] Department of Intelligent Precision Healthcare Convergence, Samsung Advanced Institute for Health Sciences and Technology (SAIHST), Sungkyunkwan University, Seoul, South Korea, [9] Department of Bio and Brain Engineering, Korea Advanced Institute of Science and Technology, Daejeon, South Korea

OPEN ACCESS

Edited by:
Kenji Toba,
Tokyo Metropolitan Institute of Gerontology, Japan

Reviewed by:
Takahito Yoshizaki,
Keio University School of Medicine, Japan
Manabu Ikeda,
Osaka University, Japan

***Correspondence:**
Sang Won Seo
sw72.seo@samsung.com
Yong Jeong
yong@kaist.ac.kr

Specialty section:
This article was submitted to Neurocognitive Aging and Behavior, a section of the journal Frontiers in Aging Neuroscience

Received: *14 February 2022*
Accepted: *27 May 2022*
Published: *20 June 2022*

Citation:
Kim SH, Kim YJ, Lee BH, Lee P, Park JH, Seo SW and Jeong Y (2022) Behavioral Reserve in Behavioral Variant Frontotemporal Dementia. Front. Aging Neurosci. 14:875589. doi: 10.3389/fnagi.2022.875589

"Reserve" refers to the individual clinical differences in response to a neuropathological burden. We explored the behavioral reserve (BR) and associated neural substrates in 40 participants with behavioral variant frontotemporal dementia (bvFTD) who were assessed with the frontal behavioral inventory (FBI) and magnetic resonance imaging. Because neuroimaging abnormality showed a high negative correlation with the FBI negative (but not positive) symptom scores, we developed a linear model only to calculate the nBR (BR for negative symptoms) marker using neuroimaging abnormalities and the FBI score. Participants were divided into high nBR and low nBR groups based on the nBR marker. The FBI negative symptom score was lower in the high nBR group than in the low nBR group having the same neuroimaging abnormalities. However, the high nBR group noted a steeper decline in cortical atrophy and showed less atrophy in the left frontotemporal cortices than the low nBR group. In addition, the fractional anisotropy (FA) values were greater in the high nBR than in the low nBR group, except in the sensory-motor and occipital areas. We identified an nBR-related functional network composed of bilateral frontotemporal areas and the left occipital pole. We propose the concept of BR in bvFTD, and these findings can help predict the disease progression.

Keywords: behavioral variant frontotemporal dementia, behavior reserve, neural correlates, brain network, MRI

Abbreviations: AD, Alzheimer's Disease; BR, behavioral reserve; bvFTD, behavioral variant frontotemporal dementia; CR, cognitive reserve; DTI, diffusion tensor imaging; DOT, Dictionary of Occupational Titles; FEW, family-wise error; FA, fractional anisotropy; FBI, frontal behavioral inventory; FTD, frontotemporal dementia; GM, gray matter; MRI, magnetic resonance imaging; mean CTh_{FT}, mean cortical thickness of the fronto-temporo-insular area; mean FA_{FT}, mean FA value of the frontotemporal WM; MR, motor reserve; MNI, Montreal Neurological Institute; nBR, behavioral reserve for negative symptoms; NBSs, network-based statistics; PD, Parkinson's Disease; ROIs, regions of interest; rs-fMRI, resting-state functional magnetic resonance imaging; SPECT, single-photon emission computed tomography; T1WI, T1-weighted images; TBSS, tract-based spatial statistics; WM, white matter.

INTRODUCTION

Frontotemporal dementia (FTD) is the second most common cause of early-onset dementia after Alzheimer's Disease (AD); also, it is associated with progressive degeneration of the frontal and temporal lobes (Bang et al., 2015). Behavioral variant FTD (bvFTD) is the most common subtype of FTD and is characterized by personality change and social dysfunction (Rascovsky et al., 2011). The severity of behavioral manifestations of bvFTD is commonly evaluated using the frontal behavioral inventory (FBI), which is a caregiver-based questionnaire consisting of 12 positive and 12 negative behavioral symptoms (Kertesz et al., 1997, 2000; Milan et al., 2008).

The concept of "reserve" refers to individual differences in the capacity to withstand the pathological burden of neurodegenerative diseases (Katzman et al., 1988). Compared with people with a low reserve, people with a higher reserve can cope with a greater pathological burden before the onset of symptoms; they may show a less severe clinical presentation under similar pathological burdens. However, if the pathological burden increases, participants with a high reserve show a faster decline in the clinical presentation than those with a low reserve (Stern, 2012; Barulli and Stern, 2013). Cognitive reserve (CR) is a widely accepted concept in AD (Stern, 2012; Lee et al., 2019). Moreover, the concept of motor reserve (MR) has recently emerged in Parkinson's Disease (PD) (Chung et al., 2020a,b). Previous research has suggested that CR is an environmental factor that contributes to heterogeneous cognitive function mediated by the neuroanatomical structure, metabolism, or cerebral blood flow; the precise mechanism remains unclear (Placek et al., 2016; Maiovis et al., 2018; Beyer et al., 2021).

Using FBI scores and statistical modeling, Borroni et al. (2012) identified four behavioral subgroups in participants with bvFTD, namely "disinhibited," "apathic," "language," and "aggressive." Furthermore, Premi et al. (2013) proposed the behavioral reserve (BR) hypothesis in FTD with cerebral single-photon emission computed tomography (SPECT); this is similar to the concepts of CR in AD and of MR in PD. These studies revealed that educational attainment was the only measure associated with a disinhibited phenotype. These studies also observed greater hypoperfusion in the right inferior frontal gyrus, left medial frontal gyrus, and right caudate in those with a higher education level than those with a lower education level.

The degree of behavioral manifestation varies in participants with bvFTD, even with similar degrees of cortical atrophy or white matter (WM) destruction. In this study, we have proposed a concept of BR to understand these individual behavioral differences. We have suggested a novel model to conceptualize BR based on the original definition of reserve, using T1 imaging and fractional anisotropy (FA) as surrogates of the neuropathological burden of gray matter (GM) and WM, respectively. Subsequently, we have tested whether BR can explain the heterogeneous clinical presentation of bvFTD.

Neural compensation, one of the neural reserve mechanisms, is a brain network newly developed to compensate for the disruption of the pre-existing brain network due to the disease pathology. In this respect, we also investigated the neural correlates and the associated networks of BR by estimating the BR of each participant with bvFTD based on their FBI score and neuroimaging abnormalities. Then, we identified the BR-associated functional brain networks using network-based statistics (NBSs) analysis.

MATERIALS AND METHODS

Ethics Approval Statement

This study was approved by the Institutional Review Board of the Samsung Medical Center. Written informed consent was obtained from the caregivers of all participants prior to conducting the study procedures.

Participants

In this study, 59 participants presenting to the Neurology Department of the Samsung Medical Center between January 2011 and September 2018 were screened. They were diagnosed with bvFTD based on the clinical criteria proposed by the International Behavioral Variant Frontotemporal Dementia Criteria Consortium for probable bvFTD (Rascovsky et al., 2011). All participants were evaluated using the FBI and through comprehensive interviews; they also underwent magnetic resonance imaging (MRI), including high-resolution T1-weighted MRI, resting-state functional MRI (rs-fMRI), and diffusion tensor imaging (DTI). Among the 59 participants screened, 1 without FBI scores and 18 without rs-fMRI and DTI scans were excluded. Finally, 40 participants were included in this study (**Figure 1**).

Blood tests, including a complete blood count, blood chemistry tests, vitamin B12/folate test, thyroid function test, and serological tests for syphilis, were performed to exclude the secondary causes of dementia. In addition, conventional brain MRI confirmed the absence of severe WM diseases and structural lesions, such as traumatic brain injuries, brain tumors, and hydrocephalus.

The basic demographical data were obtained. Considering that the years of education and occupational complexity have been widely accepted as the most relevant CR estimates, we also obtained data on these parameters to test whether they are valid estimates even for BR. Occupational complexity was measured using the Dictionary of Occupational Titles (DOT), which evaluated the complexity of dealing with data (0–6 points), people (0–8 points), and things (0–7 points) (United States Department of Labor and United States Employment Service and Center, 2006). In the DOT ratings, a lower score indicates a higher occupational complexity. Thus, we investigated the correlations between the years of education, occupational complexity, and BR markers.

Frontal Behavioral Inventory Scores

Behavioral symptoms were quantified using the FBI, which is a caregiver-based behavioral questionnaire consisting of 12 positive and 12 negative symptoms (Kertesz et al., 1997, 2000; Milan et al., 2008). The positive symptoms include obsessions, hoarding, inappropriateness, excessive jocularity, impulsivity,

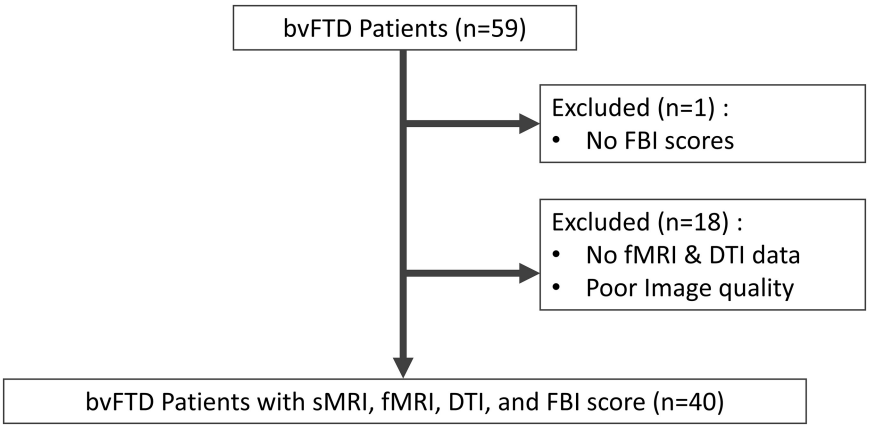

FIGURE 1 | Flowchart of the study participants and their enrolment. bvFTD, behavioral variant frontotemporal dementia; FBI, frontal behavioral inventory; fMRI, functional magnetic resonance imaging; DTI, diffusion tensor imaging; sMRI, structural magnetic resonance imaging.

restlessness, irritability, aggression, hyperorality, hypersexuality, utilization behavior, and incontinence. The negative symptoms include apathy, aspontaneity, emotional flatness, inflexibility, disorganization, inattention, personal neglect, loss of insight, logopenia, aphasia, comprehensive deficit, and alien hand. Each item is scored 0–3 points (0: no symptom, 1: mild, 2: moderate, and 3: severe); thus, the maximum score is 72. The behavioral score was newly defined so that it was directly proportional to the behavioral performance, reflecting the concept of reserve well and making it easier to understand. The positive and negative behavioral score was calculated by subtracting the FBI score of the positive items or the FBI score of the negative items from the maximum score (36 points); retrospectively, a lower score indicated severe symptoms. The FBI symptoms were categorized into the following four phenotypes (Borroni et al., 2012): (1) disinhibited phenotype (which comprised loss of insight, obsession, hoarding, excessive jocularity, impulsivity, restlessness, hyperorality, and utilization behavior), (2) apathetic phenotype (which comprised apathy and aspontaneity), (3) aggressive phenotype (which comprised inflexibility, irritability, and aggression), and (4) language phenotype (which comprised logopenia, aphasia, comprehensive deficit, and alien hand). We explored the correlations between the scores of each phenotype and the neuroimaging abnormalities.

Magnetic Resonance Imaging Acquisition

An Achieva 3.0-Tesla MRI scanner (Philips, Best, Netherlands) was used to obtain all sequences. A three-dimensional (3D), T1-weighted turbo field echo image was obtained with the following parameters: sagittal slice thickness, 1.0 mm (over contiguous slices with 50% overlap); no gap; repetition time (TR), 9.9 ms; echo time (TE), 4.6 ms; flip angle, 8°; and matrix size, 240 × 240 [reconstructed to 480 × 480 over a field of view (FOV) of 240 mm]. DTI images were obtained with sets of axial diffusion-weighted, single-shot, echo-planar images with the following parameters: acquisition matrix, 128 × 128; voxel size, 1.72 mm × 1.72 mm × 2 mm; axial slices, 70; FOV, 220 mm × 220 mm; TE, 60 ms; TR, 7,696 ms; flip angle, 90°; slice gap, 0 mm; and b-factor, 600 smm^{-2}. DTI images were acquired in 45 different directions using the baseline image without weighting (0, 0, 0). An rs-fMRI sequence was obtained using a gradient echo-planar imaging pulse sequence with the following parameters: acquisition matrix, 128 × 128; voxel size, 2.875 mm × 2.875 mm × 4 mm; axial slices, 35; FOV, 220 mm × 140 mm × 220 mm; TE, 35 ms; and TR, 3,000 ms.

Image Preprocessing and Analyses

Vertex-Wise Analysis of Cortical Thickness

T1-weighted images (T1WI) were preprocessed using Freesurfer version 6.0.[1] We reconstructed the cortical thickness maps to the fsaverage standard surface provided by Freesurfer; then, we determined the cortical thickness values in 68 bilateral Desikan–Killinay regions of interest (ROIs) in each participant (Desikan et al., 2006).

The preprocessed cortical thickness data were subjected to vertex-wise analysis using the mri-glmfit tool from Freesurfer. Cortical thickness was investigated using a generalized linear model, with age and sex as the covariates. To avoid false positives, a Monte Carlo simulation with 10,000 permutations, as implemented in Freesurfer [family-wise error (FWE), $p < 0.01$], was tested. Only those regions that survived these multiple comparisons are shown in the figures.

Tract-Based Spatial Statistics

Diffusion tensor imaging images were preprocessed using the FMRIB Software Library (FSL version 5.0.9[2]). In the preprocessing step, eddy current distortion and head motion for each raw DTI image were corrected using the eddy current function of the FSL. Individual brain binary masks were created using the Brain Extraction Tool with a fractional intensity threshold of 0.2, and an FA map was generated using DTIfit.

[1]https://surfer.nmr.mgh.harvard.edu

[2]https://www.fmrib.ox.ac.uk/fsl

Tract-based spatial statistics (TBSS) were performed to calculate the ROI-specific mean FA value and explore whether there was any regional difference in the FA values between the groups of comparison (Smith et al., 2006). First, the FA maps of all participants were non-linearly aligned to the space of a study-specific template and registered to the Montreal Neurological Institute (MNI) coordinate space. Second, mean FA maps were created for every participant, and the mean FA skeleton was generated with a threshold FA > 0.02. Third, the aligned FA maps of each participant were projected onto the FA skeleton.

Using FSL randomization, permutation-based non-parametric *t*-statistics (10,000 permutations) were performed for group comparisons. A threshold-free cluster enhancement was used to correct multiple comparisons, and a significant difference between the groups at the cluster level was obtained at $p < 0.001$ (FWE-corrected) (Smith and Nichols, 2009). The WM was labeled with the reference atlas of ICBM-DTI-81 WM labels and the JHU WM tractography atlas supported by the FSL.

Network Construction and Network-Based Statistic Analysis

The rs-fMRI images were preprocessed using the CONN functional connectivity toolbox, version 20.b,[3] from the SPM12 package.[4] All preprocessing steps were performed using the CONN's default preprocessing pipeline. In this preprocessing pipeline, the raw rs-fMRI images were realigned for motion correction, unwrapped, centered to (0, 0, 0) coordinates, corrected for slice-timing, and coregistered to each participant's 3D T1WI. These images were then normalized to the MNI coordinate space, spatially smoothed with an 8-mm Gaussian kernel with full width at half maximum, and resliced into 2 × 2 × 2-mm voxels. Moreover, a default denoising pipeline from the CONN toolbox was also used. In this denoising pipeline, the preprocessed rs-fMRI images linearly regressed out the potential confounding effects of the blood-oxygen-level-dependent signal and temporal band-pass filtering with a band-pass filter of 0.008–0.09 Hz.

To define the network nodes, we used the FSL Harvard–Oxford atlas included in the CONN toolbox (Frazier et al., 2005; Desikan et al., 2006; Makris et al., 2006; Goldstein et al., 2007). For each participant, the average rs-fMRI time series of each ROI was extracted from 106 cortical and subcortical ROIs, and the Pearson's correlation coefficients between the rs-fMRI time series of each ROI were calculated to construct the functional connectivity.

We used NBS to identify the functional networks associated with the BR; this is a nonparametric method based on the concept of cluster-based thresholding of statistical maps (Zalesky et al., 2010). First, a general linear regression was performed with the ROI-to-ROI matrix, and a statistical parametric map was created. Then, a threshold of $p < 0.001$ was applied to the statistical parametric map to extract highly associated connections and to identify the largest number of connected BR-associated networks. Finally, a permutation test (10,000 permutations) was performed to determine an empirical null distribution of the maximal BR networks, and an FDR-corrected *p*-value was assigned to each network. Networks with a corrected $p < 0.05$ were considered statistically significant. NBS analysis was performed using CONN (20.b).

[3]https://www.nitrc.org/projects/conn

[4]https://www.fil.ion.ucl.ac.uk/spm

Calculation of the Behavioral Reserve Marker and the Relationship Between the Behavioral Reserve Marker and Reserve Proxies

Based on the original definition of reserve, we defined a BR marker as a residual of the difference between the actual behavioral score and the estimated score.

$$\begin{aligned} &Behavioural\ Reserve\ (BR)\ marker \\ &= Behavioural\ Score_{observed} - Behavioural\ Score_{estimated} \end{aligned}$$

High BR marker values indicated a high BR, while low BR marker values indicated a low BR. Based on the median value of the BR marker, participants were divided into the high and low BR groups.

The estimated behavioral score was calculated based on the neuroimaging abnormalities and demographics. A general linear model was established using age, sex, cortical thickness, and the mean FA values to estimate the behavioral score. To reflect the specific neuropathological burden of FTD, we used the mean cortical thickness of the fronto-temporo-insular area (mean CTh_{FT}) and the mean FA value of the frontotemporal WM (mean FA_{FT}) (Du et al., 2007; Zhang et al., 2009; Pan et al., 2012).

$$\begin{aligned} &Behavioural\ Score_{estimated} \\ &= \alpha_1 \times Age + \alpha_2 \times Sex + \alpha_3 \times mean\ CTh_{FT} \\ &+ \alpha_4 \times mean\ FA_{FT} + \beta \end{aligned}$$

After calculating the BR marker, we calculated the Pearson's correlation coefficients between the BR marker and the previously noted reserve markers, such as the education level and occupational complexity used in CR in AD (Stern, 2012; Lee et al., 2019) and MR in PD (Chung et al., 2020a,b).

Statistical Analysis

The Pearson's correlation coefficients were calculated to assess the relationships among the continuous variables. A two-sample *t*-test was performed to compare variables between the high and low BR groups; two-tailed *p*-values < 0.05 were considered statistically significant.

To compare the slope differences between the two groups, we used the following formula (Kleinbaum et al., 2013):

$$Z\ score = \frac{\beta_1 - \beta_2}{\sqrt{Standard\ error_1{}^2 - Standard\ error_2{}^2}}$$

Using this formula, we calculated the *Z* score using a *p*-value table. We used R studio (R studio, Boston, MA, United States) for statistical and graph visualization and BrainNet Viewer for network visualization (Xia et al., 2013).

RESULTS

Demographics

The demographics and behavioral assessments of the participants and the two groups (low and high nBR) are summarized in **Table 1**. There were no differences in age, sex, education level, or occupational complexity between the high and low nBR groups. However, the FBI negative symptom scores were higher in the low nBR group than in the high nBR group (**Table 1**).

Behavioral Scores and Neuroimaging Correlates

The behavioral scores for negative symptoms were positively correlated with the global (r = 0.496, p = 0.002) and fronto-temporo-insular (r = 0.521, p = 0.0005) mean cortical thicknesses (**Figure 2A**). However, the behavioral scores for the positive symptoms were not correlated with the global (r = −0.238, p = 0.140) and fronto-temporo-insular (r = −0.228, p = 0.157) mean cortical thicknesses (**Figure 2B**).

The behavioral scores for the negative symptoms were positively correlated with the mean FA values of the global (r = 0.554, p = 0.0002) and frontotemporal (r = 0.544, p = 0.0003) WM (**Figure 3A**). Similar to the cortical thickness, the behavioral scores for the positive symptoms were not correlated with the mean FA values of the global (r = −0.023, p = 0.888) or frontotemporal (r = −0.0043, p = 0.792) WM (**Figure 3B**).

Among the four phenotype subgroups, the apathetic phenotype was positively correlated with the global (r = 0.424, 0 = 0.006) and fronto-temporo-insular (r = 0.447, p = 0.004) mean cortical thicknesses. Furthermore, the language phenotype was also positively correlated with the global (r = 0.527, p = 0.0005) and fronto-temporo-insular (r = 0.574, p = 0.0001) mean cortical thicknesses (**Figures 2D,F**). However, the global (r = −0.100, p = 0.539) and fronto-temporo-insular (r = −0.061, p = 0.710) mean cortical thicknesses were not associated with the disinhibited and aggressive phenotypes (global: r = −0.224, p = 0.165; fronto-temporo-insular: r = −0.241, p = 0.134; **Figures 2C,E**). FA maps revealed that the apathetic phenotype was positively correlated with the mean FA values of the global (r = 0.370, 0 = 0.019) and fronto-temporo-insular (r = 0.357, p = 0.024) WM. Furthermore, FA maps also revealed that the language phenotype was positively correlated with the mean FA values of the global (r = 0.464, p = 0.003) and fronto-temporo-insular (r = 0.490, p = 0.001) mean cortical thicknesses (**Figures 3D,F**). However, the mean FA values of the global (r = 0.119, p = 0.463) and fronto-temporo-insular (r = 0.126, p = 0.449) mean cortical thicknesses were not associated with the disinhibited and aggressive phenotypes (global: r = 0.061, p = 0.710; fronto-temporo-insular: r = 0.019, p = 0.908; **Figures 3C,E**).

Calculation of the Behavioral Reserve Marker and Its Relationship With the Reserve Proxies

We only used the negative symptom score for the BR because the positive symptoms did not show any significant correlation. As seen in **Table 2**, the general linear model demonstrated that the estimated behavioral score for negative symptoms was predicted by the fronto-temporo-insular cortical thickness (β = 10.504, p = 0.049) and the FA value of the frontotemporal WM (β = 75.919, p = 0.035). The R^2 value of the model was 0.386 (adjusted R^2 = 0.316; F-test: p = 0.002).

The apathetic and language phenotypes, for which significant correlations were noted between the behavioral scores and the neuroimaging abnormalities, were used for building a general linear model. Conversely, the disinhibited and aggressive phenotypes, for which no such significant correlations were noted, were not used. The general linear model demonstrated that the estimated behavioral score for the language phenotype was predicted by the fronto-temporo-insular cortical thickness (β = 4.779, p = 0.013) and the FA value of the frontotemporal WM (β = 25.891, p = 0.043). The R^2 value of the model was 0.470 (adjusted R^2 = 0.437; F-test, p = 0.0004). However, the general linear model for the apathetic phenotype did

TABLE 1 | Demographic characteristics and behavioral assessment of the participants with bvFTD classified into the low behavioral reserve for negative symptoms (nBR) group and the high nBR group.

	bvFTD (n = 40)	Low nBR (n = 20)	High nBR (n = 20)	p-Value
Demographics				
Diagnostic age, years	65.7 ± 8.4	65.1 ± 8.6	66.3 ± 8.4	0.656
Gender, women (%)	15 (37.5)	7 (35.0)	8 (40.0)	0.756
Level of education, years	11.9 ± 5.4	12.0 ± 5.9	11.7 ± 5.1	0.852
Occupational complexity (DOT rating)[a]	13.3 ± 4.6	13.3 ± 5.1	13.4 ± 4.2	0.927
Behavioral assessment				
FBI_{total}	27.8 ± 11.9	35.0 ± 10.9	20.7 ± 7.9	<0.001
$FBI_{negative}$	19.1 ± 7.9	24.4 ± 5.6	13.8 ± 6.2	<0.001
$FBI_{positive}$	8.8 ± 6.9	10.7 ± 8.2	7.0 ± 4.8	0.094
MRI-FBI interval, days	28.9 ± 136.8	45.4 ± 120.3	12.5 ± 153.0	0.454

[a]*Occupational information of one participant classified into the high nBR group was not available.*

bvFTD, behavioral variant frontotemporal dementia; DOT, Dictionary of Occupational Titles; FBI, frontal behavioral inventory.

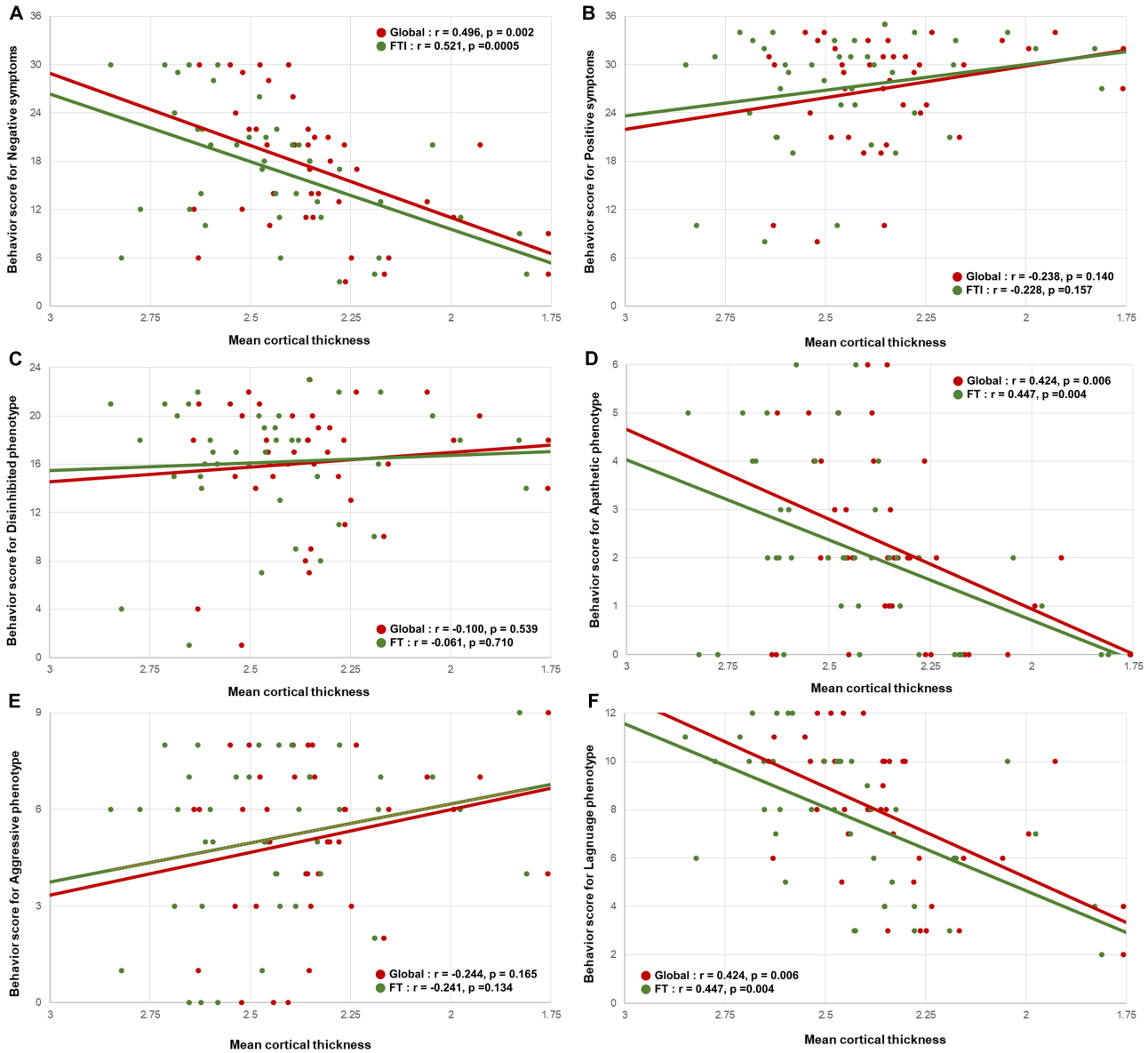

FIGURE 2 | Correlation between the mean cortical thickness and the behavioral scores. Scatterplots showing the relationship between the behavioral scores for negative symptoms and the behavioral variant frontotemporal dementia neuropathology imaging biomarkers. **(A)** The behavioral scores for negative symptoms were positively correlated with the global mean cortical thickness and fronto-temporo-insular mean cortical thickness. **(B)** The behavioral scores for positive symptoms were not correlated with the global mean cortical thickness and fronto-temporo-insular mean cortical thickness. In phenotype aspects. **(D,F)** The behavioral scores for apathetic and language phenotypes were positively correlated with the global mean cortical thickness and fronto-temporo-insular mean cortical thickness. **(C,E)** The behavioral scores for disinhibited and aggressive phenotype were not correlated with the global mean cortical thickness and fronto-temporo-insular mean cortical thickness.

not identify a significant model (adjusted R^2 = 0.221; F-test: p = 0.061).

After calculating the individual nBR markers, we calculated the relationships between the BR marker and the previously noted reserve proxies, such as the education level and occupational complexity used in CR in AD (Stern, 2012; Lee et al., 2019) and MR in PD (Chung et al., 2020a,b). As seen in **Figure 4**, the nBR marker was not correlated with the education level (r = 0.170, p = 0.293) or the occupational complexity (r = −0.004, p = 0.981). The three items of the DOT score did not correlate with the nBR marker (**Supplementary Figure 1**).

Validation of the Behavioral Reserve for Negative Symptoms Marker

We compared the relationship of the behavioral score for negative symptoms with the neuroimaging abnormalities between the high and low nBR groups. Compared to the low nBR group,

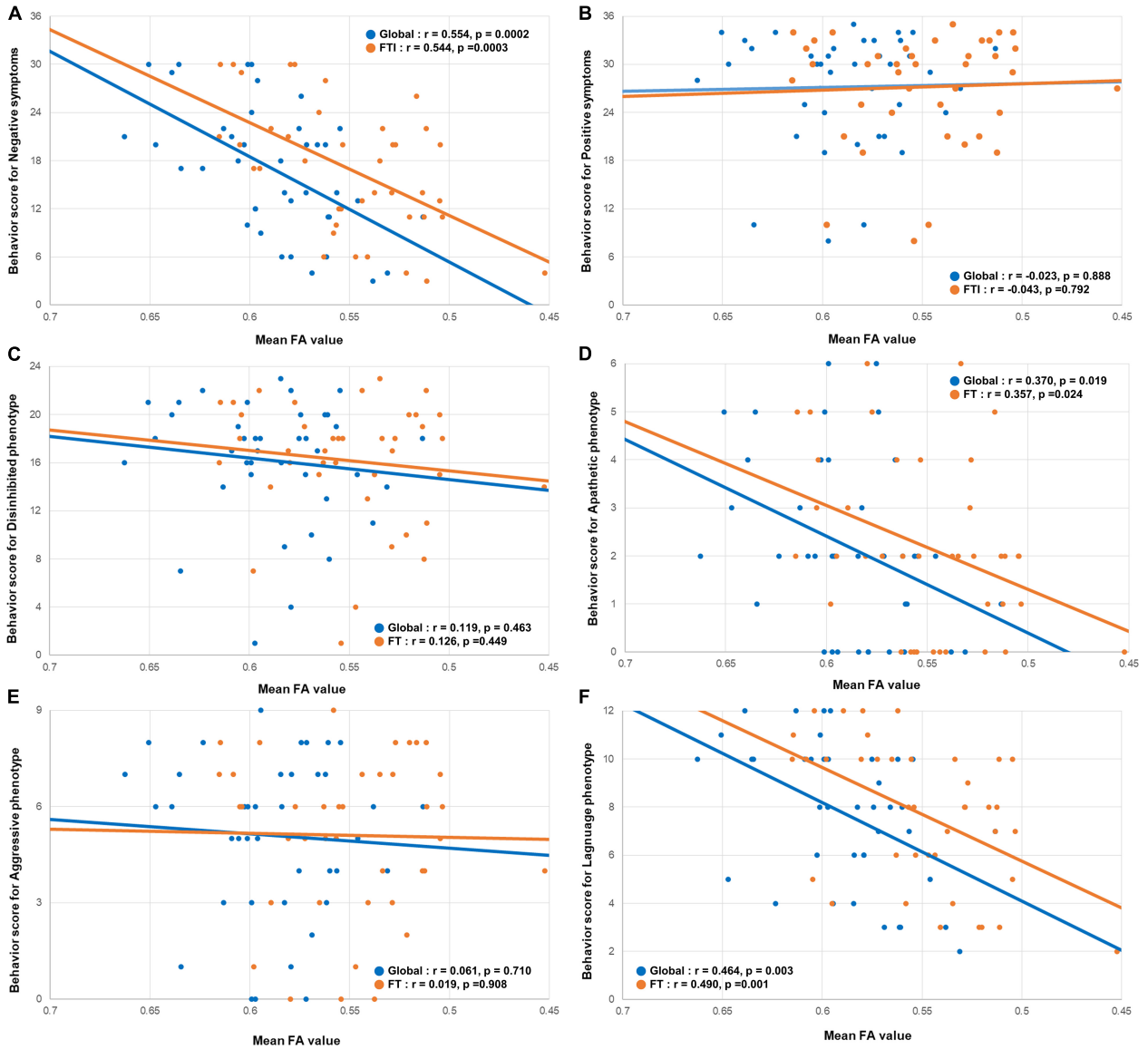

FIGURE 3 | Correlation between the mean FA value and the behavioral scores. Scatterplots showing the relationship between the behavioral scores for negative symptoms and the behavioral variant frontotemporal dementia neuropathology imaging biomarkers. **(A)** The behavioral scores for negative symptoms were positively correlated with the global mean FA, and mean FA value of the frontotemporal WM. **(B)** The behavioral scores for positive symptoms were not correlated with the global mean FA, and mean FA value of the frontotemporal WM. In phenotype aspects. **(D,F)** The behavioral scores for apathetic and language phenotypes were positively correlated with the global mean FA, and mean FA value of the frontotemporal WM. **(C,E)** The behavioral scores for disinhibited and aggressive phenotype were not correlated with the global mean FA, and mean FA value of the frontotemporal WM. FA, fraction anisotropy; WM, white matter.

the high nBR group showed a higher behavioral score (fewer symptoms) at a relatively normal cortical thickness and a steeper slope (p = 0.0005; **Figure 5A**). After adjusting for the age and sex, vertex-analysis of the cortical thickness revealed that the nBR marker was positively associated with the cortical thicknesses of the following: left superior frontal gyrus; middle frontal gyrus; orbitofrontal cortex; frontal opercularis; frontal triangularis; frontal orbitalis; middle temporal cortex; inferior temporal cortex; inferior parietal cortex; supramarginal gyrus; cingulate; precuneus; and right superior frontal, caudal middle frontal, medial orbitofrontal gyri (**Figure 5B**). Furthermore, a comparison of the FA values revealed that compared to the low nBR group, the high nBR group showed a higher behavioral score; however, the two groups had similar slopes (p = 0.63; **Figure 5C**). The TBSS of the FA value showed that the BR marker was associated with the FA value of the overall WM area, except in the sensory-motor cortices and occipital lobes (**Figure 5D**).

Regarding the language related BR (l-BR), the language scores were higher in the l-BR group than in the low l-BR group;

however, the two groups had similar slopes for the fronto-temporo-insular mean cortical thickness and the frontotemporal WM FA value. Inter-group comparisons of the cortical thickness or FA maps did not identify any significant region.

Identification of the Behavioral Reserve for Negative Symptoms Network

During group comparison, NBS analysis identified a single brain network (high nBR > low nBR) consisting of the anterior cingulate gyrus, paracingulate gyri, left frontal pole, left frontal operculum cortex, left occipital pole, right pallidum, right insular cortex, left anterior parahippocampal gyrus, and right inferior frontal gyrus (pars opercularis). The uncorrected connection threshold was $p < 0.001$, and the FDR-corrected cluster threshold was $p < 0.05$ (**Figure 6**). There was no functional connectivity related l-BR *via* NBS analysis.

DISCUSSION

In this study, we have proposed a concept of BR and investigated the neural correlates of BR in bvFTD, based on the definition of reserve (i.e., the discrepancy between the pathological burden and clinical manifestation) (Stern, 2012; Barulli and Stern, 2013). We hypothesized that the presence of BR explains the differences in the behavioral performances, despite similar pathological burdens, among participants with bvFTD. First, the nBR was defined, calculated, and validated. We then identified an interaction between the nBR marker and the neuroimaging abnormalities and its effect on behavioral performance. Finally, we identified the functional brain network associated with the nBR marker.

We wish to explain the individual variability of behavioral problems in bvFTD through the BR hypothesis. BR was considered to represent the difference between the estimated and observed behavioral performances. Our linear model calculated the estimated behavioral score from neuroimaging abnormalities. We used cortical thicknesses and FA values from DTI images to reflect the neuropathological burden of the GM and WM, respectively. Considering that AD-specific ROIs were more highly correlated with education (which is a proxy of CR) than with the global area (van Loenhoud et al., 2017), we additionally applied the neuropathological burden in the frontal, temporal, and insular lobes (these are representative pathological areas in bvFTD) (Du et al., 2007; Pan et al., 2012). Our experiments showed a higher correlation with these areas than with the global area. In the WM, the sagittal stratum (including the inferior longitudinal fasciculus and the inferior fronto-occipital fasciculus), cingulum (cingulate gyrus and hippocampus), fornix, stria terminalis, superior longitudinal fasciculus, superior fronto-occipital fasciculus, and uncinate fasciculus were selected as tracts of interest (Zhang et al., 2009).

The FBI scores and neuroimaging abnormalities were analyzed to create the model. The FBI score for negative symptoms was significantly correlated with the cortical thicknesses and FA values of the global and fronto-temporo-insular areas; however, the FBI score for positive symptoms was not. The cortical thickness and FA map-related FBI score for positive symptoms were considered to have no statistically significant areas because the difference in the scores between

TABLE 2 | General linear model to predict the behavioral score for negative symptoms.

Variables	β	Standard error	*p*-Value
Intercept	−42.788	19.550	0.035
Age	−0.117	0.132	0.379
Sex	0.134	2.311	0.954
FTI cortical thickness	10.504	5.140	0.049
FT FA	75.919	34.618	0.035

FTI, fronto-temporo-insular area; FT, frontotemporal area; FA, fraction anisotropy.

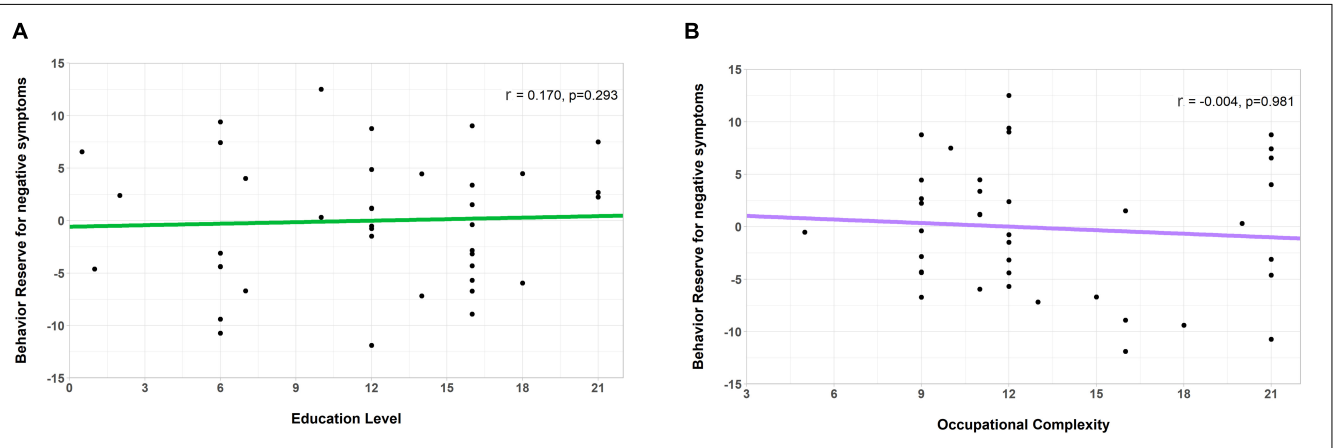

FIGURE 4 | Correlation of the behavioral reserve marker for negative symptoms (an nBR marker) with the education level and occupation complexity (markers for other reserves). Scatterplots showing the relationship between the nBR marker, education level, and occupational complexity. The nBR marker was not significantly correlated with **(A)** the education level ($r = 0.170$, $p = 0.293$) or **(B)** the occupational complexity ($r = -0.004$, $p = 0.981$). nBR, behavioral reserve for negative symptoms.

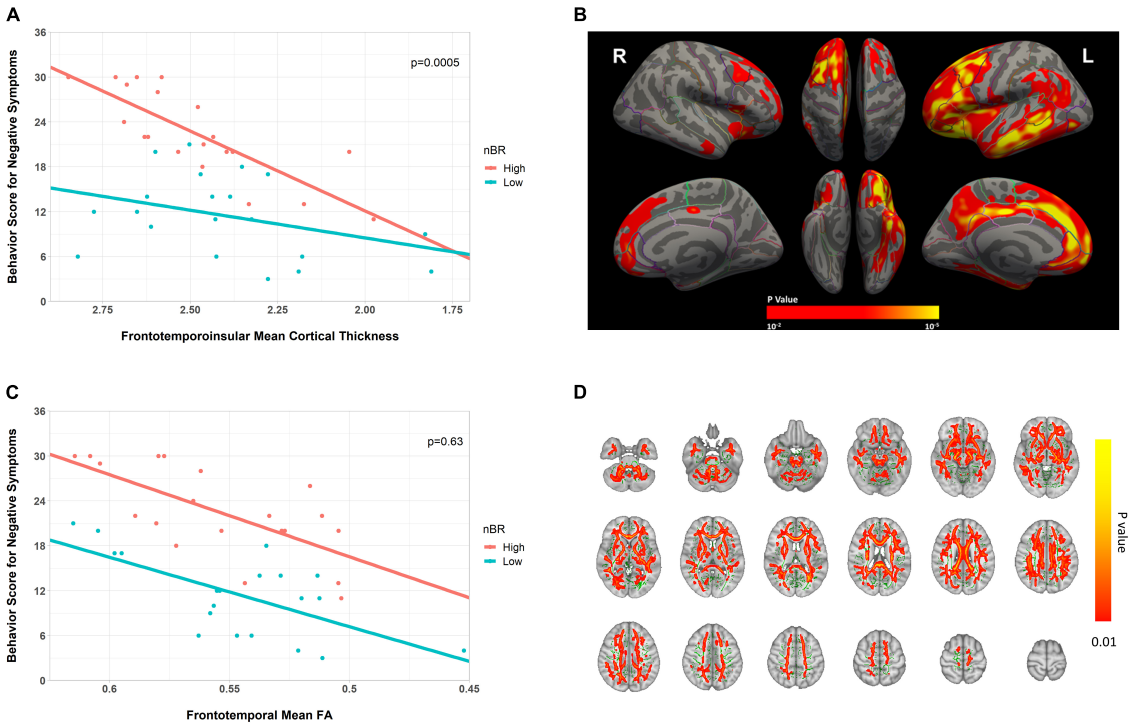

FIGURE 5 | Scatter plot for the interaction of the behavioral reserve marker for negative symptoms (nBR) and the neuroimaging abnormalities (cortical thickness and FA) on behavioral score for negative symptoms in bvFTD. **(A,C)** Scatter plots for the interaction of the nBR with **(A)** fronto-temporo-insular mean cortical thickness and **(C)** frontotemporal WM FA on behavioral score for negative symptoms in bvFTD. For illustration, groups with high and low nBR markers (defined using the median value) are plotted separately. **(B)** Cortical thickness-related nBR, adjusted for the age and sex ($p < 0.01$; corrected at the cluster level at $p < 0.01$). **(D)** FA-related nBR (in red-yellow), adjusted for the age and sex, and the mean FA skeleton (in green, FA 0.2). The results are corrected by threshold-free cluster enhancement and 10,000 permutations. Cluster significance was tested at $p < 0.01$ and subjected to multiple corrections. nBR, behavioral reserve for negative symptoms; FA, fractional anisotropy; bvFTD, behavioral variant frontotemporal dementia.

the participants was small. This can be attributed to the narrow distribution of the FBI scores for positive symptoms. Although the positive symptoms were more diagnostic for bvFTD, the negative symptoms were the most prominent symptoms at all stages (Benussi et al., 2021). According to the FBI manual, scores 25–30, 30–40, and >40 indicate mild, moderate, and severe disease states, respectively. The mean FBI score of our participants was 27.8; therefore, our data tended to represent participants with a mild disease status. In addition, the prevalence of genetic factors in bvFTD and AD is 30 and 5%, respectively (Rohrer et al., 2009). Because of the high proportion of genetic components, the environmental factors that are presumably core factors for BR may be relatively small.

The apathetic and language phenotypes (groups comprising negative items) also showed no significant correlations with neuroimaging abnormality. The apathetic phenotype included only two FBI items and excluded the major negative symptoms, such as indifference, disorganization, inattention, and personal neglect. The results for the language phenotype are thought to be because of the few language symptoms among the patients with FTD in this study, as only patients considered to have behavioral variants were selected and those considered to have semantic variants or progressive nonfluent aphasia were excluded. No significant correlations were observed between the nBR marker and the education level and occupation complexity, which were previously reported as proxies of other reserves in AD, FTD, and PD. In previous studies, only in cases with the disinhibited phenotype of bvFTD (which mostly consisted of the FBI score for positive symptoms), correlations between the education level and hypoperfusion in the frontotemporal area were observed on SPECT. However, apathic and language phenotypes, which were a part of the negative symptoms in the FBI, showed no correlated areas (Borroni et al., 2012; Maiovis et al., 2018). Our results were consistent with those of previous studies, suggesting that the education level may not be associated with BR.

Our major findings supported the BR hypothesis and demonstrated nBR marker-associated neuroimaging correlates. The high nBR group showed a higher behavioral score with lower neuroimaging abnormalities and a rapid decline of the behavioral score as reflective of cortical atrophy; this progressed similarly to CR in AD and MR in PD. Although our study is not a longitudinal study, the effect of the interaction between the nBR marker and neuroimaging abnormalities on the behavioral score was compatible with the traditional reserve concept (Stern, 2012; Barulli and Stern, 2013; Lee et al., 2019; Chung et al., 2020b). It has been reported that apathy is associated with the right

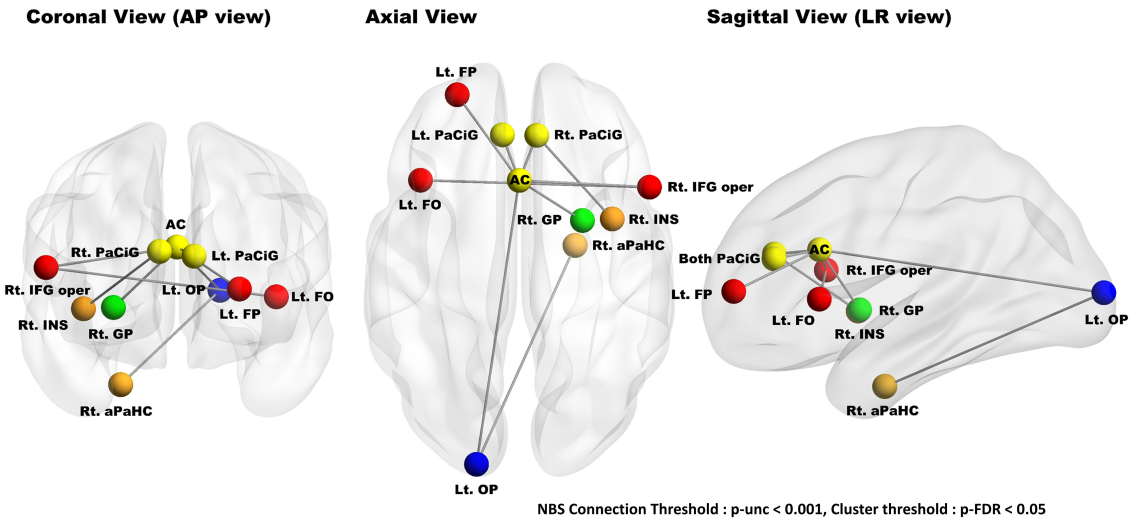

FIGURE 6 | Results of group comparisons (high nBR > low nBR) with a network-based statistical analysis. NBS analysis identified a single nBR network composed of the cingulate gyrus (anterior division), paracingulate gyri, left frontal pole, left frontal operculum cortex, left occipital pole, right pallidum, right insular cortex, left anterior parahippocampus, and right inferior frontal gyrus (pars opercularis); the connection threshold was $p < 0.001$ (uncorrected), while the cluster threshold was $p < 0.05$. The nodes located in the frontal, temporal, cingulate, basal ganglia, and occipital lobes are marked red, orange, yellow, green, and blue, respectively. NBS, network-based statistical; nBR, behavioral reserve for negative symptoms; Lt., left; Rt., right; FP, frontal pole; FO, frontal operculum cortex; PaCiG, paracingulate gyrus; AC, cingulate gyrus, anterior division; GP, globus pallidus; IFG oper, inferior frontal gyrus pars opercularis; INS, insular cortex; aPaHC, parahippocampal gyrus; OP, occipital pole.

dorsolateral prefrontal cortex, anterior cingulate, and putamen in FTD (Zamboni et al., 2008); attention is associated with the ventral prefrontal cortex in the attention-deficit/hyperactivity disorder (Durston et al., 2006); insights are associated with the orbitofrontal cortex and the frontal pole in the AD and FTD (Hornberger et al., 2014); and semantic performance is associated with the anterior temporal cortex in FTD (Williams et al., 2005).

The nBR marker was associated with the left frontal lobe, left precuneus, left cingulate, left middle and inferior temporal, left banks superior temporal, left supramarginal, and left inferior parietal cortical thicknesses. These areas overlapped with the previously reported areas associated with negative symptoms and further correlated with the default mode network (DMN). The DMN is divided into the ventral and dorsal medial prefrontal cortices (mPFCs), posterior cingulate, and precuneus (Raichle, 2015). The ventral mPFC is related to a personality change, emotional response, and mood control (Damasio, 1996; Bechara et al., 1997; Simpson et al., 2001). The dorsal mPFC is related to the regulation of emotional behavior and judgment of another person's emotional state (Ochsner et al., 2004a,b).

Given that the negative symptoms of the FBI score are apathy, emotional flatness, inflexibility, personal neglect, and loss of insight, the results of these previous studies are in line with our results. The behavioral scores in those with lesser neuroimaging abnormalities were similar between the FA maps and cortical thickness analysis. Furthermore, as the FA value decreased, the corresponding decline in the behavioral score did not differ between the high and low BR groups. In FTD, structural connectivity is known to degrade prior to cortical atrophy (Gordon et al., 2016). Thus, nBR is more closely related to the GM. In addition, the BR, similar to other reserves, can be understood by two mechanisms: neural reserve and neural compensation (Stern, 2012). Neural reserve is a pre-existing brain network with a greater capacity to cope with a neuropathological burden; on the other hand, neural compensation is a brain network newly developed to compensate for the disruption of the pre-existing brain network due to the disease pathology. However, it remains unclear whether increased brain networks related to nBR in bvFTD are mainly associated with the capacity of neural reserve or neural compensation. From this hypothesis's perspective, it can be interpreted that the GM of the high nBR group tolerated neurodegeneration better than the GM of the low nBR group (neural reserve mechanism). It can also be interpreted that compared to in the low nBR group, the WM in the high nBR group is better adapted to neurodegeneration by developing the compensation neural network identified in NBS analysis (neural compensation mechanism).

In addition, we also identified an nBR-related brain network (high nBR > low nBR) composed of the anterior cingulate gyrus, paracingulate gyri, left frontal operculum cortex, left occipital pole, right pallidum, right insular cortex, left parahippocampus, and right inferior frontal gyrus (pars opercularis). The anterior cingulate gyrus and the anterior insular cortices are a part of the salience network, and the paracingulate gyri, frontal operculum cortex, and pars opercularis of the inferior frontal gyrus are adjacent to the anterior cingulate and anterior insula. In bvFTD, salience network disruption is correlated with the clinical severity (Zhou et al., 2010; Day et al., 2013). Furthermore, the paracingulate gyri and the frontal pole were correlated with the recall performance in bvFTD. The functional connectivity

between the occipital pole and the parahippocampus may be related to language ability in the FBI's negative items.

Our study has several limitations. First, bvFTD has several genetic causes. Genetic perspectives include *C9orf72*, *MAPR*, and *GRN* genes, while proteinopathy includes the tau and TDP-43 proteins. However, we used a clinical diagnosis instead of a pathological or genetic-based diagnosis. Second, the neuropathological burden was calculated indirectly from MRI and did not include cellular or molecular data. Nevertheless, we used GM and WM to reflect the neuropathological burden as accurately as possible. Third, the estimated nBR using the residual approach could vary depending on which variables were used (Pettigrew and Soldan, 2019). Although we considered all available variables (age, sex, cortical thickness, and the mean FA values) and outcome measures (FBI score) in the model, we need to validate the nBR using another biomarker or outcome measure in the future. Finally, we could only suggest the effect of the interaction between nBR markers and neuroimaging abnormalities on the behavioral score of negative symptoms in this cross-sectional study. Hence, a longitudinal study would help confirm whether greater nBR would delay the decline of behavioral score or disease progression.

In conclusion, we propose a novel concept of BR in bvFTD, which is associated with the individual's capacity against its neuropathological burden, especially for negative symptoms. The nBR marker-related GM areas and the functional brain networks were also found centered at the frontotemporal areas. Participants with a greater nBR marker would show lesser clinical manifestations of the same neuropathological burden. These findings can be used to predict the clinical progression of each individual with bvFTD, thus enabling physicians to provide appropriate interventions when available.

DATA AVAILABILITY STATEMENT

The raw data supporting the conclusions of this article will be made available by the authors, without undue reservation.

ETHICS STATEMENT

The studies involving human participants were reviewed and approved by the Institutional Review Board of the Samsung Medical Center. The patients/participants provided their written informed consent to participate in this study.

AUTHOR CONTRIBUTIONS

SHK performed the statistical analyses. SHK, JHP, and YJ performed the study design. BHL and SWS performed the data collection. SHK, BHL, SWS, and YJ performed the drafting of the manuscript. SHK, YJK, and PL performed the imaging data processing and analysis. All authors contributed to the article and approved the submitted version.

FUNDING

This work was supported by the Basic Research Lab (BRL) Program (NRF-2020R1A4A1018714), funded by the Korean Government (MSIP) through the National Research Foundation (NRF), as well as by the 2022 Smart project of the KAIST-KU Joint Research Center, KAIST.

SUPPLEMENTARY MATERIAL

The Supplementary Material for this article can be found online at: https://www.frontiersin.org/articles/10.3389/fnagi.2022.875589/full#supplementary-material

Supplementary Figure 1 | Relationship between the behavior reserve marker for negative symptoms (nBR marker) and occupation complexity. Scatterplots showing relationship between nBR marker and occupational complexity. nBR markers were not significantly correlated with **(A)** complexity of data ($R = -0.013$, $p = 0.982$), **(B)** complexity of people ($R = 0.115$, $p = 0.779$), and **(C)** complexity of things ($R = -0.796$, $p = 0.118$).

REFERENCES

Bang, J., Spina, S., and Miller, B. L. (2015). Frontotemporal dementia. *Lancet* 386, 1672–1682.

Barulli, D., and Stern, Y. (2013). Efficiency, capacity, compensation, maintenance, plasticity: emerging concepts in cognitive reserve. *Trends Cogn. Sci.* 17, 502–509. doi: 10.1016/j.tics.2013.08.012

Bechara, A., Damasio, H., Tranel, D., and Damasio, A. R. (1997). Deciding advantageously before knowing the advantageous strategy. *Science* 275, 1293–1295.

Benussi, A., Ashton, N. J., Karikari, T. K., Alberici, A., Saraceno, C., Ghidoni, R., et al. (2021). Prodromal frontotemporal dementia: clinical features and predictors of progression. *Alzheimers Res. Ther.* 13:188. doi: 10.1186/s13195-021-00932-2

Beyer, L., Meyer-Wilmes, J., Schonecker, S., Schnabel, J., Sauerbeck, J., Scheifele, M., et al. (2021). Cognitive reserve hypothesis in frontotemporal dementia: a FDG-PET study. *Neuroimage Clin.* 29:102535. doi: 10.1016/j.nicl.2020.102535

Borroni, B., Grassi, M., Premi, E., Gazzina, S., Alberici, A., Cosseddu, M., et al. (2012). Neuroanatomical correlates of behavioural phenotypes in behavioural variant of frontotemporal dementia. *Behav. Brain Res.* 235, 124–129. doi: 10.1016/j.bbr.2012.08.003

Chung, S. J., Kim, H. R., Jung, J. H., Lee, P. H., Jeong, Y., and Sohn, Y. H. (2020a). Identifying the functional brain network of motor reserve in early parkinson's Disease. *Mov. Disord.* 35, 577–586. doi: 10.1002/mds.28012

Chung, S. J., Lee, J. J., Lee, P. H., and Sohn, Y. H. (2020b). Emerging concepts of motor reserve in parkinson's Disease. *J Mov. Disord.* 13, 171–184. doi: 10.14802/jmd.20029

Damasio, A. R. (1996). The somatic marker hypothesis and the possible functions of the prefrontal cortex. *Philos. Trans. R Soc. Lond. B Biol. Sci.* 351, 1413–1420. doi: 10.1098/rstb.1996.0125

Day, G. S., Farb, N. A., Tang-Wai, D. F., Masellis, M., Black, S. E., Freedman, M., et al. (2013). Salience network resting-state activity: prediction of frontotemporal dementia progression. *JAMA Neurol.* 70, 1249–1253. doi: 10.1001/jamaneurol.2013.3258

Desikan, R. S., Segonne, F., Fischl, B., Quinn, B. T., Dickerson, B. C., Blacker, D., et al. (2006). An automated labeling system for subdividing the human cerebral cortex on MRI scans into gyral based regions of interest. *Neuroimage* 31, 968–980. doi: 10.1016/j.neuroimage.2006.01.021

Du, A. T., Schuff, N., Kramer, J. H., Rosen, H. J., Gorno-Tempini, M. L., Rankin, K., et al. (2007). Different regional patterns of cortical thinning in Alzheimer's Disease and frontotemporal dementia. *Brain* 130, 1159–1166. doi: 10.1093/brain/awm016

Durston, S., Mulder, M., Casey, B. J., Ziermans, T., and Van Engeland, H. (2006). Activation in ventral prefrontal cortex is sensitive to genetic vulnerability for attention-deficit hyperactivity disorder. *Biol. Psychiatry* 60, 1062–1070. doi: 10.1016/j.biopsych.2005.12.020

Frazier, J. A., Chiu, S., Breeze, J. L., Makris, N., Lange, N., Kennedy, D. N., et al. (2005). Structural brain magnetic resonance imaging of limbic and thalamic volumes in pediatric bipolar disorder. *Am. J. Psychiatry* 162, 1256–1265. doi: 10.1176/appi.ajp.162.7.1256

Goldstein, J. M., Seidman, L. J., Makris, N., Ahern, T., O'brien, L. M., Caviness, V. S. Jr., et al. (2007). Hypothalamic abnormalities in schizophrenia: sex effects and genetic vulnerability. *Biol. Psychiatry* 61, 935–945. doi: 10.1016/j.biopsych.2006.06.027

Gordon, E., Rohrer, J. D., and Fox, N. C. (2016). Advances in neuroimaging in frontotemporal dementia. *J. Neurochem.* 138(Suppl. 1), 193–210. doi: 10.1111/jnc.13656

Hornberger, M., Yew, B., Gilardoni, S., Mioshi, E., Gleichgerrcht, E., Manes, F., et al. (2014). Ventromedial-frontopolar prefrontal cortex atrophy correlates with insight loss in frontotemporal dementia and Alzheimer's Disease. *Hum. Brain Mapp.* 35, 616–626. doi: 10.1002/hbm.22200

Katzman, R., Terry, R., Deteresa, R., Brown, T., Davies, P., Fuld, P., et al. (1988). Clinical, pathological, and neurochemical changes in dementia: a subgroup with preserved mental status and numerous neocortical plaques. *Ann. Neurol.* 23, 138–144. doi: 10.1002/ana.410230206

Kertesz, A., Davidson, W., and Fox, H. (1997). Frontal behavioral inventory: diagnostic criteria for frontal lobe dementia. *Can. J. Neurol. Sci.* 24, 29–36. doi: 10.1017/s0317167100021053

Kertesz, A., Nadkarni, N., Davidson, W., and Thomas, A. W. (2000). The frontal behavioral inventory in the differential diagnosis of frontotemporal dementia. *J. Int. Neuropsychol. Soc.* 6, 460–468. doi: 10.1017/s1355617700644041

Kleinbaum, D. G., Kupper, L. L., Nizam, A., and Rosenberg, E. S. (2013). *Applied Regression Analysis and other Multivariable Methods*. Boston, MA: Cengage Learning.

Lee, D. H., Lee, P., Seo, S. W., Roh, J. H., Oh, M., Oh, J. S., et al. (2019). Neural substrates of cognitive reserve in Alzheimer's Disease spectrum and normal aging. *Neuroimage* 186, 690–702. doi: 10.1016/j.neuroimage.2018.11.053

Maiovis, P., Ioannidis, P., Gerasimou, G., Gotzamani-Psarrakou, A., and Karacostas, D. (2018). Cognitive reserve hypothesis in frontotemporal dementia: evidence from a brain SPECT study in a series of Greek frontotemporal dementia patients. *Neurodegener. Dis.* 18, 69–73. doi: 10.1159/000486621

Makris, N., Goldstein, J. M., Kennedy, D., Hodge, S. M., Caviness, V. S., Faraone, S. V., et al. (2006). Decreased volume of left and total anterior insular lobule in schizophrenia. *Schizophr. Res.* 83, 155–171.

Milan, G., Lamenza, F., Iavarone, A., Galeone, F., Lore, E., De Falco, C., et al. (2008). Frontal behavioural inventory in the differential diagnosis of dementia. *Acta Neurol. Scand.* 117, 260–265. doi: 10.1111/j.1600-0404.2007.00934.x

Ochsner, K. N., Knierim, K., Ludlow, D. H., Hanelin, J., Ramachandran, T., Glover, G., et al. (2004a). Reflecting upon feelings: an fMRI study of neural systems supporting the attribution of emotion to self and other. *J. Cogn. Neurosci.* 16, 1746–1772. doi: 10.1162/0898929042947829

Ochsner, K. N., Ray, R. D., Cooper, J. C., Robertson, E. R., Chopra, S., Gabrieli, J. D., et al. (2004b). For better or for worse: neural systems supporting the cognitive down- and up-regulation of negative emotion. *Neuroimage* 23, 483–499.

Pan, P. L., Song, W., Yang, J., Huang, R., Chen, K., Gong, Q. Y., et al. (2012). Gray matter atrophy in behavioral variant frontotemporal dementia: a meta-analysis of voxel-based morphometry studies. *Dement. Geriatr. Cogn. Disord.* 33, 141–148. doi: 10.1159/000338176

Pettigrew, C., and Soldan, A. (2019). Defining cognitive reserve and implications for cognitive aging. *Curr. Neurol. Neurosci. Rep.* 19:1. doi: 10.1007/s11910-019-0917-z

Placek, K., Massimo, L., Olm, C., Ternes, K., Firn, K., Van Deerlin, V., et al. (2016). Cognitive reserve in frontotemporal degeneration: neuroanatomic and neuropsychological evidence. *Neurology* 87, 1813–1819.

Premi, E., Garibotto, V., Gazzina, S., Grassi, M., Cosseddu, M., Paghera, B., et al. (2013). Beyond cognitive reserve: behavioural reserve hypothesis in frontotemporal dementia. *Behav. Brain Res.* 245, 58–62. doi: 10.1016/j.bbr.2013.01.030

Raichle, M. E. (2015). The brain's default mode network. *Annu. Rev. Neurosci.* 38, 433–447.

Rascovsky, K., Hodges, J. R., Knopman, D., Mendez, M. F., Kramer, J. H., Neuhaus, J., et al. (2011). Sensitivity of revised diagnostic criteria for the behavioural variant of frontotemporal dementia. *Brain* 134, 2456–2477. doi: 10.1093/brain/awr179

Rohrer, J. D., Guerreiro, R., Vandrovcova, J., Uphill, J., Reiman, D., Beck, J., et al. (2009). The heritability and genetics of frontotemporal lobar degeneration. *Neurology* 73, 1451–1456. doi: 10.1212/WNL.0b013e3181bf997a

Simpson, J. R. Jr., Snyder, A. Z., Gusnard, D. A., and Raichle, M. E. (2001). Emotion-induced changes in human medial prefrontal cortex: I. During cognitive task performance. *Proc. Natl. Acad. Sci. U.S.A* 98, 683–687. doi: 10.1073/pnas.98.2.683

Smith, S. M., Jenkinson, M., Johansen-Berg, H., Rueckert, D., Nichols, T. E., Mackay, C. E., et al. (2006). Tract-based spatial statistics: voxelwise analysis of multi-subject diffusion data. *Neuroimage* 31, 1487–1505.

Smith, S. M., and Nichols, T. E. (2009). Threshold-free cluster enhancement: addressing problems of smoothing, threshold dependence and localisation in cluster inference. *Neuroimage* 44, 83–98. doi: 10.1016/j.neuroimage.2008.03.061

Stern, Y. (2012). Cognitive reserve in ageing and Alzheimer's Disease. *Lancet Neurol.* 11, 1006–1012.

United States Department of Labor and United States Employment Service and Center (2006). *Dictionary of Occupational Titles (DOT): Revised Fourth Edition, 1991*. United States Department of Labor Washington, D.C. [distributor].

van Loenhoud, A. C., Wink, A. M., Groot, C., Verfaillie, S. C. J., Twisk, J., Barkhof, F., et al. (2017). A neuroimaging approach to capture cognitive reserve: application to Alzheimer's Disease. *Hum. Brain Mapp.* 38, 4703–4715. doi: 10.1002/hbm.23695

Williams, G. B., Nestor, P. J., and Hodges, J. R. (2005). Neural correlates of semantic and behavioural deficits in frontotemporal dementia. *Neuroimage* 24, 1042–1051. doi: 10.1016/j.neuroimage.2004.10.023

Xia, M., Wang, J., and He, Y. (2013). BrainNet viewer: a network visualization tool for human brain connectomics. *PLoS One* 8:e68910. doi: 10.1371/journal.pone.0068910

Zalesky, A., Fornito, A., and Bullmore, E. T. (2010). Network-based statistic: identifying differences in brain networks. *Neuroimage* 53, 1197–1207. doi: 10.1016/j.neuroimage.2010.06.041

Zamboni, G., Huey, E. D., Krueger, F., Nichelli, P. F., and Grafman, J. (2008). Apathy and disinhibition in frontotemporal dementia: insights into their neural correlates. *Neurology* 71, 736–742. doi: 10.1212/01.wnl.0000324920.96835.95

Zhang, Y., Schuff, N., Du, A. T., Rosen, H. J., Kramer, J. H., Gorno-Tempini, M. L., et al. (2009). White matter damage in frontotemporal dementia and Alzheimer's Disease measured by diffusion MRI. *Brain* 132, 2579–2592. doi: 10.1093/brain/awp071

Zhou, J., Greicius, M. D., Gennatas, E. D., Growdon, M. E., Jang, J. Y., Rabinovici, G. D., et al. (2010). Divergent network connectivity changes in behavioural variant frontotemporal dementia and Alzheimer's Disease. *Brain* 133, 1352–1367. doi: 10.1093/brain/awq075

Conflict of Interest: The authors declare that the research was conducted in the absence of any commercial or financial relationships that could be construed as a potential conflict of interest.

Publisher's Note: All claims expressed in this article are solely those of the authors and do not necessarily represent those of their affiliated organizations, or those of the publisher, the editors and the reviewers. Any product that may be evaluated in this article, or claim that may be made by its manufacturer, is not guaranteed or endorsed by the publisher.

frontiers | Frontiers in Aging Neuroscience

ORIGINAL RESEARCH
published: 24 June 2022
doi: 10.3389/fnagi.2022.817137

Functional Connectivity Dynamics Altered of the Resting Brain in Subjective Cognitive Decline

Yi-Chia Wei[1,2,3], *Yi-Chia Kung*[1], *Wen-Yi Huang*[2,3,4], *Chemin Lin*[2,4,5], *Yao-Liang Chen*[6,7], *Chih-Ken Chen*[2,4,5], *Yu-Chiau Shyu*[2,8] *and Ching-Po Lin*[1]*

[1] *Institute of Neuroscience, National Yang Ming Chiao Tung University, Taipei, Taiwan,* [2] *Community Medicine Research Center, Chang Gung Memorial Hospital, Keelung, Taiwan,* [3] *Department of Neurology, Chang Gung Memorial Hospital, Keelung, Taiwan,* [4] *College of Medicine, Chang Gung University, Taoyuan, Taiwan,* [5] *Department of Psychiatry, Chang Gung Memorial Hospital, Keelung, Taiwan,* [6] *Department of Medical Imaging and Radiological Sciences, Chang Gung University, Taoyuan, Taiwan,* [7] *Department of Radiology, Chang Gung Memorial Hospital, Keelung, Taiwan,* [8] *Department of Nursing, Chang Gung University of Science and Technology, Taoyuan, Taiwan*

Background: Subjective cognitive decline (SCD) appears in the preclinical stage of the Alzheimer's disease continuum. In this stage, dynamic features are more sensitive than static features to reflect early subtle changes in functional brain connectivity. Therefore, we studied local and extended dynamic connectivity of the resting brain of people with SCD to determine their intrinsic brain changes.

Methods: We enrolled cognitively normal older adults from the communities and divided them into SCD and normal control (NC) groups. We used mean dynamic amplitude of low-frequency fluctuation (mdALFF) to evaluate region of interest (ROI)-wise local dynamic connectivity of resting-state functional MRI. The dynamic functional connectivity (dFC) between ROIs was tested by whole-brain-based statistics.

Results: When comparing SCD ($N = 40$) with NC ($N = 45$), $mdALFF_{mean}$ decreased at right inferior parietal lobule (IPL) of the frontoparietal network (FPN). Still, it increased at the right middle temporal gyrus (MTG) of the ventral attention network (VAN) and right calcarine of the visual network (VIS). Also, the $mdALFF_{var}$ (variance) increased at the left superior temporal gyrus of AUD, right MTG of VAN, right globus pallidum of the cingulo-opercular network (CON), and right lingual gyrus of VIS. Furthermore, $mdALFF_{mean}$ at right IPL of FPN are correlated negatively with subjective complaints and positively with objective cognitive performance. In the dFC seeded from the ROIs with local mdALFF group differences, SCD showed a generally lower dFC_{mean} and higher dFC_{var} (variance) to other regions of the brain. These weakened and unstable functional connectivity appeared among FPN, CON, the default mode network, and the salience network, the large-scale networks of the triple network model for organizing neural resource allocations.

Conclusion: The local dynamic connectivity of SCD decreased in brain regions of cognitive executive control. Meanwhile, compensatory visual efforts and bottom-up attention rose. Mixed decrease and compensatory increase of dynamics of intrinsic brain activity suggest the transitional nature of SCD. The FPN local dynamics balance

OPEN ACCESS

Edited by:
P. Hemachandra Reddy, Texas Tech University Health Sciences Center, United States

Reviewed by:
Bing Zhang, Nanjing Drum Tower Hospital, China
Stavros I. Dimitriadis, Greek Association of Alzheimer's Disease and Related Disorders, Greece

***Correspondence:**
Ching-Po Lin
chingpolin@gmail.com

Specialty section:
This article was submitted to Neurocognitive Aging and Behavior, a section of the journal Frontiers in Aging Neuroscience

Received: *17 November 2021*
Accepted: *19 May 2022*
Published: *24 June 2022*

Citation:
Wei Y-C, Kung Y-C, Huang W-Y, Lin C, Chen Y-L, Chen C-K, Shyu Y-C and Lin C-P (2022) Functional Connectivity Dynamics Altered of the Resting Brain in Subjective Cognitive Decline. Front. Aging Neurosci. 14:817137. doi: 10.3389/fnagi.2022.817137

subjective and objective cognition and maintain cognitive preservation in preclinical dementia. Aberrant triple network model features the dFC alternations of SCD. Finally, the right lateralization phenomenon emerged early in the dementia continuum and affected local dynamic connectivity.

Keywords: subjective cognitive decline (SCD), preclinical dementia, resting state functional MRI, dynamic functional connectivity, mdALFF, dynamics

INTRODUCTION

Subjective cognitive decline (SCD) refers to individuals' perceived decline in memory or other cognitive abilities relative to their previous level of performance in the absence of objective neuropsychological deficits (Jessen et al., 2014). SCD is considered a deviation from normal aging and representative for the late preclinical stage of Alzheimer's disease (AD) (Sperling et al., 2011). Cognitive changes in SCD are characterized by subtle cognitive decline and compensatory cognitive efforts (Jessen et al., 2014).

Magnetic resonance imaging (MRI) is an essential noninvasive tool in cognitive neuroscience. Functional MRI (fMRI) detects blood oxygenation level-dependent (BOLD) signals to reflect neuronal activities in the human brain (Grady, 2012). In addition, resting-state fMRI (rs-fMRI) revealed the intrinsic brain activity of human brain, networks of functional connections, and their relationships with neuropsychiatric diseases (Zhang and Raichle, 2010).

Early Local, Late Global Connectivity Changes in AD Spectrum

In neurodegeneration of the AD continuum, pathological tau deposition is closely related to cognitive performance (Hanseeuw et al., 2019) and is a good tracer of disease progression (Brier et al., 2016). The topological similarity between functional disconnection and tau deposition reflects the pathological functional coupling in AD (Ossenkoppele et al., 2019; Franzmeier et al., 2020). Measuring changes in functional connectivity is a noninvasive approach for understanding pathogenesis of AD neurodegeneration. Along the trajectory of disease progression from preclinical stage to AD, functional connectivity decreases earlier before structural destruction (Jack et al., 2010; Sperling et al., 2011). Therefore, functional disconnection can be measured in SCD, but not yet the gray matter volume reduction (Sun et al., 2016; Dong et al., 2018; Parker et al., 2020). In addition, the functional disconnection develops locally in the early stage (Sun et al., 2016) before the late global disconnection (Liu et al., 2014). For example, in a hierarchical comparison of normal people, SCD, mild cognitive impairment (MCI), and patients with AD, only local functional disconnection developed in SCD, whereas mixed local and global disconnection started in MCI and shifted to fully global compensation in AD (Wang et al., 2019). Therefore, studying local functional connectivity reveals the earliest changes in the brain of preclinical dementia.

Local Functional Activation in SCD

Local functional activation was commonly assessed by recording the spontaneous activity at the resting brain. At first, fluctuations of BOLD signals at 0.01–0.1 Hz were used to describe network features of the resting-state default mode of the brain (Fransson, 2005) and its responses to cognitive tasks (Fransson, 2006). More recently, the combined study of 18F-fluorodeoxyglucose positron emission tomography (FDG-PET) and rs-fMRI found the coupling of glucose metabolism and the amplitude of low-frequency fluctuation (ALFF) of BOLD signals. The two methods are consistent for recording brain activity (Jiao et al., 2019).

Previously, ALFF has been applied to characterize disease-related regional functional changes in the brain, such as those in the elderly with AD (He et al., 2007) and the children with attention deficit hyperactivity disorder (ADHD) (Zang et al., 2007). In SCD, when compared to healthy controls, the distinct local connectivity patterns are increased ALFF values in bilateral inferior parietal lobule (IPL), right inferior occipital gyrus, right middle occipital gyrus, right superior temporal gyrus (STG), and right cerebellar posterior lobe (Sun et al., 2016), as well as decreased ALFF values in the precuneus, anterior cingulate cortex, and cerebellum (Yang et al., 2018). In addition, the patterns of regional ALFF and fractional ALFF (fALFF) distinguished SCD, MCI, and AD from normal people in the machine learning model (accuracy 76–92%) (Yang et al., 2018). Therefore, measuring ALFF is a feasible way to characterize the early brain changes in preclinical dementia.

Why Studying Dynamic Connectivity in SCD

Currently, studies of static functional connectivity (sFC) (Viviano and Damoiseaux, 2020; Wang et al., 2020) are much abundant than that of dynamic functional connectivity (dFC) in SCD (Xie et al., 2019; Dong et al., 2020; Yang et al., 2020; Chen et al., 2021). However, brain activity is context-sensitive and activity-dependent. The intrinsic brain activity is dynamic and fluctuates overtimes. sFC may not show the full picture of the changes in the brain integrated states. In contrast, dFC can be more comprehensive than sFC in characterizing functional features of neurodegeneration. For example, dFC outperformed sFC in classifying AD from controls [area under the receiver operating characteristic curve (AUROC) 0.82 for sFC matrices and 0.84 for dFC] (de Vos et al., 2018).

In addition, dFC provides complementary information to sFC, such as in aging-related functional connectivity changes. The dFC studies of rs-fMRI showed posterior-attenuated and anterior-enhanced local hub dynamics in aging people (Zhang

et al., 2017), echoing the posterior–anterior shift in aging (PASA) model that describes asymmetric changes in aging brains by posteriorly-decreased and anteriorly-increased BOLD signals in tasks fMRI (Davis et al., 2008). However, the directions of the linear gradients were opposite for sFC and dFC, suggesting that sFC and dFC provided complementary information of intrinsic brain activity alterations in the aging brains (Zhang et al., 2017).

Because the cognitive decline of SCD is subtle and studying the dynamics of functional connectivity reveals more details of the early neurodegeneration, we compared the local dynamic connectivity in rs-fMRI between SCD and normal healthy control by the mean dynamic amplitude of low-frequency fluctuation (mdALFF). We also looked for their outward dFC to seek emerging alterations of the intrinsic brain function of preclinical dementia.

METHODS

Definition of Grouping

Subjective cognitive decline was defined by the two criteria of the Subjective Cognitive Decline Initiative Working Group: (1) self-experience of a persistent decline of cognitive capacity when compared to a previously normal cognitive status, and the change did not correlate with any acute event, and (2) the performance of standardized cognitive tests met the expected levels (Molinuevo et al., 2017). In our study setting, grouping to SCD required: (1) having SCCs, defined by a self-reported AD8 score $\geq$2 points (Galvin et al., 2005; Yang et al., 2011; Wei et al., 2019), and (2) normal cognition, defined by a MoCA score higher than the score of age- and education-matched means minus one standard deviation (Rossetti et al., 2011). In contrast, the normal control (NC) group included the cognitively normal participants without SCCs by an AD8 score of 0–2.

Measurements

AD8 is a brief measure by 8 questions to detect cognitive impairment regarding the daily cognitive abilities of judgment, interest, repeats, appliances, orientation, finance management, appointment remembering, and the consistency of cognitive changes. Endorsement of a change to each cognitive problem in the last several years scores 1 point. A total score equal to or over 2 points represents having subjective cognitive complaints (SCCs) (Galvin et al., 2005, 2006). The original English version of the AD8 questionnaire was created by Galvin et al. in 2005 (Galvin et al., 2005) and can be applied in informant-based (Galvin et al., 2006) or self-report manners (Galvin et al., 2007). We used the Traditional Chinese version of the AD8 questionnaire, which was well validated (Yang et al., 2011). Because self-endorsed decline usually occurs earlier than informant confirmed decline (Caselli et al., 2014), we applied AD8 in a self-report manner for detecting SCCs (Wei et al., 2019, 2021).

The Montreal Cognitive Assessment (MoCA) score determined their objective cognitive performance. Impairment of cognitive performance was defined by a MoCA score lower than one standard deviation below the mean of age- and education-adjusted norms (Rossetti et al., 2011). The other cognitive tests in this study included the Mini-Mental State Examination (MMSE) (Shyu and Yip, 2001), digit symbol coding (DSC), digit span test (DST), letter-number sequencing (LNS), category fluency (CF), and facial memory test (FMT). We also use the Hospital Anxiety and Depression Scale (HADS), which contained anxiety subscale (HADS-A) and depression subscales (HADS-D), for evaluating anxiety and depression tendency (Bjelland et al., 2002).

Participant Enrollment

This work was a part of the Northeastern Taiwan Community Medicine Research Cohort (NTCMRC; identifier on ClinicalTrials.gov: NCT04839796) conducted by the Community Medicine Research Center of the Chang Gung Memorial Hospital in Keelung, Taiwan. The cohort was launched in Northeastern Taiwan in 2012 and started cognitive and brain imaging recording in 2018. The Institutional Review Board of Chang Gung Memorial Hospital approved this study (approval no. 201600580B0, 201600270B0, 201600269B0, 201901350B0, 201901353B0, 201901352B0, and 200600269B0). All the participants signed informed consent before entering this study.

During 2018–2020, we enrolled healthy, right-handed, older adults aged over 50 years. Participants with major organ failure, including heart failure, renal failure, moderate-to-severe liver disease, and active thyroid diseases, were not recruited. In the initial screening, we excluded the participants who fulfilled the criteria of MCI (Petersen et al., 1999; Winblad et al., 2004) or dementia (Mckhann et al., 2011) or had other brain disorders, including stroke, epilepsy, brain tumor, traumatic brain injury, and developmental neurological diseases. Through the Mini-International Neuropsychiatric Interview (Lecrubier et al., 1997), we further excluded those participants with psychiatric disorders. Brain structural MRI screened the structural lesion(s) and excluded those participants before going through the rs-fMRI analysis.

From 136 community-dwelling healthy older adults, we excluded 29 participants for current or history of major depressive disorder, 3 participants who met the criteria of MCI, 9 participants for brain lesions in the structural MRI, and the other 10 for motion found in fMRI image preprocessing. Then, having or not of SCCs divided these 85 cognitively normal healthy older adults into SCD group ($N = 40$) and NC group ($N = 45$) (**Figure 1**).

The 85 enrolled participants had a mean age of 65.47 $\pm$ 5.69 years, a female-to-male ratio of 1.36 (49 women and 36 men), and 10.10 $\pm$ 4.19 years of school education. Between-group comparisons confirmed the equality of age, sex, and education level between SCD and NC (**Table 1**). The SCD group had higher degree of SCCs (AD8 score 4.03 $\pm$ 1.82 vs. 0.18 $\pm$ 0.39, $p < 0.001$) and poorer cognitive performance in MoCA (23.85 $\pm$ 3.29 vs. 26.31 $\pm$ 3.52, $p = 0.001$), LNS ($p = 0.021$), CF of animal ($p = 0.004$), and color ($p = 0.028$) than the NC group. Compared to NC, SCD also had higher tendency of anxiety (HADS-A score 5.40 $\pm$ 3.21 vs. 2.84 $\pm$ 2.84, $p < 0.001$) and depression (HADS-D score 5.45 $\pm$ 3.36 vs. 2.80 $\pm$ 3.29, $p < 0.001$) (**Table 1**).

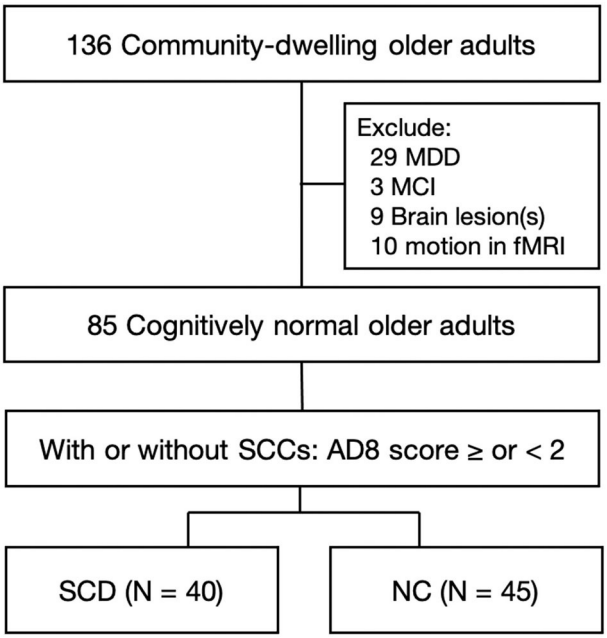

FIGURE 1 | Flow chart of enrollment. Healthy older adults aged over 50 years were enrolled from the communities. Initial screening excluded the participants who had a current state or previous history of MDD, met the criteria of MCI, had brain lesions in structural MRI, or had head motion during fMRI scans. These 85 cognitively normal older adults were further divided into the group of SCD and NC, based on having or not having SCCs by an AD8 score ≥2 or <2 points. MDD, major depressive disorder; MCI, mild cognitive impairment; SCCs, subjective cognitive complaints; SCD, subjective cognitive decline; NC, normal control.

TABLE 1 | Between group comparison.

	SCD ($N = 40$)	NC ($N = 45$)	p-value
Basic information			
Age	64.93 ± 5.65	65.96 ± 5.75	0.408
Sex, female	27 (67.5%)	22 (48.9%)	0.085
Education, year	9.80 ± 4.52	10.38 ± 3.90	0.529
Cognition			
AD8 (0-8)	4.03 ± 1.82	0.18 ± 0.39	<0.001*
MMSE (30-0)	28.13 ± 1.45	28.38 ± 1.81	0.484
MoCA (30-0)	23.85 ± 3.29	26.31 ± 3.52	0.001*
DSC	53.18 ± 17.31	60.31 ± 22.83	0.115
DST-forward	12.18 ± 2.34	12.42 ± 2.24	0.629
DST-backward	6.21 ± 3.12	7.36 ± 2.64	0.071
LNS	8.26 ± 2.55	9.76 ± 3.19	0.021*
CF-animal	16.05 ± 4.81	19.18 ± 4.86	0.004*
CF-fruit	13.26 ± 3.39	14.11 ± 3.02	0.225
CF-color	12.21 ± 4.09	14.33 ± 4.58	0.028*
CF-city	18.23 ± 5.81	20.02 ± 5.64	0.156
FMT	34.03 ± 4.06	35.89 ± 4.80	0.060
Anxiety and depression			
HADS-A (0–21)	5.40 ± 3.21	2.84 ± 2.84	<0.001*
HADS-D (0–21)	5.45 ± 3.36	2.80 ± 3.29	<0.001*

**Statistical significance at $p < 0.05$. Data were given as mean ± standard deviation or n (%). Ranges of the rating scales were annotated from normal to abnormal. Clinical meanings of the rating scale were AD8 for subjective cognitive complaints, MMSE and MoCA for general cognitive assessment, HADS-A for anxiety, and HADS-D for depression. NC, normal control; SCD, subjective cognitive decline; MMSE, Mini-Mental State Examination; MoCA, Montreal Cognitive Assessment; DSC, digit symbol coding; DST, digit span test; LNS, letter-number sequencing; CF, category fluency; FMT, facial memory test; HADS-A, Hospital Anxiety and Depression Scale—Anxiety subscale; HADS-D, Hospital Anxiety and Depression Scale—Depression subscale.*

Image Data Acquisition

Magnetic resonance imaging data were collected using a 3T Siemens Skyra system (Erlangen, Germany) and a 20-channel head-neck coil at Keelung Chang Gung Memorial Hospital. High-resolution T1-weighted anatomical images (3D-MPRAGE with 256 × 256 × 256 matrix size, 1 mm^3 isotropic cube, flip angle (FA) = 8, repeat time (TR) = 2200 ms, echo time (TE) = 2.45 ms, and inverse time = 900 ms) were acquired before the functional scans for localization reference. Customized cushions were used to minimize head motion during each scan. rs-fMRI scans were subsequently acquired using a single-shot, gradient-recalled echo-planar imaging sequence (TR/TE/FA = 2,500 ms/27 ms/90, field of view = 220 mm, matrix size = 64 × 64, 35 slices with 3 mm thickness, 200 measurements) aligned along the anterior commissure-posterior commissure line, thus allowing whole-brain coverage.

Image Preprocessing

All the fMRI data were preprocessed by the analysis of functional neuroImages (AFNI) (Cox, 1996), FMRIB Software Library (FSL) (Smith et al., 2004), and statistical parametric mapping (SPM) (Friston, 2007). The data with excessive motion resulting in translation >2 mm, rotation >2°, and a mean frame displacement exceeding 0.5 mm were excluded. The first 10 volumes were first deleted to ensure that the data were acquired with a steady-state signal. In the preprocessing stage, all the fMRI datasets were subjected to motion correction with the Friston 24-parameter model (Friston et al., 1996), skull-stripping, slice-timing, despiking, and detrending. For the anatomical information, native fMRI images were registered to the native T1-weighted image and segmented into white matter, gray matter, and cerebrospinal fluid. The fMRI datasets were spatially normalized to a standard Montreal Neurological Institute (MNI) template and resampled to an isotropic resolution of 2 × 2 × 2 mm^3. Then, the linear detrending was applied to eliminate any signal drift induced by system instability. Finally, the effects of nuisance regressors, including the six motion parameters, respiration/cardiac pulsations, white matter, and cerebrospinal fluid, were removed from the preprocessed datasets. The preprocessed data were temporally bandpass filtered between 0.01 and 0.1 Hz and then smoothed with a Gaussian kernel (full width at half maximum = 6 mm) to improve the signal-to-noise ratio.

Dynamic Analysis for Functional Metrics

Software and Atlas

The ROI-based dynamic metrics were generated by the DynamicBC toolbox (version 2.2) (Liao et al., 2014), with a

sliding-window approach (window size = 50 TRs, step size = 10 TRs) on the rs-fMRI dataset referencing our previous study (Kung et al., 2019). The window length follows the criterion (Leonardi and Van De Ville, 2015) with adequate sampling; furthermore, it is long enough with stable and reliable results and short enough to detect quick changes. The ROI-based analysis was performed in each window, resulting in multiple time-varying dynamic metrics. The functional metrics were calculated on the 300 ROI parcellation (Seitzman et al., 2020), including cortical, subcortical, and cerebellum structures with 14 predefined resting-state network parcellations. We excluded 27 ROIs belonging to the undefined network and used the 273 ROIs for the following analysis. Meanwhile, the anatomic annotation of the ROIs was obtained by referring to the Automated Anatomical Labeling (AAL) atlas (Tzourio-Mazoyer et al., 2002).

Local Dynamic Connectivity: mdALFF Analysis

We transformed voxel-wise ALFF into ROI-wise dynamic metrics to study local dynamic connectivity and then applied it to predefined functional networks. In detail, (1) we used the fast Fourier transform (FFT) (parameters: taper percent = 0, FFT length = shortest) of the filtered time series as the power spectrum. Then, the ALFF as the average square root of the power spectrum across 0.01–0.08 Hz was calculated for each voxel (Zang et al., 2007). (2) Next, the ALFF map was divided by the global mean of whole-brain ALFF to mean ALFF (mALFF). Then, the values of all the voxels in each ROI were averaged as ROI-wise mALFF. (3) After generating the ROI-wise mALFF map, we combined the sliding-window technique to summarize the mdALFF metrics of whole-brain ROIs. The mean and variance of mALFF across windows were obtained as $mdALFF_{mean}$ and $mdALFF_{var}$, respectively (Liao et al., 2019). (4) Finally, the mdALFF values of the 273 ROIs were aggregated into the predefined functional network (Seitzman et al., 2020).

Extended Dynamic Connectivity: dFC Analysis

Next, we examined the dynamics of inter-regional functional connectivity extended from the regions with significant mdALFF group differences. The ROIs with significant differences of $mdALFF_{mean}$ or $mdALFF_{var}$ between the SCD and NC groups were taken as seeds. The dFC from the seeds was calculated as follows: (1) The BOLD times series of all voxels within each ROI were averaged for calculating the Pearson's correlation coefficients in a pairwise manner of the seed ROI to the whole-brain ROIs. (2) These correlation coefficients, considered the dFC, were transformed into *Z*-scores using Fisher's *Z* formula for statistical analysis. (3) Then, the temporal series of dFC values from each sliding window were averaged and yielded the mean of dFC (dFC_{mean}) and the variance of dFC (dFC_{var}) for each participant.

Statistical Analysis

Comparing mdALFF Between SCD and NC

The group difference of the mean and variance of the mdALFF values between the SCD and NC groups were examined by a generalized linear model with adjustment for age, sex, education, and frame displacement as covariates and *post hoc* analysis with the Tukey's method. Statistical significance was considered at a confidence level of 99.5% by a $p < 0.005$. Next, we used the false discovery rate (FDR) to test the statistical significance in multiple comparisons (Benjamini and Hochberg, 1995). The FDR correction was applied in two ways: first, whole-brain correction based on the 273 ROIs; second, network-based correction using FDR to check multiple comparisons among the ROIs within each functional network. The reason for using network-based correction was that large-scale functional connectivity organizes internally and works together for specific functions, and each network was considered a processing system (Power et al., 2011).

Comparing dFC Between SCD and NC

To compare the difference in dFC between the SCD and NC groups, we used the network-based statistic (NBS) to control the family-wise error rate in identifying group difference for the clusters of connected connections. A *p*-value below 0.05 with 1,000 permutations of original data was considered statistically significant (Zalesky et al., 2010).

Correlation Analysis of mdALFF Values and Clinical Indices

A partial correlation analysis adjusted for age, sex, education, and frame displacement examined the relationship between mdALFF and the clinical variables. The $mdALFF_{mean}$ and $mdALFF_{var}$ were tested for correlations to the scores of AD8, MMSE, MoCA, DSC, DST, CF categories, FMT, HADS-A, and HADS-D using the data from all the participants. A correlation coefficient was considered statistically significant by a *p*-value < 0.05 after FDR corrections for multiple comparisons.

In addition, we tested the mdALFF clinical correlation in separated groups of SCD and NC. The partial correlation coefficients of each group underwent Fisher's Z-transformation and then two-tailed t-tests for group differences. FDR further examined the group comparison of correlation, and an FDR-corrected p-value < 0.05 was defined as statistical significance.

RESULTS

Local Dynamic Connectivity mdALFF

Comparing the local dynamic connectivity between the SCD and NC groups, $mdALFF_{mean}$ decreased at ROI(a) that located in the right IPL and belonged to the frontoparietal network (FPN) ($p = 0.002$). In contrast, we observed an increase of $mdALFF_{mean}$ at ROI(b) in the right middle temporal gyrus (MTG) of the ventral attention network (VAN) ($p < 0.001$) and ROI(c) in the right calcarine fissure and surrounding cortex (CAL) of the visual network (VIS) ($p < 0.001$) (**Figure 2**).

In the SCD group, $mdALFF_{var}$ was higher at ROI(a) in left STG of the auditory network (AUD) ($p < 0.001$), ROI(b) in right lingual gyrus (LING) of VIS ($p = 0.002$), ROI(c) in right MTG of VAN ($p < 0.001$), and ROI(d) in right lenticular nucleus pallidum (PAL) of the cingulo-opercular network (CON) ($p = 0.004$) (**Figure 3**).

In addition to the significant local dynamic connectivity changes, there were some marginal mdALFF group differences. For example, the SCD had marginal $mdALFF_{mean}$ decreases

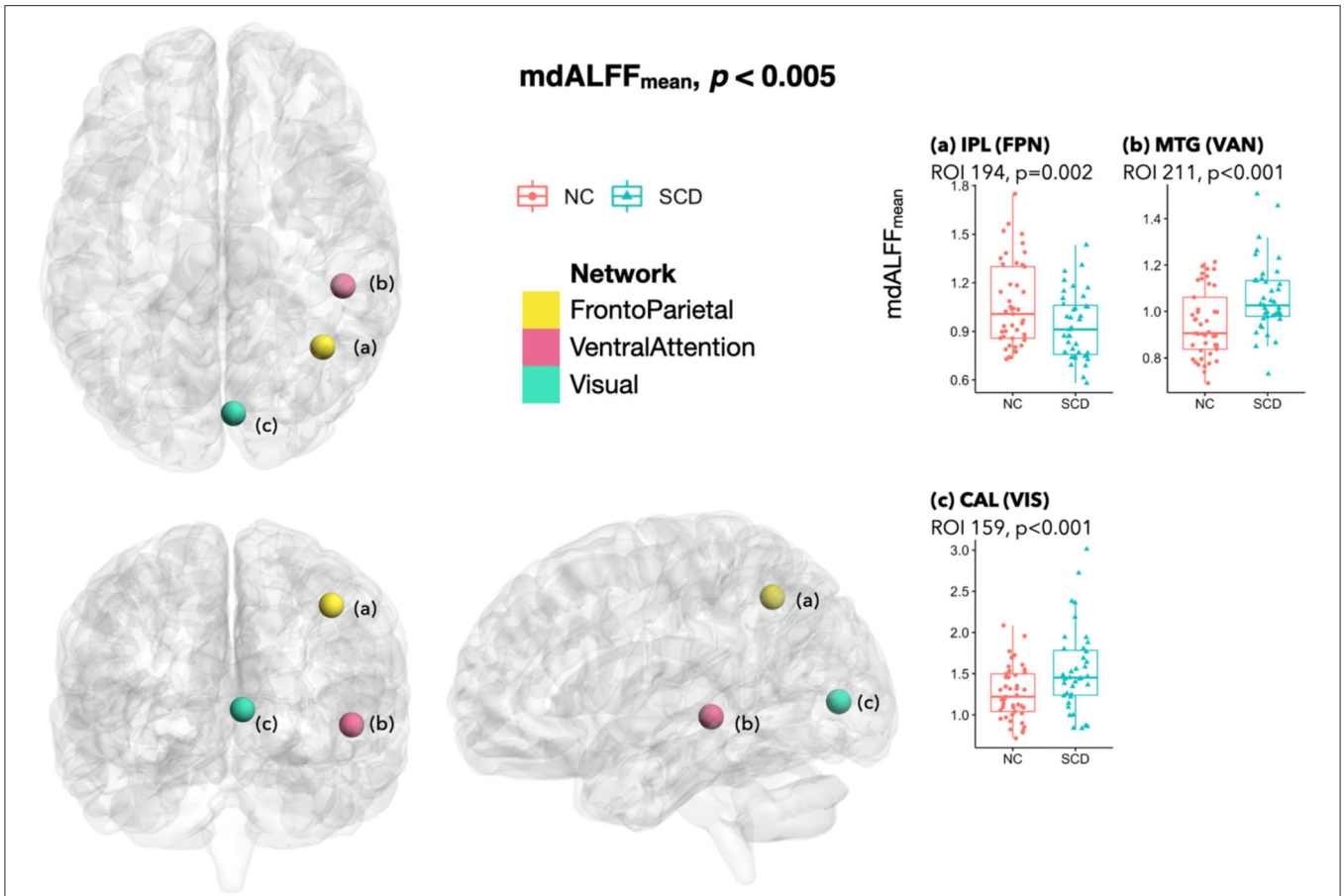

FIGURE 2 | Differences of mdALFF$_{mean}$ between SCD and NC. When comparing the SCD group with the NC group, a significant decrease of mdALFF$_{mean}$ at a $p <$ 0.005 was found at ROI(a) in right IPL of FPN. In contrast, the mdALFF$_{mean}$ increased in ROI(b) in right MTG of VAN and ROI(c) in right CAL of VIS. In addition, a marginal decrease of mdALFF$_{mean}$ was observed at a cFPN ROI in right lobule VI, two cDMN ROIs in left Crus I/II, and a AUD ROI in right Rolandic area (p-value between 0.005–0.01; not shown in the figure). The anatomical location of each ROI was referred to the Automated Anatomical Labeling atlas (Tzourio-Mazoyer et al., 2002), and their functional network attribution was classified by Seitzman et al. (Seitzman et al., 2020). SCD, subjective cognitive decline; NC, normal control; mdALFF$_{mean}$, mean of the mean dynamic amplitude of low-frequency fluctuation; ROI, region of interest; IPL, inferior parietal lobule; FPN, frontoparietal network; MTG, middle temporal gyrus; VAN, ventral attention network; CAL, calcarine fissure and surrounding primary visual cortex; VIS, visual network; cFPN, frontoparietal network in the cerebellar regions; cDMN, default mode network in the cerebellar regions; AUD, auditory network.

than the NC at an ROI of right Rolandic operculum (ROL) that belonged to AUD ($p = 0.006$), an ROI in right lobule VI that belonged to the cerebellar regions of frontoparietal network (cFPN) ($p = 0.008$), and two ROIs in left Crus I/II of the cerebellar regions of default mode network (cDMN) ($p =$ 0.006 and 0.006; not shown in figures). Moreover, mdALFF$_{var}$ marginally increased at a VIS ROI in the right CAL ($p = 0.005$; not shown in figures), but marginally decreased at a cFPN ROI in the left Crus I ($p = 0.006$) in SCD than NC.

The network-based FDR for mdALFF values was significant for mdALFF$_{mean}$ at right MTG of VAN and right CAL of VIS, as well as for mdALFF$_{var}$ at right MTG of VAN and left STG of AUD. The whole-brain ROI-wise FDR was not significant.

Difference of dFC Between SCD and NC

In SCD than NC, the extended dFC from those regions with altered local dynamic connectivity generally showed a lower mean and higher variance of functional connectivity dynamics that indicated weakened and unstable brain activity. Although the between-group NBS did not reach a significant difference, the dFC values between SCD and NC groups showed tendencies of early functional connectivity changes in SCD. To be specific, dFC$_{mean}$ decreased between the ROIs of FPN-cFPN, FPN-the default mode network (DMN), FPN-the salience network (SAL), FPN-the dorsal attention network (DAN), FPN-the reward network (REW), VIS-cFPN, CON-DMN, and CON-SAL ($p <$ 0.005; **Figure 4**). In addition, increased dFC$_{var}$ was found between the ROIs of FPN-DMN, FPN-SAL, VAN-DMN, VIS-VAN, VIS-the somatomotor network (SMN), VIS-FPN, AUD-VIS, AUD-FPN, CON-VIS, within CON, within VIS, and within AUD ($p < 0.005$; **Figure 5**).

Correlations of mdALFF to Clinical Indices

In correlation analysis, AD8 score for the degree of SCCs was negatively correlated with the mdALFF$_{mean}$ in right IPL of FPN ($r = -0.29$), but positively correlated with the mdALFF$_{mean}$ in

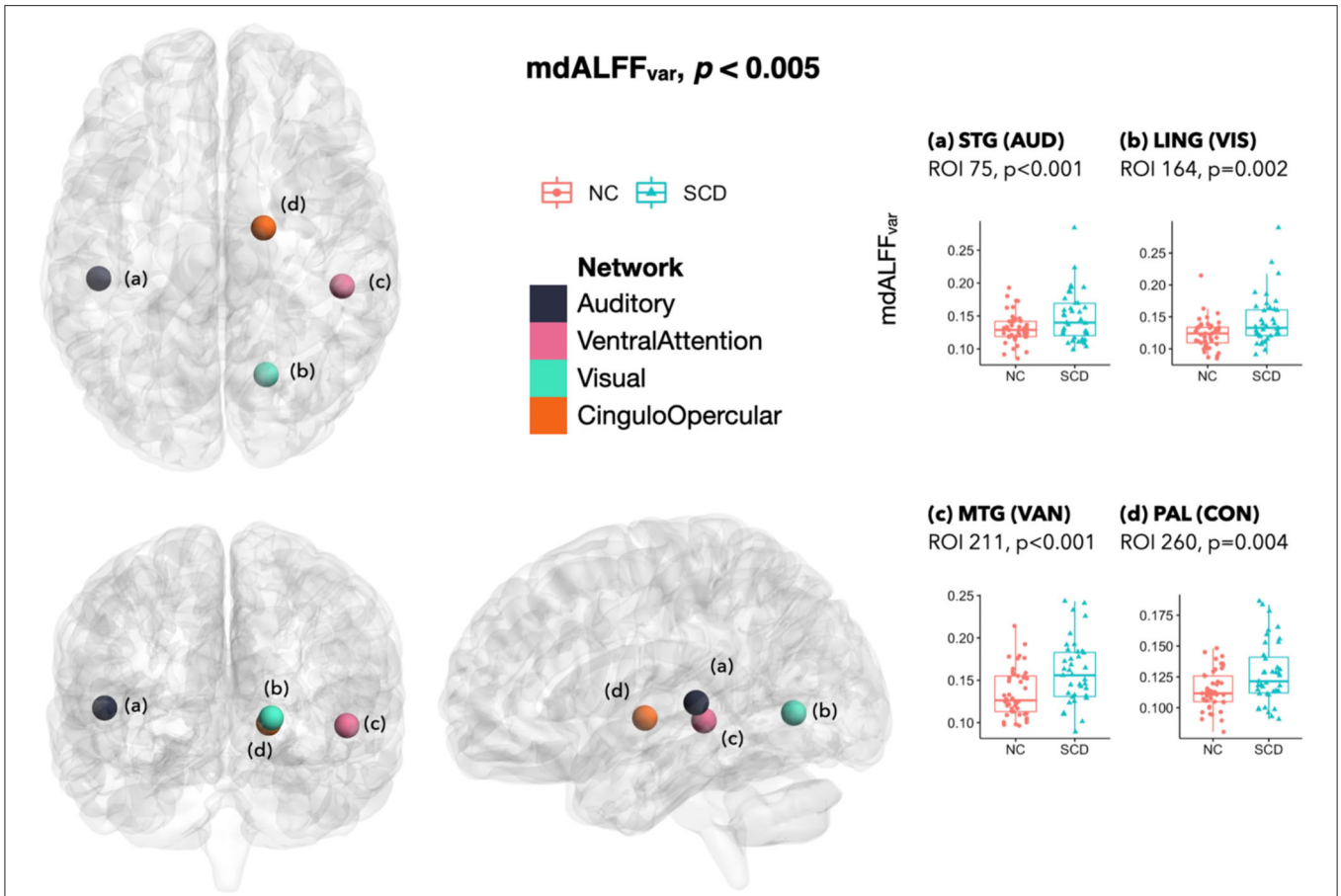

FIGURE 3 | Differences of $mdALFF_{var}$ between SCD and NC. The $mdALFF_{var}$ was higher in SCD than NC at ROI **(A)** in left STG of AUD, ROI **(B)** in right LING of VIS, ROI **(C)** in right MTG of VAN, and ROI **(D)** in right PAL of CON. In the SCD group, marginal changes of $mdALFF_{var}$ included an increase at a VIS ROI in right CAL ($p = 0.005$) and a decrease at a cFPN ROI in left Crus I ($p = 0.006$) (not in the figure). $mdALFF_{var}$, variance of the mean dynamic amplitude of low-frequency fluctuation; SCD, subjective cognitive decline; NC, normal control; ROI, region of interest; STG, superior temporal gyrus; AUD, auditory network; LING, lingual gyrus; VIS, visual network; MTG, middle temporal gyrus; VAN, ventral attention network; PAL, pallidum of lenticular nucleus; CON, cingulo-opercular network; CAL, calcarine fissure and surrounding primary visual cortex; cFPN, frontoparietal network in the cerebellar regions.

right MTG of VAN ($r = 0.30$), and right CAL of VIS ($r = 0.38$). AD8 score was also positively correlated with the $mdALFF_{var}$ in left STG of AUD ($r = 0.51$), right LING of VIS ($r = 0.42$), and right MTG of VAN ($r = 0.32$). Statistical significance was set at $p < 0.05$ after FDR correction (**Table 2**).

For the correlations with cognitive performance, $mdALFF_{mean}$ in right IPL of FPN was correlated positively with MMSE score ($r = 0.29$, FDR-corrected $p < 0.05$) and CF score of fruit category ($r = 0.32$, FDR-corrected $p < 0.05$) (**Table 2**).

In addition, $mdALFF_{var}$ in right MTG of VAN was associated with the degree of anxiety, in terms of HADS-A ($r = 0.33$, FDR-corrected $p < 0.05$) (**Table 2**).

For the group differences of mdALFF-clinical correlation, different trends of correlations between the SCD and NC groups were observed between MMSE score to $mdALFF_{var}$ in right MTG of VAN, CF scores for fruit and city categories to $mdALFF_{var}$ in right PAL of CON, HADS-D scores to $mdALFF_{mean}$ in right IPL of FPN, $mdALFF_{mean}$ in right CAL of VIS, and $mdALFF_{var}$ in left STG of AUD (FDR-corrected $p < 0.05$) (**Table 2**).

DISCUSSION

Summary

This was an rs-fMRI study of local mdALFF and related extension of dFC in community-dwelling cognitively normal older adults, who were divided into the SCD and NC groups for comparisons. In SCD, ROI-based mdALFF local dynamic connectivity analysis showed mixed changes in mean and variance. The ROIs with significant group differences of $mdALFF_{mean}$ and $mdALFF_{var}$ were mainly located in the right cerebral hemisphere. In addition, the alterations of intrinsic brain activity of SCD were toward a regional-specific mixture of deficiency-compensation mechanisms and unstable local dynamics. In detail, local dynamic connectivity became weak in FPN for central executive control and cognitive flexibility. Still, FPN balanced both

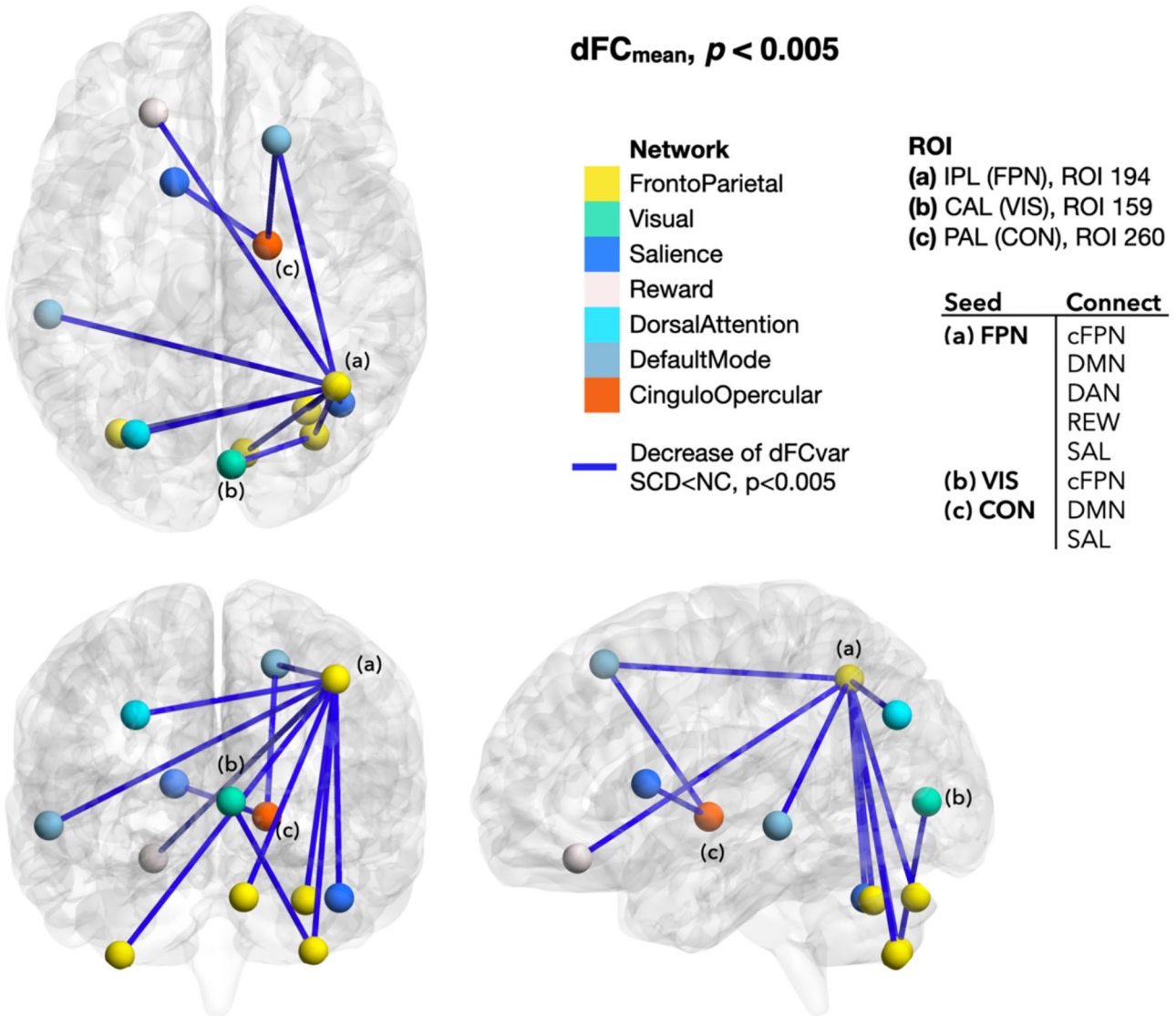

FIGURE 4 | Differences of dFC$_{mean}$ between SCD and NC. The dFC$_{mean}$ seeded from the ROIs with local mdALFF group differences generally decreased in SCD than NC, including the dFC from the FPN ROI to the cFPN, DMN, DAN, REW, and SAL ROIs ($p < 0.005$). Color of line indicated the changes of dFC. Blue was for decrease. Color of ROIs represented the functional network they belonged to. dFC$_{mean}$, mean of the dynamic functional connectivity; SCD, subjective cognitive decline; NC, normal control; ROI, region of interest; IPL, inferior parietal lobule; FPN, frontoparietal network; CAL, calcarine area; VIS, visual network; PAL, pallidum of lenticular nucleus; CON, cingulo-opercular network; cFPN, frontoparietal network in the cerebellar regions; DMN, default mode network; DAN, dorsal attention network; REW, reward network; SAL, salience network.

subjective and objective cognition and had a crucial role in cognitive reserve in preclinical dementia. In contrast, functional compensation of SCD started in visual and attention networks. To sum up, the temporal fluctuations of local BOLD signals explained regional brain changes of SCD, which responded to the subtle cognitive decline and tried to resume the homeostasis of the brain.

The dFC from those ROIs with local dynamic changes also differed between SCD and NC. Those regions with altered mdALFF$_{mean}$ of VIS, FPN, and VAN showed decreased dFC$_{mean}$ and increased dFC$_{var}$ to other brain regions. An increased variance indicated instability and fluctuation of local dynamic connectivity. The CON, VAN, and AUD regions with increased mdALFF$_{var}$ also showed unstable outward connections with an increased dFC$_{var}$. The altered dFC in SCD could result from disconnection and noise signals due to early degeneration or resource relocation to cope with the subtle cognitive decline.

The Cognitive Theories of Aging Help Interpret the Altered Dynamic Connectivity in SCD

The brain's responses to the emerging neurodegeneration and functional deterioration of SCD resembled accelerated aging

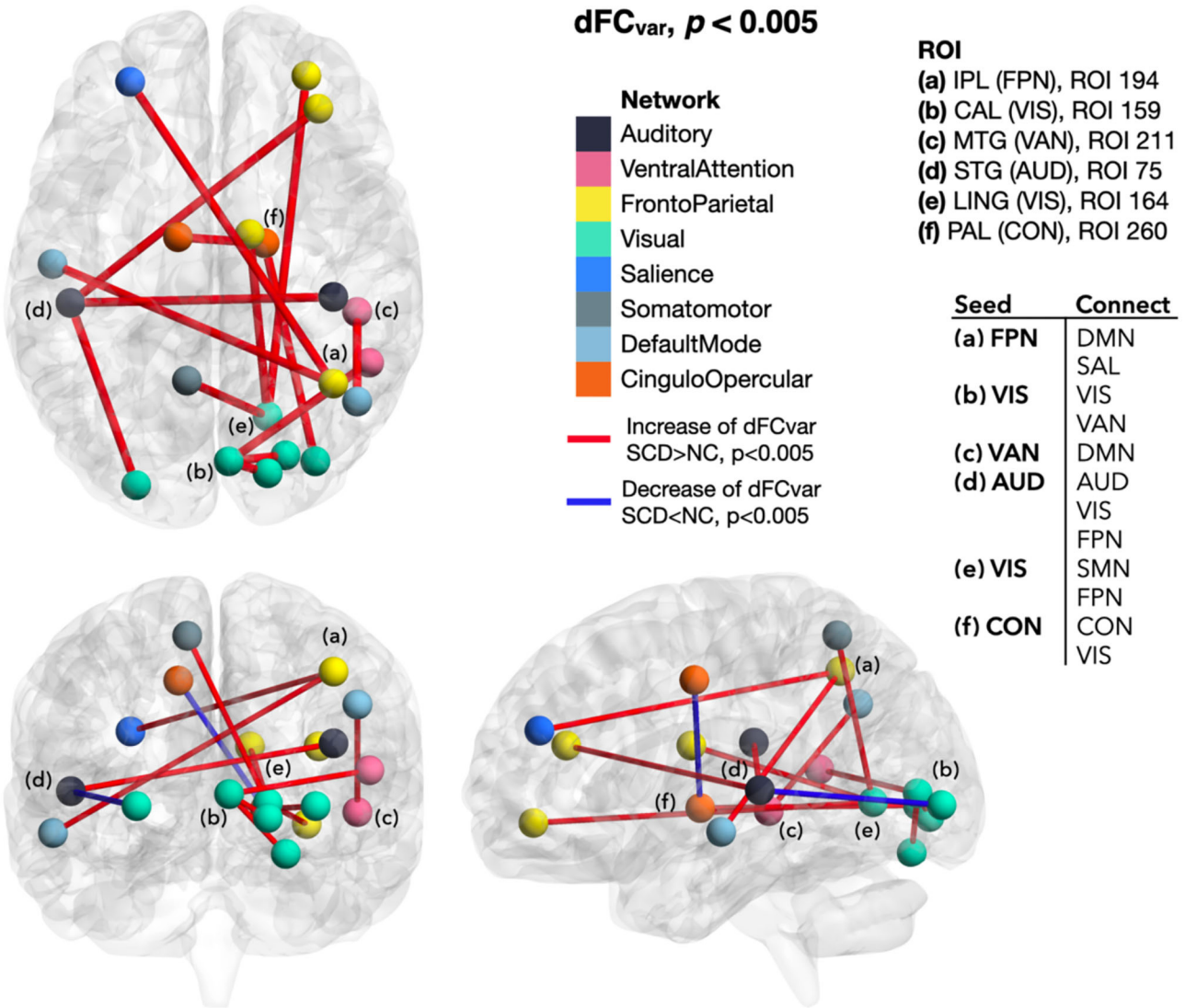

FIGURE 5 | Differences of dFC_{var} between SCD and NC. In SCD, dFC_{var} generally increased from the ROIs with local dynamic connectivity changes (seeding ROIs) to other brain regions. In contrast, the dFC_{var} decrease appeared between the ROIs of AUD-VIS and within CON. dFC_{var}, variance of the dynamic functional connectivity; SCD, subjective cognitive decline; NC, normal control; ROI, region of interest; IPL, inferior parietal lobule; FPN, frontoparietal network; CAL, calcarine area; VIS, visual network; MTG, middle temporal gyrus; VAN, ventral attention network; STG, superior temporal gyrus; AUD, auditory network; LING, lingual gyrus; VIS, visual network; PAL, pallidum of lenticular nucleus; CON, cingulo-opercular network; DMN, default mode network; SAL, salience network; SMN, somatomotor network.

(Dennis and Thompson, 2014; Chen and Arai, 2020). For example, homeostatic disinhibition by decreased GABAergic transmission in response to the defected and inefficient glutamatergic synaptic transmission is a common pathway of aging and AD (Gleichmann et al., 2011). In addition, functional compensation is one of the central theories for explaining the continuous brain changes of aging (Grady, 2012) and preclinical dementia (Jessen et al., 2014; Viviano and Damoiseaux, 2020). Overactivation of bilateral prefrontal cortex in working memory tests is considered compensations to aging in the model of *hemispheric asymmetry reduction in older adults (HAROLD)* (Cabeza, 2002). However, compensations could not fully cover the complex brain changes. Other explanations for the regionally increased brain activity include the *dedifferentiation* that reduced resource allocation and inefficient neural responses result in non-selective brain activation (Li and Lindenberger, 1999) and the *scaffolding theory of aging and cognition (STAC)* that additional networks are recruited in response to the functional decay of the initial network (Park and Reuter-Lorenz, 2009).

In recapitulating the above ideas, a highly differentiated brain reacts dynamically to the emerging and progressive destruction due to neurodegeneration. A comprehensive evaluation of behavioral, information-processing, and neurobiological evidence and referencing it to the cognitive

theories of aging helps us to understand the mechanisms of transition from normal to cognitively impaired states (Li et al., 2001).

History of Functional Connectivity Dynamics Study and What Did This Study Add to Current Knowledge?

Blood oxygenation level-dependent signals and resting-state networks have initially been considered in static states but later discovered to be fluctuating overtimes (Chang and Glover, 2010). It opened a new horizon of using BOLD dynamics to characterize disease-related brain changes in different scales from local changes, network reorganization to global brain remodeling (Biswal, 2012). By sliding-window technique, dynamic analysis of rs-fMRI can simulate neural activities of the brain by a comparable temporal resolution as that of electroencephalogram (EEG). Simultaneous resting-state EEG-fMRI showed distinct correlations between EEG power spectra and dynamic fluctuations of resting-state networks (Laufs, 2008; Hutchison et al., 2013). In addition, simultaneously recording of local field potential and fMRI found the dependence of functional connectivity dynamics to the behavior states (Hutchison et al., 2013; Pan et al., 2013). Lately, the development of analytic methods further extended the applications of sliding-window techniques to pairwise dFC comparisons, dynamic graph analysis, frame-wise analysis, state modeling, and temporal modeling. After that, dynamics of functional connectivity becomes a vital feature other than static connectivity for describing how the brain works (Preti et al., 2017).

In 2012, Jones et al. proposed the non-stationary modular architecture model of the resting brain and demonstrated temporal differences of DMN sub-network configurations in patients with AD and age-matched healthy controls. According to it, the resting brain in AD pronged to stay in the state emphasizing prefrontal anterior DMN but spend less time in the state weighting on posterior DMN (Jones et al., 2012). After that, several studies successively showed the dynamic features of AD (Gu et al., 2020), MCI (Wee et al., 2016; Jie et al., 2018), SCD (Xie et al., 2019; Dong et al., 2020; Yang et al., 2020; Chen et al., 2021), and across the AD spectrum (Cordova-Palomera et al., 2017; Demirtas et al., 2017).

The dynamics of functional connectivity are continuously changing over disease progression in the AD continuum. Combining temporal and spatial variability, dynamic features of resting-state networks can distinguish early MCI from late MCI and early MCI from healthy controls (Jie et al., 2018). It found the earliest changes in functional connectivity dynamics and its evolution over the trajectories of cognitive decline. Indeed, later studies of SCD confirmed that altered functional connectivity dynamics began in the preclinical phase. A large-scale brain dynamic study based on the graph theory described the temporospatial dynamics of SCD. Temporal flexibility and spatiotemporal diversity characterized SCD differently from NC and outperformed sFC and structural metrics in the support vector machine (SVM) classifier. This study also showed a mixed increase and decrease of connectivity dynamics across brain regions in SCD (Dong et al., 2020). Another state-modeling study of SCD found more dwell time in a state of hypoconnectivity within and between networks but less time in hyperconnectivity within and between the auditory, visual, and SMN. These altered dFC properties are further correlated significantly with cognitive performance (Chen et al., 2021). The other graphic analysis also revealed altered correlations between centrality frequency

TABLE 2 | Partial correlation coefficient (r) of $mdALFF_{mean}$ and $mdALFF_{var}$ to clinical indices.

Location†	$mdALFF_{mean}$			$mdALFF_{var}$			
	Figure 2			Figure 3			
	ROI(a)	ROI(b)	ROI(c)	ROI(a)	ROI(b)	ROI(c)	ROI(d)
Hemisphere	Right	Right	Right	Left	Right	Right	Right
AAL location	IPL	MTG	CAL	STG	LING	MTG	PAL
Network	FPN	VAN	VIS	AUD	VIS	VAN	CON
ROI number	194	211	159	75	164	211	260
AD8	**−0.29***	**0.30***	**0.38***	**0.51***	**0.42***	**0.32***	0.19
MMSE	**0.29***	0.01	−0.19	−0.20	0.10	−0.07	−0.13
MoCA	0.14	−0.14	−0.08	−0.21	−0.04	−0.07	−0.19
DSC	0.01	−0.01	0.04	0.02	−0.05	−0.02	−0.25
DST-forward	0.14	−0.04	−0.02	−0.21	−0.10	−0.07	0.01
DST-backward	0.10	−0.03	−0.08	−0.06	0.02	−0.11	0.02
LNS	−0.01	−0.09	0.10	−0.05	0.03	−0.18	−0.17
CF-animal	0.13	0.15	−0.01	−0.08	−0.23	−0.06	−0.18
CF-fruit	**0.32***	0.11	−0.09	−0.10	−0.15	−0.12	−0.07
CF-color	0.13	−0.07	0.00	−0.09	−0.11	−0.25	−0.06
CF-city	−0.19	−0.04	0.12	0.08	−0.14	−0.06	−0.21
FMT	0.20	−0.05	−0.07	−0.04	0.02	−0.07	−0.11
HADS-A	−0.20	0.17	0.10	0.14	0.21	**0.33***	0.11
HADS-D	0.17	−0.10	−0.02	0.22	0.12	0.23	0.13

Partial correlation coefficient with a FDR-corrected $p < 0.05$. The statistically significant values were in bold type. † References to ROI location in **Figures 2, **3**. Between-group differences of partial correlation coefficient were tested by Fisher's Z-transformation and one-tailed test. Boxes marked the correlations with significant group differences between SCD and NC (FDR-corrected $p < 0.05$). The following partial correlation coefficients of $mdALFF_{var}$ to cognitive scores differed between the SCD and NC groups: $mdALFF_{var}$ in right MTG of VAN with MMSE score (SCD $r = 0.398$ vs. NC $r = -0.108$), $mdALFF_{var}$ in right PAL of CON with CF-fruit score ($r = 0.297$ vs. -0.275) and CF-city score ($r = -0.293$ vs. $r = 0.325$). In addition, the correlations of the HADS-D depression score were different in the following local dynamic connectivity: $mdALFF_{mean}$ in right IPL of FPN ($r = 0.197$ vs. -0.271), $mdALFF_{mean}$ in right CAL of VIS ($r = -0.237$ vs. 0.187), $mdALFF_{var}$ in left STG of AUD ($r = -0.294$ vs. 0.235).*

ROI, region of interest; AAL, automated anatomical labeling; MMSE, Mini-Mental State Examination; MoCA, Montreal Cognitive Assessment; DSC, digit symbol coding; DST, digit span test; LNS, letter-number sequencing; CF, category fluency; FMT, facial memory test; HADS-A, Hospital Anxiety and Depression Scale—Anxiety subscale; HADS-D, Hospital Anxiety and Depression Scale—Depression subscale; mdALFF, mean dynamic amplitude of low-frequency fluctuation; var, variance; IPL, inferior parietal lobule; MTG, middle temporal gyrus; CAL, calcarine fissure and surrounding cortex; STG, superior temporal gyrus; LING, lingual gyrus; PAL, pallidum of lenticular nucleus; FPN, frontoparietal network; VAN, ventral attention network; VIS, visual network; AUD, auditory network; CON, cingulo-opercular network; FDR, false discovery rate; SCD, subjective cognitive decline; NC, normal control.

and cognitive performance in SCD when compared to NC. The correlation decreased in the anterior brain but increased in the posterior brain, especially significant within DMN (Xie et al., 2019).

The functional connectivity dynamics also change at the local level. A dynamic ALFF (dALFF) analysis comparing people with subjective memory complaints, NC, and MCI found lower regional dynamic connectivity in the hippocampus, parahippocampal gyrus, fusiform gyrus, precuneus, paracentral gyrus, and cerebellum in SCD. Furthermore, general concordance was higher in those with subjective memory decline than in NC (Yang et al., 2020). That was, the local dynamics of vulnerable areas became less active in SCD, and general connectivity dynamics became more synchronized and less favoring normal arousal state (Yan et al., 2017). Compared to this dALFF study of subjective memory decline (Yang et al., 2020), enrolling criteria of our study included multi-domain self-awareness of impaired cognitive abilities more than solely memory concerns. Our comparisons of mdALFF between SCD and NC identified more brain regions of various functional networks than the isolated memory-related regions as in the dALFF study. In addition, our analyses focused on network properties of the ROIs toward an explainable result with clinical relevance.

In summary, previous studies and our study of connectivity dynamics in SCD show the changes in both temporal and spatial aspects and from global to local scales. The dynamic disconnection moves the resting brain of SCD into a less coordinated state. With the correlations of clinical indices, regional connectivity dynamics are transformed into neuroimaging markers for indicating the transitional characteristics of the brain from a normal healthy state to the initiation of the AD spectrum disorders.

Right Brain Changes More Than Left Brain

Interestingly, the ROIs with mdALFF changes in SCD were primarily located in the right cerebral hemisphere. Even the marginal changes occurred more on the contralateral left cerebellar hemisphere that connects through cerebro-cerebellar circuits to the right cerebrum. We presume this result echoes the rightward functional lateralization phenomenon in aging and AD neurodegeneration.

As early as 2002, Cabeza established the *HAROLD* model for the aging brain that describes asymmetric functional reduction with a more significant functional loss on the left than the right cerebral hemisphere. As it states, the brain activation is more bilateral in older people than left-lateralized in younger adults regarding perception, inhibitory control, and memory function (Cabeza, 2002). Previous sFC studies of AD spectrum disorders also documented the similar right lateralization phenomenon of functional connectivity as in the aging brain. Functional deviation to the non-dominant hemisphere in MCI and AD suggests primary dysfunction of the dominant left hemisphere and corresponding compensatory functional shift to the right hemisphere (Liu et al., 2018). Furthermore, the regional cerebral metabolic rate of glucose on FDG-PET decreased more in the left hemisphere than the right hemisphere in patients with MCI and AD than in normal people (Weise et al., 2018). The asymmetric reduction in glucose metabolism in the left hemisphere may be the underlying physiological reason for the function deviation to the right hemisphere.

In this study, we focused on the SCD stage, the transition between normal and MCI. The dynamics of functional connectivity showed that the local disconnection and compensatory gain of function emerged in the non-dominant right hemisphere. Before influencing the dominant hemisphere, preclinical neurodegeneration affects first on the non-dominant hemisphere. Thus, the non-dominant cerebral hemisphere and its related contralateral cerebellar hemisphere are the precursors of functional connectivity changes. To sum up the findings of previous AD and MCI studies and our SCD study, the non-dominant right hemisphere shows early preclinical dynamic connectivity changes in the SCD stage. When cognitive decline progresses to the MCI and AD stages, the dominant left hemisphere loses function, and the non-dominant right hemisphere takes the response to rescue the functional loss.

Properties of Networks May Affect Their Vulnerability to Early Neurodegenerative Processes

We found that FPN (i.e., the central executive network, CEN) lost local dynamic connectivity in SCD. Other studies demonstrated that dynamic connectivity of DMN is affected in SCD (Xie et al., 2019). From the network property study, the properties of each network are specific for its unique functions. For example, DMN and FPN/CEN are the internally driven functional networks for higher-order mental processes. Their high integration and low coherence are in terms of high between-network connectivity, low within-network connectivity, low dynamic metastability, and low dynamic synchrony (Lee and Frangou, 2017). Furthermore, activation of FPN and DMN in task fMRI is associated with the subtle cognitive decline in cognitively normal non-MCI elderly (Zanchi et al., 2017). In our study, the regions of FPN, cFPN, and cDMN showed significant or marginal $mdALFF_{mean}$ decreases in SCD than NC. The within-network dFC_{mean} of cerebral-cerebellar parts of FPN (FPN-cFPN) also decreased in SCD. We proposed that the above networks are complicated and delicate in connecting outward and may be more vulnerable to disconnection.

In contrast, the other networks have low between-network connectivity, such as VIS and SMN (Lee and Frangou, 2017). They may contribute to functional compensation in the early stages of the AD continuum because they are relatively functioning well and can rescue the functional loss of the rest of the brain. These primary networks can work on their own and rely less on inter-network functional linkage. As in our study, $mdALFF_{mean}$ of CAL of the primary visual cortex increased while its dFC to the cFPN region decreased. Another dynamic rs-fMRI study of SCD also showed reduced dwell time of hyperconnectivity between the primary networks (i.e., VIS, AUD, and SMN) than controls (Chen et al., 2021). Therefore, we reasoned that the primary networks work more isolated in SCD.

The decentralized discrete operation is the alteration in response to the early neurodegeneration.

Functional Networks Altered in SCD

FPN and CFPN That in Charge of Central Executive Control

Fluid intelligence, including cognitive processing speed, working memory and long-term memory, is in contrast to crystalized intelligence regarding world knowledge and vocabulary (Park and Bischof, 2013). In normal aging, fluid intelligence declines with age, whereas crystallized intelligence remains at the same level. Similarly, fluid intelligence decreases more rapidly in preclinical AD than crystallized intelligence. The gap of decline between the two categories of intelligence is associated with amyloid deposition in the brain (Mcdonough et al., 2016).

Frontoparietal network is a flexible hub for flexible brain coordination for cognitive control (Zanto and Gazzaley, 2013) and adaptive task control (Cole et al., 2013). In addition, FPN maintains fluid intelligence by functional integration to the rest of the brain (Cole et al., 2015). However, FPN is affected early in preclinical AD. An rs-fMRI study of SCD demonstrated positive correlations between the comprehensive cognitive performance by the MoCA score and the static local connectivity of FPN (Wang et al., 2019). Well-functioning executive control is crucial to maintain cognitive preservation in the preclinical stage of dementia before the development of cognitive impairment.

In our study, the regions of FPN showed decreased $mdALFF_{mean}$ in SCD. The regions of cFPN also showed marginally decreased $mdALFF_{mean}$ and $mdALFF_{var}$ in SCD. These regions of FPN and cFPN have located in the cerebral association cortices and its mirroring posterior cerebellum, which are connected by cerebro-cerebellar circuits for reciprocal control of higher-order cognitive function (Buckner et al., 2011). Furthermore, dFC_{mean} showed decreased changes between the regions of FPN and cFPN in SCD than NC. The altered local and long-range dynamic connectivity in SCD represents the vulnerability of the higher-order functional networks and the related reduction in central executive control and cerebellar forward controlling. In correlation analysis, the regional $mdALFF_{mean}$ within FPN is correlated negatively with the degree of subjective cognitive concerns by the AD8 score and positively with cognitive performance in terms of the scores of MMSE and CF of fruit. Therefore, the local dynamics of FPN are crucial in balancing subjective and objective cognition in preclinical dementia, even if the cerebral-cerebellar disconnection within the central executive controls system has begun.

The Triple Network Dysfunction in SCD: FPN, DMN, and SAL/CON

In the triple network model for cognitive and affective dysfunction, SAL weights the external stimuli or internal awareness to balance the switches between cognitive controlling FPN/CEN and the self-referential DMN (Menon, 2011). The anterior cingulate cortex and anterior insula are the main parts of SAL to detect salient stimuli, coordinate, and dynamically allocate neural resources (Uddin, 2015). Besides, CON and SAL are considered equivalent or adjacent networks that CON has closer collaborations with FPN (Gratton et al., 2018).

With this background knowledge, we revisit the mdALFF and dFC results. The decreased local mdALFF within FPN, cFPN, and cDMN and the weakened outward dFC between FPN-DMN, FPN-SAL, CON-SAL, and CON-DMN suggest an imbalanced triple network organization centering the decline of FPN local connectivity in SCD. In addition, the regional FPN $mdALFF_{mean}$ is correlated with subjective and objective cognition. Similarly, in a study of dFC based on the triple network model, Xue et al. revealed aberrant dFC variability among DMN, SAL, and executive control network (i.e., FPN) in SCD and MCI compared to NC; moreover, the dFC variability within FPN is correlated with cognitive performance (Xue et al., 2021). To recap our study and Xue's study, the triple network model's aberrant dynamic activity and disorganization explain the subtle cognitive decline and awareness of cognitive impairment in SCD. These delicate dynamic changes in the triple networks appear early than the overt rise of cross-network functional connectivity in late MCI and AD (Li et al., 2019).

Attention Networks in AD Spectrum

The VAN detects unexpected stimuli and triggers attention shifting (bottom-up stimulus-driven attention), in cooperating with the goal-relevant top-down attention by the dorsal attention network (Corbetta and Shulman, 2002; Fox et al., 2006). Earlier in the AD continuum, VAN is preserved but DAN is affected in the MCI stage. However, both DAN and VAN are impaired in more advanced stages, as in the dementia stage (Sorg et al., 2007; Qian et al., 2015; Wang et al., 2019). As our results also suggested, the bottom-up attention maintained by the VAN was intact in the SCD stage. It even showed compensatory efforts for preserving cognitive performance in the SCD stage earlier before the development of MCI. In summary, when the top-down attention processing is impaired in the preclinical and MCI phases of dementia, the bottom-up attention processing retains or raises to keep the performance level.

Visual Network

The visual network controls visual signal processing, visual memory, visual learning, and visual coordination. A compensatory increase of sFC in SCD has been noticed in the medial visual network (Hafkemeijer et al., 2013) and inferior and medial occipital regions (Sun et al., 2016). In our study, the increased local dynamic connectivity was also located in the medial visual network, with increased $mdALFF_{mean}$ and $mdALFF_{var}$ of calcarine and lingual areas. The increase of visual local dynamic connectivity suggests a visual compensation for the subtle cognitive decline of SCD. In addition, the degree of SCCs was associated with this local dynamic connectivity. In addition, another rs-fMRI study also showed associations of subjective memory complaints and the sFC of the visual cortices, including the cuneus and lingual gyrus (Kawagoe et al., 2019). Therefore, the visual compensatory mechanism is one of the early modifications in response to subtle cognitive decline.

Auditory Network

The auditory cortex is one of the primary perception areas of the brain. The central auditory system receives external signals from peripheral auditory structures, and the auditory functional network operates the hearing-related cognitive processes. Auditory cognition includes auditory working memory, auditory semantic knowledge, auditory object recognition, auditory spatial processing, and auditory scene analysis (Johnson et al., 2021). Moreover, the auditory functional network does not work alone, but interplays with frontoparietal executive control and sensory networks for cognitive processes of auditory working memory (Kaiser, 2015).

In AD spectrum disorders, central auditory system dysfunction leads to distortion of the hierarchical auditory processing, loss of auditory plasticity, and impairment of auditory reciprocity. It results in a series of auditory cognitive deficits (Johnson et al., 2021). In a pathological inspection of the brains of patients with AD, senile plaques and neurofibrillary tangles were distributed throughout auditory-related nuclei (Sinha et al., 1993). In patients with AD, deficits of the auditory spatial processing are associated with gray matter volume loss, especially the posterior cortical atrophy (Golden et al., 2015). From functional aspects, the decrease of intra-network resting-state functional connectivity of the auditory network advances from normal controls, early MCI, to late MCI (Zhang et al., 2018).

In our study, the local dynamic connectivity $mdALFF_{mean}$ decreased marginally at the right ROL ($p = 0.006$) and the $mdALFF_{var}$ increased at the left STG in SCD ($p < 0.001$). In previous studies, right ROL was one of the brain regions that showed early functional changes in AD spectrum disorders. For example, the right ROL local property and its subgraph connecting to the right insula could differentiate early MCI from NC (Cui et al., 2018). Furthermore, our study showed that the dFC_{var} within AUD-AUD and between AUD-FPN regions increased significantly in SCD than NC. The unstable intra- and inter-network collaborations of the central auditory system signify the preclinical changes in SCD and correspond to the cognitive maintenance co-played by auditory and executive networks (Kaiser, 2015).

Limitations

There are several limitations of this study. First, previous studies have shown heterogeneous results of functional connectivity changes in SCD, which may be related to obtaining study groups at different phases of SCD (Viviano and Damoiseaux, 2020; Wang et al., 2020). The hypothetic model of functional connectivity changes in SCD includes a first increase of functional connectivity due to noisy signal propagation and compensation, followed by a later decrease due to the progression of disconnection (Viviano and Damoiseaux, 2020). The functional connectivity changes are continuous processes even in the SCD stage. Different research groups can enroll participants at either early SCD, late SCD, or a heterogeneous population and yield inconsistent findings. In our case, longitudinal follow-up will be a chance to know the sequential changes in functional connectivity dynamics of this community-dwelling group of people with SCD. Second, this study enrolled only SCD and NC. No advanced stages of the AD spectrum were included for comparisons. The setting of community-based research limited our studying population. Future enrollments of MCI and dementia groups from hospital-based settings will overcome this limitation and increase the generalizability of our findings to the continuum of AD. Finally, the sample size was relatively small when aiming to discover subtle brain changes in preclinical dementia, and therefore, the testing for multiple comparisons did not provide strong evidence. Thus, increasing sample size in future works is warranted to bring more convincing results for the dynamic connectivity changes in SCD.

CONCLUSIONS

Dynamic features of functional connectivity evolve along the trajectories of cognitive decline. This rs-fMRI study shows that the dynamic changes start early in the preclinical SCD stage. Local dynamic connectivity decreased in the regions of FPN but increased in VIS and VAN. Mixed weakening, compensatory enhancing, and unstable local dynamic connectivity mdALFF and their outward dFC suggest the transitional nature of the SCD stage from normal to cognitive impairment. Thus, the brain keeps a dynamic balancing between functional maintenance and subtle cognitive impairment in this stage. The altered local dynamics were associated with the degree of subjective cognitive concerns. In addition, the local dynamics of the right IPL of FPN are correlated with subjective and objective cognition and may be crucial for cognitive preservation in preclinical dementia.

DATA AVAILABILITY STATEMENT

The raw data supporting the conclusions of this article will be made available by the authors, without undue reservation.

ETHICS STATEMENT

The studies involving human participants were reviewed and approved by the Institutional Review Board of Chang Gung Memorial Hospital. The patients/participants provided their written informed consent to participate in this study.

AUTHOR CONTRIBUTIONS

Y-CW: conceptualization, methodology, data curation, formal analysis, investigation, resource, writing—original drafting, visualization, project administration, and funding acquisition. Y-CK: methodology, software, formal analysis, writing—original drafting, and visualization. W-YH: resource, data curation, and funding acquisition. CL: data curation, project administration, and funding acquisition. Y-LC: data curation and supervision. C-KC: resource, supervision, and project administration. Y-CS: data curation and resource. C-PL: conceptualization, methodology, investigation, resource, writing, review, editing, and supervision. All authors contributed to the article and approved the submitted version.

FUNDING

This research was supported by the grants of the Chang Gung Research Project to Y-CW (CRRPG2G0072), W-YH (CRRPG2K0032), C-PL (CRRPG2G0062 and CRRPG2K0022), C-KC (CRRPG2G0052 and CRRPG2K0012), and the Community Medicine Research Center of Keelung Chang Gung Memorial Hospital (CLRPG2J0011 and CLRPG2L0052). This research was also supported by grants to C-PL from the Ministry of Science and Technology (MOST) of Taiwan (MOST 110-2321-B-010-004, MOST 110-2634-F-010-001, MOST 111-2321-B-A49-003, and MOST 108-2321-B-010-010-MY2).

ACKNOWLEDGMENTS

The authors thank the Community Medicine Research Center and the Department of Medical Research and Development of Keelung Chang Gung Memorial Hospital for their great support. In addition, special thanks are given to the researchers for their devotion to this project: Jui-Yi Lee, Yi-Ting Chen, Hsin-Ju Hu, and Chun-Min Chang.

REFERENCES

Benjamini, Y., and Hochberg, Y. (1995). Controlling the false discovery rate: a practical and powerful approach to multiple testing. *J. Royal Stat. Soc. Ser. B. (Methodological)*. 57, 289–300. doi: 10.1111/j.2517-6161.1995.tb02031.x

Biswal, B. B. (2012). Resting state fMRI: a personal history. *Neuroimage*. 62, 938–944. doi: 10.1016/j.neuroimage.2012.01.090

Bjelland, I., Dahl, A. A., Haug, T. T., and Neckelmann, D. (2002). The validity of the hospital anxiety and depression scale. an updated literature review. *J. Psychosom. Res*. 52, 69–77. doi: 10.1016/S0022-3999(01)00296-3

Brier, M. R., Gordon, B., Friedrichsen, K., Mccarthy, J., Stern, A., Christensen, J., et al. (2016). Tau and Aβ imaging, CSF measures, and cognition in Alzheimer's disease. *Sci. Transl. Med.* 8, 338ra.366-338ra366. doi: 10.1126/scitranslmed.aaf2362

Buckner, R. L., Krienen, F. M., Castellanos, A., Diaz, J. C., and Yeo, B. T. T. (2011). The organization of the human cerebellum estimated by intrinsic functional connectivity. *J. Neurophysiol.* 106, 2322–2345. doi: 10.1152/jn.00339.2011

Cabeza, R. (2002). Hemispheric asymmetry reduction in older adults: the HAROLD model. *Psychol. Aging*. 17, 85–100. doi: 10.1037/0882-7974.17.1.85

Caselli, R. J., Chen, K., Locke, D. E., Lee, W., Roontiva, A., Bandy, D., et al. (2014). Subjective cognitive decline: self and informant comparisons. *Alzheimers. Dement*. 10, 93–98. doi: 10.1016/j.jalz.2013.01.003

Chang, C., and Glover, G. H. (2010). Time-frequency dynamics of resting-state brain connectivity measured with fMRI. *Neuroimage*. 50, 81–98. doi: 10.1016/j.neuroimage.2009.12.011

Chen, L. K., and Arai, H. (2020). Physio-cognitive decline as the accelerated aging phenotype. *Arch. Gerontol. Geriatr*. 104051. doi: 10.1016/j.archger.2020.104051

Chen, Q., Lu, J., Zhang, X., Sun, Y., Chen, W., Li, X., et al. (2021). Alterations in dynamic functional connectivity in individuals with subjective cognitive decline. *Front. Aging. Neurosci* 13, 646017. doi: 10.3389/fnagi.2021.646017

Cole, M. W., Ito, T., and Braver, T. S. (2015). Lateral prefrontal cortex contributes to fluid intelligence through multinetwork connectivity. *Brain. Connect*. 5, 497–504. doi: 10.1089/brain.2015.0357

Cole, M. W., Reynolds, J. R., Power, J. D., Repovs, G., Anticevic, A., and Braver, T. S. (2013). Multi-task connectivity reveals flexible hubs for adaptive task control. *Nat. Neurosci*. 16, 1348–55. doi: 10.1038/nn.3470

Corbetta, M., and Shulman, G. L. (2002). Control of goal-directed and stimulus-driven attention in the brain. *Nat. Rev. Neurosci*. 3, 201–215. doi: 10.1038/nrn755

Cordova-Palomera, A., Kaufmann, T., Persson, K., Alnaes, D., Doan, N. T., Moberget, T., et al. (2017). Disrupted global metastability and static and dynamic brain connectivity across individuals in the Alzheimer's disease continuum. *Sci. Rep*. 7, 40268. doi: 10.1038/srep40268

Cox, R. W. (1996). AFNI: software for analysis and visualization of functional magnetic resonance neuroimages. *Comput. Biomed. Res*. 29, 162–173. doi: 10.1006/cbmr.1996.0014

Cui, X., Xiang, J., Wang, B., Xiao, J., Niu, Y., and Chen, J. (2018). Integrating the local property and topological structure in the minimum spanning tree brain functional network for classification of early mild cognitive impairment. *Front. Neurosci*. 12, 701. doi: 10.3389/fnins.2018.00701

Davis, S. W., Dennis, N. A., Daselaar, S. M., Fleck, M. S., and Cabeza, R. (2008). Que PASA? The posterior-anterior shift in aging. *Cereb. Cortex*. 18, 1201–1209. doi: 10.1093/cercor/bhm155

de Vos, F., Koini, M., Schouten, T. M., Seiler, S., Van Der Grond, J., Lechner, A., et al. (2018). A comprehensive analysis of resting state fMRI measures to classify individual patients with Alzheimer's disease. *Neuroimage*. 167, 62–72. doi: 10.1016/j.neuroimage.2017.11.025

Demirtas, M., Falcon, C., Tucholka, A., Gispert, J. D., Molinuevo, J. L., and Deco, G. (2017). A whole-brain computational modeling approach to explain the alterations in resting-state functional connectivity during progression of Alzheimer's disease. *Neuroimage. Clin*. 16, 343–354. doi: 10.1016/j.nicl.2017.08.006

Dennis, E. L., and Thompson, P. M. (2014). Functional brain connectivity using fMRI in aging and Alzheimer's disease. *Neuropsychol. Rev*. 24, 49–62. doi: 10.1007/s11065-014-9249-6

Dong, C., Liu, T., Wen, W., Kochan, N. A., Jiang, J., Li, Q., et al. (2018). Altered functional connectivity strength in informant-reported subjective cognitive decline: a resting-state functional magnetic resonance imaging study. *Alzheimers. Dement. (Amst)* 10, 688–697. doi: 10.1016/j.dadm.2018.08.011

Dong, G., Yang, L., Li, C. R., Wang, X., Zhang, Y., Du, W., et al. (2020). Dynamic network connectivity predicts subjective cognitive decline: the Sino-Longitudinal Cognitive impairment and dementia study. *Brain. Imaging. Behav*. 14, 2692–2707. doi: 10.1007/s11682-019-00220-6

Fox, M. D., Corbetta, M., Snyder, A. Z., Vincent, J. L., and Raichle, M. E. (2006). Spontaneous neuronal activity distinguishes human dorsal and ventral attention systems. *Proc. Natl. Acad. Sci. U.S.A*. 103, 10046–10051. doi: 10.1073/pnas.0604187103

Fransson, P. (2005). Spontaneous low-frequency BOLD signal fluctuations: an fMRI investigation of the resting-state default mode of brain function hypothesis. *Hum. Brain. Mapp*. 26, 15–29. doi: 10.1002/hbm.20113

Fransson, P. (2006). How default is the default mode of brain function? Further evidence from intrinsic BOLD signal fluctuations. *Neuropsychologia*. 44, 2836–2845. doi: 10.1016/j.neuropsychologia.2006.06.017

Franzmeier, N., Neitzel, J., Rubinski, A., Smith, R., Strandberg, O., Ossenkoppele, R., et al. and Alzheimer's Disease Neuroimaging, I. (2020). Functional brain architecture is associated with the rate of tau accumulation in Alzheimer's disease. *Nat. Commun*. 11, 347. doi: 10.1038/s41467-019-14159-1

Friston, K. J. (2007). *Statistical Parametric Mapping: The Analysis of Funtional Brain Images*. Amsterdam, Boston: Elsevier/Academic Press.

Friston, K. J., Williams, S., Howard, R., Frackowiak, R. S. J., and Turner, R. (1996). Movement-Related effects in fMRI time-series. *Magnetic Resonance Med.* 35, 346–355. doi: 10.1002/mrm.1910350312

Galvin, J. E., Roe, C. M., Coats, M. A., and Morris, J. C. (2007). Patient's Rating of Cognitive Ability: Using the AD8, a Brief Informant Interview, as a Self-rating Tool to Detect Dementia. *JAMA Neurol.* 64, 725–730. doi: 10.1001/archneur.64.5.725

Galvin, J. E., Roe, C. M., Powlishta, K. K., Coats, M. A., Muich, S. J., Grant, E., et al. (2005). The AD8: a brief informant interview to detect dementia. *Neurology*. 65, 559–564. doi: 10.1212/01.wnl.0000172958.95282.2a

Galvin, J. E., Roe, C. M., Xiong, C., and Morris, J. C. (2006). Validity and reliability of the AD8 informant interview in dementia. *Neurology*. 67, 1942–1948. doi: 10.1212/01.wnl.0000247042.15547.eb

Gleichmann, M., Chow, V. W., and Mattson, M. P. (2011). Homeostatic disinhibition in the aging brain and Alzheimer's disease. *J. Alzheimers Dis*. 24, 15–24. doi: 10.3233/JAD-2010-101674

Golden, H. L., Nicholas, J. M., Yong, K. X., Downey, L. E., Schott, J. M., Mummery, C. J., et al. (2015). Auditory spatial processing in Alzheimer's disease. *Brain*. 138, 189–202. doi: 10.1093/brain/awu337

Grady, C. (2012). The cognitive neuroscience of ageing. *Nat. Rev. Neurosci*. 13, 491–505. doi: 10.1038/nrn3256

Gratton, C., Sun, H., and Petersen, S. E. (2018). Control networks and hubs. *Psychophysiology*. 55. doi: 10.1111/psyp.13032

Gu, Y., Lin, Y., Huang, L., Ma, J., Zhang, J., Xiao, Y., et al. and Alzheimer's Disease Neuroimaging, I. (2020). Abnormal dynamic functional connectivity in Alzheimer's disease. *CNS. Neurosci. Ther*. 26, 962–971. doi: 10.1111/cns.13387

Hafkemeijer, A., Altmann-Schneider, I., Oleksik, A. M., Van De Wiel, L., Middelkoop, H. A., Van Buchem, M. A., et al. (2013). Increased functional connectivity and brain atrophy in elderly with subjective memory complaints. *Brain. Connect*. 3, 353–362. doi: 10.1089/brain.2013.0144

Hanseeuw, B. J., Betensky, R. A., Jacobs, H. I. L., Schultz, A. P., Sepulcre, J., Becker, J. A., et al. (2019). Association of amyloid and tau with cognition in preclinical Alzheimer disease: a longitudinal study. *JAMA Neurol*. 76, 915–924. doi: 10.1001/jamaneurol.2019.1424

He, Y., Wang, L., Zang, Y., Tian, L., Zhang, X., Li, K., et al. (2007). Regional coherence changes in the early stages of Alzheimer's disease: a combined structural and resting-state functional MRI study. *Neuroimage*. 35, 488–500. doi: 10.1016/j.neuroimage.2006.11.042

Hutchison, R. M., Womelsdorf, T., Allen, E. A., Bandettini, P. A., Calhoun, V. D., Corbetta, M., et al. (2013). Dynamic functional connectivity: promise, issues, and interpretations. *Neuroimage*. 80, 360–378. doi: 10.1016/j.neuroimage.2013.05.079

Jack, C. R., Knopman, D. S., Jagust, W. J., Shaw, L. M., Aisen, P. S., Weiner, M. W., et al. (2010). Hypothetical model of dynamic biomarkers of the Alzheimer's pathological cascade. *Lancet Neurology*. 9, 119–128. doi: 10.1016/S1474-4422(09)70299-6

Jessen, F., Amariglio, R.E., Van Boxtel, M., Breteler, M., Ceccaldi, M., Chetelat, G., et al. (2014). A conceptual framework for research on subjective cognitive decline in preclinical Alzheimer's disease. *Alzheimers Dement*. 10, 844–852. doi: 10.1016/j.jalz.2014.01.001

Jiao, F., Gao, Z., Shi, K., Jia, X., Wu, P., Jiang, C., et al. (2019). Frequency-dependent relationship between resting-state fmri and glucose metabolism in the elderly. *Front. Neurol*. 10, 566. doi: 10.3389/fneur.2019.00566

Jie, B., Liu, M., and Shen, D. (2018). Integration of temporal and spatial properties of dynamic connectivity networks for automatic diagnosis of brain disease. *Med. Image. Anal*. 47, 81–94. doi: 10.1016/j.media.2018.03.013

Johnson, J. C. S., Marshall, C. R., Weil, R. S., Bamiou, D. E., Hardy, C. J. D., and Warren, J. D. (2021). Hearing and dementia: from ears to brain. *Brain*. 144, 391–401. doi: 10.1093/brain/awaa429

Jones, D. T., Vemuri, P., Murphy, M. C., Gunter, J. L., Senjem, M. L., Machulda, M. M., et al. Jr. (2012). Non-stationarity in the "resting brain's" modular architecture. *PLoS ONE*. 7, e39731. doi: 10.1371/journal.pone.0039731

Kaiser, J. (2015). Dynamics of auditory working memory. *Front. Psychol*. 6, 613. doi: 10.3389/fpsyg.2015.00613

Kawagoe, T., Onoda, K., and Yamaguchi, S. (2019). Subjective memory complaints are associated with altered resting-state functional connectivity but not structural atrophy. *Neuroimage. Clin*. 21, 101675. doi: 10.1016/j.nicl.2019.101675

Kung, Y. C., Li, C. W., Chen, S., Chen, S. C., Lo, C. Z., Lane, T. J., et al. (2019). Instability of brain connectivity during nonrapid eye movement sleep reflects altered properties of information integration. *Hum. Brain. Mapp*. 40, 3192–3202. doi: 10.1002/hbm.24590

Laufs, H. (2008). Endogenous brain oscillations and related networks detected by surface EEG-combined fMRI. *Hum. Brain. Mapp*. 29, 762–769. doi: 10.1002/hbm.20600

Lecrubier, Y., Sheehan, D., Weiller, E., Amorim, P., Bonora, I., Harnett Sheehan, K., et al. (1997). The Mini International Neuropsychiatric Interview (MINI). A short diagnostic structured interview: reliability and validity according to the CIDI. *European. Psychiatry*. 12, 224–231. doi: 10.1016/S0924-9338(97)83296-8

Lee, W. H., and Frangou, S. (2017). Linking functional connectivity and dynamic properties of resting-state networks. *Sci. Rep*. 7, 16610. doi: 10.1038/s41598-017-16789-1

Leonardi, N., and Van De Ville, D. (2015). On spurious and real fluctuations of dynamic functional connectivity during rest. *Neuroimage*. 104, 430–436. doi: 10.1016/j.neuroimage.2014.09.007

Li, C., Li, Y., Zheng, L., Zhu, X., Shao, B., Fan, G., et al. and Alzheimer's Disease Neuroimaging, I. (2019). Abnormal brain network connectivity in a triple-network model of Alzheimer's Disease. *J. Alzheimers. Dis*. 69, 237–252. doi: 10.3233/JAD-181097

Li, S-. C., and Lindenberger, U. (1999). "Cross-level unification: A computational exploration of the link between deterioration of neurotransmitter systems and dedifferentiation of cognitive abilities in old age," in *Cognitive Neuroscience of Memory* (Cambridge, MA: Hogrefe and Huber), 103–146.

Li, S. C., Lindenberger, U., and Sikstrom, S. (2001). Aging cognition: from neuromodulation to representation. *Trends. Cogn. Sci*. 5, 479–486. doi: 10.1016/S1364-6613(00)01769-1

Liao, W., Li, J., Ji, G. J., Wu, G. R., Long, Z., Xu, Q., et al. (2019). Endless fluctuations: temporal dynamics of the amplitude of low frequency fluctuations. *IEEE Transac. Med. Imag*. 38, 2523–2532. doi: 10.1109/TMI.2019.2904555

Liao, W., Wu, G. R., Xu, Q., Ji, G. J., Zhang, Z., Zang, Y. F., et al. (2014). DynamicBC: a MATLAB toolbox for dynamic brain connectome analysis. *Brain. Connect*. 4, 780–790. doi: 10.1089/brain.2014.0253

Liu, H., Zhang, L., Xi, Q., Zhao, X., Wang, F., Wang, X., et al. (2018). Changes in brain lateralization in patients with mild cognitive impairment and alzheimer's disease: a resting-state functional magnetic resonance study from Alzheimer's disease neuroimaging initiative. *Front. Neurol*. 9, 3. doi: 10.3389/fneur.2018.00003

Liu, Y., Yu, C., Zhang, X., Liu, J., Duan, Y., Alexander-Bloch, A. F., et al. (2014). Impaired long distance functional connectivity and weighted network architecture in Alzheimer's disease. *Cereb. Cortex*. 24, 1422–1435. doi: 10.1093/cercor/bhs410

Mcdonough, I. M., Bischof, G. N., Kennedy, K. M., Rodrigue, K. M., Farrell, M. E., and Park, D. C. (2016). Discrepancies between fluid and crystallized ability in healthy adults: a behavioral marker of preclinical Alzheimer's disease. *Neurobiol. Aging*. 46, 68–75. doi: 10.1016/j.neurobiolaging.2016.06.011

Mckhann, G. M., Knopman, D. S., Chertkow, H., Hyman, B. T., Jack, C. R. Jr., Kawas, C.H., et al. (2011). The diagnosis of dementia due to Alzheimer's disease: recommendations from the National Institute on Aging-Alzheimer's Association workgroups on diagnostic guidelines for Alzheimer's disease. *Alzheimers. Dement*. 7, 263–269. doi: 10.1016/j.jalz.2011.03.005

Menon, V. (2011). Large-scale brain networks and psychopathology: a unifying triple network model. *Trends. Cogn. Sci*. 15, 483–506. doi: 10.1016/j.tics.2011.08.003

Molinuevo, J. L., Rabin, L. A., Amariglio, R., Buckley, R., Dubois, B., Ellis, K. A., et al. (2017). Implementation of subjective cognitive decline criteria in research studies. *Alzheimers Dement*. 13, 296–311. doi: 10.1016/j.jalz.2016.09.012

Ossenkoppele, R., Iaccarino, L., Schonhaut, D. R., Brown, J. A., La Joie, R. O'neil, J. P., Janabi, M., et al. (2019). Tau covariance patterns in Alzheimer's disease patients match intrinsic connectivity networks in the healthy brain. *Neuroimage. Clin*. 23, 101848. doi: 10.1016/j.nicl.2019.101848

Pan, W. J., Thompson, G. J., Magnuson, M. E., Jaeger, D., and Keilholz, S. (2013). Infraslow LFP correlates to resting-state fMRI BOLD signals. *Neuroimage*. 74, 288–297. doi: 10.1016/j.neuroimage.2013.02.035

Park, D. C., and Bischof, G. N. (2013). The aging mind: neuroplasticity in response to cognitive training. *Dialogues. Clin. Neurosci*. 15, 109–119. doi: 10.31887/DCNS.2013.15.1/dpark

Park, D. C., and Reuter-Lorenz, P. (2009). The adaptive brain: aging and neurocognitive scaffolding. *Annu. Rev. Psychol*. 60, 173–196. doi: 10.1146/annurev.psych.59.103006.093656

Parker, A. F., Smart, C. M., Scarapicchia, V., and Gawryluk, J. R. and For the Alzheimer's Disease Neuroimaging, I. (2020). Identification of earlier biomarkers for alzheimer's disease: a multimodal neuroimaging study of individuals with subjective cognitive decline. *J. Alzheimers Dis*. 77, 1067–1076. doi: 10.3233/JAD-200299

Petersen, R. C., Smith, G. E., Waring, S. C., Ivnik, R. J., Tangalos, E. G., and Kokmen, E. (1999). Mild cognitive impairment: clinical characterization and outcome. *Arch. Neurol.* 56, 303–308. doi: 10.1001/archneur.56.3.303

Power, J. D., Cohen, A. L., Nelson, S. M., Wig, G. S., Barnes, K. A., Church, J. A., et al. (2011). Functional network organization of the human brain. *Neuron*. 72, 665–678. doi: 10.1016/j.neuron.2011.09.006

Preti, M. G., Bolton, T. A., and Van De Ville, D. (2017). The dynamic functional connectome: State-of-the-art and perspectives. *Neuroimage*. 160, 41–54. doi: 10.1016/j.neuroimage.2016.12.061

Qian, S., Zhang, Z., Li, B., and Sun, G. (2015). Functional-structural degeneration in dorsal and ventral attention systems for Alzheimer's disease, amnestic mild cognitive impairment. *Brain Imag. Behav*. 9, 790–800. doi: 10.1007/s11682-014-9336-6

Rossetti, H. C., Lacritz, L. H., Cullum, C. M., and Weiner, M. F. (2011). Normative data for the Montreal Cognitive Assessment (MoCA) in a population-based sample. *Neurology*. 77, 1272–1275. doi: 10.1212/WNL.0b013e318230208a

Seitzman, B. A., Gratton, C., Marek, S., Raut, R. V., Dosenbach, N. U. F., Schlaggar, B. L., et al. (2020). A set of functionally-defined brain regions with improved representation of the subcortex and cerebellum. *Neuroimage*. 206, 116290. doi: 10.1016/j.neuroimage.2019.116290

Shyu, Y. I., and Yip, P. K. (2001). Factor structure and explanatory variables of the Mini-Mental State Examination (MMSE) for elderly persons in Taiwan. *J. Formos. Med. Assoc*. 100, 676–683.

Sinha, U. K., Hollen, K. M., Rodriguez, R., and Miller, C. A. (1993). Auditory system degeneration in Alzheimer's disease. *Neurology*. 43, 779–785. doi: 10.1212/WNL.43.4.779

Smith, S. M., Jenkinson, M., Woolrich, M. W., Beckmann, C. F., Behrens, T. E. J., Johansen-Berg, H. J.M., et al. (2004). Advances in functional and structural MR image analysis and implementation as FSL. *NeuroImage*. 23, S208–S219. doi: 10.1016/j.neuroimage.2004.07.051

Sorg, C., Riedl, V., Muhlau, M., Calhoun, V. D., Eichele, T., Laer, L., et al. (2007). Selective changes of resting-state networks in individuals at risk for Alzheimer's disease. *Proc. Natl. Acad. Sci. U.S.A*. 104, 18760–18765. doi: 10.1073/pnas.0708803104

Sperling, R. A., Aisen, P. S., Beckett, L. A., Bennett, D. A., Craft, S., Fagan, A. M. Jr., et al. (2011). Toward defining the preclinical stages of Alzheimer's disease: recommendations from the National Institute on Aging-Alzheimer's Association workgroups on diagnostic guidelines for Alzheimer's disease. *Alzheimers. Dement*. 7, 280–292. doi: 10.1016/j.jalz.2011.03.003

Sun, Y., Dai, Z., Li, Y., Sheng, C., Li, H., Wang, X., et al. (2016). Subjective cognitive decline: mapping functional and structural brain changes-a combined resting-state functional and structural MR imaging study. *Radiology* 281, 185–192. doi: 10.1148/radiol.2016151771

Tzourio-Mazoyer, N., Landeau, B., Papathanassiou, D., Crivello, F., Etard, O., Delcroix, N., et al. (2002). Automated anatomical labeling of activations in SPM using a macroscopic anatomical parcellation of the MNI MRI single-subject brain. *NeuroImage*. 15, 273–289. doi: 10.1006/nimg.2001.0978

Uddin, L. Q. (2015). Salience processing and insular cortical function and dysfunction. *Nat. Rev. Neurosci*. 16, 55–61. doi: 10.1038/nrn3857

Viviano, R. P., and Damoiseaux, J. S. (2020). Functional neuroimaging in subjective cognitive decline: current status and a research path forward. *Alzheimers. Res. Ther*. 12, 23. doi: 10.1186/s13195-020-00591-9

Wang, X., Huang, W., Su, L., Xing, Y., Jessen, F., Sun, Y., et al. (2020). Neuroimaging advances regarding subjective cognitive decline in preclinical Alzheimer's disease. *Mol. Neurodegener*. 15, 55. doi: 10.1186/s13024-020-00395-3

Wang, Z., Qiao, K., Chen, G., Sui, D., Dong, H. M., Wang, Y. S., et al. (2019). Functional connectivity changes across the spectrum of subjective cognitive decline, amnestic mild cognitive impairment and Alzheimer's disease. *Front. Neuroinform*. 13, 26. doi: 10.3389/fninf.2019.00026

Wee, C. Y., Yang, S., Yap, P. T., and Shen, D. and Alzheimer's Disease Neuroimaging, I. (2016). Sparse temporally dynamic resting-state functional connectivity networks for early MCI identification. *Brain. Imaging. Behav*. 10, 342–356. doi: 10.1007/s11682-015-9408-2

Wei, Y. C., Huang, L. Y., Chen, C. K., Lin, C., Shyu, Y. C., Chen, Y. L., et al. (2019). Subjective cognitive decline in the community is affected at multiple aspects of mental health and life quality: a cross-sectional study of the community medicine of Keelung Chang Gung Memorial Hospital. *Dement. Geriatr. Cogn. Dis. Extra*. 9, 152–162. doi: 10.1159/000497222

Wei, Y-. C., Huang, L-. Y., Lin, C., Shyu, Y-. C., and Chen, C-. K. (2021). Taiwanese Depression Questionnaire and AD8 Questionnaire for Screening Late-Life Depression in Communities. *Neuropsychiatric Dis. Treat.* 17, 747–755. doi: 10.2147/NDT.S298233

Weise, C. M., Chen, K., Chen, Y., Kuang, X., Savage, C. R., and Reiman, E. M. and Alzheimer's Disease Neuroimaging, I. (2018). Left lateralized cerebral glucose metabolism declines in amyloid-beta positive persons with mild cognitive impairment. *Neuroimage. Clin*. 20, 286–296. doi: 10.1016/j.nicl.2018.07.016

Winblad, B., Palmer, K., Kivipelto, M., Jelic, V., Fratiglioni, L., Wahlund, L. O., et al. (2004). Mild cognitive impairment—beyond controversies, towards a consensus: report of the International Working Group on Mild Cognitive Impairment. *J. Intern. Med*. 256, 240–246. doi: 10.1111/j.1365-2796.2004.01380.x

Xie, Y., Liu, T., Ai, J., Chen, D., Zhuo, Y., Zhao, G., et al. (2019). Changes in centrality frequency of the default mode network in individuals with subjective cognitive decline. *Front Aging Neurosci*. 11, 118. doi: 10.3389/fnagi.2019.00118

Xue, C., Qi, W., Yuan, Q., Hu, G., Ge, H., Rao, J., et al. (2021). Disrupted dynamic functional connectivity in distinguishing subjective cognitive decline and amnestic mild cognitive impairment based on the triple-network model. *Front. Aging. Neurosci*. 13, 711009. doi: 10.3389/fnagi.2021.711009

Yan, C-. G., Yang, Z., Colcombe, S. J., Zuo, X-. N., and Milham, M. P. (2017). Concordance among indices of intrinsic brain function: insights from inter-individual variation and temporal dynamics. *Science. Bull.* 62, 1572–1584. doi: 10.1016/j.scib.2017.09.015

Yang, L., Yan, Y., Wang, Y., Hu, X., Lu, J., Chan, P., et al. (2018). Gradual Disturbances of the Amplitude of Low-Frequency Fluctuations (ALFF) and Fractional ALFF in Alzheimer Spectrum. *Front. Neurosci*. 12, 975. doi: 10.3389/fnins.2018.00975

Yang, Y., Zha, X., Zhang, X., Ke, J., Hu, S., Wang, X., et al. (2020). Dynamics and concordance abnormalities among indices of intrinsic brain activity in individuals with subjective cognitive decline: a temporal dynamics resting-state functional magnetic resonance imaging analysis. *Front. Aging. Neurosci*. 12, 584863. doi: 10.3389/fnagi.2020.584863

Yang, Y. H., Galvin, J. E., Morris, J. C., Lai, C. L., Chou, M. C., and Liu, C. K. (2011). Application of AD8 questionnaire to screen very mild dementia in Taiwanese. *Am. J. Alzheimers Dis. Other. Demen*. 26, 134–138. doi: 10.1177/1533317510397330

Zalesky, A., Fornito, A., and Bullmore, E. T. (2010). Network-based statistic: identifying differences in brain networks. *Neuroimage*. 53, 1197–1207. doi: 10.1016/j.neuroimage.2010.06.041

Zanchi, D., Montandon, M. L., Sinanaj, I., Rodriguez, C., Depoorter, A., Herrmann, F. R., et al. (2017). Decreased fronto-parietal and increased default mode network activation is associated with subtle cognitive deficits in elderly controls. *Neurosignals*. 25, 127–138. doi: 10.1159/000486152

Zang, Y. F., He, Y., Zhu, C. Z., Cao, Q. J., Sui, M. Q., Liang, M., et al. (2007). Altered baseline brain activity in children with ADHD revealed by resting-state functional MRI. *Brain. Dev*. 29, 83–91. doi: 10.1016/j.braindev.2006.07.002

Zanto, T. P., and Gazzaley, A. (2013). Fronto-parietal network: flexible hub of cognitive control. *Trends. Cogn. Sci*. 17, 602–603. doi: 10.1016/j.tics.2013.10.001

Zhang, D., and Raichle, M. E. (2010). Disease and the brain's dark energy. *Nat. Rev. Neurol*. 6, 15–28. doi: 10.1038/nrneurol.2009.198

Zhang, H., Lee, A., and Qiu, A. (2017). A posterior-to-anterior shift of brain functional dynamics in aging. *Brain. Struct. Funct*. 222, 3665–3676. doi: 10.1007/s00429-017-1425-z

Zhang, Y., Liu, X., Zhao, K., Li, L., and Ding, Y. (2018). Study of altered functional connectivity in individuals at risk for Alzheimer's Disease. *Technol. Health. Care.* 26, 103–111. doi: 10.3233/THC-174235

Conflict of Interest: The authors declare that the research was conducted in the absence of any commercial or financial relationships that could be construed as a potential conflict of interest.

Publisher's Note: All claims expressed in this article are solely those of the authors and do not necessarily represent those of their affiliated organizations, or those of the publisher, the editors and the reviewers. Any product that may be evaluated in this article, or claim that may be made by its manufacturer, is not guaranteed or endorsed by the publisher.

frontiers | Frontiers in Aging Neuroscience

TYPE Original Research
PUBLISHED 10 August 2022
DOI 10.3389/fnagi.2022.932906

OPEN ACCESS

EDITED BY
Michael Ewers,
Ludwig Maximilian University of Munich, Germany

REVIEWED BY
Yaakov Stern,
Columbia University Irving Medical Center, United States
Vijay K. Ramanan,
Mayo Clinic, United States

*CORRESPONDENCE
Takashi Kato
tkato@ncgg.go.jp

†The research group of the Study on Diagnosis of Early Alzheimer's Disease-Japan (SEAD-J) comprised investigators from nine different centers. The investigators contributed to the design and implementation of the SEAD-J and/or provided data but did not participate in the analyses of this report.

SPECIALTY SECTION
This article was submitted to Alzheimer's Disease and Related Dementias, a section of the journal Frontiers in Aging Neuroscience

RECEIVED 30 April 2022
ACCEPTED 18 July 2022
PUBLISHED 10 August 2022

CITATION
Kato T, Nishita Y, Otsuka R, Inui Y, Nakamura A, Kimura Y, Ito K and SEAD-J Study Group (2022) Effect of cognitive reserve on amnestic mild cognitive impairment due to Alzheimer's disease defined by fluorodeoxyglucose-positron emission tomography.
Front. Aging Neurosci. 14:932906.
doi: 10.3389/fnagi.2022.932906

Effect of cognitive reserve on amnestic mild cognitive impairment due to Alzheimer's disease defined by fluorodeoxyglucose-positron emission tomography

Takashi Kato[1]*, Yukiko Nishita[2], Rei Otsuka[2], Yoshitaka Inui[3], Akinori Nakamura[1,4], Yasuyuki Kimura[1], Kengo Ito[1] and SEAD-J Study Group†

[1]Department of Clinical and Experimental Neuroimaging, National Center for Geriatrics and Gerontology, Aichi, Japan, [2]Department of Epidemiology of Aging, National Center for Geriatrics and Gerontology, Aichi, Japan, [3]Department of Radiology, Fujita Health University School of Medicine, Aichi, Japan, [4]Department of Biomarker Research, National Center for Geriatrics and Gerontology, Aichi, Japan

This study aimed to investigate the effect of cognitive reserve (CR) on the rate of cognitive decline and cerebral glucose metabolism in amnestic mild cognitive impairment (MCI) using the Study on Diagnosis of Early Alzheimer's Disease-Japan (SEAD-J) dataset. The patients in SEAD-J underwent cognitive tests and fluorodeoxyglucose-positron emission tomography (FDG-PET). MCI to be studied was classified as amnestic MCI due to Alzheimer's disease (AD) with neurodegeneration. A total of 57 patients were visually interpreted as having an AD pattern (P1 pattern, Silverman's classification). The 57 individuals showing the P1 pattern were divided into a high-education group (years of school education $\geq$13, N = 18) and a low-education group (years of school education $\leq$12, N = 39). Voxel-based statistical parametric mapping revealed more severe hypometabolism in the high-education group than in the low-education group. Glucose metabolism in the hippocampus and temporoparietal area was inversely associated with the years of school education in the high- and low-education groups (N = 57). General linear mixed model analyses demonstrated that cognitive decline was more rapid in the high-education group during 3-year follow-up. These results suggest that the cerebral glucose metabolism is lower and cognitive function declines faster in patients with high CR of amnestic MCI due to AD defined by FDG-PET.

KEYWORDS

cognitive reserve, mild cognitive impairment, Alzheimer's disease (AD), cerebral glucose metabolism, education

Introduction

In aging and dementia, the concept of cognitive reserve (CR) is associated with the capacity of the brain to cope with neuropathology in order to minimize clinical manifestations (Stern, 2002). According to the CR hypothesis, in advanced degenerative dementia, individuals with a high CR should have more advanced dementia pathology than those with low CR if they have the same level of cognitive function, which has been proven in a number of studies (Lovden et al., 2020).

Stern's CR hypothesis includes another important claim wherein he predicted that individuals with a high CR would retain cognitive function despite pathology; however, once the decline begins, the rate of decline would be faster than that in individuals with a low CR. Nevertheless, the results from various research groups have been inconsistent. Compared with low CR, cognitive decline in high CR has been reported to be faster (Unverzagt et al., 1998; Andel et al., 2006; Scarmeas et al., 2006), slower (Fritsch et al., 2001; Hall et al., 2007; Bennett et al., 2015), or similar (Del Ser et al., 1999; Paradise et al., 2009; Vemuri et al., 2011). One possible reason for this discrepancy could be attributed to the varying etiologies and disease stages among the reports. In recent years by using imaging or liquid biomarkers, it has become possible to optimize examinations of CR for Alzheimer's disease (AD) related clinical progression across AD continuum (McKhann et al., 2011), including preclinical AD, amnestic mild cognitive impairment (MCI) due to AD, and AD dementia (van Loenhoud et al., 2019; Lee et al., 2021).

This study aimed to investigate the effect of CR on the rate of cognitive decline and cerebral glucose metabolism in amnestic MCI due to AD using data from the Study on Diagnosis of Early Alzheimer's Disease-Japan (SEAD-J) (Ito et al., 2015; Inui et al., 2017). The SEAD-J was a prospective study to investigate the predictive ability of fluorodeoxyglucose-positron emission tomography (FDG-PET) in the conversion from amnestic MCI to dementia in 3-year follow-up. Visual reading of the pattern of decreased glucose metabolism on FDG-PET at the baseline was employed to narrow down the included participants to MCI due to AD. Neurodegenerative progression was estimated based on the degree of cerebral glucose hypometabolism.

Patients and methods

Patient information

Study on Diagnosis of Early Alzheimer's Disease-Japan

The data used in this work were retrieved from the SEAD-J database. The SEAD-J was launched in 2005 as a multicenter (nine institutions in Japan) cohort study of amnestic MCI. The primary intent of the SEAD-J was to establish scientific evidence for the usefulness of imaging biomarkers (F-18 FDG-PET) in the early diagnosis of AD at the stage of amnestic MCI. Clinical and neuropsychological assessments can be combined to evaluate amnestic MCI progression.

A total of 114 patients (64 women and 50 men; mean age, 70.8 ± 7.5 years) were enrolled in the SEAD-J. Notably, 88 patients reached the endpoint (conversion to dementia) or completed the 3-year follow-up. In this study, 57 out of the 88 patients were examined whose FDG-PET images were visually interpreted as an AD pattern (P1, described in the visual interpretation of the FDG-PET images), respectively. The 57 individuals showing the P1 pattern were divided into a high-education group (years of school education ≥13, N = 18) and a low-education group (years of school education ≤12, N = 39) (**Table 1** and **Supplementary material**). In the survey and statistical analysis model of this study, years of school education was specified as a discrete variable. In the Japanese schooling system, as well as in the United States, 13 or more years of education usually implies some form of education beyond secondary school. The subjects were stratified into two groups using the separating point for years of education while considering the distribution of the educational attainment and the number of the subjects.

The diagnosis of amnestic MCI was based on an interview with neurologists that revealed evidence of reduced cognitive capacity, normal activities of daily living, and absence of dementia. All the patients were free of significant underlying medical, neurological, or psychiatric illnesses. All the patients were initially assessed using a series of neuropsychological

TABLE 1 Demographic characteristics of the patients at the baseline and conversion rate in a 3-year follow-up.

	Total	Low-education	High-education	*p*
N	57	39	18	
Age	71.9 (6.4)	73.1 (5.2)	69.3 (8.0)	0.054
Sex (male/female)	28/29	14/25	14/4	0.001
Years of school education	11.6 (2.9)	9.9 (1.6) (≤12)	15.1 (1.5) (≥13)	<0.001
CDR	0.5	0.5	0.5	
MMSE	25.6 (1.8)	25.8 (1.7)	26.0 (1.6)	0.826
ADAS-Jcog	10.1 (5.0)	10.5 (5.5)	9.2 (3.5)	0.294
WMS-R LM-I	7.3 (3.2)	7.3 (3.3)	7.3 (3.0)	0.930
WMS-R LM-II	2.2 (2.5)	2.2 (2.5)	2.4 (2.5)	0.677
GDS	4.4 (2.3)	4.2 (2.4)	4.8 (2.0)	0.569
Converter/non-converter	35/22	22/17	13/5	0.442

Values are presented as mean (standard deviation) or number of participants. Differences in sex and conversion/non-conversion between the high and low cognitive reserves were tested using the chi-square test. Other continuous parameters were tested using the Student's *t*-test. CDR, Clinical Dementia Rating Scale; MMSE, Mini-Mental State Examination; ADAS-Jcog, Alzheimer's Disease Assessment Scale-Cognitive Component-Japanese version; WMS-R LM-I, Wechsler Memory Scale-Revised, logical memory I; WMS-R LM-II, Wechsler Memory Scale-Revised, logical memory II; GDS, Geriatric Depression Scale.

tests, including the Mini-Mental State Examination (MMSE), Alzheimer's Disease Assessment Scale-Cognitive Component-Japanese version (ADAS-Jcog), Clinical Dementia Rating (CDR), Geriatric Depression Scale (GDS), Everyday Memory Check List (EMCL), and Logical Memory Subset of the Wechsler Memory Scale Revised (WMS-R LM). In accordance with the inclusion criteria, patients with MCI were between 50 and 80 years of age, with an MMSE score $\geq$24, GDS score $\leq$10, WMS-R LM-I score $\leq$13, WMS-R LM-II part A and part B scores $\leq$8 (maximum = 50), and a CDR memory box score of 0.5. Patients with less than 6 years of formal education were excluded. Each patient signed an informed consent form after receiving full explanation of the procedures involved.

Patients were assessed at 1-year intervals for 3 years. CDR, MMSE, EMCL, and WMS-RLM tests were readministered at each visit. Conversion to dementia was determined when CDR was $\geq$1.0. No further follow-up of patients with a CDR $\geq$1.0 was performed. AD was diagnosed when a patient fulfilled both CDR $\geq$1.0 and the National Institute of Neurological and Communicative Disorders-Alzheimer's Disease and Related Disorders Association (NINCDS-ADRDA) "probable AD" criteria. Other diseases were diagnosed based on the established clinical criteria, including vascular dementia, dementia with Lewy bodies, and frontotemporal dementia. Two researchers in the SEAD-J group, blinded to the PET results, established the final clinical outcome of each patient based on the submitted case reports. Patients diagnosed with cognitive impairment other than AD, MCI, or normal were excluded from this study.

This study was approved by the ethics committees of all the participating institutions. All participants provided informed consent in accordance with the ethics committee of the National Center for Geriatrics and Gerontology. All the datasets of the clinical and FDG-PET findings over a follow-up period of 3 years were acquired.

F-18 fluorodeoxyglucose-positron emission tomography acquisition

F-18 fluorodeoxyglucose-positron emission tomography (FDG-PET) scan was performed with the patient in the resting state for 40–60 min following a venous injection of 18F-FDG (254 $\pm$ 107 MBq). A static scan was performed for 10 $\pm$ 5 min, either in the two or three-dimensional mode. Attenuation was corrected using either a transmission scan with segmentation for dedicated PET or a computed tomography (CT) scan for PET/CT. F-18 FDG-PET images were processed to produce 3D-stereotactic surface projection (SSP) and generate z-score maps using iSSP (version 3.5; Nihon Medi-Physics, Tokyo, Japan). 3D-SSP was created using the Neurological Statistical Image Analysis Software (NEUROSTAT) developed by Minoshima et al. (1995). NEUROSTAT anatomically normalizes the individual PET data to the standard brain and compares the regional voxel data with the normal database, calculating the z-score (| normal mean - individual value| /normal standard deviation) for each voxel of the cerebral surface, and displays the sites at which the voxel value is statistically reduced. The normal database was constructed using 50 control participants (31 men and 19 women; mean age 57.6 years), with 10 participants from each of the five participating institutions. The results of their neurological and brain imaging examinations [magnetic resonance imaging (MRI) or CT] were normal, and their cognitive function was judged to be normal by experienced neurologists.

Visual interpretation of the fluorodeoxyglucose-positron emission tomography images

Three experts, blinded to the clinical information, independently assessed the reconstructed PET images. They visually evaluate the 3D-SSP z-score maps to classify the images into different dementia patterns according to Silverman's criteria (Silverman and Phelps, 2001). Based on these criteria, FDG-PET findings are classified into seven interpretive patterns as positive (P1–P3, P1 +) or negative (N1–N3) for the presence of a progressive neurodegenerative disease, in general, and AD specifically compared with the results of longitudinal or neuropathological analysis. P1 indicates progressive PET patterns consistent with the presence of AD showing hypometabolism in the parietal/temporal $\pm$ frontal cortex, while P1 +, P2, and P3 indicate progressive PET patterns but inconsistent with AD (P1 + , the presence of abnormal findings other than P1; P2, frontal predominant hypometabolism; P3, hypometabolism of both the caudate and lentiform nuclei). N1–N3 patterns indicate all the negative scans, wherein N1 represents normal metabolism. When the classification of the three raters did not match, a consensus was reached upon discussion of the cases. They referred to the patients' MRI images to exclude the partial volume effect attributed to severe atrophy, cerebral vascular lesions, and space-occupying lesions when a local hypometabolic area was observed in the PET image. Patients with patterns other than P1 pattern were excluded from this study.

Magnetic resonance imaging

All the participants were scanned using either a 1.5 T or 3T MRI system. T1-, T2-, and fluid-attenuated inversion recovery-weighted MR images were acquired to rule out neurological diseases, such as cerebrovascular diseases and brain tumors other than neurodegenerative dementia.

Statistical analyses

For analyses of baseline profiles, we used independent-sample *t*-tests to assess the differences in clinical and cognitive variables, age, years of school education, scores of cognitive tests, and PET scores. The chi-squared test was used for the analyses of sex and age differences between the high- and low-education groups. The chi-square test was also used to determine group differences in the ratio of AD conversion (AD converters vs. non-converters; stable MCI) within the 3-year period between the high- and low-education groups.

General linear mixed models (GLMMs) (Laird and Ware, 1982; Morrell et al., 2009) were employed to evaluate the effects of years of school education on the cognitive changes over a 3-year period. As GLMMs can model differences between groups as random effects, they provide a wide range of models for the analysis of grouped data. GLMMs can handle missing data more appropriately than traditional regression analysis and repeated-measures analysis. The correlations between the repeated measures are adequately accounted for by the variance-covariance structure of random effects. These models are useful for the analysis of many types of data, including longitudinal data. Therefore, a GLMM was chosen for the analysis of intellectual change in some recent studies (Nishita et al., 2019).

The model used in the current study included fixed terms for the intercept (baseline performance for an individual with value zero for all predictors), education (0 = low-education group, 1 = high-education group), time (time in years since baseline), and an education × time interaction term. Age (at baseline) and sex (0 = male; 1 = female) were included as covariates. The random effects of the intercept (baseline performance) and slope (change over time) were calculated using an unstructured covariance matrix. The term of primary interest for this study was the education × time interaction, which reflects whether the high- or low-education groups differ in the rate of change in the cognitive scores, such as the MMSE, ADAS-Jcog, and WMS-R LM I and II scores over time.

Statistical analyses were performed using SPSS Statistics V.17.0 (IBM, Armonk, NY, United States) and SAS System version 9.3 (SAS Institute, Cary, NC, United States). Statistical significance was set at $p < 0.05$.

Statistical parametric mapping analysis

For voxel-based analyses of group comparisons and multiple regression using SPM8, each FDG-PET image was spatially deformed to the Montreal Neurological Imaging template (PET.nii) using parameters derived from that image and then normalized for variations in whole-brain measurements using proportional scaling. Post-processed images were smoothed to a spatial resolution of 8 mm full width at half maximum. Voxel-based group comparisons were made between high-education and low-education groups with adjustment for the ADAS-Jcog score. Linear regression models were used to evaluate the effect of years of education on cerebral glucose metabolism by adjusting for the ADAS-Jcog score. ADAS-cog score is more precise in measuring the severity of total cognitive dysfunction than MMSE (Balsis et al., 2015). The level of significance was set at $p < 0.01$ and extent threshold >400 (uncorrected). In addition, a region of interest (ROI)-based analysis for FDG-PET data was performed using the MarsBar toolbox.[1] ROI was created from the statistical map of the regression analysis. This analysis can be a kind of circular statistics (Kriegeskorte et al., 2009), but it only aimed at estimating the strength of the linear relationship between the years of school education and the regional glucose metabolism.

Results

Table 1 presents the patients' demographic characteristics at baseline and conversion ratio during the 3-year follow-up. There were significant differences in sex ($p = 0.001$) and years of school education ($p < 0.001$) at baseline between the high- and low-education groups. The differences in age were not statistically significant ($p = 0.054$). The high-education group tended to be younger and included more men than the low-education group. No significant differences were detected between the high- and low-education groups in the CDR, MMSE, ADAS-Jcog, WMS-R LM-I, WMS-R LM-II, and GDS scores. No significant difference in the ratio of conversion to dementia was detected between the high- and low-education groups (**Table 1**).

A group comparison of FDG-PET images demonstrated that patients with high-education ($N = 18$) had significantly lower glucose metabolism than those with low-education ($N = 39$) in the left hippocampus [(−32, −11, −23), $T = 5.40$] and its surrounding area, including the amygdala, fusiform gyrus, and lingual gyrus, adjusted for ADAS-Jcog [$p < 0.01$ and extent threshold >400 (uncorrected)] (**Figure 1**). The cluster of the left hippocampus reached a significant level of family-wise error <0.05.

Voxel-based regression analyses controlling the ADAS-Jcog score revealed that years of school education were significantly and inversely associated with the regional glucose metabolism in the left hippocampus [(−32, −11, −24), $T = 4.20$] and the temporoparietal area, including the fusiform, inferior temporal, angular, and superior parietal gyrus. The left lingual and superior frontal gyri were also detected as significant areas [$p < 0.01$, extent threshold >400 (uncorrected)] (**Figure 2**). **Figure 3** shows a scatter plot representing a significant inverse relationship ($R^2 = 0.189$, $p < 0.001$) between years of school

1 http://marsbar.sourceforge.net/

10.3389/fnagi.2022.932906

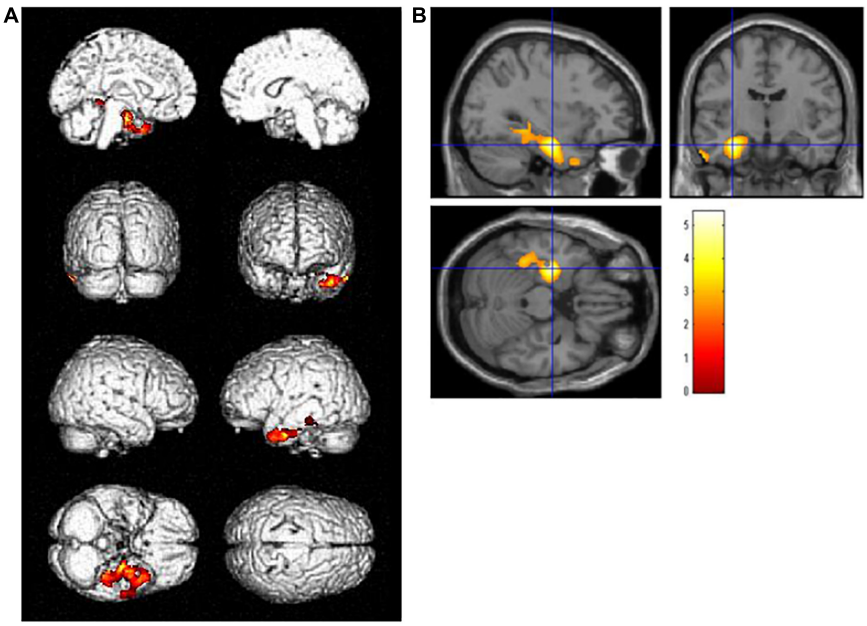

FIGURE 1
Regions with statistically significant decrease ($p < 0.01$, extent threshold >400) in glucose metabolism PET after adjusting for Alzheimer's Disease Assessment Scale-Cognitive Component-Japanese version in the high-education group (years of school education ≥13, $N = 18$) compared with the low-education group (years of school education ≤12, $N = 39$) on **(A)** the brain surface projection and **(B)** multi-planar cross-sectional views. The red-yellow scale indicates the level of statistical significance. The blue crossed lines indicate the maximum peak voxel in the left hippocampus [(−32, −11, −23), $T = 5.40$].

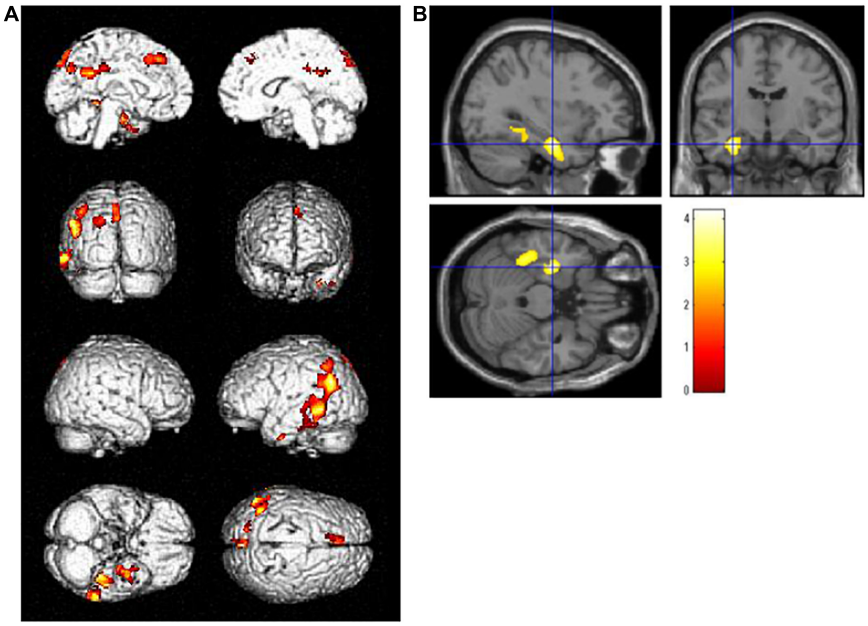

FIGURE 2
Regions where regional glucose metabolism was inversely associated with years of school education upon controlling for the Alzheimer's Disease Assessment Scale-Cognitive Component-Japanese version score in a combined group ($N = 57$) of high- and low-education group. Statistically significant areas ($p < 0.01$, extent threshold >400) are displayed on **(A)** the brain surface projection and **(B)** multiplanar cross-sectional views. The red-yellow scale indicates the level of statistical significance. The blue crossed lines indicate the maximum peak voxel in the left hippocampus [(−32, −11, −24), $T = 4.20$].

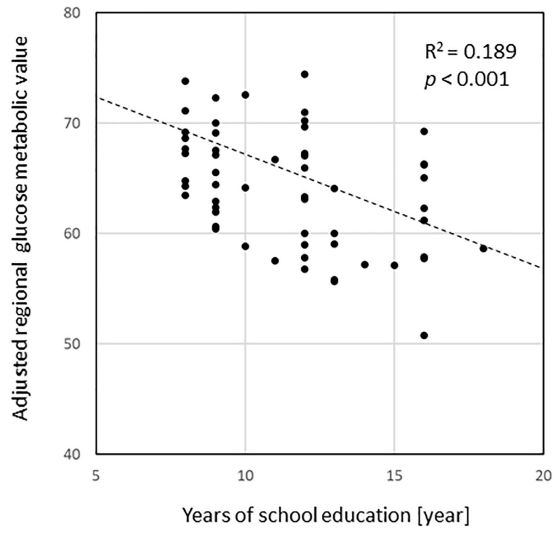

FIGURE 3
A scatterplot representing a significant inverse relationship (R^2 = 0.189, p < 0.001) between the years of education (x-axis) and regional cerebral glucose metabolism in the left hippocampal cluster detected in the regression analysis (y-axis). Glucose metabolism values were normalized with the mean value in individual images as 50.

education (x-axis) and regional cerebral glucose metabolism in the left hippocampal cluster (y-axis).

Table 2 and Figure 4 show the results of the analyses of the GLMMs. The term for education was not significant for any of the subtests (MMSE, β = −0.3080, p = 0.6172; ADAS-Jcog, β = 0.5188, p = 0.7489; WMS-R LM I, β = 0.2624, p = 0.8182; WMS-R LM II, β = 0.4242, p = 0.5665), which represents no significance in any of the estimated cognitive scores between high- and low-education groups at the baseline. The term for time was significant for all the subtests (MMSE, β = −1.8162, p < 0.0001; ADAS-Jcog, β = 3.7829, p < 0.0001; WMS-R LM I, β = −1.2465, p = 0.0012; WMS-R LM II, β = −0.7317, p = 0.0240), which shows that significant cognitive decline over 3 years was estimated for all the cognitive scores. Education × time, which was the interaction effect of education and time, was significant for all the subtests except MMSE (MMSE, β = 0.3627, p = 0.4982; ADAS-Jcog, β = −1.9065, p = 0.0367; WMS-R LM I, β = 0.9491, p = 0.0326; WMS-R LM II, β = 0.9133, p = 0.0183).

Discussion

This study examined the effect of CR on amnestic MCI due to AD with neurodegeneration, as determined by FDG-PET.

All 57 patients with amnestic MCI included in this study showed AD-like hypometabolic pattern on FDG-PET images. They were not tested for amyloid by PET, CSF, or blood. Therefore, they can be categorized as MCI due to AD-intermediate likelihood based on the 2011 MCI criteria by the National Institute on Aging and Alzheimer's Association (Albert et al., 2011).

Fluorodeoxyglucose-positron emission tomography is a downstream marker of neurodegeneration in AD (Dubois et al., 2014) that corresponds to N+ in ATN system in AD continuum (Jack et al., 2016). Although the topographic pattern of hypometabolism in the parietotemporal association cortex, posterior cingulate gyrus, and precuneus is useful for diagnosing AD and may be an alternative to amyloid PET in some conditions (Rabinovici et al., 2011), such a pattern can be observed in neurological diseases other than AD (Kato et al., 2016). Tau PET and amyloid PET would provide all the information on ATN and would allow a more reliable and detailed evaluation of the CR of amnestic MCI in the AD continuum.

Years of school education was used as a surrogate index of CR for this study. In the statistical group comparison adjusting for the cognitive performance, significantly more severe hypometabolism was detected in the left hippocampus and surrounding regions, including the fusiform and parahippocampal gyrus, in the high-education group than in the low-education group (Figure 1). In addition, areas where regional glucose metabolism was negatively correlated with years of school education adjusting for the cognitive score

TABLE 2 Parameter values estimated by the mixed general linear model.

	Model terms	Parameter estimate	SE	*P*-Value
MMSE	Education	−0.3080	0.6142	0.6172
	Time	−1.8162	0.4423	<0.0001
	Education × time	0.3627	0.5333	0.4982
ADAS-Jcog	Education	0.5188	1.6151	0.7489
	Time	3.7829	0.7218	<0.0001
	Education × time	−1.9065	0.8970	0.0367
WMS-R LM I	Education	0.2624	1.1380	0.8182
	Time	−1.2465	0.3643	0.0012
	Education × time	0.9491	0.4397	0.0326
WMS-R LM II	Education	0.4242	0.7373	0.5665
	Time	−0.7317	0.3151	0.0240
	Education × time	0.9133	0.3796	0.0183

Higher scores indicate better performance in the MMSE, LM I, and LM II and lower performance in the ADAS-Jcog. Possible scores for MMSE are 0–30; ADAS-Jcog, 0–70; LM-I, 0–50; and LM-II, 50. Time = years since baseline, Education = 0 [high-education: reference (years of school education ≥13) or 1 (low-education, years of school education ≤12)]. In addition to the variables shown in the table, each model included terms to control the fixed effects of age at baseline, sex as a covariate, and the random effects of the intercept (baseline performance) and slope (change over time). The estimated parameters are the effect of education at baseline (education), effect of elapsed time (time), and effect of interaction of education and time (education × time). MMSE, Mini-Mental State Examination; ADAS-Jcog, Alzheimer's Disease Assessment Scale-Cognitive Component-Japanese version; WMS-R LM-I, Wechsler Memory Scale-Revised, logical memory I; WMS-R LM-II, Wechsler Memory Scale-Revised, logical memory II; SE, standard error of mean.

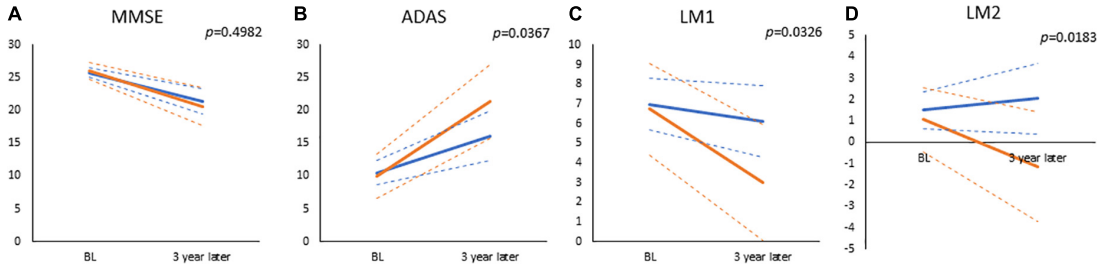

FIGURE 4
The results of general mixed linear models, which estimated values at baseline and visit of 3-year follow-up for **(A)** Mini-Mental State Examination (MMSE), **(B)** Alzheimer's Disease Assessment Scale-Cognitive Component-Japanese version (ADAS), **(C)** Wechsler Memory Scale-Revised, logical memory I (LM1), and **(D)** Wechsler Memory Scale-Revised, logical memory II (LM2). Displayed *p*-values are significant for the interaction of time and education (high or low cognitive reserve). The solid and dashed lines connect the mean and 95% confidence interval at baseline and 3 years, respectively. Blue lines: low-education group (years of school education ≤12); Red lines: high-education group (years of school education ≥13).

were found in the left temporal to parietal lobes (**Figure 2**). In both analyses, the clusters of the left hippocampal regions had the highest *T*-values. These brain regions are within the area where tau accumulation and neurodegeneration are observed in AD. These results revealed that in amnestic MCI due to AD, if cognitive function is set at the same level, the longer years of education are associated with more advanced neurodegeneration of AD. The concept of CR relates to the capacity of the brain to cope with neuropathology so as to minimize clinical manifestations in aging and dementia (Stern, 2002). Accordingly, we can reason out that the CR effect manifests as a decline in the cerebral glucose metabolism in amnestic MCI due to AD with the same level of cognition.

The cerebral regions related to CR were distributed in a strong left-dominant manner, which was not seen in the z-score mapping of mean FDG-PET images showing the P1 pattern (Ito et al., 2015). This may be explained by the fact that the performance of language-based neuropsychological tests has been shown to correlate with the lateralization of gray matter loss to the left hemisphere in MCI and AD (Derflinger et al., 2011).

This study also examined the effect of educational attainment on the estimated rate of cognitive decline during a 3-year follow-up period using GLMMs. An interaction effect of years of school education on the cognitive decline rate was found for the ADAS-Jcog, LM-I, and LM-II (**Table 2** and **Figure 4**). These results indicate that cognitive decline following the onset of AD is faster for those with a high-education than for those with low-education. No significant difference in the cognitive function at baseline was observed between the high- and low-education groups. This finding could be attributed to the inclusion criteria, which encompassed amnestic MCI and a combination of MMSE, WMS-R-LM-I/II, CDR, and GDS scores. The narrow range of cognitive scores may have resulted in the inclusion of amnestic MCI with relatively uniform cognitive function scores. If the inclusion criteria had been more relaxed, significant differences caused by CR between the high- and low-education groups might have been detected. The rates of cognitive decline of the patients might have been influenced by the difference of cognitive status.

Recently, biomarkers reflecting amyloid and tau, which are involved in the pathology of AD, have become available. It has become possible to narrow the focus of CR studies to AD continuum or preclinical AD by incorporating these biomarkers. The results of these studies have indicated that the rate of cognitive decline in the high-education group is slower in the preclinical AD stage and faster after the onset of AD (van Loenhoud et al., 2019; Lee et al., 2021). The results of this study were consistent with the above findings.

Epidemiological studies examining CR suggest that CR is linked to socioeconomic status and literacy (Stern, 2009). Years of schooling is a strong proxy for CR, but it is not a decisive factor. Years of schooling are correlated with family environment and general socioeconomic attainment. Therefore, the characteristics of years of schooling as a proxy indicator of CR may vary based on conditions, such as race and social environment. In the United States, the effect of years of education reportedly varies by race (Avila et al., 2020). This could be attributed to the social and economic environment in which the people of a particular race live, rather than a factor of race itself. The participants of this study were Japanese individuals born during or shortly after World War II. College and university enrollment rates among this population were generally around 10%, suggesting that most individuals with 13 or more years of education (i.e., more than secondary schooling) belonged to a relatively high social and economic stratum. The division between up to and beyond secondary education is found in several CR studies (Nishita et al., 2019; Wilson et al., 2019; Avila et al., 2020). The appropriate separating point for educational length may vary based on the distribution of the years of education and socioeconomic background of the studied population. It may be useful to

utilize sensitivity analysis (Qian and Mahdi, 2020) to optimize the split points. Additional analyses dividing the subjects into the compulsory education level (years of school education $\leq$9, N = 21) and higher education level (years of school education $\geq$13, N = 18) provided nearly identical results that are shown in the **Supplementary Materials 3A–E**. The general direction that the results of the present analyses represent is maintained.

We should be cautious about the extent to which results of this study can be generalized. These results may not be equally applicable to subjects with different characteristics using different analysis methods (Lovden et al., 2020). The findings of this study are for patients with amnestic MCI due to AD-intermediate likelihood with a narrow range of cognitive scores and an average age of approximately 71 years. Younger age may have increased the proportion of hippocampal-sparing AD type, while older age may have raised the proportion of limbic predominant AD subtype (Ferreira et al., 2020). These subtypes differ in terms of the affected brain regions and the degree of atrophy, as well as in the rate of progression of cognitive decline. With increasing age, more pathological changes other than AD become evident (Jellinger, 1998; Spina et al., 2021). Even if diagnosis of AD is narrowed using imaging or fluid biomarkers, the results may differ from this study depending on the characteristics of the recruited subjects. The same may be true for targeting non-AD dementias. The measured cognitive scores should also be considered. In a cohort study with a larger sample size, the higher education group demonstrated accelerated declines in composite scores of episodic memory and perceptual speed, but not in the composite score of global cognition (Wilson et al., 2019).

The other potential factors such as sleeping disturbance (Cordone et al., 2019), ApoE type (Vemuri et al., 2017), physical activity (Pedrero-Chamizo et al., 2021), and cerebrovascular disease (Saito and Ihara, 2016) are ideally also to be analyzed, because they may be linked to disease progression through amyloid and tau deposition or other pathways. Patients with cerebrovascular disease were excluded in this study. Unfortunately, ApoE type, sleeping disorder, and physical activities were not evaluated. It is expected that such modifying factors will be examined in the future.

This study has certain limitations. First, the sample size was relatively small. As the significance level of the present results is not sufficiently high, a study with a larger sample size is necessary to obtain more robust results. Second, there was a lack of biomarker information directly indicating the presence or absence of amyloid and tau. Third, information on *ApoE* was not available; *ApoE* is a risk factor for AD, which could result in a bias in the present findings. Finally, the assessment measures could also be a limitation of the study. We used years of education as a proxy measure of CR. CR is defined not only by years of education but also by socioeconomic activities, language proficiency, leisure activity level, and physical activity level. The use of a composite proxy index that includes these factors could result in a more accurate assessment (Ko et al., 2022). Considering cognitive function, this study examined limited cognitive function scores, such as the ADAS-Jcog; however, previous studies have demonstrated that the CR effect varies based on the cognitive function (Kang et al., 2018). It might be desirable to evaluate various brain functions, including executive functions, individually and as a combination.

In conclusion, this study demonstrated that cerebral glucose metabolism is lower and cognitive function declines faster in patients with high CR in amnestic MCI due to AD defined by FDG-PET.

Data availability statement

The dataset can be requested from the principal investigator upon reasonable request. Requests to access the datasets should be directed to TK, tkato@ncgg.go.jp.

Ethics statement

The studies involving human participants were reviewed and approved by the Ethics Committee of the National Center for Geriatrics and Gerontology. The patients/participants provided their written informed consent to participate in this study.

Members of SEAD-J Study Group

Hidenao Fukuyama (Kyoto University, Kyoto, Japan), Michio Senda (Institute of Biomedical Research and Innovation, Kobe, Japan), Kenji Ishii (Tokyo Metropolitan Institute of Gerontology, Tokyo, Japan), Kazunari Ishii (Kindai University, Osaka, Japan), Kiyoshi Maeda (Kobe Gakuin University, Kobe, Japan), Yasuji Yamamoto (Kobe University Graduate School of Medicine, Kobe, Japan), Yasuomi Ouchi (Hamamatsu University School of Medicine, Hamamatsu, Japan), Ayumu Okamura (Kizawa Memorial Hospital, Gifu, Japan), Yutaka Arahata (National Center for Geriatrics and Gerontology, Aichi, Japan), Yukihiko Washimi (National Center for Geriatrics and Gerontology, Aichi, Japan), Kenichi Meguro (Tohoku University Graduate School of Medicine, Sendai, Japan), and Mitsuru Ikeda (Nagoya University School of Health Sciences, Nagoya, Japan).

Author contributions

KI was the principal investigator who contributed to the design and administration of the SEAD-J study.

YI made basic data preparation and analyses. TK performed voxel-based statistical analyses and wrote the first draft of the manuscript. YN and RO analyzed the general mixed linear models. YK and AN contributed to the structure and the discussion of the manuscript. All authors contributed to the article and approved the submitted version.

Funding

This study was supported by the Health Labour Sciences Research Grant from the Ministry of Health, Labour, and Welfare of Japan (H17-Tyojyu-023), (16dk0207022h0001), AMED under Grant Number JP21km0908001, and Research Funding for Longevity Sciences from National Center for Geriatrics and Gerontology, Japan (20-1, 30-3). The funding sources had no role in the study design, data collection, data analyses, or data interpretation.

Acknowledgments

We thank those who contributed to the patients' care, and collection and preprocessing of the PET images and clinical reports.

Conflict of interest

The authors declare that the research was conducted in the absence of any commercial or financial relationships that could be construed as a potential conflict of interest.

Publisher's note

Supplementary material

The Supplementary Material for this article can be found online at: https://www.frontiersin.org/articles/10.3389/fnagi.2022.932906/full#supplementary-material

References

Albert, M. S., DeKosky, S. T., Dickson, D., Dubois, B., Feldman, H. H., Fox, N. C., et al. (2011). The diagnosis of mild cognitive impairment due to Alzheimer's disease: Recommendations from the National Institute on Aging-Alzheimer's Association workgroups on diagnostic guidelines for Alzheimer's disease. *Alzheimers Dement.* 7, 270–279. doi: 10.1016/j.jalz.2011.03.008

Andel, R., Vigen, C., Mack, W. J., Clark, L. J., and Gatz, M. (2006). The effect of education and occupational complexity on rate of cognitive decline in Alzheimer's patients. *J. Int. Neuropsychol. Soc.* 12, 147–152. doi: 10.1017/S1355617706060206

Avila, J. F., Renteria, M. A., Jones, R. N., Vonk, J. M. J., Turney, I., Sol, K., et al. (2020). Education differentially contributes to cognitive reserve across racial/ethnic groups. *Alzheimers Dement.* 17, 70–80. doi: 10.1002/alz.12176

Balsis, S., Benge, J. F., Lowe, D. A., Geraci, L., and Doody, R. S. (2015). How do scores on the ADAS-Cog, MMSE, and CDR-SOB correspond? *Clin. Neuropsychol.* 29, 1002–1009. doi: 10.1080/13854046.2015.1119312

Bennett, K. K., Buchanan, D. M., Jones, P. G., and Spertus, J. A. (2015). Socioeconomic status, cognitive-emotional factors, and health status following myocardial infarction: Testing the reserve capacity model. *J. Behav. Med.* 38, 110–121. doi: 10.1007/s10865-014-9583-4

Cordone, S., Annarumma, L., Rossini, P. M., and De Gennaro, L. (2019). Sleep and beta-amyloid deposition in Alzheimer disease: Insights on mechanisms and possible innovative treatments. *Front. Pharmacol.* 10:695. doi: 10.3389/fphar.2019.00695

Del Ser, T., Hachinski, V., Merskey, H., and Munoz, D. G. (1999). An autopsy-verified study of the effect of education on degenerative dementia. *Brain* 122(Pt 12), 2309–2319. doi: 10.1093/brain/122.12.2309

Derflinger, S., Sorg, C., Gaser, C., Myers, N., Arsic, M., Kurz, A., et al. (2011). Grey-matter atrophy in Alzheimer's disease is asymmetric but not lateralized. *J. Alzheimers Dis.* 25, 347–357. doi: 10.3233/JAD-2011-110041

Dubois, B., Feldman, H. H., Jacova, C., Hampel, H., Molinuevo, J. L., Blennow, K., et al. (2014). Advancing research diagnostic criteria for Alzheimer's disease: The IWG-2 criteria. *Lancet Neurol.* 13, 614–629. doi: 10.1016/S1474-4422(14)70090-0

Ferreira, D., Nordberg, A., and Westman, E. (2020). Biological subtypes of Alzheimer disease: A systematic review and meta-analysis. *Neurology* 94, 436–448. doi: 10.1212/WNL.0000000000009058

Fritsch, T., McClendon, M. J., Smyth, K. A., Lerner, A. J., Chen, C. H., Petot, G. J., et al. (2001). Effects of educational attainment on the clinical expression of Alzheimer's disease: Results from a research registry. *Am. J. Alzheimers Dis. Other Dement.* 16, 369–376. doi: 10.1177/153331750101600606

Hall, C. B., Derby, C., LeValley, A., Katz, M. J., Verghese, J., and Lipton, R. B. (2007). Education delays accelerated decline on a memory test in persons who develop dementia. *Neurology* 69, 1657–1664. doi: 10.1212/01.wnl.0000278163.82636.30

Inui, Y., Ito, K., Kato, T., and Group, S.-J. S. (2017). Longer-term investigation of the value of 18F-FDG-PET and magnetic resonance imaging for predicting the conversion of mild cognitive impairment to Alzheimer's disease: A multicenter study. *J. Alzheimers Dis.* 60, 877–887. doi: 10.3233/JAD-170395

Ito, K., Fukuyama, H., Senda, M., Ishii, K., Maeda, K., Yamamoto, Y., et al. (2015). Prediction of outcomes in mild cognitive impairment by using 18F-FDG-PET: A multicenter study. *J. Alzheimers Dis.* 45, 543–552. doi: 10.3233/JAD-141338

Jack, C. R. Jr., Bennett, D. A., Blennow, K., Carrillo, M. C., Feldman, H. H., Frisoni, G. B., et al. (2016). A/T/N: An unbiased descriptive classification scheme for Alzheimer disease biomarkers. *Neurology* 87, 539–547. doi: 10.1212/WNL.0000000000002923

Jellinger, K. A. (1998). Dementia with grains (argyrophilic grain disease). *Brain Pathol.* 8, 377–386. doi: 10.1111/j.1750-3639.1998.tb00161.x

Kang, J. M., Cho, Y. S., Park, S., Lee, B. H., Sohn, B. K., Choi, C. H., et al. (2018). Montreal cognitive assessment reflects cognitive reserve. *BMC Geriatr.* 18:261. doi: 10.1186/s12877-018-0951-8

Kato, T., Inui, Y., Nakamura, A., and Ito, K. (2016). Brain fluorodeoxyglucose (FDG) PET in dementia. *Ageing Res. Rev.* 30, 73–84. doi: 10.1016/j.arr.2016.02.003

Ko, K., Yi, D., Byun, M. S., Lee, J. H., Jeon, S. Y., Kim, W. J., et al. (2022). Cognitive reserve proxies, Alzheimer pathologies, and cognition. *Neurobiol. Aging* 110, 88–95. doi: 10.1016/j.neurobiolaging.2021.10.005

Kriegeskorte, N., Simmons, W. K., Bellgowan, P. S., and Baker, C. I. (2009). Circular analysis in systems neuroscience: The dangers of double dipping. *Nat. Neurosci.* 12, 535–540. doi: 10.1038/nn.2303

Laird, N. M., and Ware, J. H. (1982). Random-effects models for longitudinal data. *Biometrics* 38, 963–974.

Lee, D. H., Seo, S. W., Roh, J. H., Oh, M., Oh, J. S., Oh, S. J., et al. (2021). Effects of cognitive reserve in Alzheimer's disease and cognitively unimpaired individuals. *Front. Aging Neurosci.* 13:784054. doi: 10.3389/fnagi.2021.784054

Lovden, M., Fratiglioni, L., Glymour, M. M., Lindenberger, U., and Tucker-Drob, E. M. (2020). Education and cognitive functioning across the life span. *Psychol. Sci. Public Interest* 21, 6–41. doi: 10.1177/1529100620920576

McKhann, G. M., Knopman, D. S., Chertkow, H., Hyman, B. T., Jack, C. R. Jr., Kawas, C. H., et al. (2011). The diagnosis of dementia due to Alzheimer's disease: Recommendations from the National Institute on Aging-Alzheimer's Association workgroups on diagnostic guidelines for Alzheimer's disease. *Alzheimers Dement.* 7, 263–269. doi: 10.1016/j.jalz.2011.03.005

Minoshima, S., Frey, K. A., Koeppe, R. A., Foster, N. L., and Kuhl, D. E. (1995). A diagnostic approach in Alzheimer's disease using three-dimensional stereotactic surface projections of fluorine-18-FDG PET. *J. Nucl. Med.* 36, 1238–1248.

Morrell, C. H., Brant, L. J., and Ferrucci, L. (2009). Model choice can obscure results in longitudinal studies. *J. Gerontol. A Biol. Sci. Med. Sci.* 64, 215–222. doi: 10.1093/gerona/gln024

Nishita, Y., Tange, C., Tomida, M., Otsuka, R., Ando, F., and Shimokata, H. (2019). Positive effects of openness on cognitive aging in middle-aged and older adults: A 13-year longitudinal study. *Int. J. Environ. Res. Public Health* 16:2072. doi: 10.3390/ijerph16122072

Paradise, M., Cooper, C., and Livingston, G. (2009). Systematic review of the effect of education on survival in Alzheimer's disease. *Int. Psychogeriatr.* 21, 25–32. doi: 10.1017/S1041610208008053

Pedrero-Chamizo, R., Szoeke, C., Dennerstein, L., and Campbell, S. (2021). Influence of physical activity levels and functional capacity on brain beta-amyloid deposition in older women. *Front. Aging Neurosci.* 13:697528. doi: 10.3389/fnagi.2021.697528

Qian, G., and Mahdi, A. (2020). Sensitivity analysis methods in the biomedical sciences. *Math. Biosci.* 323:108306. doi: 10.1016/j.mbs.2020.108306

Rabinovici, G. D., Rosen, H. J., Alkalay, A., Kornak, J., Furst, A. J., Agarwal, N., et al. (2011). Amyloid vs. FDG-PET in the differential diagnosis of AD and FTLD. *Neurology* 77, 2034–2042. doi: 10.1212/WNL.0b013e31823b9c5e

Saito, S., and Ihara, M. (2016). Interaction between cerebrovascular disease and Alzheimer pathology. *Curr. Opin. Psychiatry* 29, 168–173. doi: 10.1097/YCO.0000000000000239

Scarmeas, N., Albert, S. M., Manly, J. J., and Stern, Y. (2006). Education and rates of cognitive decline in incident Alzheimer's disease. *J. Neurol. Neurosurg. Psychiatry* 77, 308–316. doi: 10.1136/jnnp.2005.072306

Silverman, D. H., and Phelps, M. E. (2001). Application of positron emission tomography for evaluation of metabolism and blood flow in human brain: Normal development, aging, dementia, and stroke. *Mol. Genet. Metab.* 74, 128–138. doi: 10.1006/mgme.2001.3236

Spina, S., La Joie, R., Petersen, C., Nolan, A. L., Cuevas, D., Cosme, C., et al. (2021). Comorbid neuropathological diagnoses in early versus late-onset Alzheimer's disease. *Brain* 144, 2186–2198. doi: 10.1093/brain/awab099

Stern, Y. (2002). What is cognitive reserve? Theory and research application of the reserve concept. *J. Int. Neuropsychol. Soc.* 8, 448–460.

Stern, Y. (2009). Cognitive reserve. *Neuropsychologia* 47, 2015–2028. doi: 10.1016/j.neuropsychologia.2009.03.004

Unverzagt, F. W., Hui, S. L., Farlow, M. R., Hall, K. S., and Hendrie, H. C. (1998). Cognitive decline and education in mild dementia. *Neurology* 50, 181–185. doi: 10.1212/wnl.50.1.181

van Loenhoud, A. C., van der Flier, W. M., Wink, A. M., Dicks, E., Groot, C., Twisk, J., et al. (2019). Cognitive reserve and clinical progression in Alzheimer disease: A paradoxical relationship. *Neurology* 93, e334–e346. doi: 10.1212/WNL.0000000000007821

Vemuri, P., Knopman, D. S., Lesnick, T. G., Przybelski, S. A., Mielke, M. M., Graff-Radford, J., et al. (2017). Evaluation of amyloid protective factors and Alzheimer disease neurodegeneration protective factors in elderly individuals. *JAMA Neurol.* 74, 718–726. doi: 10.1001/jamaneurol.2017.0244

Vemuri, P., Weigand, S. D., Przybelski, S. A., Knopman, D. S., Smith, G. E., Trojanowski, J. Q., et al. (2011). Cognitive reserve and Alzheimer's disease biomarkers are independent determinants of cognition. *Brain* 134(Pt 5), 1479–1492. doi: 10.1093/brain/awr049

Wilson, R. S., Yu, L., Lamar, M., Schneider, J. A., Boyle, P. A., and Bennett, D. A. (2019). Education and cognitive reserve in old age. *Neurology* 92, e1041–e1050. doi: 10.1212/WNL.0000000000007036

Advantages of publishing in Frontiers

OPEN ACCESS
Articles are free to read for greatest visibility and readership

FAST PUBLICATION
Around 90 days from submission to decision

HIGH QUALITY PEER-REVIEW
Rigorous, collaborative, and constructive peer-review

TRANSPARENT PEER-REVIEW
Editors and reviewers acknowledged by name on published articles

Frontiers
Avenue du Tribunal-Fédéral 34
1005 Lausanne | Switzerland

Visit us: www.frontiersin.org
Contact us: frontiersin.org/about/contact

REPRODUCIBILITY OF RESEARCH
Support open data and methods to enhance research reproducibility

DIGITAL PUBLISHING
Articles designed for optimal readership across devices

FOLLOW US
@frontiersin

IMPACT METRICS
Advanced article metrics track visibility across digital media

EXTENSIVE PROMOTION
Marketing and promotion of impactful research

LOOP RESEARCH NETWORK
Our network increases your article's readership